
Synthesis and Characterization of Silicon Polyoxolenes

INAUGURAL – DISSERTATION

to obtain the academic degree
Doctor rerum naturalium (Dr. rer. nat.)

submitted to the Faculty of Mathematics,
Engineering Sciences and Natural Sciences
of Heidelberg University

by

Rezisha Maskey, M. Sc.
b. in Bhaktapur, Nepal

2023

DISSERTATION

to obtain the academic degree
Doctor rerum naturalium (Dr. rer. nat.)

submitted to the Faculty of Mathematics,
Engineering Sciences and Natural Sciences
of Heidelberg University

by

Rezisha Maskey, M. Sc.
b. in Bhaktapur, Nepal

Date of Defense: 17.02.2023

1st Reviewer: Prof. Dr. Lutz Greb
2nd Reviewer: Prof. Dr. Dr. Hans-Jörg Himmel

The experimental part of this work was carried out under the supervision of Prof. Dr. *Lutz Greb* at the Institute of Inorganic Chemistry of Heidelberg University from January 2019 to October 2022. Parts of the results described here were obtained by *Christoph Bendel*, *Simone Ebel*, *Angelina Jovic*, *Jonas Malzacher*, *Qingqing Luo* and *Annabelle Sonn* as part of their research internships or bachelor theses in the group of Prof. Dr. GREB under my guidance.

Parts of this dissertation have already been published in scientific articles or presented at conferences.

Talks:

- I. *Siliziumtris(perchloro)dioxolen*
Skilizium, Lantsch/Lenz, Switzerland, **2019**.
- II. *Silizium Trisdioxolene – stabile Triplett Diradikale*
5th Closed Conference Edersee, Vöhl, Germany **2019**.
- III. *Synthese und Redox Chemie von Siliziumtrisdioxolenen*
Skilizium, Engelberg, Switzerland, **2020**.



Publications:

- I. *Bis(perchlorocatecholato)silane – A Neutral Silicon Lewis Super Acid*
R. Maskey, M. Schädler, C. Legler and L. Greb, *Angew. Chem. Int. Ed.* **2018**, *57*, 1717-1720, DOI: 10.1002/anie.201712155; *Angew. Chem.* **2018**, *130*, 1733-1736, DOI: 10.1002/ange.201712155.
- II. *Silicon Tris(perchloro)dioxolene: A Neutral Triplet Diradical*
R. Maskey, H. Wadepohl and L. Greb, *Angew. Chem. Int. Ed.* **2019**, *58*, 3616-3619, DOI: 10.1002/anie.201812989; *Angew. Chem.* **2019**, *131*, 3655-3658, DOI: 10.1002/ange.201812989.
- III. *Completing the Redox-Series of Silicon Trisdioxolene: ortho-Quinone and Lewis Superacid Make a Powerful Redox Catalyst*
R. Maskey, C. Bendel, J. Malzacher and L. Greb, *Chem. Eur. J.* **2020**, *26*, 17386-17389, DOI: 10.1002/chem.202004712.
- IV. *Synthesis and Characterization of Hypercoordinated Silicate Anions: Catching Intermediates of Lewis Base Catalysis*
D. Hartmann,† N. Ansmann,† S. Sailer, P. Erdmann, R. Maskey, M. Schorpp and L. Greb, *Angew. Chem. Int. Ed.* **2022**, e202203947, DOI: 10.1002/anie.202203947.
- V. *Catecholate Complexes of p-Block Elements: Redox Activity*
R. Maskey and L. Greb, *Encyclopedia of Inorganic and Bioinorganic Chemistry*, **2022**.
- VI. *Redox-Active Lewis Pairs Yield Diradicaloids and Enable Modular Control of the Diradical Character*
R. Maskey, T. Thorwart, S. Ebel, A. Jovic, D. Hartmann and L. Greb, *Manuscript submitted*.

To my Family

and to my younger self..

*Those who dwell, as scientist or laymen
- among the beauties and mysteries of the earth -
are never alone or weary of life.*

Rachel Carson
27 May 1907 – 14 April 1964

ABSTRACT

Tris(catecholato)silicate dianions, a compound class that is already known for over a century, can be readily prepared by reacting sand with catechol under basic conditions. Strikingly, the two-electron-oxidized derivative – silicon tris(perchloro)dioxolene $\mathbf{1}^{\text{Cl}}$ – has been recently accessed, representing a thermally stable, neutral triplet diradical and the first non-metal complex with redox-active and mixed-valence substituents.

In the present work, the redox properties of $\mathbf{1}^{\text{Cl}}$ are investigated and by the synthesis of the corresponding monoradical anion $[\mathbf{1}^{\text{Cl}}]^{\bullet-}$, the redox series of tris(catecholato)silicates in general is completed. With cyclic voltammetry the redox potentials $E_{1/2} = 0.43$ V and 0.88 V (*vs.* Fc/Fc⁺) were finally determined. Comparing the redox potentials of $\mathbf{1}^{\text{Cl}}$ with *free* tetrachloro-*o*-benzoquinone, a tremendous shift of about 1.2 V becomes apparent. Moreover, $\mathbf{1}^{\text{Cl}}$ is applicable as efficient redox catalyst.

By varying the quinone ligands and the silicon source, further homo- and heteroleptic derivatives are prepared. Variable temperature EPR measurements disclose the existence of diradicals with a triplet ground state.

With a more profound understanding of the monomeric species, the synthesis is extended to higher nuclearity. A straightforward approach is established by introducing substituted 2,5-dihydroxy-*p*-benzoquinone ($\text{H}_2\text{d}hbq^{\text{Y}}$) as $[\text{d}hbq^{\text{Y}}][\text{Na}@15\text{c}5]_2$ ($\text{Y} = \text{Cl}, \text{Br}, \text{Ph}, \text{NO}_2$) salts and mixing with bis(catecholato)silanes $\mathbf{2}^{\text{X}}$ ($\text{X} = \text{Cl}, \text{Br}, \text{CF}_3, \text{iPr}$) to obtain the dinuclear species $[\mathbf{4}^{\text{X,Y}}][\text{Na}@15\text{c}5]_2$, which are robust to coordinating environments. By selective combination of more electron-rich $\mathbf{2}^{\text{X}}$ and electron-poor *d}hbq* linkers diradicaloid complexes $[\mathbf{4}^{\text{X,Y}}]^{2-}$ ($\text{X} = \text{Cl}, \text{iPr}$ and $\text{Y} = \text{Cl}, \text{Br}, \text{NO}_2$) were obtained and characterized. The opposite extreme with the smallest diradical character was accomplished by combining electron-poor $\mathbf{2}^{\text{CF}_3}$ and electron-rich *d}hbq^{\text{Ph}}. The underlying design principle is further disclosed by computational analyses. Conclusively, this one-step protocol grants access to dimeric silicon polyoxolenes with control over and fine-tuning of the spin ground state. Lastly, preliminary results are obtained for the trimeric structures by implementing the six-fold deprotonated tritopic linker 2,3,6,7,10,11-hexahydroxytriphenylene ($\text{H}_6\text{h}htp$) with $\mathbf{2}^{\text{Cl}}$.*

The results gathered in this work present a fundamental understanding of silicon-bridged polyoxolenes and thus are valuable extensions based on a non-metal main group element to known works based on transition metals.

KURZZUSAMMENFASSUNG

Tris(catecholato)silikat-Dianionen – eine Substanzklasse, die bereits seit über einem Jahrhundert bekannt ist, können leicht durch eine Reaktion von Sand mit Catechol in basischem Milieu hergestellt werden. Kürzlich wurde die zweifach oxidierte Form – Silizium Tris(perchloro)dioxolen $\mathbf{1}^{\text{Cl}}$ – zugänglich gemacht, welches ein thermisch stabiles, neutrales Triplett-Diradikal sowie den ersten nichtmetallischen Komplex mit redoxaktiven und gemischtvalenten Substituenten darstellt.

In der vorliegenden Arbeit werden die Redox-Eigenschaften von $\mathbf{1}^{\text{Cl}}$ untersucht und durch die Synthese des entsprechenden Monoradikalanions $[\mathbf{1}^{\text{Cl}}]^{\bullet-}$ die Redox-Serie von Tris(catecholato)silikaten im Allgemeinen vervollständigt. Mittels Cyclovoltammetrie konnten die Redoxpotentiale $E_{1/2} = 0.43$ V und 0.88 V (*vs.* Fc/Fc⁺) bestimmt werden. Bei einem Vergleich der Redoxpotentiale von $\mathbf{1}^{\text{Cl}}$ mit dem *freien* Tetrachlor-*o*-benzochinon, zeigt sich eine enorme Potentialverschiebung um etwa 1.2 V. Außerdem kann $\mathbf{1}^{\text{Cl}}$ als effizienter Redoxkatalysator eingesetzt werden.

Durch Veränderung der Chinon-Liganden und der Siliziumquellen werden weitere homo- und heteroleptische Derivate hergestellt. EPR-Messungen bei variabler Temperatur zeigen das Vorliegen von Diradikalen mit einem Triplett Grundzustand, analog zum perchlorierten Derivat.

Mit einem tieferen Verständnis für die monomeren Verbindungen wird schließlich die Nuklearität der Substanzklasse erhöht. Durch die Einführung von substituierten 2,5-Dihydroxy-*p*-Benzochinonen ($\text{H}_2\text{d}hbq^{\text{Y}}$) als $[\text{d}hbq^{\text{Y}}][\text{Na}@15\text{c}5]_2$ ($\text{Y} = \text{Cl}, \text{Br}, \text{Ph}, \text{NO}_2$) Salze und das anschließende Umsetzen mit Bis(catecholato)silanen $\mathbf{2}^{\text{X}}$ ($\text{X} = \text{Cl}, \text{Br}, \text{CF}_3, \text{iPr}$) wird eine einfache Vorschrift geschaffen, um die zweikernigen Verbindungen $[\mathbf{4}^{\text{X,Y}}][\text{Na}@15\text{c}5]_2$ herzustellen, die in Gegenwart von koordinierenden Lösungsmitteln robust sind. Durch gezielte Kombination von elektronenreicheren $\mathbf{2}^{\text{X}}$ und elektronenarmen *dhbq*-Linkern werden diradikaloide Komplexe $[\mathbf{4}^{\text{X,Y}}]^{2-}$ ($\text{X} = \text{Cl}, \text{iPr}$ und $\text{Y} = \text{Cl}, \text{Br}, \text{NO}_2$) erhalten und untersucht. Das entgegengesetzte Extrem mit dem kleinsten Diradikal-Charakter wird durch die Kombination von $\mathbf{2}^{\text{CF}_3}$ (elektronenarm) und *dhbq*^{Ph} (elektronenreich) erreicht. Das zugrundeliegende Syntheseprinzip wird durch quantenchemische Berechnungen bestätigt. Schlussendlich, ermöglicht dieser einstufige Ansatz den Zugang zu dimeren Siliziumpolyoxolenen mit Kontrolle über und Feinabstimmung des Spin-Grundzustands. Zuletzt werden erste Ergebnisse für trimere Strukturen durch die Umsetzung des sechsfach deprotonierten tritropischen Linkers 2,3,6,7,10,11-Hexahydroxytriphenylen (*H6hhtp*) mit $\mathbf{2}^{\text{Cl}}$ erzielt.

Die in dieser Arbeit gesammelten Ergebnisse stellen ein grundlegendes Verständnis von Silizium-verbrückten Polyoxolenen dar und sind somit eine wertvolle Erweiterung bekannter Arbeiten auf der Basis von Übergangsmetallen, die auf einem nichtmetallischen Hauptgruppenelement basieren.

TABLE OF CONTENTS

1	Introduction	1
1.1	Redox-Active Ligands: <i>ortho</i>-Dioxolenes	2
1.1.1	Dioxolene Complexes of <i>p</i> -Block Elements	4
1.1.2	Silicon Dioxolene Complexes	11
1.2	Porous Functional Materials	14
2	Motivation and Aim	19
3	Results and Discussion	21
3.1	Completing the Redox Series	21
3.1.1	Synthesis and Characterization of 1^{Cl}	22
3.1.2	Synthesis and Characterization of $[1^{\text{Cl}}]^{2-}$	25
3.1.3	Investigating the Redox Properties	26
3.1.4	Synthesis and Characterization of $[1^{\text{Cl}}]^{\bullet-}$	29
3.1.5	Redox Catalysis.....	33
3.1.6	Conclusion.....	35
3.2	Further Silicon Trisdioxolenes	37
3.2.1	Synthesis of Precursors.....	37
3.2.2	Synthesis and Characterization of 1^{X}	40
3.2.3	Synthesis of $[1^{\text{X}}]^{2-}$	44
3.2.4	Synthesis of $[1^{\text{Br}}]^{\bullet-}$	46
3.2.5	Formation Mechanism towards 1^{X}	47
3.2.6	Heteroleptic Silicon Trisdioxolenes.....	49
3.2.7	Investigating the Magnetic Properties of 1^{tBu} and $1^{\text{X,Y}}$	52
3.2.8	Conclusion.....	54
3.3	Tetraoxolene-bridged Bis(catecholato)silanes	57

3.3.1	Synthesis and Characterization of Precursors.....	57
3.3.2	Synthesis and Characterization of 2 ^{iPr}	64
3.3.3	Synthesis and Characterization of [4 ^{X,Y}][Na@15c5] ₂	65
3.3.4	Investigating the Magnetic Properties.....	75
3.3.5	Conclusion.....	80
3.4	Hexaoxolene-bridged Bis(catecholato)silanes	83
3.4.1	Synthesis of Precursors.....	83
3.4.2	Deprotonation of H ₆ <i>hhtp</i> and Synthesis of [5 ^{Cl}][HB] ₆	85
3.4.3	Conclusion.....	97
4	Summary.....	99
5	Experimental Section	103
5.1	General Information.....	103
5.1.1	Materials and Methods.....	103
5.1.2	Analytical Methods.....	104
5.1.3	Theoretical Methods	108
5.2	Syntheses.....	112
5.2.1	Precursors	114
5.2.2	Silicon Lewis Acids	125
5.2.3	Homoleptic Silicon Trisdioxolene Compounds	127
5.2.4	Heteroleptic Silicon Trisdioxolene Compounds	140
5.2.5	Tetraoxolene-bridged Bis(catecholato)silanes	141
5.2.6	Hexaoxolene-bridged Bis(catecholato)silanes	147
5.2.7	Catalysis.....	150
5.2.8	Miscellaneous.....	153
6	References.....	155
7	Appendix.....	I
7.1	List of Abbreviations.....	I

7.2	List of Symbols.....	IV
7.3	Computational Data Tables.....	V
7.3.1	Data Tables for Chapters 3.1 and 3.2	V
7.3.2	Data Tables for Chapter 3.3.....	VIII
7.4	Computation of Metrical Oxidation State.....	XI
7.5	EPR Spectroscopy	XIII
7.6	NMR Spectroscopy.....	XV
7.7	Cyclic Voltammetry Experiments	XVI
7.8	Crystallographic Data.....	XX
	Danksagung.....	XXX
	Eidesstattliche Versicherung	XXXIV

1

INTRODUCTION

Many chemical transformations can be facilitated by catalytic processes based on transition metals. These catalytic processes are usually accompanied by a change in the redox state, typically taking place at the metal center (Figure 1). A distinction can be made between reductive, oxidative, and intrinsically redox neutral processes. The coordinating ligands thereby serve as stabilizing skeleton for the corresponding metal center and regulate the catalyst performance with the help of their properties (e.g., steric hindrance), but themselves are only indirectly involved in the reaction. Thus, such ligands only partake as *spectators* and are also called redox-inactive ligands.¹⁻⁴

A lot of the catalytic systems known today, and which are of industrial usage benefit from the features of (noble) transition metals. In contrast to base metals favoring one electron processes that lead to undefined reactions, precious metals participate in well-defined two electron redox reactions. However, due to their low natural abundance, effortful and costly production, these metals also bear many disadvantages.^{2,5} Therefore, it is of particular importance to develop adequate catalytic systems based on elements that are more accessible and abundant. Here, silicon stands out with a mass fraction of up to 28 % as the second-most abundant element in the earth's crust.⁶ Accordingly, cost-effective and environmentally benign compounds, as well as novel reaction pathways, which for example are not mediated *via* the metal center, have received a significant upturn.⁵ Within the last decades, new types of catalytic approaches have been discovered in which the ligand system plays a significantly more active role by interacting cooperatively in the determining step for bond activation or by contributing features like redox activity.⁷⁻⁹

Nature already paved the way for this concept since various metalloenzymes are known to have redox-active ligands within their active site, that interact with the corresponding metal ions. Such ligand-centered redox reactions found in enzymatic processes are essential in plenty of metabolic pathways.¹⁰

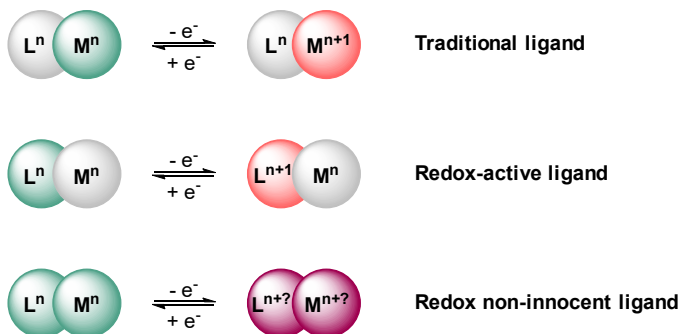


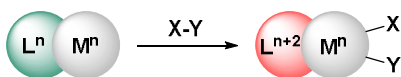
Figure 1: Classification of ligand (L) types in metal (M) complexes upon electron transfer reactions.

1.1 Redox-Active Ligands: *ortho*-Dioxolenes

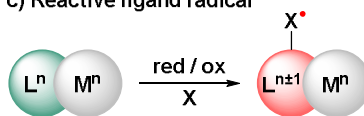
Ligands that are redox-active typically have an energetically higher-lying HOMO (highest occupied molecular orbital) or an energetically lower-lying LUMO (lowest occupied molecular orbital) compared with *traditional* ligands.^{3,5} This leads to more accessible energy levels than the single metal center can provide, widening the range for possible redox events and modifying the reactivity of the whole complex.¹¹ Accordingly, multi-electron reactions are unraveled into sub-steps, which means that ligand-centered redox processes can be more easily initiated. Thereby, the metal center can retain its electronic state, or the redox-active ligand may interact in synergy with the central ion, enabling delocalization of the electrons leading to ambiguous redox states (Figure 1).^{1,12} In 1966, JØRGENSEN stated that *ligands are innocent when they allow oxidation states of the central atom to be defined*.¹³ With that, the terminology of *suspect* or rather (redox) non-innocent ligands was introduced to describe the ambiguity in the redox state of the metal center occurring through the ligand system.

Redox-active ligands can expand the reactivity of the metal center and the whole complex through different reaction modes (Figure 2). They can function as (a) electron reservoir by providing or receiving electrons, (b) change the Lewis acidity/basicity of the central atom, (c) generate reactive ligand-centered radicals, or (d) directly activate substrates by single electron transfer reactions.^{1-3,9} Regarding radical-type reactivity, it is important to mention that thereby different spin states can be accessed. This likewise broadens the reactivity in catalysis as lower reaction barriers can be generated through different open shell configurations.¹⁴

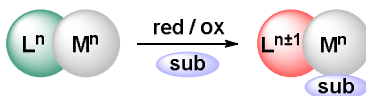
a) Electron reservoir



c) Reactive ligand radical



b) Change in Lewis acidity or basicity



d) Activation of substrate by SET

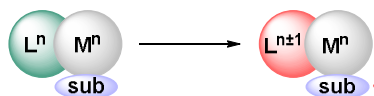
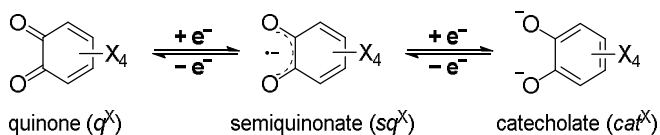


Figure 2: Enhancing the reactivity of a metal center (M) with redox-active ligands (L) as a) electron reservoir or by b) changing the Lewis acidity or basicity of the metal center, c) generation of reactive ligand radicals or d) activation of substrate (sub) by single electron transfer (SET) from the ligand.

Catechol, also known as 1,2-dihydroxybenzene, is an excellent example of a redox-active ligand. It was first isolated by REINSCH in the first half of the nineteenth century and a variety of natural substances, derived from the catechol moiety, play an important role in many biological processes.¹⁵⁻¹⁶ For example, catecholamines make up an essential class of compounds for neurotransmitters, hormones, and other narcotic drugs. Also, catechol-type siderophores possess the ability to specifically bind to iron(III) cations, making them soluble and thus increasing their biological availability.

The redox activity of the catechol is displayed by two reversible one electron oxidations resulting in three stable redox isomers (Scheme 1) which are all suitable for coordination.¹⁷ In the 1970s, the members of this redox series were first mentioned and coined as dioxolenes (*diox*) by BALCH *et al.*¹⁸⁻¹⁹ To date, dioxolene ligands have

found broad usage in the fields of coordination chemistry. Numerous transition metal dioxolene complexes are well established and intensively studied.²⁰⁻²² Due to similar orbital energies between the ligand and the metal center and hence the occurrence of redox non-innocence, to date, promising applications within the fields of redox-active ligand-based catalysis and functional materials could be spawned.^{2, 9, 23-26}



Scheme 1: Redox isomers of *ortho*-dioxolene ligands with their respective notation and abbreviations used in the following.

1.1.1 Dioxolene Complexes of *p*-Block Elements

As with the transition metal complexes, the chemistry of dioxolene complexes with *p*-block elements has also been investigated and resumed appropriately.²⁷⁻³⁰ There, the dioxolene ligands usually behave chemically innocent, which means the redox state of the element center is well-defined. In many *p*-block element dioxolene complexes, the ligand tends to adopt the fully reduced catecholate state which imparts features such as strong Lewis acidity.³¹⁻³⁴ The differences in the energies of the frontier molecule orbitals of the dioxolene ligands and the (lighter) *p*-block elements, unlike the orbital energies regarding the *d*-block metals (*vide supra*), yield in redox unambiguous performance.³⁵ This means that redox reactions are prone to be only ligand- or element-based. Consequently, characteristics such as valence electromerism are scarce within the *p*-block elements³⁶ compared to the transition metals.³⁷ However, the heavier *p*-block elements show more distinct redox flexibility and therefore are inclined to be involved in redox processes alongside the dioxolene ligands.³⁵ In the following, some selected examples for *p*-block element dioxolene complexes in view of redox activity will be presented.

1.1.1.1 Group 13

The first aluminum catecholate complex $\text{Al}(\text{cat}^{\text{H}})_2$ (Figure 3a), reported in the 1960s, could be oxidized in the presence of sodium peroxide at higher temperatures, whereas the analogous boron complexes remained in their reduced state.³⁸ A decade later

further group 13 dioxolene complexes were discovered by reacting the metal halides MX_3 ($\text{M} = \text{Al}, \text{Ga}, \text{In}$ and $\text{X} = \text{Cl}, \text{Br}, \text{I}$) with $q^{3,6\text{-dtb}}$ (Figure 3b), resulting in paramagnetic monosemiquinoidal dihalide complexes as indicated by EPR spectroscopy.³⁹

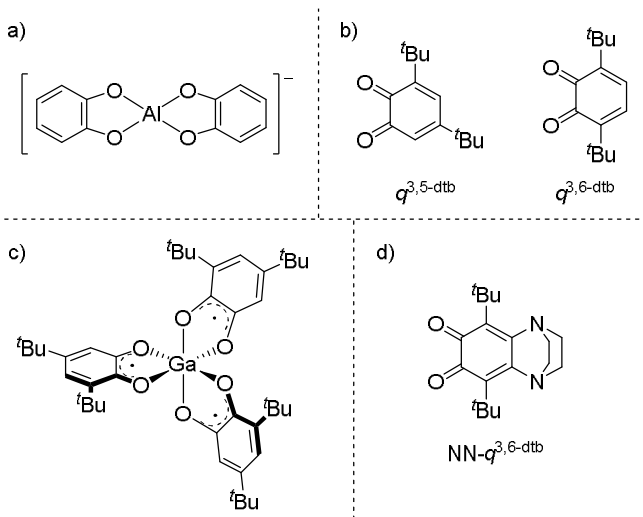


Figure 3: a) Anionic aluminum catecholate complex.³⁸ b) 3,5-Di- tBu - and 3,6-di- tBu -substituted o -dioxolenes represented in the quinone state. c) Neutral triradical tris(3,5-di- tBu -semiquinonato)gallium complex.⁴⁰⁻⁴¹ d) Sterically hindered ligand: 5,8-di- tBu -2,3-dihydro-1,4-ethanoquinoxaline-6,7-dione.

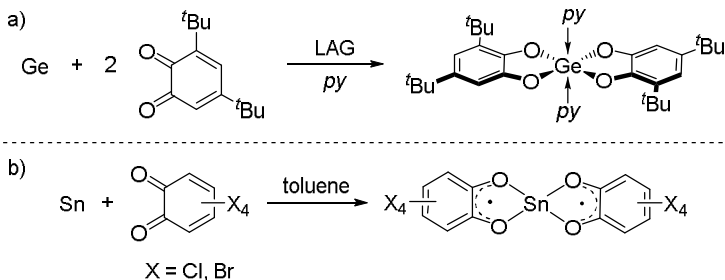
Later, in 1993, the groups of HENDRICKSON and MCGARVEY independently isolated the triradical $\text{Ga}(sq^{3,5\text{-dtb}})$ (Figure 3c).⁴⁰⁻⁴¹ Green crystalline material was obtained either from oxidative addition of $q^{3,5\text{-dtb}}$ (Figure 3b) to elemental gallium or by salt exchange between GaI_3 and $\text{Na}(sq^{3,5\text{-dtb}})$. Single crystal structure analysis showed that the dioxolene ligands were coordinated octahedrally around the gallium center and the bond lengths confirmed the presence of the semiquinone state for all three ligands. Similar results were obtained for the isostructural chromium complex.⁴² Magnetic investigations on $\text{Ga}(sq^{3,5\text{-dtb}})_3$ showed an increase of the magnetic moment from $3.0 \mu_B$ at 320 K to $3.58 \mu_B$ at 9 K, indicating a ferromagnetically coupled $S = 3/2$ ground state. The exchange parameter was calculated as $J_{sqsq} = 7.8 \text{ cm}^{-1}$ and low-temperature EPR measurements revealed signals for the forbidden transition at

$\Delta m_s = 3$ at $g = 6$, corroborating the presence of a quartet state ($S = 3/2$) for the triradical.⁴¹ Later, these findings were additionally validated by the group of SCHMIDT, who prepared $M(\text{diox}^X)_{2/3}$ complexes ($M = \text{Al, In, Cd, Sn}$ and $X = 3,5\text{-dtb}; 3,6\text{-dtb}$) following a mechanochemical route by grinding the metals with the respective quinones.⁴³ Besides, the dipolar coupling parameters were calculated and found to be $D > 0$ for triradicals, consistent with theoretical predictions. Furthermore, semiempirical PM3 (CI) calculations on dioxolene complexes by PEREKHODTSEV and LEBEDEV consolidated the theoretical concepts and the experiments.⁴⁴

In 2014, an analogous aluminum dioxolene complex was synthesized and characterized by scXRD. Thereby, PISKUNOV *et al.* made use of the sterically hindered ligand 5,8-di-*t*-butyl-2,3-dihydro-1,4-ethanoquinoxaline-6,7-dione (NN-*q*^{3,6-dtb}, Figure 3d) and drew comparisons of the magnetic properties between the group 13 elements.⁴⁵ Single crystal structure analysis showed an octahedral configuration for the aluminum and gallium semiquinonate complexes, whereas the respective indium complex adopted a trigonal prismatic structure. Similar observations for indium dioxolene complexes were made before by the same group but with the 3,6-di-*t*-butyl-dioxolene ligand.⁴⁶ Having a look at the magnetic properties, the unpaired electrons in $M(\text{NN-}s\text{q}^{3,6\text{-dtb}})_3$ ($M = \text{Al, Ga}$) coupled ferromagnetically at 30 K, as expected by previous results with similar complexes (*vide supra*). By contrast, the indium analogues were present in a doublet ground state and the coupling was found to be antiferromagnetic. These examples neatly present the control over and dependency of the magnetic properties through the complexes' geometry. Here it should be noted that for magnetic couplings between unpaired electrons two exchange pathways are possible.⁴³ The first one proceeds through direct exchange, for example, between the electrons and the *p*-orbitals of adjacent oxygens, resulting in non-zero overlap, meaning antiferromagnetic coupling. The second pathway is mediated through the empty *p*-orbital of the element center, which leads to an orthogonal overlap due to the symmetry of the *p*-orbitals, and thus yields ferromagnetic coupling.^{40,43} Lastly, for related thallium dioxolene complexes prepared by STEGMANN and coworkers from diphenyl thallium hydroxide and substituted catechols, oxidation with atmospheric oxygen led to respective stable semiquinonate complexes, which presumably exist as ions pairs.⁴⁷

1.1.1.2 Group 14

RIVIÈRE and coworkers realized the first bis(catecholato)germanes in 1986 by reacting $q^{3,5\text{-dtb}}$ with GeF_2 or $\text{GeF}_2(\text{THF})$ in benzene.⁴⁸ Later, the synthesis could be extended onto GeCl_2 or GeCl_4 .⁴⁹ Reactions with elemental gallium could also be enabled⁵⁰ and accelerated by liquid-assisted grinding (*LAG*) with donor molecules, such as pyridine (*py*), resulting in the adduct complexes (Scheme 2a).⁵¹ GeO_2 could also be utilized with the respective catechol. GREB and coworkers were also able to compound $\text{Ge}(\text{cat}^{\text{Cl}})_2$ under milder conditions. Simply mixing of GeO_2 with $\text{H}_2\text{cat}^{\text{Cl}}$ at 60°C directly in water yielded the respective bis-adduct. Hence, $\text{Ge}(\text{cat}^{\text{Cl}})_2$ marks the first neutral Lewis superacid (see chapter 1.1.2 for definition) showing entire stability in aqueous media.³⁴ Using cyano-substituted pyridines as donor ligand resulted in yellow- and orange-colored solids,⁵² instead of colorless ones as with THF or *py*.^{49,51} This was explained by charge transfer happening between the catecholates and the *py* ligands (LLCT). Later, GRISHIN *et al.* discovered that $\text{M}(\text{cat}^{3,6\text{-dtb}})_2$ ($\text{M} = \text{Ge}, \text{Sn}$) reacted with radicals emerging in the radical polymerization of styrene. EPR experiments showed that thereby semiquinone intermediates were formed, thus, suggesting a direct participation of the bis(catecholate) complexes within the propagation steps. The resulting polymers could be further used as macroinitiators to promote chain growth.⁵³



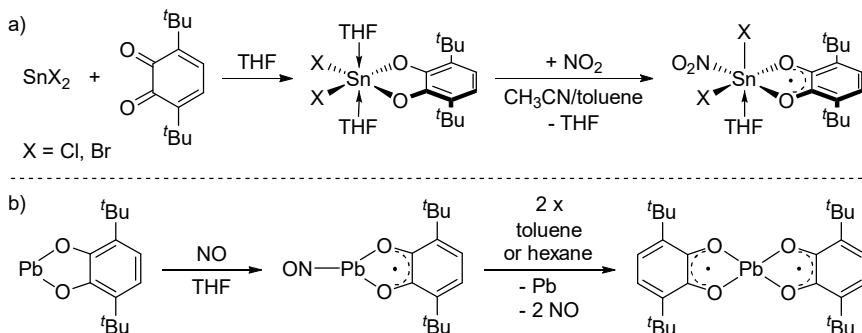
Scheme 2: a) Synthesis of $\text{Ge}(\text{cat}^{3,5\text{-dtb}})_2(\text{py})_2$ via oxidative addition of $q^{3,5\text{-dtb}}$ to germanium metal under *LAG* conditions in presence of pyridine.⁵¹ b) Synthesis of neutral diradical $\text{Sn}(\text{sq}^{\text{X}})_2$ ($\text{X} = \text{Cl}, \text{Br}$) via oxidative addition of q^{X} onto elemental tin in toluene.⁵⁴⁻⁵⁵

Investigations on tin dioxolene compounds started in the 1980s with reactions between triorganyltin hydroxides with substituted catechols⁵⁶ or tin halides with quinones,⁵⁷⁻⁵⁸ in which the appearance of paramagnetic intermediates was observed by means of

EPR spectroscopy. Later, DAVIES and HAWARI used chlorinated organotin reagents with 3,6-di-*t*-butyl-benzoquinone to purposefully synthesize similar radical tin derivatives $X_3Sn(sq^{3,6-dtb})$ ($X = \text{alkyl, Cl}$), which were isolated as stable adducts with donor ligands (*phen*, *bipy*, TMEDA).⁵⁹ Following an electrochemical setup by conducting the anodic oxidation of tin metal in presence of cat^X ($X = \text{H, Br}$), MABROUK and TUCK were able to synthesize $Sn(cat^X)$ complexes.⁶⁰ Addition of another equivalent of quinone led to $Sn(IV)$ bis(catecholato) complexes. Implementation of elemental tin with quinones in toluene, directly led to tin(II) semiquinonate species (Scheme 2b).⁵⁴⁻⁵⁵ In 2005, ABAKUMOV and PISKUNOV synthesized $Cl_2Sn(cat^{3,6-dtb})(THF)_2$ (Scheme 3a) and $Ph_2Sn(cat^{3,6-dtb})(THF)_n$ ($n = 0, 1$), which turned out to be useful as radical traps for some short-lived C-, O- and S-centered radicals, whereby the catecholato ligands were oxidized to the semiquinone state.⁶¹⁻⁶² Furthermore, ferrocene was able to reduce $Sn(sq^{3,6-dtb})_2Cl_2$ in acetonitrile leading to the mixed-valence complex $[(cat^{3,6-dtb})(sq^{3,6-dtb})SnCl_2][Cp_2Fe]$, which gave rise to ferromagnetic coupling between the ferrocenium radical cation and the tin radical anion complex.⁶³ The reaction could be reversed into the starting material by changing the solvent to THF. Oxidative fixation of NO_2 could be realized by $X_2Sn(cat^{3,6-dtb})(THF)_2$ ($X = \text{Cl, Br}$) in a mixture of acetonitrile/toluene (Scheme 3a).⁶⁴ The resulting semiquinonate complex then quickly dimerized to the respective halogenated diradical compound, evidenced by typical splitting patterns observed in EPR spectra at lower temperatures. Finally in 2016, the synthesis and crystallization of free $Sn(cat^{3,6-dtb})$ was reattempted with $SnCl_2$ (dioxane) and $Na_2(cat^{3,6-dtb})$ as starting materials.⁶⁵ SCXRD analysis finally revealed that the complex existed as trimeric aggregate, substantiating the results that were already made ten years before by ABAKUMOVA and coworkers, who prepared $Sn(cat^{3,6-dtb})$ in minor yields from tin amalgam and $q^{3,6-dtb}$.⁶⁶

Lead(II) dioxolene complexes were first tackled in 2003 by mixing lead metal with different quinones, but the synthesis was accompanied with difficulties as the reaction only resulted in insoluble diamagnetic precipitate, whereas with phenanthrenequinone stable bis(semiquinonate) complexes could be realized.⁶⁷ Following an electrochemical approach, as done with tin,⁶⁰ lead catecholates could be successfully prepared.⁶⁷ In 2012, $Pb(cat^{3,6-dtb})$ was discovered to be the first non-transition metal complex able to fixate nitric oxide in THF yielding $Pb(sq^{3,6-dtb})NO$ (Scheme 3b).⁶⁸ Switching to

nonpolar solvents such as toluene or hexane, led to the elimination of NO gas and disproportionation to metallic lead and the desired diradical species $\text{Pb}(sq^{3,6\text{-dtb}})_2$.



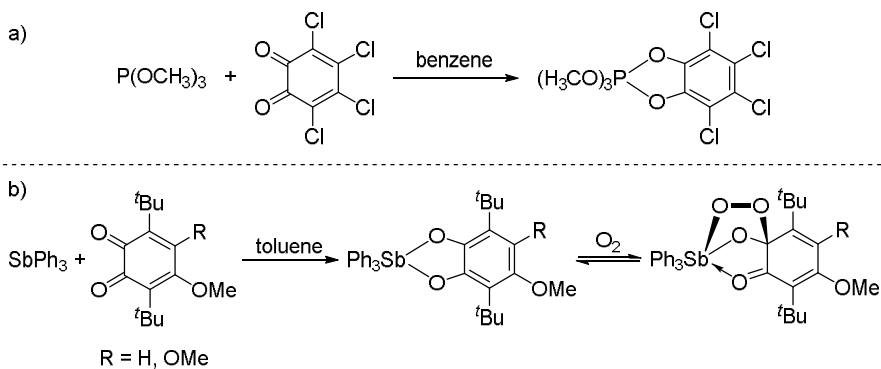
Scheme 3: a) Oxidative addition of $q^{3,6\text{-dtb}}$ to tin halides in THF leading to $\text{X}_2\text{Sn}(\text{cat}^{3,6\text{-dtb}})(\text{THF})_2$ ($\text{X} = \text{Cl, Br}$),⁶¹ followed by a subsequent reaction with NO_2 gas in $\text{CH}_3\text{CN}/\text{toluene}$.⁶⁴ b) Fixation of nitric acid by $\text{Pb}(\text{cat}^{3,6\text{-dtb}})$ in THF leading to the respective monoradical complex $\text{Pb}(\text{sq}^{3,6\text{-dtb}})\text{NO}$, which dimerizes in non-polar solvents under loss of NO gas to the neutral diradical $\text{Pb}(\text{sq}^{3,6\text{-dtb}})_2$.⁶⁸

1.1.1.3 Group 15

Pioneering works of the group of RAMIREZ in the late 1950s led to the first group 15 dioxolene complexes.⁶⁹⁻⁷⁰ For example, trimethyl phosphite and tetrachloro-*o*-benzoquinone in benzene under inert conditions react to form a neutral monocatecholato phosphorane (Scheme 4a).⁷¹ Later on, phosphorus trihalides also were employed, leading to $\text{Cl}_3\text{P}(\text{cat}^{\text{Cl}})$, which in presence of acetic anhydride assembled to the bis(catecholato) complex $\text{ClP}(\text{cat}^{\text{Cl}})_2$.⁷² The same outcome could be obtained by mixing quinone with ethyl dichlorophosphite. STEPHAN *et al.* synthesized coordinatively saturated phosphorus(V) dications by using substituted quinones to oxidize phosphorus(III) terpyridine (*terpy*) dications.⁷³ Interestingly, the complex $[(\text{terpy})(\text{cat}^{\text{Cl}})\text{PPh}]^{2+}$ still exerted weak Lewis acidity and operated as effective initiator for hydrodefluorination reactions of fluoroalkanes. In 1991, the group of TUCK were able to prepare $\text{BrP}(\text{cat}^{\text{X}})_2$ ($\text{X} = \text{Cl, Br}$) *via* one-pot reaction with halogenated quinones, bromine and red phosphorus,⁷⁴ avoiding the usage of corrosive phosphorus halides.^{72, 75} Without bromine the synthesis yielded indistinct paramagnetic intermediates as detected by EPR spectroscopy.

In 1973, the reactivity above could be applied to arsenic by WIEBER *et al.*, resulting in bis(catecholato) compounds such as $\text{MeAs}(\text{cat}^{\text{H}})_2$ and $\text{MeAs}(\text{cat}^{\text{H}})(\text{cat}^{\text{Cl}})$.⁷⁶

Additionally, ABAKUMOVA and coworkers synthesized neutral antimony(V) catecholate complexes by oxidative addition of methoxy substituted 3,6-di-*t*-butyl-*o*-benzoquinone to SbPh_3 (Scheme 4b).⁷⁷ By storing the complexes under ambient conditions, they were found to react reversibly with molecular dioxygen furnishing spiro endoperoxides with trioxastibolane rings. A radical pathway was postulated as mechanism, wherein the catecholate ligand is first oxidized to the semiquinonate state by oxygen. This leads to the formation of a diradical intermediate with a semiquinonate and a peroxy ligand, which rapidly recombines to the bicyclic endoperoxides. Interestingly, the antimony catecholate complexes with more electron deficient ligands were stable in the presence of O_2 .⁷⁸ Hereby, electrochemical investigations showed that the redox potentials of the dioxolene ligands played a crucial role. Besides MOVCHAN *et al.* prepared further neutral antimony complexes which could serve as radical traps for the autooxidation of oleic acid.⁷⁹

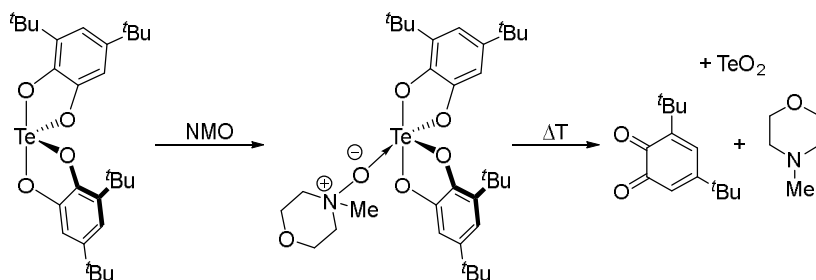


Scheme 4: a) Ramirez reaction of trimethyl phosphite with q^{Cl} in benzene to $(\text{H}_3\text{CO})_3\text{P}(\text{cat}^{\text{Cl}})$.⁷¹ b) Oxidative addition of methoxy-substituted $q^{3,6\text{-dtb}}$ onto triphenylstibine in toluene to the respective catecholate complex, which reversibly reacts with molecular oxygen.⁷⁷

1.1.1.4 Group 16

$\text{Te}(\text{cat}^{\text{H}})_2$ was first synthesized in 1959 by ANTIKAINEN and MÄLKÖNEN from telluric acid and catechol in aqueous media.⁸⁰ Single crystal structure analysis revealed a distorted trigonal bipyramidal structure in which an equatorial position was unoccupied.⁸¹ Over thirty years later, further stable dioxolene complexes containing tellurium also could be prepared by TUCK *et al.* via oxidative addition of substituted quinones to elemental tellurium.⁸² There, the ligands were present in the catecholate

state and the tellurium owned the oxidation state +IV. Regarding the redox behavior, BART *et al.* reinvestigated it only recently and found the compounds to be quite stable and relatively unresponsive towards further oxidation by heating.⁸³ Reactions with organic oxidants, such as pyridine-N-oxide or N-methylmorpholine-N-oxide (NMO) yielded in the formation of the respective adducts as observed with other Lewis bases, such as 2,2'-bipyridine or BCl_3 .⁸² Heating the adduct complex $\text{Te}(\text{cat}^{\beta,5\text{-dtb}})_2(\text{NMO})$ only led to decomposition, meaning complete oxidation of the ligands and formation of N-methylmorpholine and TeO_2 , leaving the redox state of tellurium unchanged (Scheme 5).⁸³



Scheme 5: Reaction of $\text{Te}(\text{cat}^{\beta,5\text{-dtb}})_2$ with NMO leading to adduct formation. Subsequent heating results in decomposition of the adduct.⁸³

1.1.2 Silicon Dioxolene Complexes

The synthesis of the first silicon dioxolene complexes goes back to the year 1920, over a century ago. At that time, ROSENHEIM and SORGE realized the highly robust tris(catecholato)silicate salts $[\text{Si}(\text{cat}^{\text{H}})]_3[\text{HB}]_2$ ($\text{HB} = \text{NH}_4$ or Hpy) by reacting silicon tetrachloride and catechol in diethyl ether, followed by a work up with ammoniacal or pyridine-containing alcoholic solutions.⁸⁴ Later, SCHENDEL and RAIBMANN discovered that the dianions can be prepared from freshly precipitated silicon dioxide in boiling hot ammoniacal catechol solution.⁸⁵ In the early sixties, WEISS and coworkers demonstrated that the reaction also proceeds under milder conditions and even with quartz glass or other modifications of SiO_2 .⁸⁶ For a long time, the structure of the silicate dianions had been controversial. WEISS *et al.* postulated that the dianions existed as dimers.⁸⁶ However, in 1969, single crystal structure analysis by

FLYNN and BOER showed that the catecholates are indeed octahedrally arranged around the silicon center,⁸⁷ as already assumed by ROSENHEIM (Figure 4a).⁸⁴

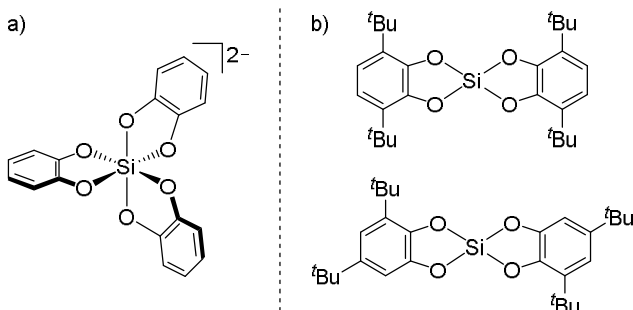


Figure 4: a) Octahedral arrangement of the catecholates in the dianion $[\text{Si}(\text{cat}^{\text{H}})_3]^{2-}$.^{84,87} b) Examples of 3,6- and 3,5-di-^tBu substituted bis(catecholato)silanes synthesized by KABACHNIK *et al.*⁸⁸⁻⁸⁹

Around 1980, KABACHNIK and coworkers studied the oxidized species of hexacoordinate silicon dioxolene compounds. Thereby, the bis(catecholato)silane derivative $\text{Si}(\text{cat}^{3,6\text{-dtb}})_2$ was synthesized (Figure 4b)⁹⁰⁻⁹¹ and converted with alkali salts of sq^{X} ($\text{X} = 3,5\text{-dtb}; 3,6\text{-dtb}; 2\text{-Cl-}3,5\text{-dtb}; \text{Cl}$) to yield the respective monoradical anions $[\text{Si}(\text{cat}^{\text{X}})_2(\text{sq}^{\text{X}})]^-$.⁸⁸ With low-temperature EPR experiments, both intra- and interligand electron exchange was observed, dependent on the solvent polarity and the substituent pattern on the dioxolene ligands. Furthermore, mixing various *o*-benzoquinones with $\text{Si}(\text{cat}^{\text{X}})_2$ ($\text{X} = 3,5\text{-dtb}; 3,6\text{-dtb}$, see Figure 4b) furnished putative homo- and heteroleptic neutral diradical compounds $\text{Si}(\text{diox})_3$.⁸⁸⁻⁸⁹ Their diradical character was unveiled by variable temperature EPR measurements of frozen solutions in toluene. There, the characteristic coupling for two unpaired electrons at normal field and the forbidden transition at half-field could be examined. However, aside from the EPR studies, no further evidence was provided either by other spectroscopic methods or through single crystal X-ray diffraction.

In 2012, RAO *et al.* prepared further derivatives of tris(catecholato)silicate salts by reacting substituted cat^{X} ($\text{X} = \text{Cl}; \text{Br}; 3,5\text{-dtb}$) with tetraethoxysilane (TEOS) in the presence of an amine base in acetonitrile.⁹² $[\text{Si}(\text{cat}^{\text{X}})_3][\text{H}_2\text{N}^n\text{Pr}_2]$ ($\text{X} = \text{Cl}, \text{Br}$) and $[\text{Si}(\text{cat}^{3,5\text{-dtb}})_3][\text{H}_2\text{N}^n\text{Bu}_2]$ were afforded and the structural properties were characterized by various methods including scXRD. Interestingly, hydrogen bond interactions were observed only within the solid phase structure of the chlorinated

salt $[\text{Si}(\text{cat}^{\text{Cl}})_3][\text{H}_2\text{N}^n\text{Pr}_2]_2$. Both cations were found to interact with the oxygen atoms of one catechol ligand and with solvent molecules.

Finally in 2018, the fully oxidized redox isomer of the perchlorinated silicate dianion was isolated by GREB and coworkers.⁹³ Thereby, the mixed-valence compound $\text{Si}(\text{sq}^{\text{Cl}})_2(\text{cat}^{\text{Cl}})$ was prepared by mixing silicon tetraiodide (SiI_4) with q^{Cl} in dichloromethane under inert conditions (Figure 5a). As confirmed by the bond lengths obtained from the single crystal structure, the quinone ligands were reduced to the semiquinonate and catecholate states with concurrent oxidation of the iodides to molecular iodine. Variable temperature EPR measurements of the diradical in dilute state and DFT calculations on the isolated compound verified an intramolecular ferromagnetic coupling of the unpaired electrons, leading to a triplet ground state. In contrast, preliminary SQUID magnetometry measurements of the solid state indicated an intermolecular antiferromagnetic coupling between the open shell dioxolene units. Furthermore, $\text{Si}(\text{sq}^{\text{Cl}})_2(\text{cat}^{\text{Cl}})$ also represents the first example of mixed valence ligands bridged by a non-metal center.

With the 21st century, more attention was also devoted to further neutral bis(catecholato)silane derivatives regarding their Lewis acidity. In 2015, TILLEY *et al.* synthesized the perfluorinated complex $\text{Si}(\text{cat}^{\text{F}})_2$ (Figure 5b), which was found to be the first neutral silane that was able to catalyze the hydrosilylation of aldehydes.⁹⁴ Some years later, GREB and coworkers found that changing the substituents to less electronegative chloride increased the compounds' Lewis acidity (Figure 5c).³¹ This could be experimentally demonstrated by fluoride ion abstraction from the SbF_6^- anion, which marks the threshold for Lewis superacidity.⁹⁵ Additionally, the computed fluoride ion affinities (FIAs), a valuable measure for the Lewis acidity of hard Lewis acids in the gas phase, were consulted for comparison.⁹⁶⁻⁹⁷ Hereby, the FIA for $\text{Si}(\text{cat}^{\text{Cl}})_2$ of $507 \text{ kJ}\cdot\text{mol}^{-1}$ exceeded that of SbF_5 with $501 \text{ kJ}\cdot\text{mol}^{-1}$. Thus, by definition, $\text{Si}(\text{cat}^{\text{Cl}})_2$ represented the first neutral silicon Lewis superacid and, for example, could be successfully used as catalyst for a hydrodefluorination reaction.

Making use of the heavier homologue bromine or sterically hindered and electron-withdrawing CF_3 -groups (Figure 5c), led to further increases of the Lewis acidity ($538 \text{ kJ}\cdot\text{mol}^{-1}$ and $584 \text{ kJ}\cdot\text{mol}^{-1}$, respectively).³²⁻³³ Moreover, $\text{Si}(\text{cat}^{\text{CF}_3})_2$ exhibited enhanced solubility compared to the perhalogenated analogues. Coupled with its increased Lewis superacidity broader applicability was enabled, which could be

disclosed by using $\text{Si}(\text{cat}^{\text{CF}_3})_2$ as catalyst for deoxygenation reactions of aldehydes, ketones, amides, and phosphine oxides, as well as for carbonyl olefin metathesis. Further investigations on the counter-intuitive course of the Lewis acidity regarding the substituents of $\text{Si}(\text{cat}^{\text{X}})_2$ ($\text{X} = \text{F}, \text{Cl}, \text{Br}$) showed that the trend correlates not to the electronegativity, but to the Hammett parameters σ_m ($\text{F} = 0.337 < \text{Cl} = 0.373 < \text{Br} = 0.391$).⁹⁸ More positive values indicate stronger electron-withdrawing properties, as a result of the decreased ability to π -backbond to the aromatic system of the catechol ligands and thereby leading to an increased electron deficiency at the silicon center.³¹⁻³²

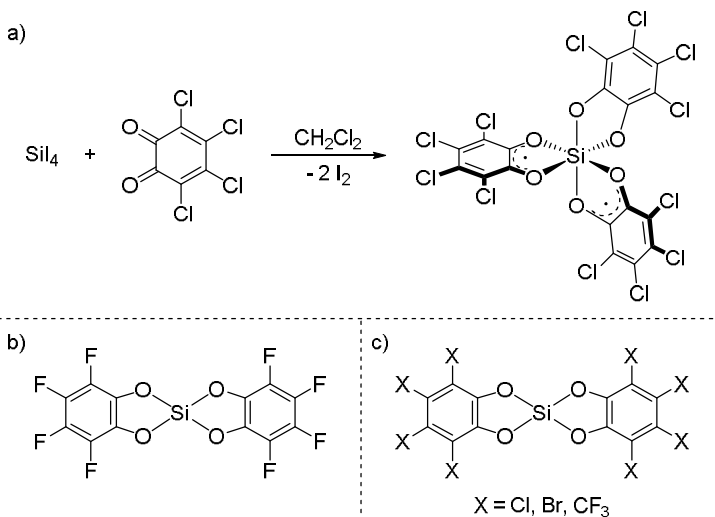


Figure 5: a) Synthesis of neutral diradical $\text{Si}(\text{cat}^{\text{Cl}})_2(\text{cat}^{\text{Cl}})$ by mixing SiI_4 with cat^{Cl} in non-donor solvent, like CH_2Cl_2 .⁹³ b) Lewis acid $\text{Si}(\text{cat}^{\text{F}})_2$ synthesized by TILLEY *et al.*⁹⁴ c). Lewis superacids $\text{Si}(\text{cat}^{\text{X}})_2$ ($\text{X} = \text{Cl}, \text{Br}, \text{CF}_3$) synthesized by GREB *et al.*³¹⁻³³

1.2 Porous Functional Materials

In 1756, the Swedish mineralogist CRONSTEDT observed vigorous steam development while heating stilbite, a tectosilicate mineral.⁹⁹ This illustrative example might be one of the first recorded proofs made for porous substances. Based on this observation, these materials were coined as zeolites (Greek for *boiling stone*). Zeolites own a porous structure with differing pore sizes and are composed of an aluminosilicate framework,

which are made up of AlO_4^- and SiO_4 tetrahedrons.¹⁰⁰ They can be naturally found in form of various minerals but nowadays are also of great industrial interest due to their large surface area and adsorption capacity, and therefore produced in large scale.¹⁰¹⁻¹⁰² First applications for natural zeolites have been found as ion exchanger,¹⁰³ molecular sieves¹⁰⁴ or as gas absorber.¹⁰⁵ But due to the commonly inhomogeneous composition of natural zeolites, synthetically produced materials are of high industrial demand.¹⁰⁶ A considerable example hereby is *Zeolite Y*, afforded by BRECK,¹⁰⁷ which is predominantly used in petrochemistry as catalyst in processes like fluid catalytic cracking (FCC)¹⁰⁸ and hydrocracking¹⁰⁹ – a substantial progress in industrial catalysis.

Aside from zeolites, which can be declared as purely inorganic, novel microporous materials composed of inorganic and organic compounds were prepared in the early nineties. Pioneering works of YAGHI and coworkers in 1995 thereby established the term metal organic framework (MOF) and prepared one of the first examples (*MOF-2*) with permanent porosity.¹¹⁰⁻¹¹¹ Since then, the construction of three-dimensional microporous solids containing metallic nodes and organic linkers has been further investigated and mastered.¹¹²⁻¹¹³ Remarkable success was made by using reticular chemistry to produce extremely low-density materials.¹¹⁴⁻¹¹⁵ With the help of large organic diamagnetic linkers, framework stability and permanent porosity could be promoted, logically, accompanied by large metal-metal distances. This prevented effective electronic exchange among the metal centers that are crucial for charge transfer and magnetic coupling. Finally, the usage of redox-active polytopic linkers allowed to merge both fields, smoothing the way for magnetic and conductive MOFs.¹¹⁶⁻¹¹⁸ These porous functional materials promise a wealth of applications, for example as porous battery electrodes, electrochemical sensors or in lightweight magnetoelectric materials.¹¹⁹⁻¹²⁰ In the following, some seminal examples shall be highlighted.

In 2015, the groups of LONG and HARRIS synthesized MOFs based on Fe(III) nodes and 2,5-dihydroxy-*p*-benzoquinone ($\text{H}_2\text{d}hbq^{\text{H}}$, Figure 6a) as organic linker in the paramagnetic state. Back then, they were able to realize record conductivities and magnetic ordering temperatures.¹²¹⁻¹²² Later, YAGHI and coworkers employed 2,3,6,7,10,11-hexahydroxytriphenylene ($\text{H}_6\text{h}htp$, Figure 6b) as spacer to construct two-dimensional MOFs with pronounced charge storage capacity and conductivity.¹²³ By

now, the *hhtp* linker has been employed to assemble two- and three-dimensional frameworks that are applied in electronic devices among others.¹²⁴⁻¹²⁶

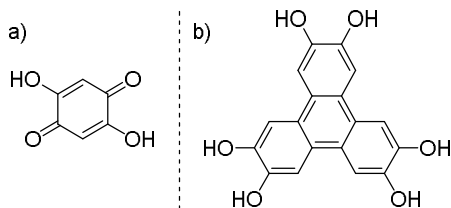


Figure 6: The organic linkers a) 2,5-dihydroxy-*p*-benzoquinone (H_2dhbq^H) and b) 2,3,6,7,10,11-hexahydroxytriphenylene (H_6hhtp) used in various MOFs.

Another class of porous materials are displayed by the covalent organic frameworks (COFs).¹²⁷⁻¹²⁹ In contrast to MOFs, COFs are metal-free and constituted of covalently bonded organic building blocks. The first COFs with permanent porosity were realized by the group of YAGHI in 2005.¹³⁰ *COF-1* was synthesized *via* condensation reactions between boronic acids (Figure 7a) and *COF-5* in similar fashion by the condensation of boronic acids with the polyoxolene *hhtp* (Figure 7b). Thenceforth, two- and three-dimensional COFs have been established and prepared by making use of dynamic condensation reactions between various organic building blocks with different geometries, yielding in B-O, C-N or B-N bond formation.^{128, 131}

Later, the usage of polyoxolenes with silanes as building blocks for silicon-based COFs (SiCOFs) was inspired by successful syntheses of respective macrocycles and cages.¹³²⁻¹³⁶ In 1992, early attempts towards silicate network materials were accomplished by the group of SHEA, where TEOS was condensed with 1,2,4,5-tetrahydroxybenzene, which easily oxidizes to *dhbq*, but the material was not further examined.¹³⁷ However, the synthesis was only carried out at ambient temperature, so that the criteria of reversibility, which is often crucial for equilibration toward ordered topologies, was not met.¹²⁸

Recently, the first synthesis of a two-dimensional SiCOF was successfully achieved by THOMAS *et al.*, where reversible Si-O bond formation under solvothermal conditions was exploited (Figure 7c).¹³⁸ Subsequently, implementation of *hhtp* as linker allowed the construction of three-dimensional SiCOFs,¹³⁹ structurally comparable with analogous transition metal-bridged networks.¹²⁴

So far, COFs with magnetic, conductive, or charge-storing features have only been achieved by using, e.g., π -conjugated systems or by incorporating magnetic metal nanoparticles.¹⁴⁰⁻¹⁴² Architectures exhibiting electronic exchange *via* non-metallic single atom connectors in terms of MOFs, however, are unexplored.

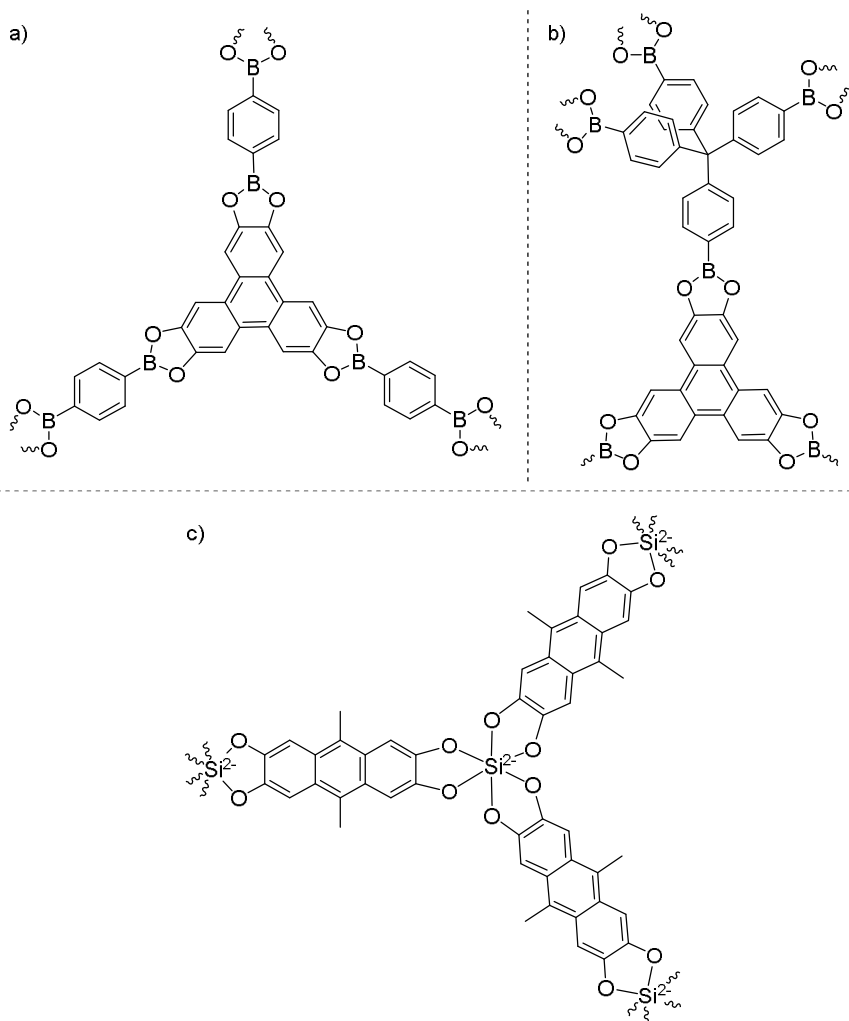


Figure 7: Linkage in the frameworks of a) *COF-1*, b) *COF-5130* and c) one of the first SiCOFs by THOMAS *et al.*¹³⁸

2

MOTIVATION AND AIM

As a thematic starting point for this work serves the diradical of the homoleptic compound $\text{Si}(\text{diox}^{\text{Cl}})_3$, that demonstrates the first example of an oxidized form of a tris(catecholato)silicate – a substance class known for over a century.⁹³ Constituting the first non-metal complex with redox-active and mixed-valence substituents, the thermally stable compound allowed the investigation regarding magnetic properties, revealing *intramolecular* ferromagnetic coupling (triplet ground state) in the dilute state and *intermolecular* antiferromagnetic coupling in the solid state. Strikingly, such properties state a novelty for a non-metal compound, yet a more comprehensive understanding of the redox properties is required for possible applications in diradical research (such as non-linear optics, conductors, energy storage, singlet fission or spintronics).¹⁴³⁻¹⁴⁶

Therefore, the first part of this work deals with the investigation of the redox chemistry and the completion of the redox series of $\text{Si}(\text{diox}^{\text{Cl}})_3$ – and thus of tris(catecholato)silicates in general – by catching the elusive monoradical anion. Subsequently, the application of the oxidized form in redox catalysis shall be studied. Consecutively, a variation of the substituents at the dioxolene ligands shall be performed by introducing different *ortho*-quinones (*q*) and silicon sources, resulting in a new series of homo- and heteroleptic mononuclear compounds. These will be in turn investigated regarding their electronic structure and redox properties in order to make comparisons with $\text{Si}(\text{diox}^{\text{Cl}})_3$.

The next step towards extended systems will be covered in the last two sections of this work. By introducing rationally chosen polytopic linkers, such as 2,5-dihydroxy-*p*-benzoquinone ($\text{H}_2\text{d}hbq^{\text{H}}$) and 2,3,6,7,10,11-hexahydroxytriphenylene ($\text{H}_6\text{h}htp$), the controlled assembly of dimeric and, in continuation, trimeric forms of the silicon

dioxolene motif will be investigated. It is known, that both *dhbq* and *hhtp* linkers readily stabilize various diamagnetic and paramagnetic (semiquinonate) states in transition metal complexes and mediate extremely strong magnetic interactions.¹⁴⁷⁻¹⁵⁰ Thus, a synthetic strategy towards dimeric compounds involving the reaction of Lewis acids $\text{Si}(\text{cat})_2$ and H_2dhbq shall be established, and first characterizations be made. Outgoing from these gained insights, lastly a synthesis for the consecutive trimeric species utilizing the linker H_6hhtp shall be designed.

In summary, the aim of this work is to increase the complexity of the mononuclear homoleptic complexes $\text{Si}(\text{diox})_3$ by 1) variation of the redox state, 2) variation of the substitution at the ligands and 3) finally by increasing the nuclearity. A systematic *bottom-up* approach will disclose the magnetic properties within the homo- and heteroleptic monomeric complexes first, followed by subsequent investigation of the dimeric and trimeric analogues connected through conjugated polytopic linkers. The understanding of electron-exchange within metal free silicon polyoxolenes is not only a valuable extension from a fundamental perspective, but a structure-effect relationship gained from those smaller systems will be crucial for the rational design of redox-active SiCOFs, which in turn would constitute a major step toward an ecologically and economically benign alternative for this future type of functional materials – based on the most abundant elements in the Earth's crust.

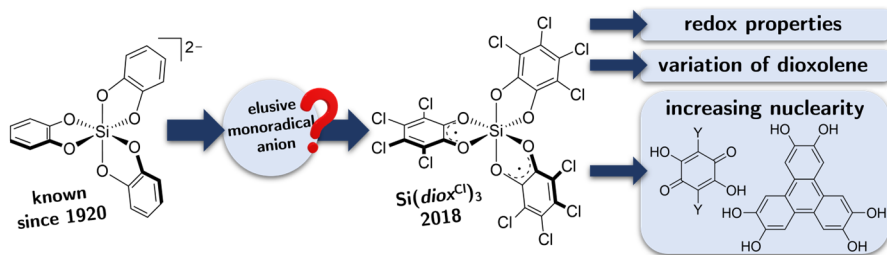


Figure 8: Overview of the aims of this work: investigating the redox chemistry of $\text{Si}(\text{diox}^{\text{Cl}})_3$ by catching the intermediate monoradical anion as well as the synthesis and characterization of new silicon polyoxolene derivatives by varying the dioxolene ligand and increasing the nuclearity.

3

RESULTS AND DISCUSSION

3.1 Completing the Redox Series^a

In the following chapter, the redox chemistry of silicon tris(perchloro)dioxolene $\mathbf{1}^{\text{Cl}}$, an easily prepared neutral triplet diradical (see chapter 1.1.2 and Figure 5a)⁹³ and also the fully oxidized form of a century-old class of dianions $[\mathbf{1}^{\text{Cl}}]^{2-}$, will be covered. This will be approached by CV studies of $\mathbf{1}^{\text{Cl}}$ and its dianionic representatives. Besides, to complete the redox series of silicon trisdioxolenes, the elusive monoradical anion $[\mathbf{1}^{\text{Cl}}]^{\bullet-}$ will be synthesized and thoroughly characterized.

Recent research works have addressed the enhancement of the redox potential of quinones by supramolecular interactions. For example, through encapsulation as guests in dimeric palladium cages, tetrahalogenated *p*-benzoquinones have found to operate as potent one-electron oxidants, which were used as catalyst in cycloaddition reactions.¹⁵¹ Further, JACOBSEN *et al.* used dicationic bis(amidinium) salts as dual hydrogen bond donors to increase the redox force of q^{Cl} for the catalysis of an oxidative lactonization.¹⁵² However, redox amplification through Lewis acid binding has not been investigated yet. From a hypothetical view, $\mathbf{1}^{\text{Cl}}$ can also be considered as the formal adduct of q^{Cl} with the Lewis superacid $\text{Si}(\text{cat}^{\text{Cl}})_2$ $\mathbf{2}^{\text{Cl}}$ (Figure 5c). Therefore, the concept to transform quinones into potent two-electron acceptors by Lewis acid binding will be introduced and the usage of $\mathbf{1}^{\text{Cl}}$ as redox catalyst will be studied hereafter.

^a Initial works of this project were already part of the Master thesis. Corresponding parts are marked with the respective reference.⁹³

3.1.1 Synthesis and Characterization of 1^{Cl}

1^{Cl} was synthesized according to a straightforward procedure (Figure 5a).⁹³ Thereby, q^{Cl} was mixed with SiI_4 in dichloromethane. The reaction mixture immediately turned black red and was left at room temperature without stirring for 72 h. Afterwards a thick layer of black solids was observed, and the solution was dark purple due to the formation of iodine. The supernatant solution was decanted off. Then the remaining solids were washed with pentane by suspending and vigorous stirring in copious amounts of solvent, which turned pink. The solids were left to settle down and pentane was exchanged repeatedly until the solution stayed colorless (after around 150 mL pentane). After removing the final pentane phase and drying the solids *in vacuo* for 24 h the product 1^{Cl} was obtained as a fine green powder in yields up to 86 %.

The successful preparation and structure of 1^{Cl} was confirmed by various analytical methods, such as scXRD analysis, HR-MS and elemental analysis. Additionally, the magnetic properties were thoroughly examined with EPR spectroscopy (Figure 9a) and SQUID measurements.⁹³ With density functional theoretical data (restricted and unrestricted PBE0-D3(BJ)/def2-TZVPP level of theory) the triplet state was found to be 63 $\text{kJ}\cdot\text{mol}^{-1}$ lower in energy than the closed shell singlet state (see Appendix 7.3.1, Table 5). The optimized structure for a triplet state was also in accordance with the metrical data obtained from scXRD analysis. Also, the spin density is mainly located over two of the three dioxolene ligands (Figure 9b). Besides, Kohn-Sham broken-symmetry computations revealed a positive value for the coupling constant J of 1^{Cl} , underlining the experimentally observed triplet ground state (see Appendix 7.3.1, Table 6).

Resonance Raman measurements showed characteristic C-O stretching bands for the semiquinonate ($\tilde{\nu} = 1476$ and 1348 cm^{-1}) and catecholate ($\tilde{\nu} = 1209 \text{ cm}^{-1}$) ligands, which are also observed by IR spectroscopy (Figure 10a and b).¹⁵³ In the UV-vis-NIR spectra of solutions of 1^{Cl} in dichloromethane absorptions at $\lambda = 453 \text{ nm}$ were revealed, which can be referred to the intraligand $\pi\pi^*$ and $n\pi^*$ transitions within the semiquinonates.¹⁵³⁻¹⁵⁴ Besides, an intense absorption in the near-IR region at $\lambda = 1127 \text{ nm}$ and a weaker one at $\lambda = 2843 \text{ nm}$ were assigned to interligand valence charge transfers (*IVCT*) between the catecholate and semiquinonates (Figure 10c). Similar

electronic properties were also found for chromium(III) complexes with identical assembly and oxidation states of the ligands.¹⁵⁵⁻¹⁵⁶

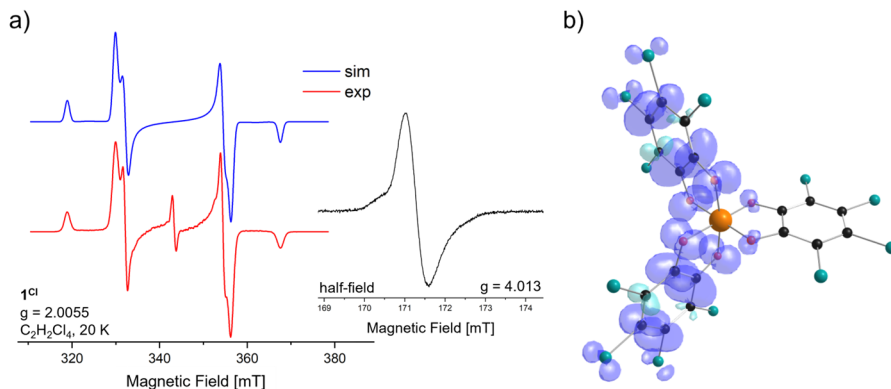


Figure 9: a) Experimental (red) and simulated¹⁵⁷ (blue) EPR spectra of 1^{Cl} in 1,1,2,2-tetrachloroethane (TCE, $C_2H_2Cl_4$) at 20 K and the half-field signal. Parameters: frequency = 9.636 GHz, power 2.0 mW (6.3 mW for half-field signal), modulation 1 mT. Simulation parameters: $S = 1$, $g = 2.0055$, $D = 0.2278 \text{ cm}^{-1}$, $E = 0.000097 \text{ cm}^{-1}$. b) Contour plot of spin density distribution of the triplet state of 1^{Cl} at PBE0-D3(BJ)/def2-TZVPP level of theory (isodensity value 0.003 au).

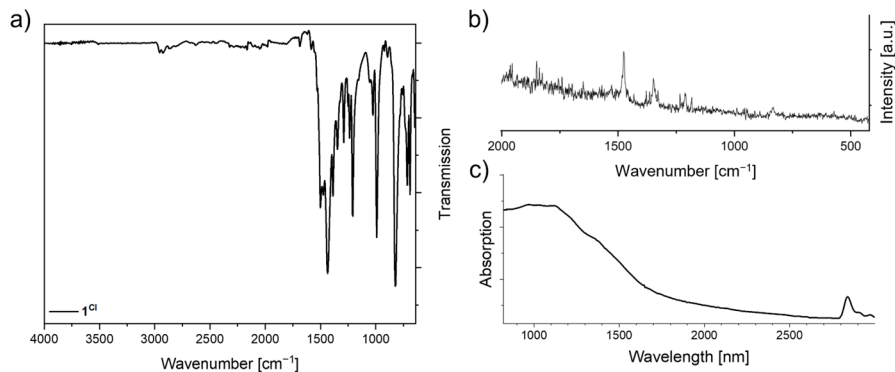


Figure 10: a) ATR-IR and b) resonance Raman (excitation wavelength $\lambda = 476 \text{ nm}$) spectra of solid-state sample of 1^{Cl} and c) absorption spectrum in the near-IR region of a solution of 1^{Cl} in CH_2Cl_2 (10^{-2} M).

Single crystals of 1^{Cl} could be produced in various solvents, like dichloromethane.⁹³ From the bond lengths obtained for the dioxolene ligands the metrical oxidation state

(MOS) was calculated (see Appendix 7.4, Table 15).¹⁵⁸ Two of the ligands were existent in the monoanionic semiquinonate state (unit A and B) and the other one in the fully reduced catecholate state (unit C), consistent with the Lewis formulation $\text{Si}(sq^{\text{Cl}})_2(\text{cat}^{\text{Cl}})$ (Figure 11a). The octahedral coordination sphere within $\mathbf{1}^{\text{Cl}}$ is slightly distorted, disclosed by the O-Si-O angles $\angle_{\text{cis}} = 85.8(1)^\circ$ to $95.6(1)^\circ$ and $\angle_{\text{trans}} = 170.3(1)^\circ$ to $178.4(1)^\circ$. Regarding the crystal packing, compact anisotropic π -stacking occurs with close aromatic rings, such as the dioxolene ligands from another molecule of $\mathbf{1}^{\text{Cl}}$, resulting in plane-to-plane centroid distances of 3.49 Å (e.g., between the units B and C in Figure 11b). These values can be compared to similar distances found in donor-acceptor complexes (e.g., benzoquinone-hydroquinone 3.20 Å)¹⁵⁹ or conductive stacked structures (e.g., 2,2'-bis-1,3-dithiole (TTF) - 7,7,8,8-tetracyanoquinodimethane (TCNQ), separated stacks of 3.47 Å and 3.17 Å, respectively).¹⁶⁰ Besides, the semiquinonate and catecholate units alternate within the stacking in the order B-C'-B'-C (Figure 11b). The remaining semiquinonate units stack with each other (A-A') irrespective of the other dioxolenes.

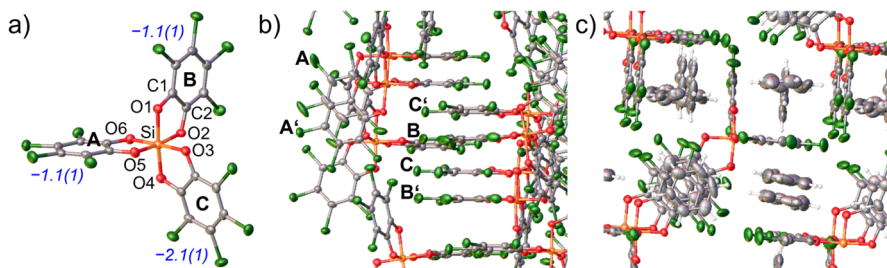


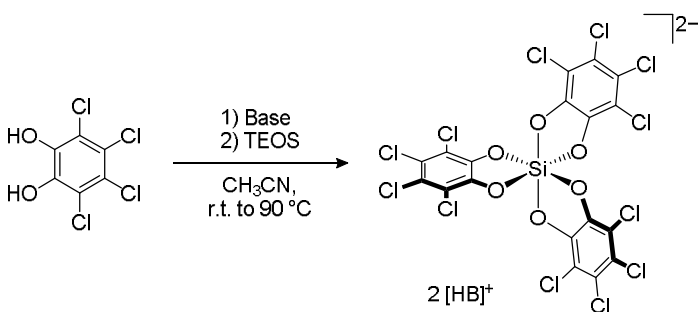
Figure 11: a) Crystal structure of and picture detail of the b) crystal packing for $\mathbf{1}^{\text{Cl}}$ obtained from a solution in CH_2Cl_2 with the assignment of the semiquinonate (unit A and B) and catecholate (unit C) ligands and the respective MOS values (in blue and italic). The thermal displacement ellipsoids are shown at the probability level of 50 %. c) Picture detail of the crystal packing for $\mathbf{1}^{\text{Cl}}$ obtained from a solution in $\text{CH}_2\text{Cl}_2/\text{C}_6\text{H}_6$. The thermal displacement ellipsoids are shown at the probability level of 50 %.

Single crystals were also received in benzene or *o*-dichlorobenzene (*o*-dcb, $\text{o-C}_6\text{H}_4\text{Cl}_2$) as the respective adducts $\mathbf{1}^{\text{Cl}}\cdot(\text{C}_6\text{H}_6)_4$ and $\mathbf{1}^{\text{Cl}}\cdot(\text{o-dcb})_4$. Similar bond lengths as in the structure from dichloromethane but a different crystal packing was apparent. In fact, the units of $\mathbf{1}^{\text{Cl}}$ were isolated from each other due to intercalation of aromatic solvents between the electron-poor dioxolene rings of $\mathbf{1}^{\text{Cl}}$ (Figure 11c). Analogue solid-state structures are already known from Cr/V/Fe-*diox*^{Cl} complexes.¹⁶¹ Interestingly, when

calculating the sum of the MOS for the dioxolene rings of $1^{\text{Cl}}\cdot(\text{C}_6\text{H}_6)_4$ a significantly larger value of -4.75 is obtained than the expected -4 . Possible intermolecular charge transfer between benzene and the semiquinonates could explain this observation, whereby the MOS for sq^{Cl} is increased from -1 to -1.3 . Indeed, the stacking between benzene and the semiquinonate ring (plane-to-plane distance of 3.3 \AA) is closer compared with benzene and the catechalote ones (3.7 \AA).

3.1.2 Synthesis and Characterization of $[1^{\text{Cl}}]^{2-}$

The syntheses of the dianionic representatives $[1^{\text{Cl}}][\text{HB}]_2$ ($\text{HB} = \text{HN}^n\text{Pr}_2$ or NEt_3) are based on the procedure of RAO *et. al.*⁹² In general, a secondary or tertiary amine base is mixed with a catechol in acetonitrile to generate the respective ammonium salts, which are converted with tetraethyl orthosilicate (TEOS) to the respective dianionic silicate salts $[1^{\text{Cl}}][\text{HB}]_2$ (Scheme 6). $\text{H}_2\text{cat}^{\text{Cl}}$ was synthesized according to literature known procedure.³¹ For di- n -propylamine the reaction was stirred for 1 h at room temperature and 2 h at $90 \text{ }^\circ\text{C}$, for triethylamine it was stirred for 2 h at room temperature and 18 h at $90 \text{ }^\circ\text{C}$. The reactions were then left to cool down, leading to the development of colorless precipitate, which could be increased by maintaining the suspension at $-20 \text{ }^\circ\text{C}$ for 1-2 h. The solids were collected by filtration and washed several times with diethyl ether. After drying under reduced pressure for 24 h the respective product salts $[1^{\text{Cl}}][\text{HB}]_2$ ($\text{HB} = \text{HN}^n\text{Pr}_2$ or NEt_3) were obtained as colorless solids in yields up 51% and 61% , respectively.



Scheme 6: General synthesis of $[1^{\text{Cl}}][\text{HB}]_2$ ($\text{HB} = \text{HN}^n\text{Pr}_2$ or NEt_3) by reacting ammonium perchlorocatecholate salts with tetraethyl orthosilicate (TEOS).⁹²

Besides, the preparation of $[\mathbf{1}^{\text{Cl}}][\text{N}^n\text{Bu}_4]_2$ was aimed. For that $[\mathbf{1}^{\text{Cl}}][\text{HNEt}_3]_2$ was suspended in dichloromethane and 2 eq. ${}^n\text{NBu}_4\text{Cl}$ were added to conduct salt metathesis. The mixture was stirred and immediately cleared up. By cooling down the solution to $-20\text{ }^\circ\text{C}$ and keeping it for 24 h HNEt_3Cl could be easily precipitated. After removing the solids and drying the supernatant solution over anhydrous NaSO_4 , the solvent was removed *in vacuo* to obtain $[\mathbf{1}^{\text{Cl}}][\text{N}^n\text{Bu}_4]_2$ as colorless powder in yields up to 74 %.

All three silicate salts from above were thoroughly characterized and found to be consistent with literature, where possible. ${}^{29}\text{Si}$ -INVGATE NMR measurements revealed chemical shifts at $\delta = -143.7$, -138.3 and -138.2 ppm, respectively, confirming the presence of hexacoordinate silicon species.¹⁶² In the IR spectra characteristic bands for N-H, C-H and C-O vibration modes can be observed. For $[\mathbf{1}^{\text{Cl}}][\text{N}^n\text{Bu}_4]_2$ no N-H stretching vibration was observed anymore, which means that the salt metathesis proceeded successfully and the side-product HNEt_3Cl could be removed completely. In addition to that single crystals of $[\mathbf{1}^{\text{Cl}}][\text{H}_2\text{N}^n\text{Pr}_2]_2$ and $[\mathbf{1}^{\text{Cl}}][\text{N}^n\text{Bu}_4]_2$ could be obtained by cooling down concentrated solutions in acetonitrile or dichloromethane.

3.1.3 Investigating the Redox Properties

To gather first insights into the redox properties of silicon trisdioxolenes, cyclic voltammetry (CV) measurements were contemplated. Investigations were started with the two-electron reduced complex $[\mathbf{1}^{\text{Cl}}][\text{N}^n\text{Bu}_4]_2$ representing the most stable form of this compound series. Besides, it was tried to avoid fluorinated electrolytes such as $[\text{PF}_6][\text{N}^n\text{Bu}_4]$ or $[\text{BArF}_2\text{4}][\text{N}^n\text{Bu}_4]$ since defluorinating side-reactions could be easily triggered by intermediate complexes containing the Lewis superacid $\mathbf{2}^{\text{Cl}}$. Finally, $[\text{BArF}_2\text{0}][\text{N}^n\text{Bu}_4]$ proved to be suitable as electrolyte and CV measurements of $[\mathbf{1}^{\text{Cl}}][\text{N}^n\text{Bu}_4]_2$ in dichloromethane revealed two well-separated but non-reversible oxidation waves at $E_{ox} = 0.45\text{ V}$ and 0.88 V (*vs.* Fc/Fc^+ , Figure 12a). These oxidation peaks were assigned to the redox couples $[\mathbf{1}^{\text{Cl}}]^{2-}/[\mathbf{1}^{\text{Cl}}]^{\bullet-}$ and $[\mathbf{1}^{\text{Cl}}]^{\bullet-}/\mathbf{1}^{\text{Cl}}$, respectively. Interestingly, measuring CV only up to $E = 0.70\text{ V}$, resulted in the isolation of a quasi-reversible redox wave at $E_{1/2} = 0.43\text{ V}$ (Figure 12b). Only after further oxidation to the diradical irreversibility within the redox events is observed. This

indicates, that $[1^{Cl}]^{\bullet-}$ must at least be stable in the presence of the dianionic species but subsequent formation of 1^{Cl} leads to unfavored side-reactions.

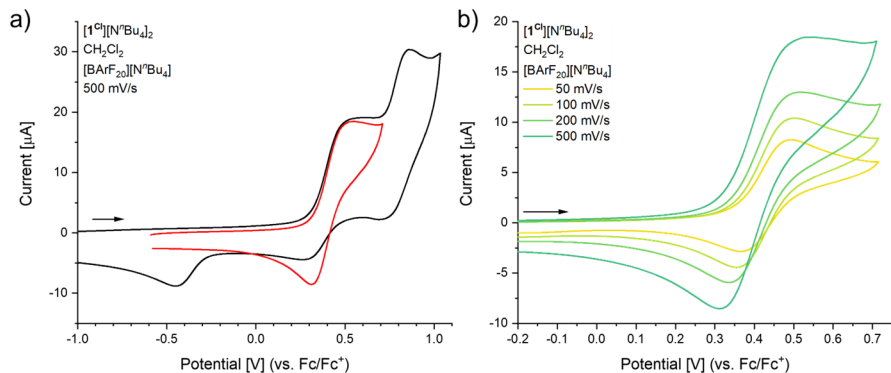


Figure 12: a) CV measurement of the first quasi-reversible redox wave of $[1^{Cl}][N^tBu_4]_2$ at 500 mV/s (red trace), measuring further to the second redox event leads to two oxidation and three reduction events (black trace). b) CV measurement of the first quasi reversible redox wave of $[1^{Cl}][N^tBu_4]_2$ at different scan rates.

CV measurements of 1^{Cl} were attempted as well. However, this led to more confusing voltammograms with no reversible reduction events, which might be explained by incompatibility issues and thus instability of 1^{Cl} with the given CV conditions.

To narrow down the redox range of 1^{Cl} more precisely, reactions with substrates of known redox potentials within the range were carried out.¹⁶³ In Table 1 the different substrates are listed of which the redox potentials were remeasured under similar conditions as $[1^{Cl}]^{2-}$ for better comparability.

In general, equimolar amounts of 1^{Cl} and the substrates were mixed in CD_2Cl_2 , and the reaction outcome was monitored *via* EPR and NMR spectroscopy. Indeed, successful oxidations of thianthrene and tris(4-bromophenyl)amine^b ($N(Ph-Br)_3$) could be observed (see Appendix 7.5 for EPR spectra). An upper limit of 1^{Cl} was reached with tris(2,4-dibromophenyl)amine ($N(Ph-Br)_3$).¹⁶⁴ There, formation of the ammoniumyl radical cation was not detected by EPR spectrum. However, significant

^b The respective amine radical cation is also known as *magic blue* due to its intense color.¹⁶³

line broadening of the aromatic signals of $\text{N}(\text{Ph-Br}_2)_3$ was observed in the ^1H NMR spectrum, implying that an electron transfer had taken place (see Appendix, Figure 63). Thus, with the experimental findings the redox potential of $\mathbf{1}^{\text{Cl}}$ can be ranged between thianthrene and $\text{N}(\text{Ph-Br}_2)_3$ ($E = 0.84\text{-}1.12$ V *vs.* Fc/Fc^+), which are also in accordance with the electroanalytical results.

Table 1: Redox potentials of the compounds measured in CH_2Cl_2 with the respective electrolyte (0.1 M) at room temperature under N_2 atmosphere. Values are internally referenced *vs.* Fc/Fc^+ . For the voltammograms see Appendix 7.7.

Compound	$E_{1/2}$ [V]	Compound	E_{ox} [V]
$\mathbf{1}^{\text{Cl}}$	0.43 ^[a] / 0.88 ^[a]	HMB	1.14 ^[b]
\mathbf{q}^{Cl}	-1.19 ^[a] / -0.33 ^[a]	PMB	1.27 ^[b]
thianthrene	0.84 ^[b]	TMB	1.65 ^[b]
$\text{N}(\text{Ph-Br})_3$	0.72 ^[b]		
$\text{N}(\text{Ph-Br}_2)_3$	1.12 ^[b]		

^[a] $[\text{BARF}_{20}][\text{N}^n\text{Bu}_4]$, ^[b] $[\text{PF}_6][\text{N}^n\text{Bu}_4]$

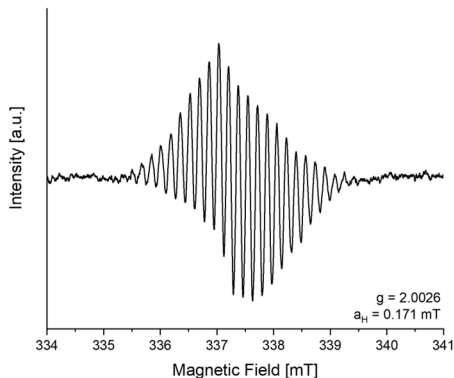


Figure 13: EPR spectrum of the oxidation of hexamethylbenzene with $\mathbf{1}^{\text{Cl}}$ in CD_2Cl_2 at room temperature. The asymmetry in the signal can be explained by the presence of the underlying monoradical anion $[\mathbf{1}^{\text{Cl}}]^\bullet^-$. Parameters: $B_0 = 3377$ G, sweep = 100 G, sweep time = 40 s, modulation = 2000 mG, microwave power = 1 mW, gain = $9 \cdot 10^2$.

In addition to that, oxidation of alkylated benzene derivatives was attempted and examined by EPR spectroscopy. Mixing $\mathbf{1}^{\text{Cl}}$ with hexamethylbenzene (HMB, Figure 13), pentamethylbenzene (PMB) or 1,2,3,4-tetramethylbenzene (TMB) in CD_2Cl_2 led

to the development the respective radical cations, identifiable by the characteristic hyperfine coupling patterns in the EPR spectra (see Appendix 7.5).¹⁶⁵ With mesitylene no reaction was observed.

The redox potentials of the substrates were also remeasured under comparable conditions since they were only poorly documented (Table 1). Remarkably, these values were way beyond the oxidative power of $\mathbf{1}^{\text{Cl}}$. A possible proton-coupled electron transfer carried out by $\mathbf{1}^{\text{Cl}}$ could explain this observation. Indeed, π -stacking with much less strong electron donors like benzene or *o*-dcb has already been observed in solid state (see chapter 3.1.1). Accordingly, these preorganized structures may act as precursor complexes for the aforesaid electron transfer.

3.1.4 Synthesis and Characterization of $[\mathbf{1}^{\text{Cl}}]^{\bullet-}$

The substantial separation of the redox waves (ΔE_{ox}) observed in the voltammogram of $[\mathbf{1}^{\text{Cl}}][\text{N}^n\text{Bu}_4]_2$ (Figure 12) enabled the calculation of the comproportionation constant K_c given by the equations (1) and (2).¹⁶⁶

$$\Delta G^0 = -RT(\ln K_c) = -nF(\Delta E_{ox}) \quad (1)$$

$$K_c = e^{F(\Delta E_{ox})/RT} \quad (2)$$

F = Faraday constant

R = universal gas constant

For $T = 298$ K a comproportionation constant of $K_c \approx 18.5 \cdot 10^6$ was calculated with equation (2). Elated by the large value for K_c , which is crucial for the isolation of the $[\mathbf{1}^{\text{Cl}}]^{\bullet-}$, the synthesis of the elusive silicon trisdioxolene monoradical anion was tackled by reacting $\mathbf{1}^{\text{Cl}}$ with $[\mathbf{1}^{\text{Cl}}]^{2-}$.

For that equimolar amounts of $\mathbf{1}^{\text{Cl}}$ and $[\mathbf{1}^{\text{Cl}}][\text{N}^n\text{Bu}_4]_2$ were mixed in dichloromethane at -40 °C (Figure 17). An intense dark green colored solution was obtained. Maintaining the low temperatures for further 24 h led to the development of green crystalline material. After removing the supernatant solution and drying the precipitate *in vacuo* for 24 h, the product was obtained as green powder in yields up to 64 %. NMR spectroscopy showed broad signals in the ^1H NMR spectrum for the

cation. The anionic part of the salt was ^{13}C and ^{29}Si -INVGATE NMR silent. Conducting EPR measurements at room temperature revealed a strong singlet signal with $g = 2.0064$, which indicates a paramagnetic substance in the $S = \frac{1}{2}$ state (Figure 14a). Indeed, scXRD analysis revealed the single crystal structure of $[\mathbf{1}^{\text{Cl}}][\text{N}^n\text{Bu}_4]$ and ultimately confirmed the spectroscopic interpretation. With the respective bond lengths the MOS were calculated for the dioxolene ligands, of which two were found to be present in the catecholate state and one in the open shell semiquinonate state (see Appendix 7.4, Table 15), consistent with the proposed Lewis formulation $[\mathbf{1}^{\text{Cl}}]^\bullet$.

The IR spectrum showed typical N-H stretching vibrations at $\tilde{\nu} = 3059\text{ cm}^{-1}$ for the cation and C-O stretching vibrations at $\tilde{\nu} = 1236$ and 1212 cm^{-1} for catecholate and semiquinonate ligands (Figure 14b). Moreover, characteristic absorption bands at $\lambda = 303$ and 456 nm were observed in the UV-vis spectrum. Examining further into the near-IR region revealed strong *IVCT* bands around $\lambda = 1003\text{ nm}$ and some smaller ones at $\lambda = 2844$ and 2974 nm , which were also expected from the large value for K_c (*vide supra*).¹⁶⁶

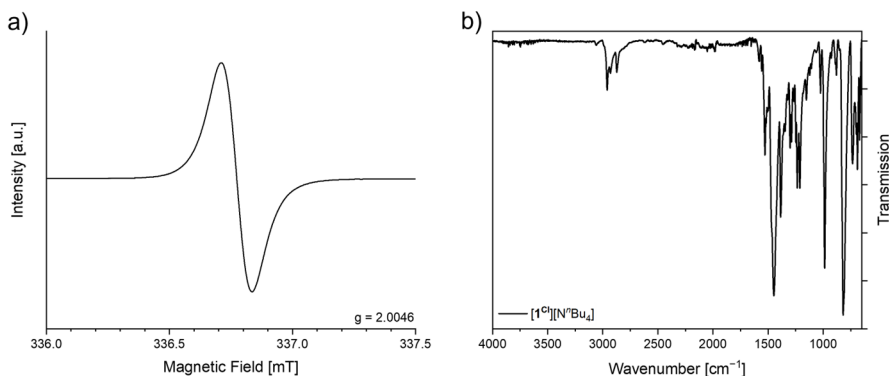


Figure 14: a) EPR spectrum of $[\mathbf{1}^{\text{Cl}}][\text{N}^n\text{Bu}_4]$ in CH_2Cl_2 . EPR parameters: $B_0 = 3368\text{ G}$, sweep = 25 G, sweep time = 30 s, modulation = 2000 mG, microwave power = 10 mW, gain = 3. b) ATR-IR spectrum of solid $[\mathbf{1}^{\text{Cl}}][\text{N}^n\text{Bu}_4]$.

Attention was also given to the redox properties of $[\mathbf{1}^{\text{Cl}}][\text{N}^n\text{Bu}_4]$. Indeed, CV measurements in dichloromethane with $[\text{BArF}_{20}][\text{N}^n\text{Bu}_4]$ (0.1 M) provided two quasi-reversible redox events at $E_{1/2} = 0.43\text{ V}$ and 0.88 V (*vs.* Fc/Fc^+ , Figure 15), very much consistent with the values obtained for the respective dianionic species (see

chapter 3.1.2). In view of the separated redox events and also the intense *IVCT* bands observed in the NIR region for $\mathbf{1}^{\text{Cl}}$ and $[\mathbf{1}^{\text{Cl}}]^{\bullet-}$, the complexes can be sorted into the classes II/III of mixed valence compounds according to ROBIN and DAY.¹⁶⁷⁻¹⁶⁸

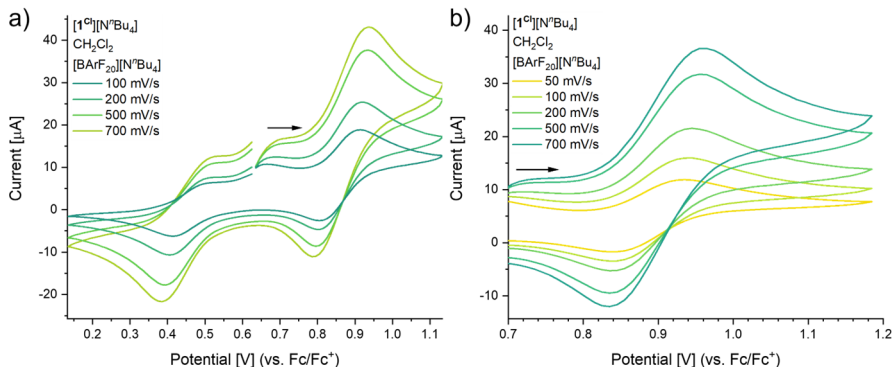


Figure 15: a) CV measurement of the two separated quasi reversible redox waves of $[\mathbf{1}^{\text{Cl}}][\text{N}^t\text{Bu}_4]$ at different scan rates. b) Isolation of the second quasi reversible redox wave of $[\mathbf{1}^{\text{Cl}}][\text{N}^t\text{Bu}_4]$ at different scan rates.

Finally having the electrochemical parameters in hand, comparing the redox properties of $\mathbf{1}^{\text{Cl}}$ with the quinone ligand q^{Cl} was mandatory. Therefore, a cyclic voltammogram of q^{Cl} was measured under same conditions delivering quasi-reversible redox events at $E_{1/2} = -1.19$ V and -0.33 V (*vs.* Fc/Fc^+ , Figure 16, black trace).

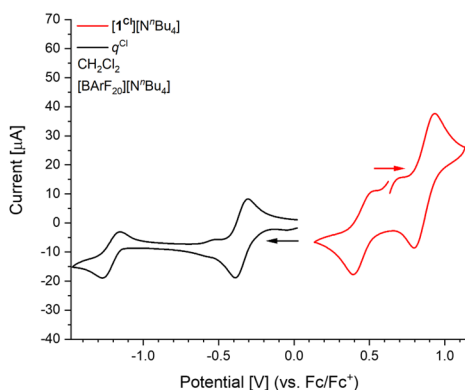


Figure 16: Comparison of the (quasi) reversible redox waves of q^{Cl} (black trace, 100 mV/s) and of $[\mathbf{1}^{\text{Cl}}][\text{N}^t\text{Bu}_4]$ (red trace, 500 mV/s).

Thus, within 1^{Cl} a redox potential shift of $\Delta E \approx 1.2$ V into the anodic direction can be observed (Figure 16). Similar redox amplification of substituted quinones were also found recently. For example, the encapsulation of perhalogenated *p*-benzoquinones in Pd-cages leads to an anodic shift of $\Delta E \approx 1.0$ V.¹⁵¹ Also, coordination of q^{Cl} to dicationic hydrogen bond donors yields a shift of $\Delta E \approx 0.6$ V.¹⁵² In this case, however, formally binding q^{Cl} to the Lewis superacid 2^{Cl} outperforms those potential shifts.

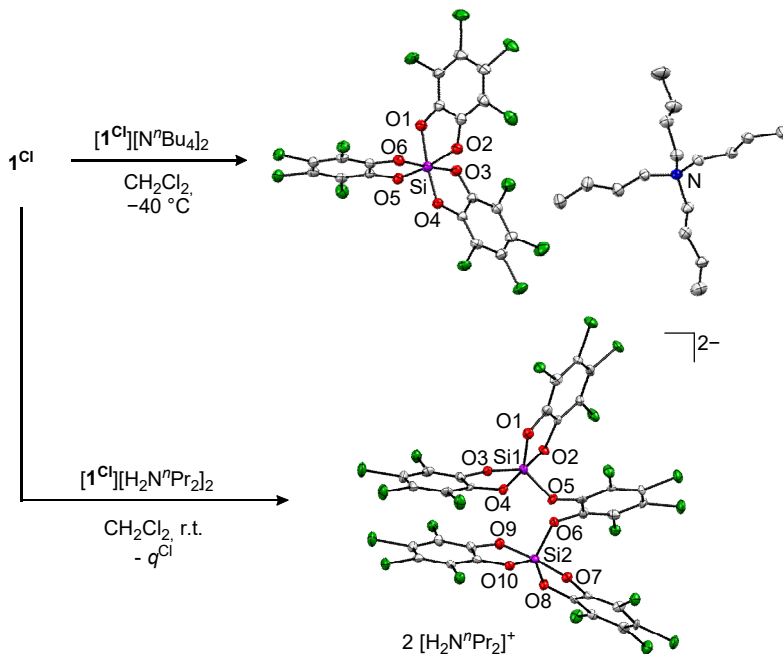


Figure 17: Comproportionation reaction of 1^{Cl} with $[1^{\text{Cl}}][\text{N}^n\text{Bu}_4]_2$ leading to the monoradical anion $[1^{\text{Cl}}]^{\bullet-}$. The thermal displacement ellipsoids are shown at the probability level of 50 %. Protons are omitted for clarity. Alternate reaction outcome of 1^{Cl} with $[1^{\text{Cl}}][\text{H}_2\text{N}^n\text{Pr}_2]_2$ yielding $[3^{\text{Cl}}][\text{H}_2\text{N}^n\text{Pr}_2]_2$ and release of q^{Cl} . The thermal displacement ellipsoids are shown at the probability level of 50 %. Cations are omitted for clarity.

Besides, during the synthetical attempts to the monoradical anion another reaction outcome was observed, however only with the use of $[1^{\text{Cl}}]^{2-}$ with a protic counter cation. Mixing of 1^{Cl} and $[1^{\text{Cl}}][\text{H}_2\text{N}^n\text{Pr}_2]_2$ in dichloromethane led to the release of one equivalent q^{Cl} and the formation of a new diamagnetic silicon catecholates species

monitored by NMR spectroscopy. In the ^{29}Si -INVGATE NMR spectrum a signal at $\delta = -109.6$ ppm was detected, speaking for a pentacoordinated silicon center.¹⁶²

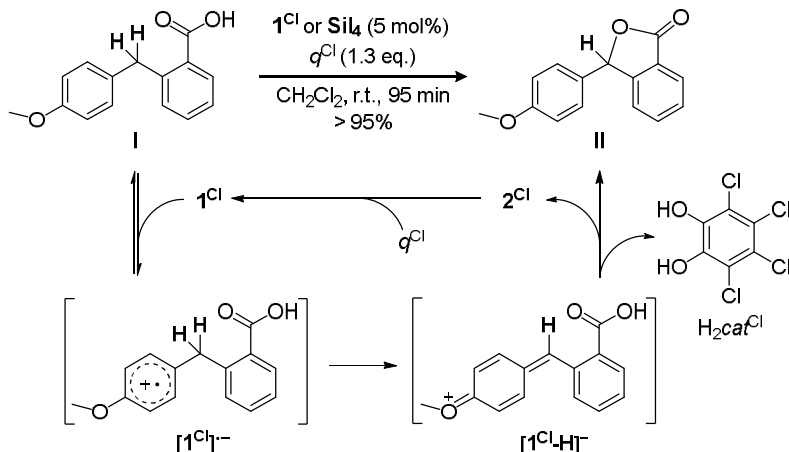
Fortunately, gaseous diffusion of pentane into the reaction solution in CD_2Cl_2 led to colorless crystals. SCXRD analysis finally revealed the solid-state structure of a dinuclear silicon complex. Surprisingly, two units of $\mathbf{2}^{\text{Cl}}$ are bridged by a cat^{Cl} unit resulting in $[(\text{cat}^{\text{Cl}})_2\text{Si}(\text{cat}^{\text{Cl}})\text{Si}(\text{cat}^{\text{Cl}})_2][\text{H}_2\text{N}^n\text{Pr}_2]_2$ ($[\mathbf{3}^{\text{Cl}}][\text{H}_2\text{N}^n\text{Pr}_2]_2$, Figure 17). Thus, ligand scrambling was presumably induced by hydrogen bond activation *via* the protic cation, coupled with an electron redistribution since a neutral quinone is released. Yet, after isolating $[\mathbf{3}^{\text{Cl}}][\text{H}_2\text{N}^n\text{Pr}_2]_2$, only one set of catecholate signals was observed in the ^{13}C spectrum, which means that a fast exchange of the catecholate units must be apparent. To explain this observation DFT calculations (PW6B95-D3/def2-QZVPP level; geometry optimization and frequencies on PBEh-3c/def2-mSVP level) of the respective exchange pathway were conducted. Indeed, thereby a very low barrier of $\Delta G^\ddagger = 49.5$ kJ·mol $^{-1}$ was revealed (see Appendix 7.3.1, Table 7 and Figure 58), emphasizing the dynamic covalent nature of the Si-O bonds in these silicon-based catecholate complexes.^{136, 138, 169-170}

3.1.5 Redox Catalysis

Encouraged by the now tangible redox properties of $\mathbf{1}^{\text{Cl}}$ and the preliminary results regarding the oxidation reactions with the alkylated benzenes, $\mathbf{1}^{\text{Cl}}$ was further investigated regarding its potential to function as redox catalyst.

In this regard, the intramolecular oxidative lactonization reaction of 2-(4-methoxybenzyl)benzoic acid **I** was investigated.¹⁵² First, **I** was synthesized as per literature known procedure and obtained analytically pure in 87 % yield.¹⁷¹⁻¹⁷² With a catalyst loading of 5 mol% of $\mathbf{1}^{\text{Cl}}$ and 1.3 eq. of q^{Cl} a quantitative conversion of **I** to the respective lactone **II** was achieved at room temperature in 95 min (Scheme 7). Because of the straightforward synthesis, $\mathbf{1}^{\text{Cl}}$ was also attempted to form *in situ*. Premixing 5 mol% of SiI_4 with 1.3 eq. of q^{Cl} and adding the substrate **I** after 30 min led to a similar efficient conversion to **II**, thus not stringently requiring the pre-isolation of $\mathbf{1}^{\text{Cl}}$. Compared to the system with hydrogen bond donors, $\mathbf{1}^{\text{Cl}}$ shows improved efficiency according to the more positive shift of the redox potentials for q^{Cl} . In terms of the mechanism, a total of $2e^-/2\text{H}^+$ are transferred from the substrate

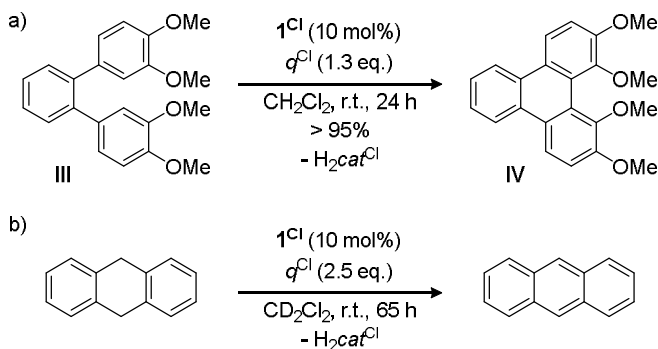
I to 1^{Cl} . This leads to the formation and cleavage of $\text{H}_2\text{cat}^{\text{Cl}}$, which is replaced by another q^{Cl} delivering the catalyst 1^{Cl} again (Scheme 7). This proposal was supported by NMR spectroscopy, where the signals for $\text{H}_2\text{cat}^{\text{Cl}}$ were observed in the ^1H and ^{13}C NMR spectra.



Scheme 7: Oxidative lactonization of **I** to **II** under redox-catalytic conditions with either 5 mol% of 1^{Cl} or *in situ* formed 1^{Cl} by premixing 5 mol% SiI_4 and q^{Cl} , supplemented with the proposed reaction mechanism.

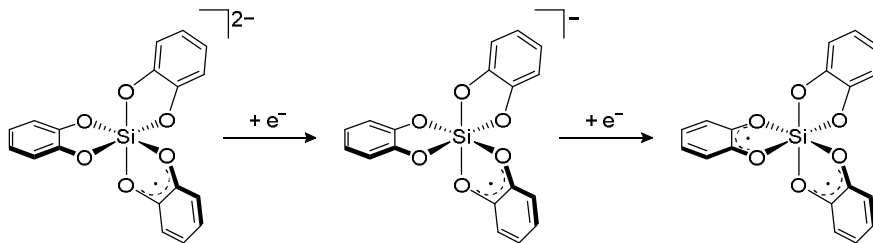
Further reactions were tested to establish the general applicability of 1^{Cl} as an efficient redox catalyst. It was found that dehydrogenative intramolecular coupling of 3,3',4,4'-tetramethoxy-*o*-terphenyl^c **III** to the respective triphenylene **IV** could be accomplished quantitatively with 10 mol% of 1^{Cl} within 24 h at room temperature (Scheme 8a).¹⁷³⁻¹⁷⁴ Additionally, dihydroanthracene was successfully oxidized to anthracene with the same catalyst loading (Scheme 8b). However, reactivity between 1^{Cl} and the product led to secondary oxidation products, observed by NMR spectroscopy, which is why the isolation of anthracene was not attempted.

^c **III** was synthesized by U. WILD (HIMMEL group, University of Heidelberg).¹⁷⁴



Scheme 8: a) Dehydrogenative intramolecular coupling of **III** to **IV** and b) oxidation of dihydroanthracene to anthracene with catalytic amounts of **1^{Cl}**.

3.1.6 Conclusion



Scheme 9: Lewis formulation of the silicon trisdioxolene redox isomers: $[1]^{2-}$, $[1]^{\bullet-}$ and **1**.

In this chapter, the redox chemistry of a century old compound class, the silicon trisdioxolenes was examined and described. The respective redox series was finally completed, and each member was thoroughly characterized (Scheme 9). Thereby, **1^{Cl}** as stable and easily preparable diradical was found to hold potential for vibrant diradical-based research areas.¹⁴³⁻¹⁴⁶ Observations of *IVCT* bands in the NIR region for **1^{Cl}** highlighted the suitability of silicon as central atom for the construction of metal-free magnetic materials and electronic devices.¹⁷⁵

Moreover, comproportionation reaction between **1^{Cl}** and $[1^{\text{Cl}}]^{2-}$ resulted in the monoradical anion $[1^{\text{Cl}}]^{\bullet-}$ confirmed by sXRD analysis. With CV measurements, the redox potentials $E_{1/2} = 0.43 \text{ V}$ and 0.88 V (*vs.* Fc/Fc^+) could be determined, but

guiding redox reactions revealed an even higher redox potential of $E_{1/2} \approx 1.0$ V (*vs.* Fc/Fc⁺), depicting **1**^{Cl} as strong oxidant like [N(Ph-Br₂)₃]^{•+} (*magic blue*) and NO⁺. However, the latter oxidants suffer limitations due to their charged nature, non-innocence, and effortful synthesis, whereas **1**^{Cl} stands out as neutral oxidant with a straightforward synthesis by only combining two commercially available starting materials. At the same time, upon reduction of **1**^{Cl} an easy-to-handle weakly coordinating anion (*WCA*) is delivered (reminiscent of SbF₅).⁹³

Besides, **1**^{Cl} proved to be an efficient redox catalyst, which can be even generated *in situ*. Further, DFT calculations (PW6B95-D3/def2-TZVPP (CH₂Cl₂, CPCM) level; geometry optimization and frequencies on BP86-D3/def2-SVP level) of the solvated electron affinities revealed higher values for **1**^{Cl} ($EA_{solv} = 5.43$ eV, see Appendix 7.3.1, Table 8) compared to *q*^{Cl} ($EA_{solv} = 4.52$ eV), consistent with the experimental findings. Thus, the concept of redox amplification through Lewis superacid-binding was successfully demonstrated to be a powerful instrument, whenever high oxidation potentials are needed.

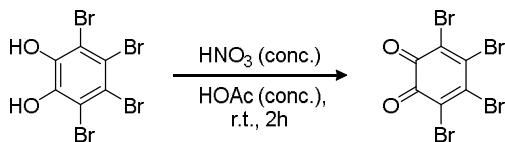
3.2 Further Silicon Trisdioxolenes

Driven by the successful synthesis and characterization of $\mathbf{1}^{\text{Cl}}$ further derivatives of the same constitution but with different substitution patterns were envisaged. For the preparation of $\mathbf{1}^{\text{X}}$ the respective quinone ligands are needed as starting material. Fortunately, q^{Cl} is commercially available, just as 3,5-di-*t*-butyl-benzoquinone (q^{tBu}).^d Further substitutions, like X = F, Br, *i*Pr^e were tackled by oxidizing the respective catechols. The synthesis of $\mathbf{1}^{\text{X}}$ was also tested with other silicon sources, such as SiBr₄ or elemental silicon under mechanochemical conditions.

Besides, DFT calculations (PW6B95-D3/def2-QZVPP level; geometry optimization and frequencies on PB86-D3/def2-SVP level) showed that the synthesis of $\mathbf{1}^{\text{X}}$ (X = F, Br, *t*Bu, *i*Pr) starting from SiI₄ and 3 eq. of the respective quinone under solvated conditions were highly exergonic (see Appendix 7.3.1, Table 10).

Additionally, the question arises if and how the substitution pattern influences the magnetic properties of $\mathbf{1}^{\text{X}}$. By the introduction of bigger atoms or bulkier remainders within the dioxolene ligands the distance between the molecules $\mathbf{1}^{\text{X}}$ might be enlarged in solid state leading to the observation of altered magnetic interactions. Besides, a brief insight will be given into heteroleptic silicon trisdioxolenes regarding their synthesis and magnetic properties.

3.2.1 Synthesis of Precursors



Scheme 10: Synthesis of q^{Br} via oxidation of $\text{H}_2\text{cat}^{\text{Br}}$ with conc. HNO_3 .¹⁷⁶

Like ZINCKE, tetrabromocatechol ($\text{H}_2\text{cat}^{\text{Br}}$) was oxidized at room temperature with 1.6 eq. of concentrated HNO_3 in glacial acetic acid (Scheme 10).¹⁷⁶ After 2 h of

^d Abbreviation: *t*Bu = 3,5-dt**t** = 3,5-di-*tert*-butylated.

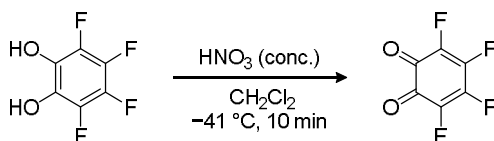
^e Abbreviation: *i*Pr = 3,4,6-t**i**p = 3,4,6-tri-*iso*-propylated.

stirring, water was added to precipitate the product. The red solids were redissolved in dichloromethane and dried over Na_2SO_4 . After removing the solvent and drying *in vacuo* for 24 h, q^{Br} was obtained as red powder in up to 56 % yield, confirmed by NMR spectroscopy where no signal for the hydroxyl group was observed in the ^1H NMR spectrum anymore, but a carbonyl signal at $\delta = 169.2$ ppm in the ^{13}C NMR spectrum.

Then, the synthesis of tetrafluoro-*o*-benzoquinone (q^{F}) was tackled. First, tetrafluorocatechol ($\text{H}_2\text{cat}^{\text{F}}$)¹⁷⁷ was purified by Kugelrohr distillation at 85 °C and 29 mbar.^f Colorless and crystalline solids were obtained in up to 55 % yield. In an initial attempt, the procedure of LEMAL *et al.* was followed, where q^{F} was prepared by oxidizing a solution of $\text{H}_2\text{cat}^{\text{F}}$ in nitromethane with concentrated HNO_3 .¹⁷⁸ The reaction was conducted at -10 °C and darkened after adding the acid. It was stirred for 10 min before adding water. The phases were separated, and the aqueous phase was extracted with benzene, which turned orange. After drying the combined organic phases over Na_2SO_4 , the solution was concentrated cautiously without heating at a reduced pressure of 145 mbar. However, this was not successful due to the high boiling points of benzene and nitromethane. Since q^{F} melts already at 67 °C and sublimates as well,¹⁷⁸ the solvent residues could not be removed completely without loss of the product itself. At least in the ^{19}F NMR spectrum the formation of q^{F} with minor impurities could be observed.¹⁷⁹ Attempts to crystallize the product from solutions in diethyl ether layered with petroleum ether according to SAH and PEOPLES failed.¹⁸⁰ Heating to 50 °C and letting the residual solvent evaporate did also not work. According to the many signals in the ^{19}F NMR spectroscopy the product underwent polymerization and possibly fluorinated dibenzo-1,4-dioxin derivatives were formed.¹⁸¹

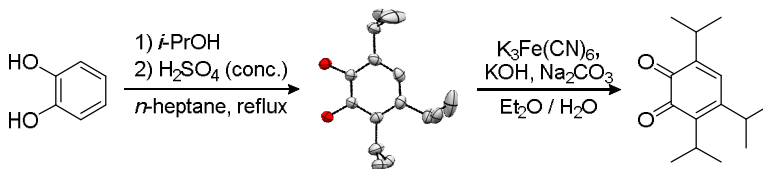
In another attempt, the oxidation of $\text{H}_2\text{cat}^{\text{F}}$ was again conducted with concentrated HNO_3 but in dichloromethane at -41 °C with an acetonitrile/dry ice bath (Scheme 11). Then, the reaction was worked up as stated above. Here, the solvent could be easily removed under reduced pressure with no need of heating. NMR spectroscopy confirmed a successful conversion to q^{F} . Upon cooling the remaining orange oil to -18 °C the product solidified and was obtained in quantitative yields.

^f $\text{H}_2\text{cat}^{\text{F}}$ was synthesized by undergraduate students during their inorganic chemistry practical course of the Bachelor's studies (MCII-AC, University of Heidelberg).¹⁷⁷



Scheme 11: Synthesis of q^F via oxidation of H_2cat^F with conc. HNO_3 .

Next, 3,4,6-triisopropylcatechol (H_2cat^{iPr}) was synthesized according to literature known procedure (Scheme 12).¹⁸² Catechol was suspended in hexane and isopropanol and heated to reflux. Upon addition of concentrated sulfuric acid, the reaction mixture darkened. The temperature and stirring was maintained for further 5 h. After cooling down, the black-colored phases were separated with the help of additional ethyl acetate and a flashlight to determine the phase boundary. The organic layer was washed with diluted aqueous NaOH (0.5 M) solution and with water. After drying over Na_2SO_4 and removal of the solvent, a viscous black-brown residue was obtained in around 80 % yield. By NMR spectroscopy and mass spectrometry it could be shown that the crude material contained other isopropylated and oxidized derivatives besides the main product. Therefore, it was further purified by silica gel flash column chromatography with petroleum ether and ethyl acetate (10:1), giving H_2cat^{iPr} as brownish oil in yields of 35 %. Much to our delight, solidifying the oil at -40 °C and slowly warming back to room temperature led to sublimation and yielded colorless crystals suitable for scXRD analysis (Scheme 12).



Scheme 12: Synthesis of H_2cat^{iPr} followed by the oxidation to q^{iPr} according to SHAVYRIN *et al.*¹⁸². The solid-state molecular structure of H_2cat^{iPr} is displayed as ORTEP plot within the reaction scheme. The thermal displacement ellipsoids are shown at the probability level of 50 %. Only one molecule per asymmetric unit is shown. Hydrogen atoms, co-crystallized solvent molecules and structural disorders are omitted for clarity.

Subsequently, q^{iPr} was prepared as described by SHAVYRIN *et al.*¹⁸² The catechol H_2cat^{iPr} was oxidized with $K_3Fe(CN)_6$ under basic conditions (KOH and Na_2CO_3) in a diethyl ether/water mixture (Scheme 12). After workup, a dark red organic phase

was obtained. The solvent was removed under reduced pressure leaving a dark red oil. Further drying *in vacuo* and storing the oil at $-40\text{ }^{\circ}\text{C}$ led to solidification. Finally, q^{Br} was obtained as dark green solids in quantitative yields.

3.2.2 Synthesis and Characterization of 1^{X}

The preparation of 1^{Br} was accomplished in the same manner as the perchlorinated example with the difference that the reaction proceeded faster. After leaving the reaction mixture of SiI_4 and q^{Br} in dichloromethane at room temperature for 24 h, dark violet precipitate was observed. Washing vigorously with pentane and drying *in vacuo* yielded elementally pure product as a violet powder in up to 76 % yield. From saturated solutions in dichloromethane or benzene suitable crystals for scXRD analysis could be obtained (Figure 18). Alike to 1^{Cl} the octahedral coordination sphere within 1^{Br} is slightly distorted disclosed by the O-Si-O angles $\angle_{\text{cis}} = 85.0(4)^{\circ}$ to $95.4(4)^{\circ}$ and $\angle_{\text{trans}} = 169.0(4)^{\circ}$ to $179.5(5)^{\circ}$. As expected, the sum of the MOS for the dioxolene rings of 1^{Br} is about -4.1 . Interestingly, having a closer look reveals an imbalance of charge between the semiquinonate ligands (-0.9 and -1.2).

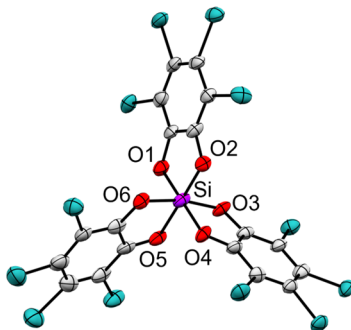


Figure 18: Solid-state molecular structure of 1^{Br} from solutions in CH_2Cl_2 . The thermal displacement ellipsoids are shown at the probability level of 50 %. Co-crystallized solvent molecules are omitted for clarity.

With IR spectroscopy, characteristic C-O stretching bands for the semiquinonate ($\tilde{\nu} = 1416\text{ cm}^{-1}$) and catecholate ($\tilde{\nu} = 1265\text{ cm}^{-1}$) ligands could be observed (Figure 19a). In the UV-vis-NIR spectra of solutions of 1^{Br} in *o*-dcb absorptions at $\lambda = 491\text{ nm}$ were revealed. Besides, an intense absorption in the near-IR region at $\lambda = 1054$ and

1154 nm and a weaker one at $\lambda = 2852$ nm could be assigned to the *IVCT* bands (Figure 19b), resembling the observations for **1^{Cl}** (Figure 10c).

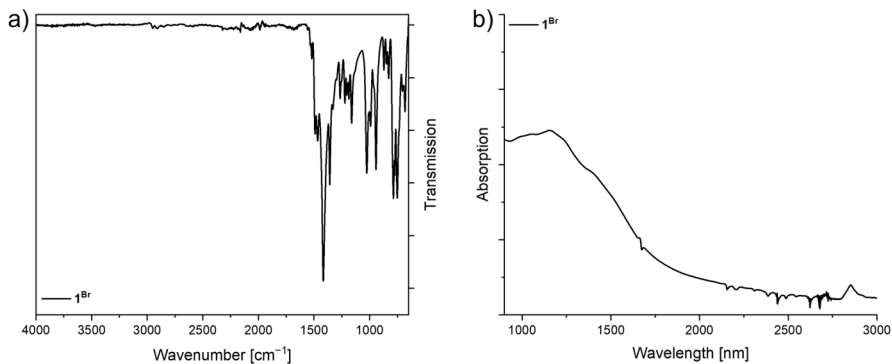


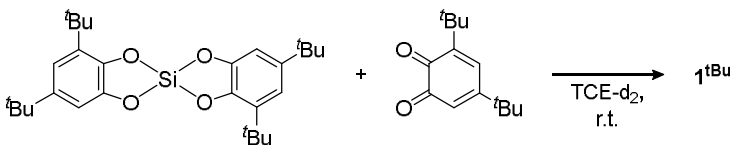
Figure 19: a) ATR-IR spectrum of solid-state sample of **1^{Br}**. b) Absorption spectrum in the near-IR region of a solution of **1^{Br}** in *o*-dcb (10^{-3} M). The irregularities in the graph from $\lambda = 1650$ to 2750 nm originate from the subtraction of the strong near-IR absorptions of the solvent.

For the synthesis of the diradical **1^{tBu}** in the first attempt the respective starting materials were mixed in dichloromethane and left at room temperature for 24 h. Brown colored solids were observed. Leaving the mixture for further days resulted in the additional formation of colorless solids. At first, mass spectrometry confirmed the formation of the product, but elemental analysis referred more to the Lewis acid **2^{tBu}**. Since **2^{tBu}** is an insoluble colorless solid, this would also be consistent with the observations above. The reaction was repeated and a green solution with black solids was obtained. After 24 h, the supernatant solution was removed, and the solids were washed with pentane until the iodine was completely removed. However, the solids turned more light brown during the washing process. Again, NMR spectroscopy revealed the isolation of **2^{tBu}**.³² Thus, the 3,5-di-^tbutylated diradical derivative seems to be less stable than the preceding perhalogenated examples.

Given that **1^{tBu}** can also be thought of as an adduct between **2^{tBu}** and q^{tBu} (as in chapter 3.1.4), the instability of the diradical could be explained by the fact that **2^{tBu}** is a much weaker Lewis acid than its perhalogenated counterparts.³² Depending on the polarity of the solvent, it is possible that the quinone can be easily cleaved when its solubility is higher than of the product **1^{tBu}**. Therefore, working up the reaction

with pentane should be avoided. However, the removal of iodine remains unavoidable. Consequently, other silicon sources were contemplated for the synthesis. The most straight-forward approach was to simply combine the Lewis acid with the respective quinone.

Thus, it was tried to afford 1^{tBu} by oxidative addition of quinone onto the Lewis acid (Scheme 13). For that 2^{tBu} was freshly sublimed[§] as it dimerizes during its synthesis.^{32, 183} It was mixed with q^{tBu} in TCE- d_2 resulting in a dark green solution with residual colorless solids. In the ^1H NMR spectrum broad signals for the ^tBu -groups and no signals in the ^{13}C NMR spectrum were observed. Since the starting materials are diamagnetic, this speaks for a paramagnetic product compound, also confirmed by initial EPR measurements at room temperature. The mixture was further stirred until the solids were completely consumed. A similar outcome was also observed in toluene- d_8 or *o*-difluorobenzene (*o*-dfb), which additionally needed heating. Interestingly, heating the reaction mixtures up to 110 °C resulted in the formation of a deep blue solution. Unfortunately, crystallization attempts were not successful.



Scheme 13: Alternative preparation of diradical 1^{tBu} in NMR scale by oxidative addition of q^{tBu} onto the Lewis acid 2^{tBu} .

Next, SiBr_4 and SiCl_4 were tested as silicon sources since bromine and chlorine would be easier to remove due to their volatility. But, as expected, side reactions occurred where the dioxolene ligands were halogenated which was confirmed by GC-MS measurements. Lastly, elemental silicon was considered, where it was mechanochemically grinded with q^{tBu} with small amounts of solvent, also known as liquid-assisted grinding (LAG).⁵¹ The reaction was conducted in toluene- d_8 but after grinding no visible change was observed. Only after heating the mixture to 120 °C for

[§] 2^{tBu} was synthesized and sublimed by Dr. D. HARTMANN during her doctoral thesis according to literature known procedure.³²

several days a weak singlet signal in the EPR spectrum could be observed. Unfortunately, these attempts did not lead to the successful synthesis of **1^{tBu}** on a preparative scale.

Nevertheless, the synthesis of **1^{tBu}** *via* SiI₄ and q^{tBu} was further pursued since mass spectrometry revealed the successful composition. Still, the removal of iodine had to be taken care of without the possibility to wash it out. This was tackled by various methods. As **1^{tBu}** seems to be stable in dichloromethane for several days, removal of iodine with the solvent under reduced pressure was attempted. This turned out to be not very successful. Then, it was further tried to remove iodine from the solids by sublimation *in vacuo* for 24 h. A green appearance of the solids was observed. However, residuals of iodine were still present recognizable by the violet discoloration of grease or vial caps when it was stored in Schlenk tubes or vials for several hours. Lastly, the usage of activated charcoal was considered since it is known to adsorb small molecules. Also, the specific iodine number indicates the efficiency of adsorption.¹⁸⁴ Prior to use, the activated charcoal^h was dried *in vacuo* for 24 h. Then the crude product was dissolved in dichloromethane and filtered over layers of activated charcoal and celite. After filtration an intense green solution was obtained. However, re-filtration of the green solution or washing out the residuals with dichloromethane eventually led to a brown filtrate which, according to NMR spectroscopy, could be assigned to the catechol H₂cat^{tBu} and thus speaks for the decomposition of **1^{tBu}**. Finally, conducting a fast filtration and removing the solvent under reduced pressure gave elementally pure **1^{tBu}** as bright green powder in yields up to 51 %. The IR spectrum showed characteristic C-H and C-O stretching bands at $\tilde{\nu} = 2954 \text{ cm}^{-1}$ and $\tilde{\nu} = 1480$ (catecholate) and 1242 cm^{-1} (semiquinonate), respectively.

The synthesis of **1^F** was approached on NMR scale. Mixing of SiI₄ and q^F in CD₂Cl₂ led to a red solution. After 24 h, the mixture had darkened, presumably by the development of iodine. EPR measurements at room temperature revealed a signal with hyperfine splitting arising from the fluorine remainders, thus confirming a conversion to a paramagnetic fluorinated compound. Iodine was removed by washing

^h Activated charcoal (Supelco 05105) was purchased from Sigma-Aldrich, Merck KGaA, Darmstadt, Germany. Iodine-adsorption: 0.05 mol/L, 70 mL/g

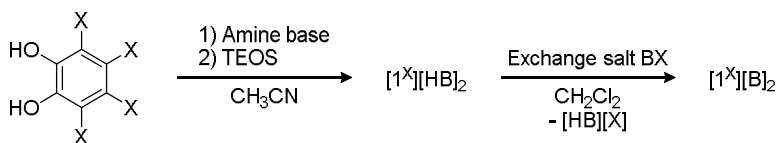
and an attempt to crystallize the product by gaseous diffusion of pentane failed. Since q^F is not very stable at ambient conditions and not easy to handle as a semisolid and volatile substance the synthesis of $\mathbf{1}^F$ had been put on hold for now.

In similar fashion, the preparation of $\mathbf{1}^{iPr}$ was also attempted. SiI_4 and q^{iPr} were mixed in dichloromethane. After 24 h, black solids were obtained in the reaction, but NMR measurements displayed the existence of a diamagnetic silicon species. With a ^{29}Si -INVGATE shift of $\delta = -41.2$ ppm, the bis(catecholato)silane $\mathbf{2}^{iPr}$ (see chapter 3.3.2) was most likely isolated, comparable with the shift obtained for freshly sublimed $\mathbf{2}^{tBu}$ (^{29}Si MAS: $\delta = -40.7$ ppm).¹⁸³ Thus, it is questionable whether $\mathbf{1}^{iPr}$ was prepared at all. Moreover, $\mathbf{2}^{iPr}$ and $\mathbf{2}^{tBu}$ should be similarly weakly acidic, which means, according to the *Lewis acid-quinone adduct* model (see chapter 3.1.4), coordination of another dioxolene ligand is less favored and thus could hamper the formation of the respective diradical. Regarding the ^{29}Si NMR shift, $\mathbf{2}^{iPr}$ seems to be existent in monomeric form in solution, whereas $\mathbf{2}^{tBu}$ tends to dimerize ($\delta = -69.3$ ppm).^{183,185} This should lead to an increased solubility of $\mathbf{2}^{iPr}$ which again calls the stability of the diradical in solvated state into question. Hence, the workup and isolation of partially formed $\mathbf{1}^{iPr}$ becomes more difficult as well.

$\mathbf{1}^{Cl}$ was also synthesized with $SiBr_4$ and $SiCl_4$. Compared to the approach with SiI_4 , the reactions proceeded much slower. Also, iodine as byproduct is much easier to handle than elemental bromine or chlorine, which are much more volatile and corrosive.

3.2.3 Synthesis of $[\mathbf{1}^X]^{2-}$

The synthesis of the dianionic salts $[\mathbf{1}^X]^{2-}$ was accomplished analogous to the synthetical route for the perchlorinated ones (Scheme 14). At first, it was tried to prepare $[\mathbf{1}^{Br}][NEt_4]_2$ via $[\mathbf{1}^{Br}][HNEt_3]_2$ and subsequent salt metathesis with NEt_4Cl (Table 2, entry a). However, problems occurred during the isolation of the product salt due to similar solubilities with the byproduct $HNEt_3Cl$. Washing with water was not sufficient but washing with diethyl ether worked well which however came along with loss of yield. NMR and HR-MS measurements at least confirmed the successful conversion to $[\mathbf{1}^{Br}][NEt_4]_2$.



Scheme 14: General synthetic route towards tris(catecholato)silicate salts. For the definition of X, Amine base, HB and BX see Table 2.

Table 2: Summary of the synthetical attempts towards $[1^X]^{2-}$ with different counteranions under varying conditions and yields.

Entry	X	HB/B	Procedure (Amine base, BX)	Conditions	Yield
(a)	Br	$[\text{NEt}_4]^+$ <i>via</i> $[\text{HNEt}_3]^+$	Conversion with NEt_3 Salt metathesis with NEt_4Cl	16 h reflux 1.5 h r.t.	Isolation of product failed
(b)		$[\text{Hpy}]^+$	Conversion with pyridine	2 h r.t., 2 h reflux	68 %
(c)	tBu	$[\text{N}^n\text{Bu}_4]^+$	Salt metathesis with $\text{N}^n\text{Bu}_4\text{Br}$	2 h r.t.	50 %
(d)		$[\text{H}_2\text{N}^n\text{Pr}_2]^+$	Conversion with HN^nPr_2 Salt metathesis with $\text{N}^n\text{Bu}_4\text{Br}$	16 h r.t., 2 h reflux 2 h r.t.	Salt metathesis failed
(e)		$[\text{NBu}_4]^+$ <i>via</i> $[\text{Hpy}]^+$	Conversion with pyridine Salt metathesis with $\text{N}^n\text{Bu}_4\text{Br}$	30 min r.t., 2 h reflux 2 h r.t.	79 %
(f)	F	$[\text{N}^n\text{Bu}_4]^+$ <i>via</i> $[\text{H}_2\text{N}(\text{nPr})_2]^+$	Conversion with HN^nPr_2 Salt metathesis with $\text{N}^n\text{Bu}_4\text{Br}$	16 h r.t., 2 h reflux 16 h r.t.	Isolation of product failed
(g)		$[\text{Hpy}]^+$	Conversion with pyridine	16 h r.t.	72 %
(h)		$[\text{N}^n\text{Bu}_4]^+$	Salt metathesis with $\text{N}^n\text{Bu}_4\text{Br}$	2 h r.t.	50 %

Hence, it was considered to prepare a salt with very low solubility with which exchange reactions could be done more easily. Thus, pyridine was used as amine base and indeed $[1^{\text{Br}}][\text{Hpy}]_2$ could be obtained as yellow powder in up to 68 % yield (Table 2, entry b). Since the basicity of pyridine (in water: $pK_a = 5.23$, conjugated acid)¹⁸⁶

is half as strong compared to triethylamine ($pK_a = 10.68$)¹⁸⁷, it might be advisable to make sure the reaction time is long enough. Salt metathesis of $[\mathbf{1}^{\text{Br}}][\text{Hpy}]_2$ with $\text{N}^n\text{Bu}_4\text{Br}$ afforded $[\mathbf{1}^{\text{Br}}][\text{N}^n\text{Bu}_4]_2$ as brown powder in 50 % yield (Table 2, entry c), confirmed by scXRD analysis and NMR spectroscopy.

For the synthesis of $[\mathbf{1}^{\text{tBu}}][\text{N}^n\text{Bu}_4]_2$, $[\mathbf{1}^{\text{tBu}}][\text{H}_2\text{N}^n\text{Pr}_2]_2$ was prepared and salt exchange was conducted with $\text{N}^n\text{Bu}_4\text{Br}$ (Table 2, entry d). But the metathesis did not happen completely, and isolation of the product failed. Therefore, the same procedure as for the brominated species was followed. Subsequently, $[\mathbf{1}^{\text{tBu}}][\text{N}^n\text{Bu}_4]_2$ *via* $[\mathbf{1}^{\text{tBu}}][\text{Hpy}]_2$ was successfully afforded as brown oil in 79 % yield (Table 2, entry e), confirmed by NMR spectroscopy.

In case of $X = \text{F}$, initial attempts towards $[\mathbf{1}^{\text{F}}][\text{N}^n\text{Bu}_4]_2$ *via* $[\mathbf{1}^{\text{F}}][\text{H}_2\text{N}^n\text{Pr}_2]_2$ did not work out as well (Table 2, entry f). Therefore, the pyridinium salt was prepared directly and obtained as brown solids in 72 % yield (Table 2, entry g). Salt metathesis with $\text{N}^n\text{Bu}_4\text{Br}$ finally led to $[\mathbf{1}^{\text{F}}][\text{N}^n\text{Bu}_4]_2$ as light brown powder in up to 50 % yield (Table 2, entry h). Due to the high fluorine content, the catechol signals for $[\mathbf{1}^{\text{F}}][\text{N}^n\text{Bu}_4]_2$ were not observed in the ^{13}C NMR spectrum. But additional HR-MS measurements confirmed the successful synthesis of both salts.

The synthesized silicate salts $[\mathbf{1}^{\text{X}}][\text{N}^n\text{Bu}_4]_2$ were also investigated by CV. Initial measurements showed similar irreversible oxidation potentials in similar range as for $[\mathbf{1}^{\text{Cl}}][\text{N}^n\text{Bu}_4]_2$. However, $[\text{PF}_6][\text{N}^n\text{Bu}_4]$ was used as electrolyte at that time, which only later proved to be unsuitable for this compound class.

3.2.4 Synthesis of $[\mathbf{1}^{\text{Br}}]^{\bullet-}$

For the synthesis of the brominated monoradical anion, disproportionation between $\mathbf{1}^{\text{Br}}$ and $[\mathbf{1}^{\text{Br}}][\text{N}^n\text{Bu}_4]_2$ was carried out as for the chlorinated species. Solutions of each of the starting materials in dichloromethane were cooled down to -40 °C and combined. A red brown suspension was obtained. The temperature was maintained for further 24 h leading to a dark brown solution. After two weeks, the supernatant solution was clear brown and black crystalline solids were observed in the reaction mixture. SCXRD analysis finally revealed the molecular structure of $[\mathbf{1}^{\text{Br}}][\text{N}^n\text{Bu}_4]$ (Figure 20) and the resulting MOS were in line with the proposed Lewis formulation

as $[\text{Si}(\text{sq}^{\text{Br}})(\text{cat}^{\text{Br}})_2]^\bullet-$ (see Appendix 7.4, Table 15). Removing the supernatant solution and drying the black solids *in vacuo* led to the product in quantitative yields.

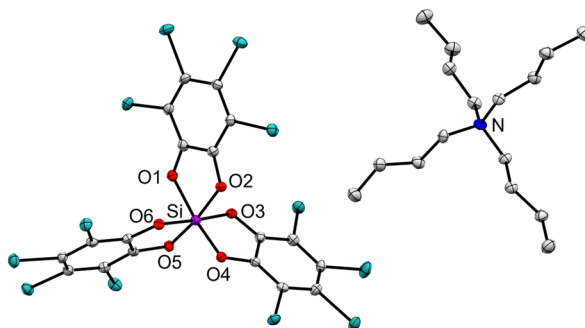
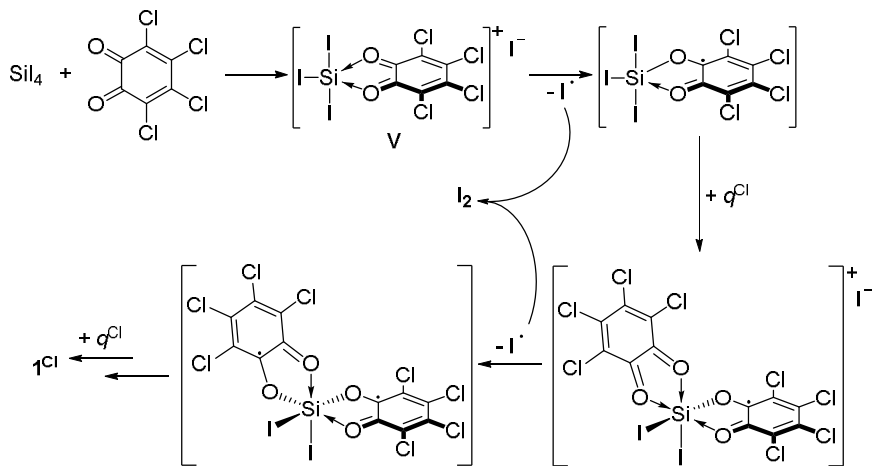


Figure 20: Solid-state molecular structure of $[\mathbf{1}^{\text{Br}}][\text{N}^t\text{Bu}_4]$. The thermal displacement ellipsoids are shown at the probability level of 50 %. Hydrogen atoms and co-crystallized solvent molecules are omitted for clarity.

3.2.5 Formation Mechanism towards $\mathbf{1}^{\text{X}}$

After completing the redox series of silicon trisdioxolenes and thorough investigation of the redox properties, the formation mechanism towards $\mathbf{1}^{\text{X}}$ was examined. The preparation of $\mathbf{1}^{\text{Cl}}$ proceeds *via* q^{Cl} and SiI_4 . During the reaction course, the quinones are reduced to a catecholate and two semiquinonate ligands and the formally monoanionic substituents of SiI_4 are oxidized to form elemental iodine. Thus, the first assumption was that the formation of $\mathbf{1}^{\text{Cl}}$ is simply initiated by a redox process, wherefore CV measurements of the starting materials were conducted. For the redox couple $q^{\text{Cl}}/\text{sq}^{\text{Cl}}$ the redox potential $E_{1/2} = -0.33$ V (*vs.* Fc/Fc^+) was found, whereas SiI_4 was not oxidized until $E_{\text{ox}} = 0.03$ V (*vs.* Fc/Fc^+ , see Appendix 7.7, Figure 71). Conclusively, the first step of the reaction towards $\mathbf{1}^{\text{Cl}}$ does not involve a redox process since the redox potential of $q^{\text{Cl}}/\text{sq}^{\text{Cl}}$ is lower than the oxidation potential of SiI_4 . Another proposal would be that the conversion proceeds *via* substitution reaction, in which the iodides serve as leaving groups. This could result in the intermediate **V** as shown in (Scheme 15), from which the actual redox process may take place, leading to the formation of iodine.

Additionally, the reaction was also tested with tetrachloro-*p*-benzoquinone. Mixing with SiI_4 in CD_2Cl_2 led to a yellow solution. The mixture was stirred at room temperature and monitored for several days, which led to no change in habitus. NMR measurements confirmed that no reaction had occurred. This observation reasserts the fact that in this synthetical approach between SiI_4 and quinones initially no redox process is involved and for the substitution of iodides a chelating ligand, such as q^{Cl} is of need.



Scheme 15: Proposed mechanism for the synthesis of 1^{Cl} via SiI_4 and q^{Cl} .

To further support this assumption, the electron affinities of **V** and q^{Cl} were computed with DFT methods (PW6B95-D3/def2-TZVPP (CH_2Cl_2 , CPCM) level; geometry optimization and frequencies on BP86-D3/def2-SVP level). Thereby, a higher value for the electron affinity for **V** ($EA_{\text{solv}} = 6.61$ eV, see Appendix 7.3.1, Table 8) was found than compared to the starting material q^{Cl} ($EA_{\text{solv}} = 4.52$ eV). To substantiate this hypothesis, the formation of 1^{Cl} was monitored by UV-vis spectroscopy. Apart from the absorption bands at $\lambda = 504$ nm which can be assigned to the formation of I_2 , bands at $\lambda = 298$ and 376 nm developed and decreased over the reaction course, speaking for the presence of triiodide. Especially during the formation of 1^{Br} , which should proceed in analogous way, this progress could be well observed *via* UV-vis spectroscopy (Figure 21).

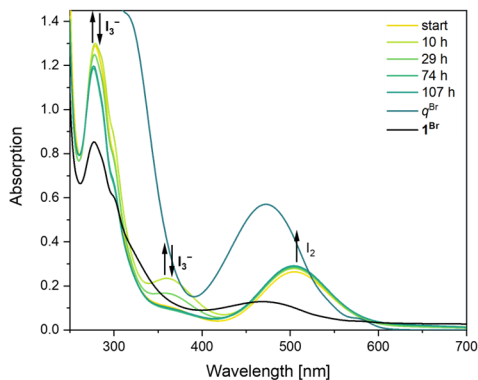


Figure 21: UV-vis reaction monitoring of the synthesis of 1^{Br} in CH_2Cl_2 (10^{-4} M) at room temperature in a quartz cuvette with *Normag* valve.

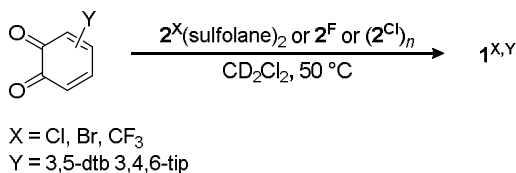
Initially, there was also the consideration that in the synthesis of 1^{Cl} first the free form of 2^{Cl} is assembled *via* redox chemical pathway, which due to its high Lewis acidity then has no choice but to coordinate another quinone ligand in non-donor solvents, finally leading to 1^{Cl} . Indeed, 2^{Cl} has recently been prepared donor-free and found to oligomerize to $(2^{\text{Cl}})_n$, which means that the solubility was still low in common organic solvents.¹⁸⁸ Thus, if the synthesis towards 1^{Cl} would proceed over 2^{Cl} , colorless precipitation should be eventually observed during the reaction, which has not been the case while repeatedly monitoring the synthesis.

3.2.6 Heteroleptic Silicon Trisdioxolenes

Initial efforts towards heteroleptic silicon trisdioxolenes $1^{\text{X,Y}}$ were pursued on NMR scale. Thereby, the synthetical route *via* oxidative addition of quinones onto the respective Lewis acids was chosen, which does not involve any byproducts (Scheme 16).

The first synthesis was attempted with the bis-acetonitrile adduct of 2^{Cl} and q^{iPr} to afford $1^{\text{Cl,iPr}}$. The reaction did not proceed successfully (Table 3, entry a), presumably because acetonitrile is a stronger donor compared to the quinone and thus cannot be displaced. Therefore, the bis-sulfolane adduct of 2^{Cl} was used and reacted with q^{iPr} (Table 3, entry b). The reaction mixture slowly turned into a dark green

suspension. After heating to 50 °C no colorless solids were observed anymore, and the conversion seemed to be complete. EPR spectroscopy confirmed the presence of a new paramagnetic substance whereby a doublet signal was detected at room temperature, caused by hyperfine splitting of the hydrogen atom (nuclear spin $I = \frac{1}{2}$) at the isopropylated dioxolene ligand. Accordingly, no signals were observed by ^{29}Si -INVGATE NMR spectroscopy. Since both starting materials both were diamagnetic substances, the observations indicate full conversion to the product $\mathbf{1}^{\text{Cl},\text{iPr}}$.



Scheme 16: General synthesis of $\mathbf{1}^{\text{X},\text{Y}}$ by oxidative addition of quinone onto bis(catecholato)silanes.

Based on these preliminary results, the reaction was repeated with the Lewis acids $\mathbf{2}^{\text{X}}(\text{sulfolane})_2$ ($\text{X} = \text{Cl, Br, CF}_3$) and $\mathbf{2}^{\text{F}}$ as well as the quinones q^{iPr} and q^{tBu} (Table 3, entries c-i).^{33,94} Thereby dark green, brown, and black solutions were obtained after heating the mixtures to 50 °C. Investigations *via* NMR and EPR spectroscopy delivered similar results as above, indicating successful oxidative additions.

In the course of the syntheses towards $\mathbf{1}^{\text{Cl},\text{Y}}$, the Lewis acid $\mathbf{2}^{\text{Cl}}$ was also introduced in its oligomeric donor-free form $(\mathbf{2}^{\text{Cl}})_n$,¹⁸⁸ since the removal of sulfolane, a byproduct of the reactions, rendered difficult. For test purposes the syntheses of $\mathbf{1}^{\text{Cl},\text{iPr}}$ and $\mathbf{1}^{\text{Cl},\text{tBu}}$ were repeated with $(\mathbf{2}^{\text{Cl}})_n$, which resulted in similar observations (Table 3, entries j and k). Dark green solutions were obtained. Removal of the solvent *in vacuo* delivered the products as green solids in quantitative yields.

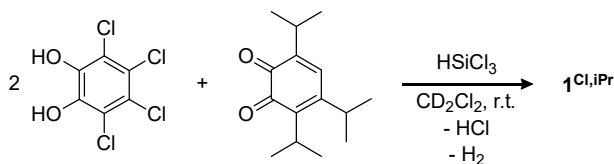
Moreover, another route to prepare heteroleptic silicon trisdioxolenes could be realized. A mixture of 2 eq. of catechol and 1 eq. of quinone in CD_2Cl_2 was reacted with HSiCl_3 (Scheme 17). The combination of $\text{H}_2\text{cat}^{\text{Cl}}$ with q^{iPr} was attempted. Immediately the development of gaseous hydrogen chloride and dihydrogen could be observed. The mixture was stirred at room temperature, leading to a clear green solution. ^1H NMR spectroscopy revealed broad signals for the isopropyl groups. Excess

HSiCl_3 and the solvent were removed under reduced pressure to give $1^{\text{Cl},\text{iPr}}$ as green solids in quantitative yields.

Table 3: Summary of the synthetical attempts towards $1^{\text{X},\text{Y}}$. All reactions were carried out in CD_2Cl_2 at $50\text{ }^\circ\text{C}$.ⁱ

Entry	Lewis Acid 2^{X}	Y	Reaction Color	EPR ^[a]
(a)	$2^{\text{Cl}} \cdot (\text{CH}_3\text{CN})_2$	iPr	no reaction	no signal
(b)	$2^{\text{Cl}} \cdot (\text{sulfolane})_2$	iPr	dark green	doublet
(c)	$2^{\text{Br}} \cdot (\text{sulfolane})_2$	iPr	dark green	doublet
(d)	$2^{\text{CF}_3} \cdot (\text{sulfolane})_2$	iPr	dark green	doublet
(e)	2^{F}	iPr	dark green	doublet
(f)	$2^{\text{Cl}} \cdot (\text{sulfolane})_2$	tBu	dark green	doublet
(g)	$2^{\text{Br}} \cdot (\text{sulfolane})_2$	tBu	dark brown	doublet
(h)	$2^{\text{CF}_3} \cdot (\text{sulfolane})_2$	tBu	black	doublet
(i)	2^{F}	tBu	dark green	doublet
(j)	$(2^{\text{Cl}})_n$	iPr	dark green	doublet
(k)	$(2^{\text{Cl}})_n$	tBu	dark green	doublet

^[a] splitting of the signal at r.t.



Scheme 17: Alternate synthesis of $1^{\text{Cl},\text{iPr}}$ by reacting $\text{H}_2\text{cat}^{\text{Cl}}$ and q^{iPr} with HSiCl_3 in CD_2Cl_2 .

To ultimately confirm the solid-state molecular structures of the heteroleptic derivatives $1^{\text{X},\text{Y}}$ crystallizations were attempted, but without success.

ⁱ The Lewis acids $2^{\text{X}}(\text{sulfolane})_2$, 2^{F} and $(2^{\text{Cl}})_n$ were prepared by T. THORWART, Dr. D. HARTMANN during their doctoral thesis and N. ANSMANN during his Master's thesis according to literature known procedures.^{33,94,188}

3.2.7 Investigating the Magnetic Properties of 1^{tBu} and $1^{\text{X.Y}}$

Open shell electronic structures of the new diradical 1^{tBu} were investigated with X-band *cw*-EPR spectroscopy. Frozen solutions of 1^{tBu} in TCE were examined at 7 K. The recorded spectra featured peak patterns which are characteristic for a triplet state ($S = 1$) centered at $g = 2.0069$ (Figure 22a). At half-field a distinct signal for the forbidden transition $\Delta m_s = 2$ at $g = 4.0272$ was additionally detected (Figure 22b). From the distances between the signals at normal field the respective zero-field splitting parameters were determined as $D = 288$ G and $E = 20.5$ G.¹⁸⁹ Thus, with equation (3) an average distance between the unpaired electrons was calculated as $r_{av} = 4.6$ Å, which is slightly shorter than already obtained theoretically ($r_{calc} = 4.9$ Å) and experimentally ($r_{exp} \approx 5$ Å) for 1^{Cl} .⁹³

$$D = 1.39 \cdot 10^4 \cdot (g/r^3) \quad (3)$$

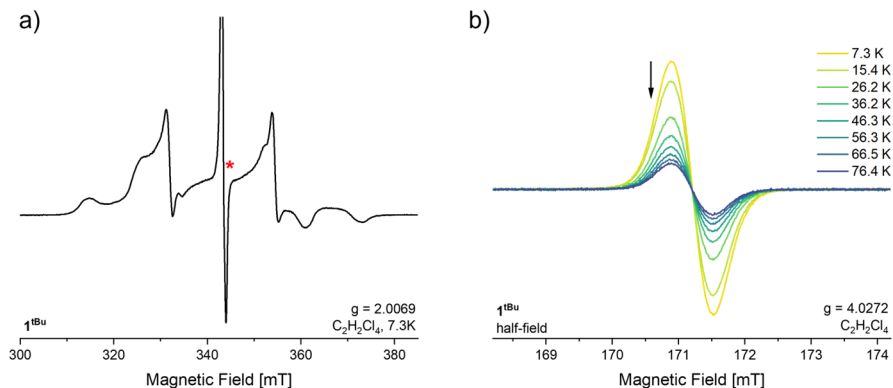


Figure 22: a) X-band EPR spectra of 1^{tBu} in TCE ($\text{C}_2\text{H}_2\text{Cl}_4$) at 7.3 K (monoradical impurity*). b) Variable temperature spectra at half-field from 7 to 80 K. Parameters: frequency = 9.632 GHz, power = 0.63 mW, modulation = 1 G.

According to ABE, the observation of the forbidden transition strongly indicates the presence of a triplet diradical.¹⁸⁹ To consolidate the electronic ground state of 1^{tBu} , variable temperature (VT) EPR measurements were conducted in the range of 7 to 80 K. The resulting $I \times T$ vs. T plot ultimately confirmed the triplet ground state. Due to the population of the singlet open shell state, which is EPR inactive, the intensity of the signal decreases upon increasing the temperature (Figure 22b). Such a

ferromagnetic coupling seems reasonable in view of the orthogonality of the magnetic ligand orbitals and of the empty $3p$ orbitals at the silicon center.

1Cl,tBu and **1**Cl,iPr, as representatives for the heteroleptic analogues, were investigated by EPR spectroscopy. Frozen solutions in dichloromethane and TCE, respectively, were measured at 6 K revealing peak patterns characteristic for triplet diradicals (Figure 23). Furthermore, a hyperfine splitting can be observed (blue area) in both spectra, unlike with the homoleptic diradical **1**tBu (Figure 22a). From this, it can be concluded that the unpaired electrons of **1**tBu are equally delocalized over the three dioxolene ligands, whereas for **1**Cl,tBu and **1**Cl,iPr the unpaired electrons must be more localized at the alkylated dioxolene ligand to make the splitting observable. Since *diox*^{tBu} is an electron-rich ligand, it preferably exists in the semiquinonate state rather than in the catecholate state, which should be more favored by the electron poor *diox*^{Cl} ligand. Thus, within the mentioned heteroleptic diradicals the *intramolecular* electron transfer can be observed by EPR spectroscopical methods.

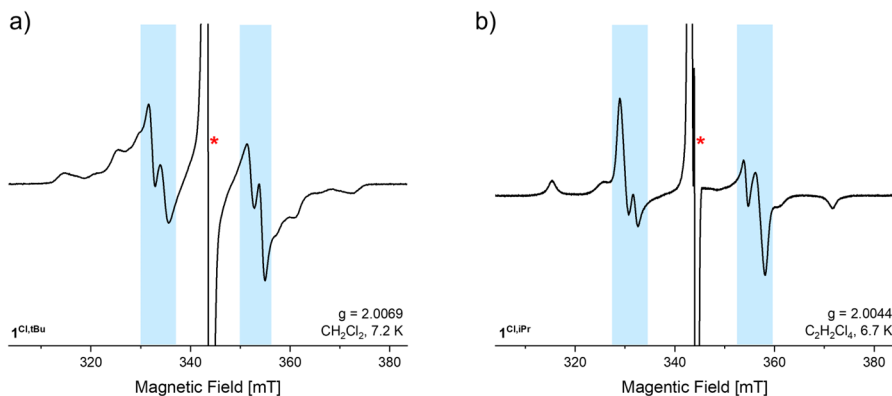


Figure 23: X-band EPR spectra of frozen solutions of a) **1**Cl,tBu at 7.2 K and b) **1**Cl,iPr at 6.7 K. Hyperfine splitting highlighted by blue area. Parameters: a) frequency = 9.632 GHz, power = 0.02 mW, modulation = 1 G, b) frequency = 9.633 GHz, power = 0.06 mW, modulation = 1 G.

At half-field distinct signals for the forbidden transition $\Delta m_s = 2$ were detected for both compounds (Figure 24). VT measurements revealed triplet ground states for **1**Cl,tBu and **1**Cl,iPr, as the intensity of the signals decreased with increasing temperature. Since the molecular geometry of heteroleptic diradicals should not differ

significantly from that of the homoleptic diradicals, ferromagnetic coupling could be also expected here.

Furthermore, the zero-field splitting parameters were determined for $\mathbf{1}^{\text{Cl,tBu}}$ as $D = 273.5$ G and $E = 26$ G and for $\mathbf{1}^{\text{Cl,iPr}}$ as $D = 300$ G and $E = 16$ G. Calculations of the average distances between the unpaired electrons with equation (3) yielded $r_{av} = 4.7$ Å and $r_{av} = 4.5$ Å, respectively, which are in a similar range to that of $\mathbf{1}^{\text{Cl}}$ and $\mathbf{1}^{\text{tBu}}$.⁹³

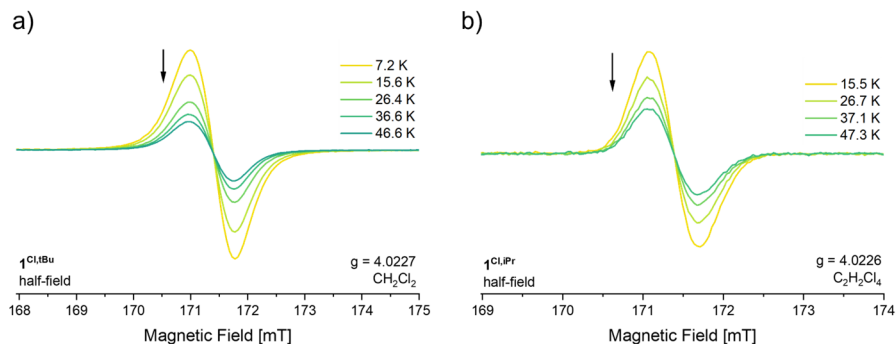


Figure 24: VT X-band EPR spectra of frozen solutions of a) $\mathbf{1}^{\text{Cl,tBu}}$ b) $\mathbf{1}^{\text{Cl,iPr}}$ at half-field from 7 to 50 K. Parameters: frequency = 9.632 GHz, power = 0.63 mW, modulation = 1 G.

3.2.8 Conclusion

According to the synthesis of $\mathbf{1}^{\text{Cl}}$, the analogous homoleptic diradical $\mathbf{1}^{\text{Br}}$ was successfully prepared in good yields. *Via* comproportionation reaction with $[\mathbf{1}^{\text{Br}}][\text{N}^n\text{Bu}_4]_2$ the brominated monoradical anion $[\mathbf{1}^{\text{Br}}][\text{N}^n\text{Bu}_4]$ could be obtained, confirmed by scXRD analysis and calculated MOS, thus completing the redox series of the silicon tris(perbromo)dioxolene. For $\mathbf{1}^{\text{Br}}$ *IVCT* bands were observed in the near-IR region, as for $\mathbf{1}^{\text{Cl}}$. Further, the derivative $\mathbf{1}^{\text{tBu}}$ could be finally synthesized and isolated. Investigations of the magnetic properties by EPR spectroscopy confirmed the diradical character with a triplet ground state.

Moreover, several tris(catecholato)silicates $[\mathbf{1}^{\text{X}}][\text{HB}]_2$ ($X = \text{F}, \text{Br}, \text{tBu}$; $\text{HB} = \text{NEt}_4^+, \text{N}^n\text{Bu}_4^+, \text{Hpy}^+$) were prepared and characterized by NMR spectroscopy and mass

spectrometry. Preliminary CV experiments showed similar oxidation potentials as for **1**^{Cl}.

With CV experiments and reaction monitoring through UV-vis spectroscopy, the formation mechanism of **1**^X was studied. It was found that the first step of the reaction cannot be initiated by a redox process, but more likely by a substitution of an iodide by the quinone. This presumably leads to the intermediate [*q*^XSiI₃]⁺, which, according to DFT calculations, has a higher electron affinity than the respective quinones and could therefore undergo reduction. Moreover, no reactivity was observed between SiI₄ and tetrachloro-*p*-benzoquinone, substantiating the proposed mechanism.

Last, the synthesis of the heteroleptic diradical species was attempted on NMR scale. Thereby, oxidative addition of *q*^Y (Y = tBu and iPr) to the Lewis acid **2**^X (X = F, Cl, Br, CF₃) led to the formation of **1**^{X,Y}, as observed by preliminary EPR measurements. Alternatively, mixing of 2 eq. H₂*cat*^X and 1 eq. *q*^Y with HSiCl₃ gave similar results for **1**^{Cl,iPr}. VT EPR measurements confirmed a triplet diradical character for **1**^{Cl,tBu} and **1**^{Cl,iPr}.

3.3 Tetraoxolene-bridged Bis(catecholato)silanes

In the following chapter the preparation and investigation of dimeric silicon polyoxolenes will be covered. At first the synthesis and the characterization of the precursors, especially the polytopic substituted 2,5-dihydroxy-*p*-benzoquinone H_2dhhbq^Y ($Y = Cl, Br, Ph, NO_2$) linkers and the new silicon Lewis acid 2^{iPr} , will be discussed in detail. Subsequently, the substituted tetraoxolene linkers will be assembled with various GREB-type silanes 2^X ($X = Cl, Br, CF_3, iPr$) to yield tetraoxolene-bridged bis(catecholato)silanes, which will be thoroughly characterized regarding their structural and magnetic properties.

3.3.1 Synthesis and Characterization of Precursors

Unsubstituted 1,4-dihydroxy-*p*-benzoquinone (H_2dhhbq^H) and its chlorinated derivative H_2dhhbq^{Cl} were purchased from commercial suppliers. H_2dhhbq^{Br} was obtained as red-brown powder by a twofold bromination of H_2dhhbq^H with elemental bromine in ethanol in 36 % yield.¹⁹⁰ The phenylated derivative, also known as polyporic acid (H_2dhhbq^{Ph}), was prepared following a two-step synthesis.¹⁹¹⁻¹⁹² First, 2,5-diphenyl-*p*-benzoquinone was brominated in hot glacial acetic acid to afford the respective dibromo compound as orange powder in 93 % yield. Subsequently, the addition of aqueous NaOH solution (10 %) to 3,6-dibromo-2,5-diphenyl-*p*-benzoquinone suspended in methanol caused a drastic color change to dark purple, which indicated an instant hydrolysis to Na_2dhhbq^{Ph} . Acidification with concentrated HCl solution led to discoloration and formation of a brown precipitate. After filtration, vigorous washing with water and drying under reduced pressure at 50 °C for two days, H_2dhhbq^{Ph} was obtained as light brown powder in 71 % yield. Lastly, the NO_2 -derivative could be directly accessed as disodium salt *via* nucleophilic substitution reaction.¹⁹³ There, tetrachloro-*p*-benzoquinone and sodium nitrate in water yielded an orange crystalline material (73 %) which was identified by elemental analysis to be the di-water adduct of $Na_2dhhbq^{NO_2}$. For further usage the crystal water needed to be removed. This could not be accomplished by drying under reduced pressure but by dissolving $Na_2dhhbq^{NO_2} \cdot (H_2O)_2$ in DMSO and storing over molecular sieves (4 Å) for 24 h. Addition of dichloromethane led to a yellow precipitation. Vigorous washing with dichloromethane/pentane and drying *in vacuo* led to water-free $Na_2dhhbq^{NO_2}$ as bright

yellow powder in quantitative yields. The above synthesized $dhbq^Y$ -precursors were thoroughly analyzed, and the data found to be consistent with the respective references.

For further usage of the $dhbq^Y$ -precursors a two-fold deprotonation was necessary. This was at first conducted for $Y = \text{Cl}$ and Br . Therefor $\text{H}_2dhbq^{\text{Cl/Br}}$ was mixed with 2 eq. of NaH and suspended in acetonitrile (method 1). Stirring at room temperature immediately led to vigorous gas development and formation of pink and purple solids, respectively. During the reaction period the gaseous phase was exchanged frequently. After stirring for 18 h the solids were collected by filtration and washed with acetonitrile/dichloromethane. After drying *in vacuo* $\text{Na}_2dhbq^{\text{Cl}}$ was obtained in quantitative and the brominated derivative in 84 % yield. The deprotonated species could be verified by NMR and IR spectroscopy. The specific OH valence vibration was no longer present while the broad C=O vibration bands retained ($\tilde{\nu} = 1488 \text{ cm}^{-1}$ for $Y = \text{Cl}$ and $\tilde{\nu} = 1504 \text{ cm}^{-1}$ for $Y = \text{Br}$, Figure 25).

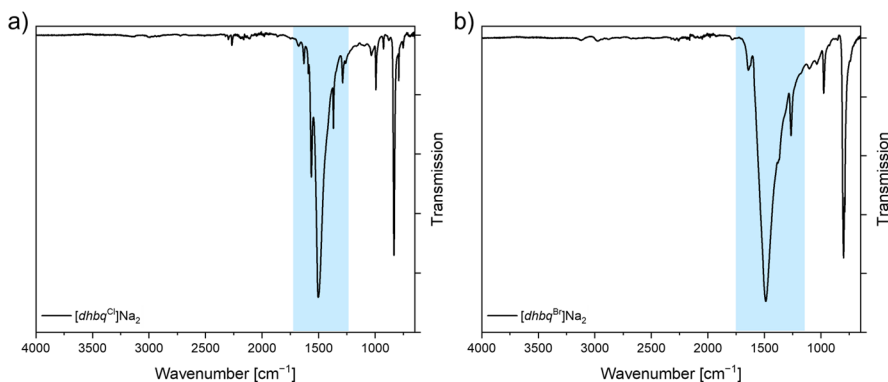


Figure 25: ATR-IR spectra of a) $[dhbq^{\text{Cl}}]\text{Na}_2$ and b) $[dhbq^{\text{Br}}]\text{Na}_2$ with no longer observed OH valence vibration but intense C=O vibration bands (blue area).

The organo-salts $\text{Na}_2dhbq^{\text{Cl/Br}}$ were insoluble in common organic solvents and only found to be soluble in water and DMSO. To increase the poor solubility 15-crown-5 was employed. Indeed, due to the complexation of the sodium cation by the crown ether and thus enlarging the counter ion, the solubility was increased, and single crystals of the chlorinated derivative could be obtained by gaseous diffusion of pentane into solutions of dichloromethane at $-40 \text{ }^\circ\text{C}$. SCXRD analysis showed that the sodium

cations are coordinated by the crown ethers and also interact with the oxygens of the $dhbq^{Cl}$ unit (Figure 26a)

. According to the structural data, the two oxygen atoms on the same side of the tetraoxolene linker interact equally and have the same distance to one of the sodium counter ions, which is also consistent with ^{13}C NMR spectroscopical data which only shows two carbon signals for the anion $[dhbq^{Cl}]^{2-}$. Additionally, the 15-crown-5 ethers are located perpendicular and slightly tilted regarding the planar $dhbq^{Cl}$ unit (Figure 26b). The brominated analogue was less soluble in common solvents even after the addition of the crown ether, which rendered the growth of single crystals impossible.

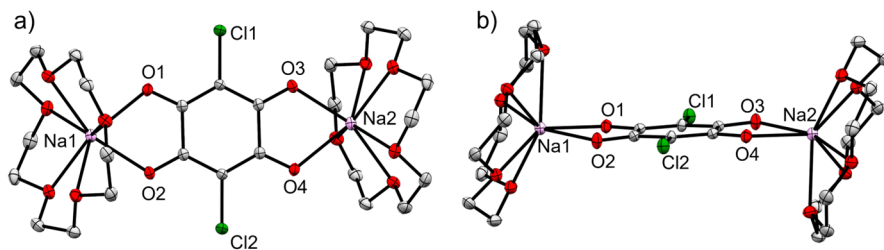


Figure 26: a) Front view and b) side view of the solid-state molecular structure of $[dhbq^{Cl}][Na@15c5]_2$ as ORTEP plot. The thermal displacement ellipsoids are shown at the probability level of 50 %. Hydrogen atoms and co-crystallized solvent molecules are omitted for clarity.

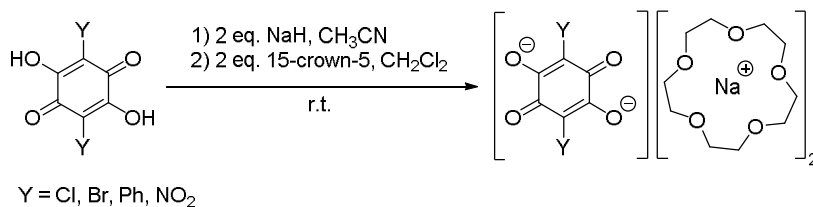
According to literature another strategy was carried out to obtain the salts $Na_2dhbq^{Cl/Br}$. Thereby, sodium methoxide was used for deprotonation (method 2).¹⁹⁴ To a sodium methanolate solution $H_2dhbq^{Cl/Br}$ was added and the resulting mixture was stirred at room temperature for two days. Pink and purple precipitates were obtained respectively and collected by filtration. The solids were washed with methanol and dried *in vacuo* at 70 °C for 2 days to obtain Na_2dhbq^{Cl} in quantitative and Na_2dhbq^{Br} in 88 % yield. Compared to method 1 from above, method 2 seemed more advantageous due to the higher solubility of deprotonating agent in methanol. Consequently, the reagent, if used in excess, can be easily removed from the products by washing only. However, although the products were dried under reduced pressure at 70 °C for 2 days, the 1H NMR spectrum still showed traces of methanol, which might derive from coordinated solvent molecules to the cation. The amount of the

solvent should be rather negligible as no specific OH stretching vibration was observed in the respective IR-spectrum. Nevertheless, even little residues of methanol might induce hydrolysis or other side-reactions regarding the subsequent synthesis of the dimeric structures and extended frameworks. With method 1 the products were obtained solvent-free and analytically pure after drying *in vacuo*. Therefore, the deprotonation of the tetraoxolenes were only conducted with method 1 (NaH), which should be more sufficient for follow-up reactions.

As the salts $\text{Na}_2\text{d}hbq^Y$ ($Y = \text{Cl}, \text{Br}, \text{Ph}, \text{NO}_2$) still were quite insoluble in common organic solvents, attempts for salt metathesis reactions were made. For test purposes, the reactions were again only conducted for the derivatives $Y = \text{Cl}$ and Br . First, salt exchange was approached for $\text{Na}_2\text{d}hbq^{\text{Cl}}$ with PPh_4Cl . There, one could observe that the reaction either proceeded in water or in a mixture of dichloromethane/acetone with a certain amount of water. Problems occurred trying to isolate the final product as their solubility was very similar to the starting materials. The phases were separated, and the aqueous phase was extracted once with dichloromethane. The organic phases were combined, and the solvent was removed under reduced pressure. The resulting solids were suspended in pentane and dichloromethane was added until everything dissolved. After cooling to $-20\text{ }^\circ\text{C}$ for 24 h, fine precipitate developed which was collected by filtration and washed with little cold dichloromethane. After drying *in vacuo* for several hours, the product was obtained as light pink powder in good yield. Red crystals could be obtained by gaseous diffusion of pentane into solutions of dichloromethane. But scXRD analysis revealed that the cation exchange was incomplete, meaning $[\text{d}hbq^{\text{Cl}}][\text{PPh}_4][\text{Na}]$ was obtained. However, after some synthetic attempts the final product $[\text{d}hbq^{\text{Cl}}][\text{PPh}_4]_2$ was obtained in yields of 83 % as confirmed by NMR spectroscopy and elemental analysis. Similar problems as above were observed when carrying out the salt metathesis with $\text{N}^n\text{Bu}_4\text{Cl}$. Isolation of the chlorinated and brominated products resulted in dark red wax-like solids. The product $[\text{d}hbq^{\text{Cl}}][\text{N}^n\text{Bu}_4]_2$ was obtained in yields up to 92 % as confirmed by NMR spectroscopy and elemental analysis, whereas for the brominated species the elemental analysis was not consistent with the theoretical data. Here, the isolation of the main product was also problematic due to very similar solubility features compared to $\text{N}^n\text{Bu}_4\text{Cl}$ or the side product NaCl . Due to the wax-like consistency it may be possible that the strong deviation in the elemental analysis originates from NaCl or extant starting material

$N^{\bullet}Bu_4Cl$. Both potential impurities cannot be properly observed by NMR spectroscopy in presence of the main product.

Since the salt metatheses proved to be difficult, the reaction was not extended to further derivatives and was left at the results from above. However, as the enhancement of solubility and thus crystallization with addition of 15-crown-5 was successful, at least for the chlorinated derivative, it was decided to subsequently react all other Na_2dhhq^Y salts with crown ether and isolate the outcome (Scheme 18). To ensure complete complexation the mixtures were stirred for 18 h in dichloromethane at room temperature. The resulting colored and voluminous solids were collected by filtration, washed with dichloromethane/pentane and dried *in vacuo* for one day. For $Y = Cl, Br, Ph$ and NO_2 yields of 77 %, 87 %, 90 % and 71 % were obtained, respectively.



Scheme 18: Deprotonation and subsequent complexation of substituted 1,4-dihydroxy-*p*-benzoquinone H_2dhhq^Y ($Y = Cl, Br, Ph, NO_2$) to the tetraoxolene salts $[dhhq^Y][Na@15c5]_2$.

Moreover, $[dhhq^{Ph}][Na@15c5]_2$ could be crystallized from saturated solutions in dichloromethane at room temperature (Figure 27a) and $[dhhq^{NO_2}][Na@15c5]_2$ from saturated solutions in DMSO (Figure 27b), each with residual solvent molecules. Analytical purity of the linkers could be confirmed by NMR spectroscopy and elemental analysis.

Synthesis of the fluorinated derivate *via* nucleophilic substitution reaction according to SUTTON and coworkers was also attempted.¹⁹⁵ 2,3,5,6-Tetrafluoro-*p*-benzoquinone was reacted with aqueous NaOH (8 M) solution in 1,4-dioxane yielding a brown precipitate, which should represent Na_2dhhq^F . The brown solid was collected by filtration and dried *in vacuo*. The ^{19}F NMR spectrum in D_2O revealed one main signal with a chemical shift at $\delta = -122.3$ ppm and a smaller one at $\delta = -177.4$ ppm. While the downfield shifted main signal could be assigned to Na_2dhhq^F , for which only one

signal is expected, absolute proof is pending due to missing comparisons from the literature. However, the second smaller signal could not be further explained. For the starting material a different chemical shift at $\delta = -146.6$ ppm in acetone- d_6 is reported.¹⁹⁶ Also ^{13}C NMR spectroscopy failed to give further insights.

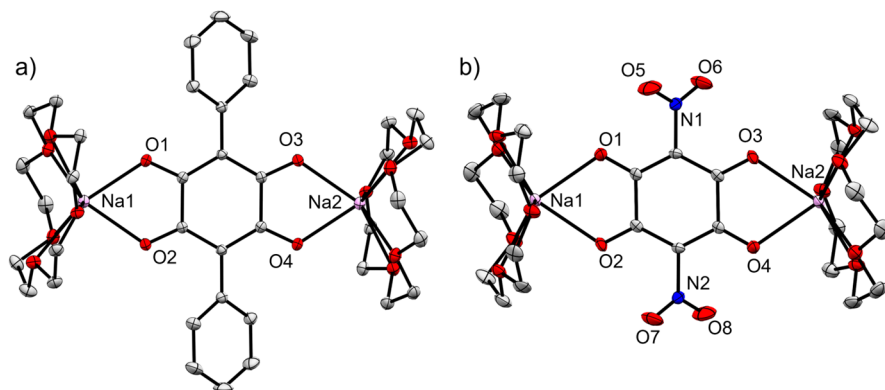


Figure 27: Front view of the solid-state molecular structures of a) $[\text{dhbq}^{\text{Ph}}][\text{Na@15c5}]_2$ and b) $[\text{dhbq}^{\text{NO}_2}][\text{Na@15c5}]_2$ as ORTEP plot. The thermal displacement ellipsoids are shown at the probability level of 50 %. Hydrogen atoms and co-crystallized solvent molecules are omitted for clarity.

In addition, attempts were made to deprotonate the unsubstituted $\text{H}_2\text{dhbq}^{\text{H}}$ with NaH in acetonitrile. The mixture turned blood red and a vigorous gas development was observed. The reaction was further stirred at room temperature for 18 h yielding a brown suspension. The brown solids were collected by filtration and washed with acetonitrile/dichloromethane. After drying *in vacuo*, the product was obtained in quantitative yields. IR spectroscopy confirmed the absence of OH stretching vibrations. Due to the pronounced insolubility of the solids in common organic solvents, NMR spectra were measured in D_2O , giving a wine-red solution. A signal was observed at $\delta = 5.36$ ppm (Figure 28a) in the ^1H NMR spectrum which does not fit the chemical shift according to the literature.¹⁹⁷ However, in the ^{13}C NMR spectrum, two signals were observed at $\delta = 181.9$ and 101.3 ppm, of which the latter one was observed as a triplet with 1:1:1 intensity and a coupling constant of $J = 24.0$ Hz (Figure 28b). This was in good agreement with reported couplings between carbon and deuterium nuclei,¹⁹⁸ meaning that a H/D exchange must have happened. Measuring another ^1H NMR experiment of the exact same sample the next day, revealed the disappearance of the signal at $\delta = 5.36$ ppm. To eliminate any errors,

the synthesis was repeated according to the literature with sodium methoxide in DMSO. Similar outcome was observed as above, and IR spectroscopy and elemental analysis indicated successful deprotonation. Nevertheless, investigation of the obtained compound by NMR spectroscopy confirmed the correctness of the results above, which means that the signal at $\delta = 5.36$ ppm can be assigned to the protons of $\text{Na}_2\text{d}hbq^{\text{H}}$ and that a fast H/D exchange seems to happen in D_2O . Apparently the corresponding authors in the literature procedure have mistakenly assigned the residual proton signal of the deuterated solvent to the product.¹⁹⁷ Aside from that, further implementation of $[\text{d}hbq^{\text{H}}]\text{Na}_2$ with 15-crown-5 unfortunately did not work out as with the substituted analogues.

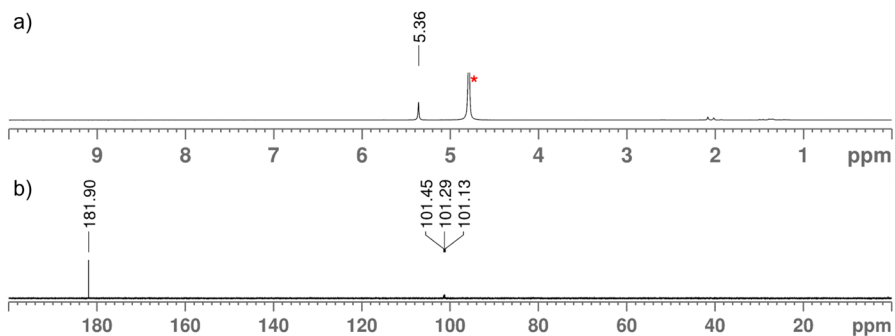


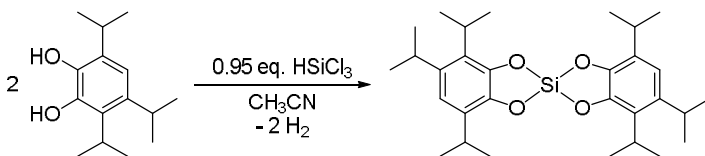
Figure 28: a) ¹H NMR (200 MHz) and b) ¹³C NMR (151 MHz) spectra of $\text{Na}_2\text{d}hbq^{\text{H}}$ in D_2O .

Lastly, the synthesis of $\text{Na}_2\text{d}hbq^{\text{CF}_3}$ was tested by reacting $\text{Na}_2\text{d}hbq^{\text{H}}$ with trifluoromethyl thianthrenium triflate ($\text{TT-CF}_3\text{-OTf}$)^j as novel trifluoromethylation reagent.¹⁹⁹ The reaction mixture was stirred in acetonitrile at -40 °C and slowly warmed to room temperature overnight. A brown suspension was obtained. Unfortunately, investigations of the solids and the supernatant confirmed that no reaction took place. Since this challenging type of reaction is beyond the scope of this work, no further efforts regarding $\text{Na}_2\text{d}hbq^{\text{CF}_3}$ were made.

^j $\text{TT-CF}_3\text{-OTf}$ was prepared by T. THORWART during his doctoral thesis according to literature known procedure.¹⁹⁹

3.3.2 Synthesis and Characterization of 2^{iPr}

With analytically pure $\text{H}_2\text{cat}^{\text{iPr}}$ (chapter 3.2.1) in hand the synthesis of the new GREB-type silicon Lewis acid 2^{iPr} now could be tackled.^k This was accomplished analogous to the established synthesis of 2^{X} ($\text{X} = \text{Cl}, \text{Br}, \text{CF}_3$).³¹⁻³³ Thereby, $\text{H}_2\text{cat}^{\text{iPr}}$ was dissolved in acetonitrile and reacted with an excess of HSiCl_3 (1.2 eq.). The mixture immediately darkened, and gas development was observed. Over time the solution decolored, and light brown solids formed. The precipitate was of very sticky nature, whereas the usage of a broad Schlenk tube was more advantageous for proper stirring and thus complete conversion. After isolating the solids by washing with acetonitrile and drying under reduced pressure, NMR measurements were conducted. The ^{29}Si -INVGATE NMR spectrum revealed a signal at $\delta = -41.0$ ppm and indicated the successful synthesis of 2^{iPr} . For comparison, the similar Lewis acid 2^{tBu} exhibited a chemical shift of $\delta = -41.7$ ppm (^{29}Si MAS NMR) in its monomeric form after sublimation.¹⁸³ However, another small signal at $\delta = -26.8$ ppm was observed additionally. It was hypothesized that the latter signal must originate from an incomplete conversion, due to the usage of excess HSiCl_3 . This might lead to intermediates such as $\text{Cl}_2\text{Si}(\text{cat}^{\text{iPr}})$, which could be consistent with the mentioned chemical shift, when drawing comparisons to similar silanes from literature.^{162, 200} Therefore, the reaction was repeated but this time with a shortfall of HSiCl_3 (0.95 eq.). Indeed, following this synthetic route 2^{iPr} could be synthesized as analytically pure and colorless powder (Scheme 19).



Scheme 19: Synthesis of the new silicon Lewis acid 2^{iPr} analogous to the procedure of GREB *et al.*³¹⁻³³

The amount of solvent used for the synthesis of 2^{iPr} should not be increased proportionally when upscaling the synthesis since the Lewis acid is partially soluble

^k The synthesis of 2^{iPr} was compiled in cooperative work with T. THORWART.

in acetonitrile. Additionally, washing with little amounts of cold acetonitrile is sufficient for the workup of 2^{iPr} . So far, yields up to 64 % were obtained.

Aside from that, it was possible to recycle H_2cat^{iPr} from failed reactions or from the supernatant and washing solutions above. The residues were combined and dried under reduced pressure. After redissolving in dichloromethane, the organic phase was washed with water and with saturated aqueous NaCl solution. Drying over Na_2SO_4 resulted in a clear red solution. Finally, removing the solvent *in vacuo* yielded a dark red and sticky residue. According to NMR spectroscopy H_2cat^{iPr} was thereby obtained in quantitative yields.

3.3.3 Synthesis and Characterization of $[4^{X,Y}][Na@15c5]_2$

Preliminary synthetical approaches towards dimeric structures were at first conducted *in situ* at NMR experiment scale. Thus, the deprotonation was followed by NMR spectroscopy. Subsequently, the Lewis acid was added, and the course of the reaction further monitored. In fact, first single crystal structures could be obtained from such initial NMR experiments. For example, the dimeric dianion $[(cat^{Cl})_2Si(dhbbq^{Cl})Si(cat^{Cl})_2]^{2-}$ $[4^{X,Y}]^{2-}$ was crystallized as PPh_4^+ salt. This could be accomplished in μ mol scale by deprotonating H_2dhbbq^{Cl} with 2 eq. NaH in CD_3CN . After stirring for 1 h 2 eq. PPh_4Cl were added. Over 24 h a colorless precipitate, supposedly NaCl, was observed and removed *via* filtration. Then, addition of 2 eq. $2^{Cl} \cdot (CH_3CN)_2$ facilitated the precipitation of solids, which showed a limited solubility in CD_2Cl_2 . Characterization *via* NMR spectroscopy failed, whereas crystallization by gaseous diffusion of pentane into concentrated solutions in dichloromethane at -40 °C was attempted. Indeed, clear dark red single crystals developed within two months.

SCXRD analysis finally confirmed the successful synthesis and for the first time the solid-state structure of the perchlorinated dimeric derivative $[4^{Cl,Cl}]^{2-}$ as conceptualized in the beginning (Figure 29a). In the same one-pot manner as above, but with the addition of 15-crown-5 after deprotonation, the perbrominated dimeric dianion $[4^{Br,Br}]^{2-}$ could be synthesized as $[Na@15c5]^+$ salt (Figure 29b). Black-violet single crystals were as well obtained after two months from saturated solutions in acetonitrile stored at -40 °C.

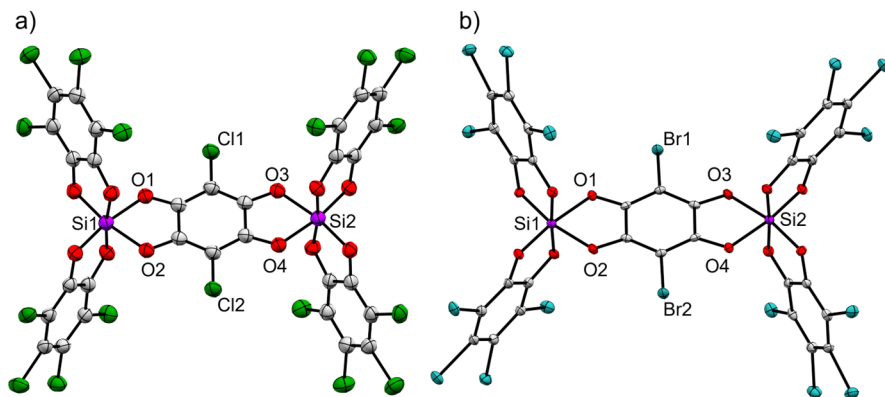


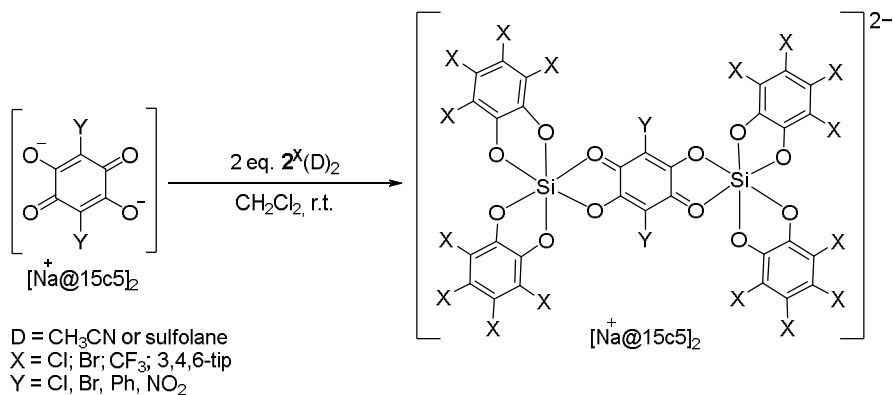
Figure 29: Solid-state molecular structure of a) $[4^{\text{Cl},\text{Cl}}][\text{Na}@15\text{c}5]_2$ and b) $[4^{\text{Br},\text{Br}}][\text{Na}@15\text{c}5]_2$ as ORTEP plot. The thermal displacement ellipsoids are shown at the probability level of 50 %. Cations and co-crystallized solvent molecules are omitted for clarity.

For clean preparative synthesis of the dimeric structures, we decided to isolate and purify the intermediate precursors before implementing them with the Lewis acids. This ensures the usage of the correct amount of starting material and thus complete conversion. Due to the low mass of NaH and its inherent weighing error, the sodium salts of $dhbq^Y$ were first prepared in large-scale amounts and isolated as 15-crown-5 salts (see chapter 3.3.1).

Above all, the linkers $[dhbq^{\text{Cl}}][\text{M}]_2$ ($\text{M} = \text{PPh}_4$ or N^nBu_4) were reacted with $2^{\text{Cl}/\text{Br}}\cdot(\text{CH}_3\text{CN})_2$. Thereby, very different outcomes were obtained. Reproduction of the salt $[4^{\text{Cl},\text{Cl}}][\text{PPh}_4]_2$ in larger scale turned out to be tricky. Mixing the starting materials in dichloromethane yielded a dark red reaction solution. Since $2^{\text{Cl}}(\text{CH}_3\text{CN})$ as very insoluble reagent was completely consumed, a conversion to the expected product was assumed. But crystallization attempts and scXRD analysis revealed the synthesis of half of the dimeric compound only, meaning $[(\text{cat}^{\text{Cl}})_2\text{Si}(dhbq^{\text{Cl}})][\text{PPh}_4]_2$. Yet, another crystallization sample yielded crystals of $[4^{\text{Cl},\text{Cl}}][\text{PPh}_4]_2$ with the same cell parameters as the structure obtained from initial NMR experiments. Moreover, implementation of the linker with $2^{\text{Br}}\cdot(\text{CH}_3\text{CN})_2$ led to the synthesis of $[4^{\text{Br},\text{Cl}}][\text{PPh}_4][\text{Na}]$. It seems that $[dhbq^{\text{Cl}}][\text{PPh}_4]_2$ is still contaminated with NaCl, leading to undetermined reactivity. Still, the single crystal structure showed the successful compounding of the first mixed halogenated dimer $[4^{\text{Br},\text{Cl}}]^{2-}$.

The combination of $[dhbq^{Cl}][N^nBu_4]_2$ with $2^{Cl} \cdot (CH_3CN)_2$ delivered $[4^{Cl,Cl}][N^nBu_4]_2$ in fair yields of 55 %. Single crystals were obtained, of which scXRD analysis could confirm solely the connectivity of the dianion. However, reaction with $2^{Br} \cdot (CH_3CN)_2$ did not provide the favored dimeric compound, but the chloride adduct $[2^{Br-Cl}][N^nBu_4]$, which crystallized from the reaction mixture. Similar outcome was observed when using $[dhbq^{Br}][N^nBu_4]_2$, which suggests that those linkers still must be impure with NaCl. Consequently, due to the ambiguous reactivity of $[dhbq^{Cl/Br}][M]_2$ ($M = PPh_4$ or N^nBu_4) presumably originating from impurities that were not detectable *via* NMR spectroscopy, and the relatively effortful synthesis, further application of those linkers was discontinued for now.

The synthesis of $[4^{X,Y}]^{2-}$ was thenceforth conducted with the $[dhbq^Y][Na@15c5]_2$ salts (Scheme 20). At first, the perhalogenated compounds were addressed. The linkers $[dhbq^Y][Na@15c5]_2$ ($Y = Cl$ and Br) were mixed with 2 eq. of Lewis acid $2^{Cl/Br} \cdot (CH_3CN)_2$ and suspended in dichloromethane under inert conditions. Thereby, the red suspensions rapidly turned to black-red and opaque mixtures. After stirring for 18 h at room temperature, the reaction mixtures appeared grey, implying that the starting materials had been consumed. The solids were collected by filtration, washed with dichloromethane/pentane several times and dried *in vacuo* for 24 h.



Scheme 20: Synthesis of the dinuclear silicon tetraoxolene salts $[4^{X,Y}][Na@15c5]_2$ ($X = Cl, Br, CF_3, iPr$ and $Y = Cl, Br, Ph, NO_2$) starting from $[dhbq^Y][Na@15c5]_2$ and $2^X(D)_2$ ($D = CH_3CN, sulfolane$ or none).

The dinuclear silicon tetraoxolene salts $[4^{X,Y}][\text{Na}@15\text{c}5]_2$ were isolated as elementally pure, grey powders in all possible combinations ($X, Y = \text{Cl, Cl; Br, Br; Cl, Br}$ and Br, Cl) in yields of 80-95 %. For $X, Y = \text{Cl, Cl; Br, Br}$ and Cl, Br single crystals suitable for scXRD analysis could be obtained by gaseous diffusion of dichloromethane into concentrated solutions in acetonitrile at -40°C . SCXRD analysis confirmed the dimeric structure as obtained from initial *in situ* NMR experiments (*vide supra*, Figure 30a). For $X, Y = \text{Br, Cl}$ the connectivity could be verified as well.

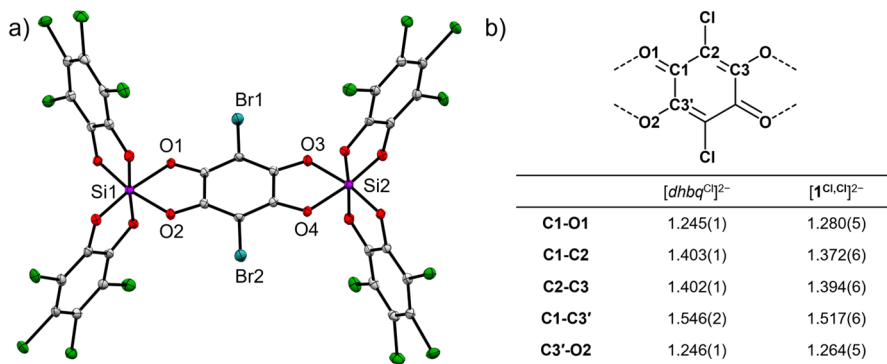


Figure 30: a) Solid-state molecular structure of the hetero-perhalogenated dimeric derivative $[\mathbf{4}^{\text{Cl,Br}}][\text{Na}@15\text{c}5]_2$ as ORTEP plot. The thermal displacement ellipsoids are shown at the probability level of 50 %. Cations and co-crystallized solvent molecules are omitted for clarity. b) Selected bond lengths [Å] of $[\text{dhbq}^{\text{Cl}}]^{2-}$ and $[\mathbf{4}^{\text{Cl,Cl}}]^{2-}$ given in tabular form for comparison.

Comparison of the metric parameters of $[\mathbf{4}^{\text{Cl,Cl}}]^{2-}$ with the respective free linker $[\text{dhbq}^{\text{Cl}}]^{2-}$ showed significant changes in bond lengths. Shortening of the C1-C2, C2-C3, C1-C3' and elongation of the C1-O1 and C3'-O2 bonds were observed within the dimeric complex (Figure 30b), being in line with a more reduced state of the dhbq^{Cl} linker.¹⁴⁷ Similar observations were made within dinuclear cobalt(III) complex $[\text{Co}_2(\text{dhbq}^{\text{H}})(\text{triphos})_2][\text{BF}_4]_2$ synthesized by HUTNER *et al.*²⁰¹ Hence, the external catecholates were suspected as source of electron density. In regard of the MOS a slight decrease was observed for the average of the four catecholates (see Appendix, Table 15).

Further, the four complexes were characterized by NMR spectroscopy. Signals for the cation were clearly visible in the ^1H and ^{13}C NMR spectrum. In addition, the ^{13}C NMR spectra allowed a clear assignment of characteristic signals for the catecholato

units and for the *dhbq*-linker of the dimeric disilicates (Figure 31). The signals for the linker within the dimers were shifted upfield compared to the linker as *free* sodium salts (*e.g.* for Y = Cl,Cl; $C_{dhbq}O$ 170.6 vs. 174.1 ppm, respectively). In the ^{29}Si -INVGATE NMR spectra only one signal for each of the complexes was observed as well (Figure 32a-d). For example, the perchlorinated derivative exhibited a signal with a chemical shift at $\delta = -130.1$ ppm, which lies in the range of hexacoordinated silicon species.¹⁶²

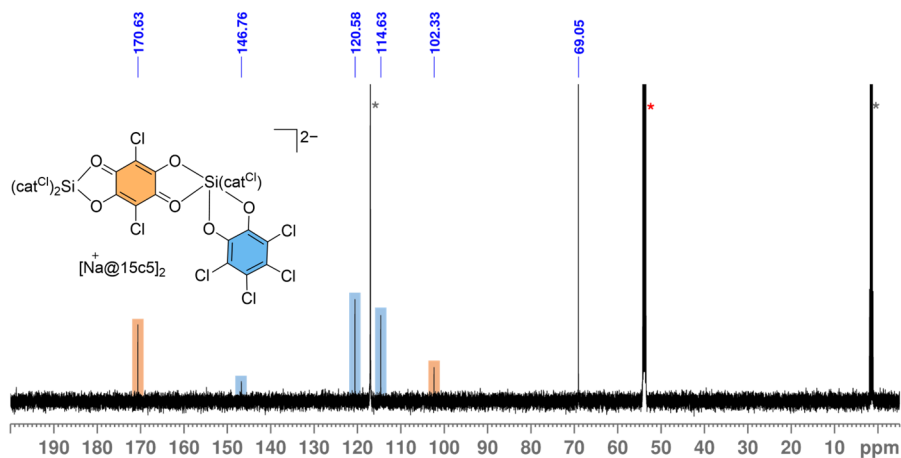


Figure 31: ^{13}C NMR spectrum (151 MHz, $CD_2Cl_2^*$) of $[4^{Cl,Cl}][Na@15c5]_2$ with residual acetonitrile (*). The set of signals for the carbon atoms of the catechol ligands is marked with blue boxes and of the tetraoxolene linker with orange boxes.

Despite their grey appearance in solid state, dissolving the perhalogenated dimers in dichloromethane yields dark red colored solutions. Investigations of a solution of $[4^{Cl,Cl}][Na@15c5]_2$ via UV-vis spectroscopy thereby revealed absorptions bands at $\lambda = 472$ nm with broad shoulders at $\lambda = 440$ and 500 nm, which are absent for the respective free linker and in line with the color of the complexes in solution or in crystalline state (Figure 33). Besides, the dimeric complexes were found to be stable and remain soluble in acetonitrile for prolonged time, whereas the Lewis acids $2^{Cl/Br}$ form insoluble bis-acetonitrile adducts. However, using the stronger donating solvent THF yielded colorless precipitation, which means the products are reverted to *dhbq*^{Cl/Br} salts and $2^{Cl/Br} \cdot (THF)_2$ and thus displaying a possibility for reversible product formation.

3 Results and Discussion

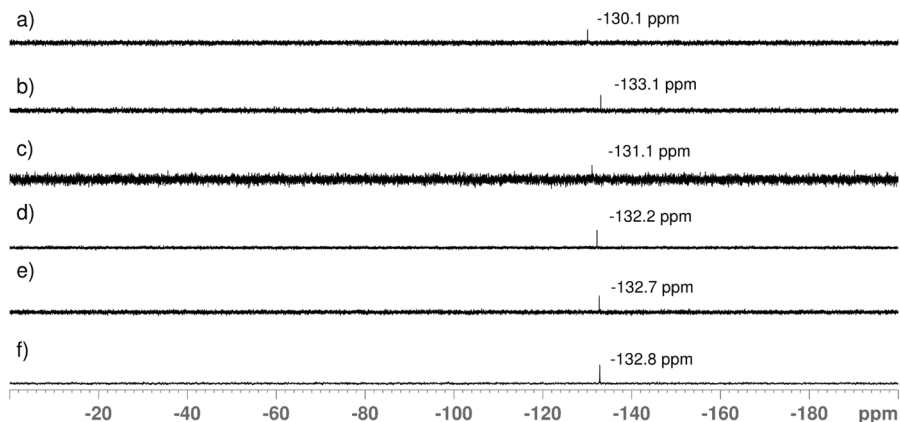


Figure 32: ^{29}Si -INVGATE NMR spectra (119 MHz, CD_2Cl_2) of $[\mathbf{4}^{\text{X,Y}}][\text{Na}@15\text{c}5]_2$ with X,Y = a) Cl,Cl b) Br,Br c) Cl,Br d) Br,Cl e) Cl,Ph and f) CF_3 ,Ph.

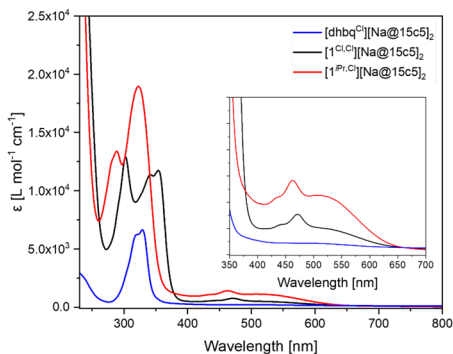


Figure 33: Comparison of UV-vis absorption spectra of identical concentrations (0.65 mM) of $[\text{dhubq}^{\text{Cl}}][\text{Na}@15\text{c}5]_2$ (blue), $[\mathbf{1}^{\text{Cl,Cl}}][\text{Na}@15\text{c}5]_2$ (black) and $[\mathbf{1}^{\text{Pr,Cl}}][\text{Na}@15\text{c}5]_2$ (red) in CH_2Cl_2 with a closer view between $\lambda = 350$ and 700 nm (inset).

Moreover, it was attempted to influence the electronic structure of the system through structural variations of the Lewis acid or dhubq^{Y} -linker. At first, the linker was altered by introducing $[\text{dhubq}^{\text{Ph}}][\text{Na}@15\text{c}5]_2$ as more electron-rich linker. Similar to the synthesis of the perhalogenated derivative, combination with $\mathbf{2}^{\text{Cl/Br}} \cdot (\text{CH}_3\text{CN})_2$ led to green and brown reaction mixtures, respectively. $[\mathbf{4}^{\text{Cl,Ph}}][\text{Na}@15\text{c}5]_2$ was isolated as green powder in 78 % yield. The compound could be characterized *via* elemental analysis and NMR spectroscopy. The ^{29}Si -INVGATE NMR spectrum revealed a signal

with the chemical shift at $\delta = -132.7$ ppm, consistent with the derivatives from above (Figure 32e). Saturated solutions in dichloromethane yielded dark-green single crystals suitable for scXRD analysis (Figure 34a).

As for the perhalogenated dimeric derivative (Figure 30b), the solid state molecular structure of $[4^{\text{Cl,Ph}}]^{2-}$ shows a significant shortening of the C1-C2, C2-C3, C1-C3' bonds and elongation of the C1-O1 and C3'-O2 bonds compared to the free linker $[d\text{hbq}^{\text{Ph}}]^{2-}$ (Figure 34b), which speaks for a more reduced state of the linker in $[4^{\text{Cl,Ph}}][\text{Na}@15\text{c}5]_2$. Accordingly, the calculation of the MOS of the external catecholates describes a slight reduction of their oxidation state (see Appendix 7.4, Table 15).

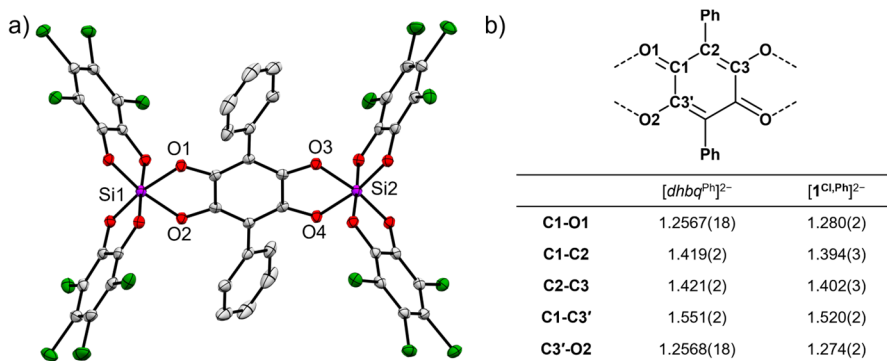


Figure 34: a) Solid-state molecular structure of $[4^{\text{Cl,Ph}}][\text{Na}@15\text{c}5]_2$ as ORTEP plot. The thermal displacement ellipsoids are shown at the probability level of 50 %. Cations and co-crystallized solvent molecules are omitted for clarity. b) Selected bond lengths [Å] of $[d\text{hbq}^{\text{Ph}}]^{2-}$ and $[4^{\text{Cl,Ph}}]^{2-}$ given in tabular form for comparison.

In contrast, the combination X,Y = Br,Ph turned out to be less stable and thus difficult to isolate. The reaction in dichloromethane yielded a dark brown solution alongside with colorless precipitate, which firstly implied an incomplete reaction. It was further stirred for some days, after which still no change in reaction could be observed. Thus, the solids were removed by filtration. Pentane was added to the filtrate to precipitate the product. The dark brown solids were then washed with pentane and dried under reduced pressure. However, investigations *via* NMR spectroscopy revealed the existence of several silicon species in the ^{29}Si -INVGATE NMR spectrum. Also, the elemental analysis did not fit with the calculated data.

Saturated solutions in dichloromethane yielded dark crystalline material which, however, could not be examined *via* scXRD analysis. From the washing solutions colorless precipitation was observed, which were assigned to the starting material **2**^{Br}·(CH₃CN)₂ by IR spectroscopy. In conclusion, the compound does not appear to be long-term stable in solution.

Then, another more electron-deficient linker was introduced. [*dhbq*^{NO₂}][Na@15c5]₂ was implemented with **2**^{Cl}·(CH₃CN)₂ in dichloromethane, yielding a grey solid in 75 % yield, similar to the perhalogenated derivatives. The low solubility of [**4**^{Cl,NO₂}][Na@15c5]₂ did not allow its characterization *via* NMR spectroscopy and decomposition was observed in acetonitrile already after some minutes. However, the purity of [**4**^{Cl,NO₂}][Na@15c5]₂ could be finally confirmed through elemental analysis.

After altering the linker, modification of the Lewis acid was carried out. For this purpose, **2**^{CF₃}·(sulfolane)₂ and **2**^{iPr} were introduced. At first, the highly electron-deficient Lewis superacid **2**^{CF₃} was combined with [*dhbq*^{Ph}][Na@15c5]₂ in dichloromethane, yielding a dark yellow solution. The product seemed to have an improved stability compared to the perhalogenated dimers only allowing its isolation after the addition of excess pentane. The solids were collected by filtration and dried *in vacuo* for 24 h. [**4**^{CF₃,Ph}][Na@15c5]₂ was obtained analytically pure as brown powder in yields up to 92 %. Sharp signals were observed in the NMR spectra. Due to the intense fluorine content and coupling, not all signals could be properly assigned in the ¹³C NMR spectrum, but the ²⁹Si-INVGATE shift provided a signal at $\delta = -132.8$ ppm (Figure 32f), implying a hexavalent silicon center in solution. Later, the connectivity of [**4**^{CF₃,Ph}][Na@15c5]₂ could be confirmed by scXRD analysis of single crystals obtained through gaseous diffusion of dichloromethane into concentrated solutions of acetonitrile at room temperature (Figure 35).

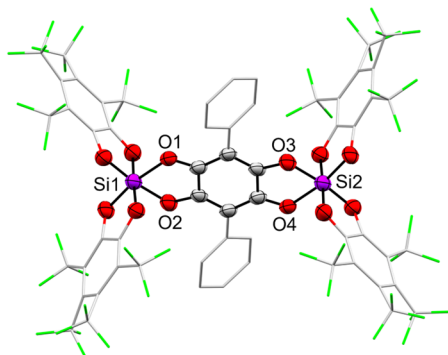


Figure 35: Solid-state molecular structure of $[4^{CF_3,Ph}][Na@15c5]_2$, connectivity shown only. The thermal displacement ellipsoids are shown at the probability level of 50 %. Cations, protons, and co-crystallized solvent molecules are omitted for clarity.

Next, 2^{iPr} was compounded with $[dhhq^{Cl/Br}][Na@15c5]_2$ in dichloromethane yielding dark red to violet solutions. The presence of numerous isopropyl groups resulted in pronounced solubilities of the products in common organic solvents. Therefore, precipitation with pentane did not allow quantitative isolation of the respective dimeric compounds. Thus, the solvent was removed *in vacuo*, and the resulting solids were further dried. Elemental analysis indicated that the samples still contained residual solvent, however drying for another 24 h *in vacuo* did not improve its purity. Also, various crystallization attempts failed since the products only separated as oils from the solvent mixtures. Interestingly, investigations *via* 1H NMR spectroscopy revealed a peak integral ratio of anion/cation that is smaller than the expected 1:2 ratio. Besides, broader signals for the isopropyl groups were observed, indicating a populated triplet diradical state of the anion (*vide infra*, chapter 3.3.4). Accordingly, no signal was obtained in the ^{29}Si -INVGATE NMR spectrum. UV-vis spectroscopy of $[4^{iPr,Cl}][Na@15c5]_2$ in dichloromethane in the visible range showed absorption bands at $\lambda = 462$ nm with two broad shoulders at $\lambda = 430$ and 525 nm, being in line with the dark red appearance both in solid state and solution (Figure 33). Similar features were found for the perchlorinated analogue but with a weaker extinction coefficient. With electrospray ionization (ESI⁻) mass spectrometry of samples in dichloromethane, reasonable high-resolution masses were observed for fragments of the derivatives X, Y = iPr, Cl/Br (Figure 36). With that, the connectivity between the *dhhq* linker and the catecholato ligand with silicon could be demonstrated as existent.

3 Results and Discussion

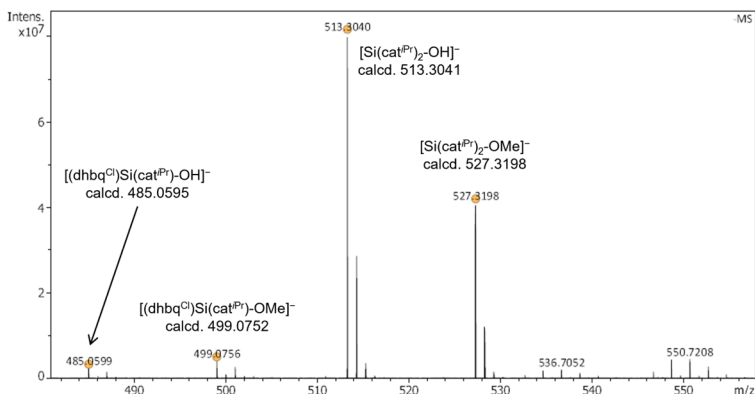


Figure 36: High resolution mass spectrum (ESI neg.) of $[4^{iPr,Cl}][Na@15c5]_2$ dissolved in CH_2Cl_2 (10^{-6} M) with the assignment of respective mass fragments.

Lastly, 2^{iPr} was combined with $[dhbq^{NO_2}][Na@15c5]_2$. A green-brown solution was obtained. After removing the solvent and drying the solids *in vacuo*, $[4^{iPr,NO_2}][Na@15c5]_2$ was obtained as green-brown powder in quantitative yields. Similar features as for the derivatives X, Y = iPr, Cl/Br could be observed. Signals in the 1H NMR spectrum were very broad and barely visible in the ^{13}C NMR spectrum, except for the cation. Also, no signal for a diamagnetic silicon species could be found.

Moreover, $[4^{iPr,Y}][Na@15c5]_2$ (Y = Cl, Br, NO_2) were found to be soluble and stable in THF, in contrast to the other dimeric derivatives. Yet, crystallization attempts by gaseous diffusion of pentane into solutions of THF were not successful. To decrease the solubility of those compounds, it was probed to synthesize the dinuclear silicon species starting from the crown-ether free sodium salts. Subsequently, 2^{iPr} was mixed with $[dhbq^Cl]Na_2$ in dichloromethane. At first no reaction occurred. This can be probably explained by the low solubility of the sodium salts in dichloromethane. Therefore, the solvent was changed to the more polar solvent acetonitrile which immediately led to a darkening of the mixture. After some hours a violet solution was obtained. Broad signals in the 1H NMR spectrum and no signals in the ^{13}C and ^{29}Si -INGATE NMR spectra confirmed that the consumption of the starting materials. Through gaseous diffusion of dichloromethane into concentrated solutions of acetonitrile dark crystalline as well as colorless precipitate could be obtained. However, only the latter ones were suitable for scXRD analysis revealing the structure

of fully reduced dimeric silicon catecholato species $[(cat^{iPr})_2Si(cat^{iPr})Si(cat^{iPr})_2]^{2-}$ $[3^{iPr}]^{2-}$ as sodium salt with an acetonitrile molecule coordinated to each cation (Figure 37), reminiscent of an alternate product obtained in the comproportionation reaction between 1^{Cl} and $[1^{Cl}][H_2N^oPr_2]_2$ through hydrogen bond activation (see chapter 3.1.4).

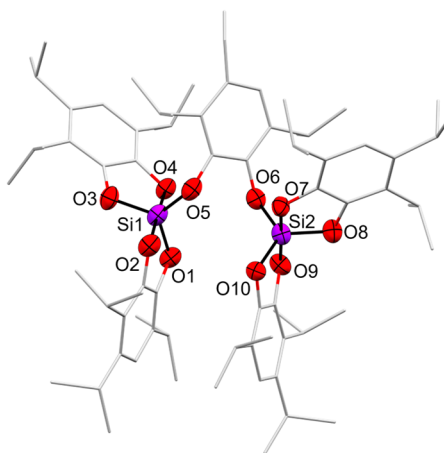


Figure 37: Unrefined solid-state molecular structure of $[3^{iPr}]Na_2$. The thermal displacement ellipsoids are shown at the probability level of 50 %. Cations, hydrogen atoms and co-crystallized solvent molecules are omitted for clarity.

3.3.4 Investigating the Magnetic Properties¹

Since it was attempted to influence the electronic structure of the system by varying the Lewis acid 2^X and the $dhbq^Y$ linker, the magnetic properties of the dimeric compounds were additionally studied by EPR spectroscopy.

The sharp peaks in the NMR spectra of $[4^{Cl,Cl}][Na@15c5]_2$ suggested a predominant closed shell character in solution (Figure 31 and Figure 32). Surprisingly, EPR spectroscopy of analytically pure $[4^{Cl,Cl}][Na@15c5]_2$ in acetonitrile or the solid sample at 7.5 K exhibited signals at normal field and a weak signal at half-field, confirming

¹ The quantum chemical computations in this chapter were conducted by Prof. Dr. L. GREB and T. THORWART.

a populated triplet diradical state. However, EPR measurements of the same samples in dichloromethane or TCE showed barely visible signals at normal field and no signal at half-field, rendering the diradical state stability strongly depending on the environmental polarity. For the electronically similar derivatives $[4^{X,Y}][\text{Na}@15\text{c}5]_2$ ($X,Y = \text{Br,Br}; \text{Cl,Br}; \text{Br,Cl}$) identical EPR spectroscopic observations as for $[4^{\text{Cl,Cl}}][\text{Na}@15\text{c}5]_2$ were made.

Interestingly, NMR investigations of solutions of analytically pure $[4^{\text{iPr,Cl}}][\text{Na}@15\text{c}5]_2$ (see chapter 3.3.3) indicated an extensively populated triplet diradical state of the anion. Accordingly, a solution of $[4^{\text{iPr,Cl}}][\text{Na}@15\text{c}5]_2$ already in less polar TCE showed an intense EPR signal at normal field and a strong peak at half-field at 6.4 K (Figure 38). VT EPR measurements from 6 to 110 K led to a decreasing $I \times T$ vs. T plot (Figure 39), characteristic of a triplet ground state with a thermally populated singlet state.

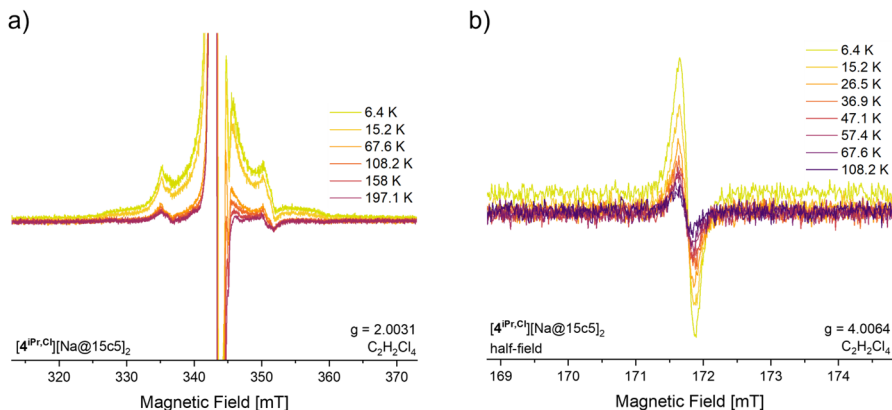


Figure 38: VT EPR of $[4^{\text{iPr,Cl}}][\text{Na}@15\text{c}5]_2$ in TCE ($\text{C}_2\text{H}_2\text{Cl}_4$) at a) normal field and b) half-field. Parameters: frequency 9.6321 GHz, power 1.258 mW, modulation 1 G.

Hence, quantum theoretical computations (restricted and unrestricted PW6B95-D4/def2-QZVPP//r2scan-D4 level of theory) were performed to guide the experimental findings. Computations of anionic or dianionic diradicals have been found difficult in earlier reports, but were tackled by the explicit consideration of counteranions.²⁰²⁻²⁰⁵ Thus, all computations were performed on the respective salts with $[\text{Na}@15\text{c}5]^+$ and one additional CH_3CN coordinated to sodium, in analogy to the

available scXRD structures. The triplet state of the precursor linker salt $[d\text{hb}q^{\text{Cl}}][\text{Na}@15\text{c}5]_2$ lies at $143 \text{ kJ}\cdot\text{mol}^{-1}$ above the closed shell singlet state (Table 4, entry a). In agreement with the experimental observations, this appears inaccessibly high for a population at room temperature. For $[4^{\text{Cl}\cdot\text{Cl}}][\text{Na}@15\text{c}5]_2$, a substantially diminished gap between closed shell and triplet state energies was computed ($30.9 \text{ kJ}\cdot\text{mol}^{-1}$, Table 4, entry b). The triplet state appears still relatively high in energy to be populated at room temperature (as observed by experiment), but alternative orientations of the cation (e.g., *via* coordination of $[\text{Na}@15\text{c}5]^+$ to the $-\text{Cl}$ at $d\text{hb}q^{\text{Cl}}$) are suspected of causing further triplet state lowering in solution. The open shell singlet solution (broken symmetry, *BS*) is comparable to the triplet state, and an antiferromagnetic (negative) coupling constant J is obtained. Excitingly, for $[4^{\text{iPr}\cdot\text{Cl}}][\text{Na}@15\text{c}5]_2$, the triplet state becomes indeed favored by $-4.7 \text{ kJ}\cdot\text{mol}^{-1}$ in comparison to the closed shell solution (Table 4, entry c). The spin density within $[4^{\text{iPr}\cdot\text{Cl}}]$ is delocalized across the central $d\text{hb}q^{\text{Cl}}$ unit and the external 2^{iPr} fragments (Figure 40).

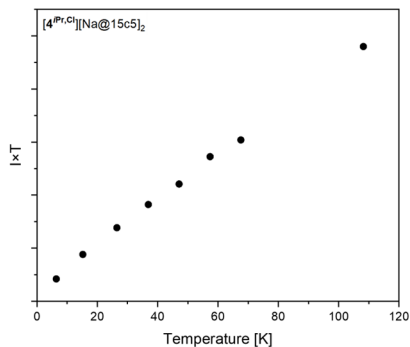


Figure 39: $I \times T$ vs. T plot based on VT EPR measurements of frozen solution samples of $[4^{\text{iPr}\cdot\text{Cl}}][\text{Na}@15\text{c}5]_2$ in TCE, $I \times T$ is the product of the intensity (I) for the forbidden resonance ($\Delta m_s = 2$) at half-field and the respective temperature.

3 Results and Discussion

Table 4: Computed energies and properties of compounds $[4^{X,Y}][\text{Na}@15\text{c}5]_2$.

Entry	Compound ^[a]	ΔE [kJ·mol ⁻¹] vs CS ^[b]		J [cm ⁻¹]	FOD ^[c]
		T ^[b]	BS ^[b]		
(a)	[d h bq ^{Cl}]	143	-	-	0.497
(b)	[4 ^{Cl,Cl}]	30.9	29.9	-79.0	1.679
(c)	[4 ^{iPr,Cl}]	-4.7	-4.6	+4.1	1.902
(d)	[4 ^{Cl,Ph}]	42.1	39.2	-207.0	1.633
(e)	[4 ^{Cl,NO₂}]	8.8	8.6	-15.7	1.869
(f)	[4 ^{CF₃,Ph}]	87.6	-	-	1.397
(g)	[4 ^{iPr,NO₂}]	-40.8	-40.6	+18.8	2.303

^[a] all compounds computed as salts with two $[\text{CH}_3\text{CN-Na}@15\text{c}5]^+$

^[b] CS = closed shell, T = triplet open shell, BS = broken symmetry open shell singlet

^[c] FOD = fractional occupation density

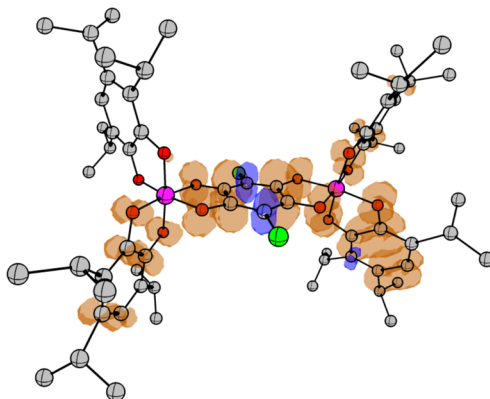


Figure 40: Spin density distribution in the triplet state of $[4^{i\text{Pr,Cl}}][\text{Na}@15\text{c}5]_2$. Cations are omitted for clarity.

The fractional occupation density (FOD), a parameter proportional to the diradical index, was examined next (Table 4).²⁰⁶⁻²⁰⁷ In line with expectations, an increasing FOD occurs the more stabilized the open shell state becomes. Overall, the computed results agree with the observed qualitative trends of EPR and NMR spectroscopy.

Next, it was probed if modifications in $dhbq^Y$ linker provided another handle for tuning the diradical character in the adducts. Combination of the phenyl-substituted $dhbq^{Ph}$ linker with 2^{Cl} yielded $[4^{Cl,Ph}][Na@15c5]_2$. Interestingly, NMR spectra of the salt in CD_2Cl_2 were sharp, and the expected 1:2 peak integral ratio of cation/anion was observed in this case. No EPR activity could be detected in apolar and polar solutions or the solid state. Accordingly, the triplet state is computed more unfavorable as for $[4^{Cl,Cl}][Na@15c5]_2$, along with a lower FOD (Table 4, entry d).

In contrast, the combination of 2^{Cl} with the NO_2 -substituted linker, $[4^{Cl,NO_2}][Na@15c5]_2$, revealed a sample with a strong EPR signal (Figure 41). In line with the experiment, the triplet state of this salt was computed at only 8.8 kJ·mol⁻¹ above the singlet state, along with a larger FOD (Table 4, entry e). Hence, with the more electron-rich linker $dhbq^{Ph}$, the equilibrium is tilted towards the closed shell state, while a more pronounced diradical character is obtained using the electron-poor linker $dhbq^{NO_2}$.

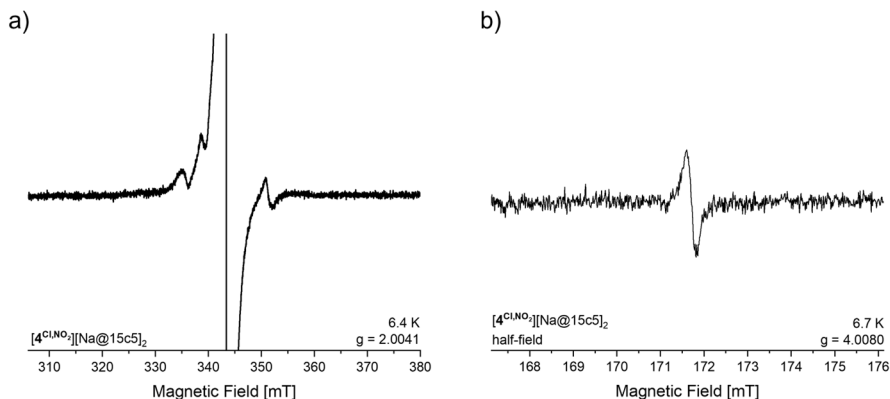


Figure 41: EPR spectrum of $[4^{Cl,NO_2}][Na@15c5]_2$ in solid state at a) normal field, 6.4 K and b) half-field, 7.7 K. Parameters: frequency 9.632 GHz, power 0.6295 mW (3.155 mW for b)), modulation 1 G.

Based on these design principles, two additional Lewis acid/linker combinations were expected to reach most toward the extremes. In line with the hypothesis, the combination of 2^{CF_3} and $dhbq^{Ph}$, $[4^{CF_3,Ph}][Na@15c5]_2$, provided sharp NMR signals and absent EPR activity, while the computed singlet-triplet gap increased

substantially (Table 4, entry f). FOD analysis delivered the smallest diradical character of all considered combinations.

The opposite direction was addressed by combining the electron-rich **2iPr** (the strongest donor) with *dhbq*^{NO₂} (the most potent acceptor). In agreement with the broad signals observed in the ¹H NMR spectrum (see chapter 3.3.3), EPR spectroscopic measurement of [**4iPr,NO₂**][Na@15c5]₂ gave a strong signal at half and normal field (Figure 42). DFT computations confirmed an open shell state that is the most preferred among all combinations, along with the largest FOD (Table 4, entry g).

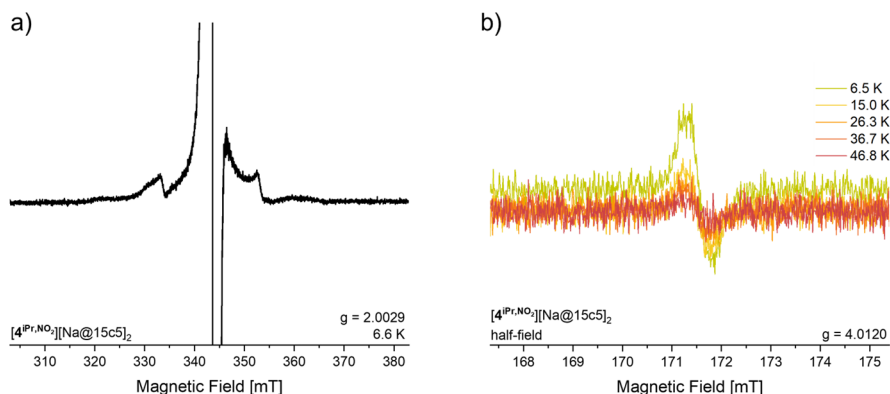


Figure 42: a) EPR spectrum of [**1iPr,NO₂**][Na@15c5]₂ in solid state at 6.6 K at normal field. b) VT EPR spectra of [**4iPr,NO₂**][Na@15c5]₂ in solid state at half-field. Parameters: frequency 9.633 GHz, power 1.257 mW (3.152 mW for b)), modulation 100 kHz.

Unfortunately, due to the low effective magnetic moments of all samples, no quantitative characterization of the magnetic properties, *e.g.*, by VT EPR, Evans' NMR method, or SQUID magnetometry, could be achieved.

3.3.5 Conclusion

In this chapter, a series of ditopic *dhbq*^Y (Y = Cl, Br, Ph, NO₂) linker was synthesized as [Na@15c5]⁺ salts and the new bis(catecholato)silane Lewis acid **2iPr** was introduced. By simply combining the Lewis acids **2^X** (X = Cl, Br, CF₃, iPr) with the

linkers [$dhbq^Y$][Na@15c5]₂ a variety of dinuclear silicon polyoxolenes [$4^{X,Y}$][Na@15c5]₂ was prepared in very good yields. For [$4^{X,Y}$]²⁻ (X = Cl, Br, CF₃ and Y = Cl, Br, Ph) solid-state molecular structures could be obtained, confirming the Lewis formulation for the anionic part as [(*cat*^X)₂Si(*dhbq*^Y)Si(*cat*^X)₂]²⁻. Through scXRD analysis and comparison with the *free* linker salts [$dhbq^Y$]²⁻ (Y = Cl, Ph) a more reduced state of the *dhbq* linker within the complexes could be observed. Sharp NMR-signals were obtained, however EPR spectroscopy revealed also signals for a populated triplet diradical state. An electron transfer from the external catecholates to the internal *dhbq* linker was suspected to be responsible for the EPR activity.

Thus, selective combination of electron-rich Lewis acids and electron-poor *dhbq* linkers was attempted and indeed led to the formation of diradicaloid complexes [$4^{X,Y}$]²⁻ (X = Cl, iPr and Y = Cl, Br, NO₂). Furthermore, with the combination of electron-poor **2**^{CF₃} and electron-rich *dhbq*^{Ph} the opposite extreme, meaning the smallest diradical character, was accomplished. The underlying design principal was additionally disclosed by computational analyses.

It can be concluded that the Lewis acid **2**^X has a twofold task: 1) enhancing the acceptor property of the bridging *dhbq*-unit (lowering the LUMO energy) and 2) providing electron density with the electron-rich catecholato π -systems. Indeed, the FIAs of the employed **2**^X correlate with the LUMO energy lowering in the *dhbq*^Y units caused by Lewis acid binding. The larger the FIA (see Appendix 7.3.2, Table 13), the more pronounced the LUMO lowering. In turn, the HOMO energies of **2**^X determine the ability to donate electron density into the central unit (see Appendix 7.3.2, Table 14). The features of the central *dhbq* provided complementary handles.

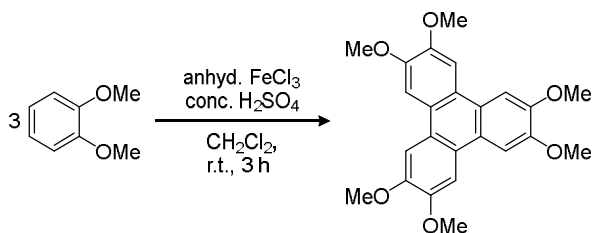
Besides, the dinuclear complexes [$4^{X,Y}$]²⁻ were found to be long-term stable in coordinating environments, such as acetonitrile and THF (partially), which is not possible for the mononuclear silicon diradicals from chapter 3.1 and 3.2.

3.4 Hexaoxolene-bridged Bis(catecholato)silanes

In the following chapter the preparation and investigation of trinuclear silicon polyoxolenes will be covered. At first the synthesis of the precursors 2,3,6,7,10,11-hexamethyltriphenylene (*hmtp*) and 2,3,6,7,10,11-hexahydroxytriphenylene (H_6hhtp) will be discussed. For the formation of neutral open shell structures 2,3,6,7,10,11-hexaketotriphenylene (*hktp*) is required as linking part. Therefore, the oxidation of H_6hhtp to *hktp* will be attempted, which turned out to be synthetically more challenging than expected. Thus, the assembly of the hexaoxolene-bridged bis(catecholato)silanes will be approached over H_6hhtp , wherefor the triphenylene first needs to get deprotonated and subsequently implemented with the perchlorinated Lewis acid 2^{Cl} as bis-acetonitrile adduct. Further, the trimeric complex salts are going to be characterized by NMR and IR spectroscopy.

3.4.1 Synthesis of Precursors

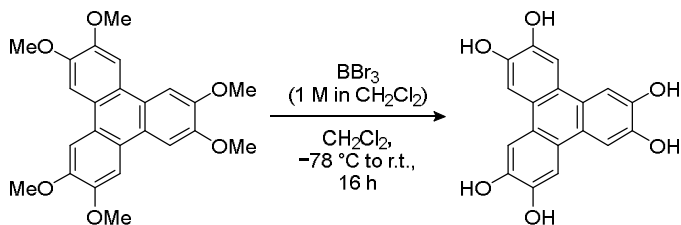
According to the group of WHITE, the triphenylene framework of the polytopic linker *hmtp* is constituted *via* C-C bond formation between three veratrole molecules.²⁰⁸ This was achieved through a SCHOLL reaction in the presence of anhydrous $FeCl_3$ as Lewis acid and concentrated sulfuric acid in dry dichloromethane (Scheme 21). After stirring for 3 h at room temperature, methanol was added to quench the reaction. A grey suspension was observed, of which the solids were collected by filtration and dried *in vacuo* for 24 h to give *hmtp* in yields up to 84 %. Here, it is important to mention, that the usage of anhydrous $FeCl_3$ is crucial for receiving good yields in the preceding reaction step.



Scheme 21: Synthesis of *hmtp* *via* oxidative trimerization of veratrole.²⁰⁸

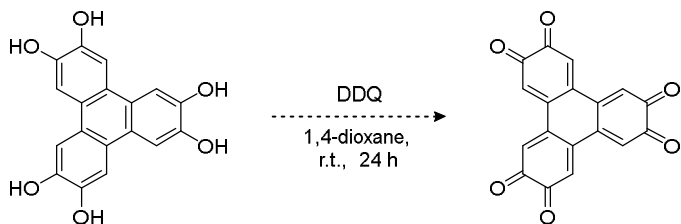
3 Results and Discussion

Next, the cleavage of the methyl ethers of *hmtp* was accomplished using the strong Lewis acid BBr_3 (1 M in CH_2Cl_2) to give H_6hhtp (Scheme 22).¹³⁹ Thereby, the reactants were mixed in dry dichloromethane at -78°C and allowed to warm to room temperature over 16 h. Afterwards the suspension was poured onto ice, the solids were collected by filtration and washed with water. Drying under reduced pressure at 60°C for 24 h finally gave analytically pure H_6hhtp as grey powder in 76 % yields.



Scheme 22: Synthesis of H_6hhtp from *hmtp* via deprotection of the methyl ether groups.¹³⁹

Lastly, it was attempted to generate *hktp* by a sixfold oxidation. Thereby, H_6hhtp was mixed with 2,3-dichloro-5,6-dicyano-*p*-benzoquinone (DDQ) in 1,4-dioxane and stirred at room temperature for 24 h under the exclusion of light (Scheme 23).²⁰⁹



Scheme 23: Synthetic approach to *hktp* by a sixfold oxidation of H_6hhtp with DDQ.²⁰⁹

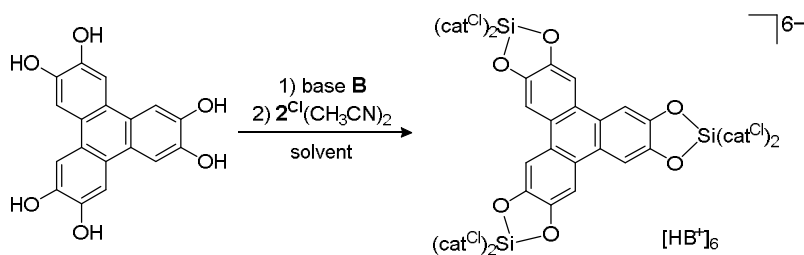
Brown precipitate was obtained and removed. The supernatant solution was concentrated under reduced pressure yielding dark brown solids that were further dried *in vacuo*. Investigations of the solids *via* ^1H NMR spectroscopy indicated a conversion as only one signal was observed at $\delta = 3.64$ ppm in CD_2Cl_2 . But the ^{13}C NMR spectrum also revealed solely one signal at $\delta = 67.4$ ppm. However, the signals were not in agreement with the literature.²⁰⁹ To gain further insights IR measurements were conducted. Surprisingly, in the IR spectrum still a broad band at

$\tilde{\nu} = 3215 \text{ cm}^{-1}$ was observed but none around $\tilde{\nu} = 1750 \text{ cm}^{-1}$ for the ketone moiety, suggesting that either the starting material H_6hhtp or the reduced form of the oxidant (H_2DDQ) must have been isolated. Yet, the signals found in the NMR spectra did not fit to any of the mentioned components. Unfortunately, mass spectrometry and elemental analysis did as well not provide any clear results as well. In summary, while conversion of H_6hhtp with DDQ could be observed through primary reaction monitoring *via* NMR spectroscopy, the obtained analytical data is very much inconclusive. Owing to the fact that the product is very sensitive,²¹⁰ and probably decomposes rapidly in solution, the formation of side- or decomposition products was considered a plausible explanation. Consequently, the following preparation of trimeric hexaoxolene-bridged bis(catecholato)silanes were further conducted with H_6hhtp .

3.4.2 Deprotonation of H_6hhtp and Synthesis of $[\text{5}^{\text{Cl}}][\text{HB}]_6$

For the use of H_6hhtp as precursor for the aimed trimeric silicon complexes, the linker formally needs to undergo a sixfold deprotonation. This was attempted with different bases bearing different basicities.

When the deprotonation was found successful, the resulting salt $[\text{hhtp}][\text{HB}]_6$ was converted with the Lewis acid $2^{\text{Cl}} \cdot (\text{CH}_3\text{CN})_2$ under varying conditions (Scheme 24) in a consecutive step.



Scheme 24: Synthetical route to the trinuclear silicon hexaoxolene salts $[\text{5}^{\text{Cl}}][\text{HB}]_6$ *via* deprotonation of H_6hhtp and subsequent conversion with $2^{\text{Cl}} \cdot (\text{CH}_3\text{CN})_2$.

3.4.2.1 Method 2: Triethylamine

The polytopic linker H_6hhtp was mixed with 6 eq. of triethylamine in CD_3CN on NMR scale. Already after 10 min 1H NMR measurements showed the absence of the phenolic hydrogens, suggesting that the deprotonation is probably facilitated by the increased solubility of triethylamine compared to NaH. However, the disappearance of the signals demonstrates the poor solubility of the deprotonated product. The reaction was further shaken for 30 min to assure completeness and then 3 eq. of $2^{Cl} \cdot (CH_3CN)_2$ were added. After shaking for additional 24 h the outcome was examined *via* NMR spectroscopy again. In the 1H NMR spectrum new and different signals in the aromatic region could be observed (Figure 43b). However, those signals were rather broad and undefined. After 24 h, the reaction mixture darkened and EPR spectroscopy revealed a broad singlet signal, thus the existence of paramagnetic impurities, which may explain the broader signal in the 1H NMR spectrum.

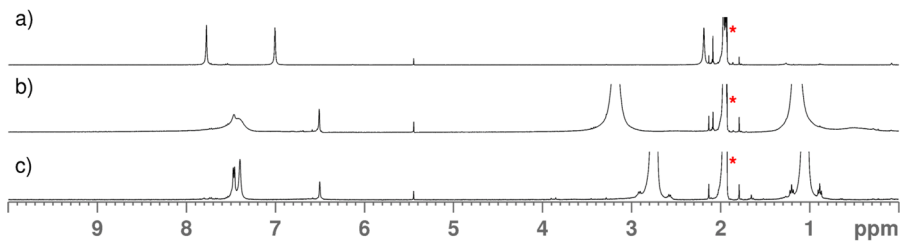


Figure 43: a) 1H NMR (400 MHz, CD_3CN^*) spectrum of H_6hhtp as reference. 1H NMR (400 MHz, CD_3CN^*) spectra of NMR scale synthesis of $[5^{Cl}][HNEt_3]_6$ with b) 6 eq. and c) 12 eq. of NEt_3 .

Since triethylamine is a mild base, it was taken into account that the deprotonation of H_6hhtp may be an equilibrium reaction. So, after the addition of the silicon Lewis acid the reaction equilibrium is shifted to the side of the starting materials, which results in partially deprotonated $[H_xhhtp]^{(x-6)}$. Thus, the conversion of the Lewis acid with different degrees of deprotonated linker leads to undesired or incomplete side-products, explaining the asymmetric NMR spectrum and other additional peaks. There is also the possibility that the protic cation $[HNEt_3]^+$ may cause problems for the silicon Lewis acid. Thereto, polymerization of the solvent acetonitrile was observed.

To improve this, it was considered to increase the amount of triethylamine to 12 eq. The use of a superstoichiometric amount of base should guarantee the equilibrium not

to undergo a strong shift and to stay at the product side. In addition, this might suppress the acid-catalyzed polymerization of acetonitrile.²¹¹⁻²¹² Repeating the synthesis with the altered conditions indeed yielded a reaction mixture which exhibited much clearer signals in the NMR spectra. In the ^1H NMR spectrum two signals in the aromatic region were observed, assignable to the protons of the triethylammonium cation and the *hhtp* core (Figure 43c). Besides, another peak at $\delta = 6.5$ ppm was visible. Conducting the reaction in THF-d_8 yielded similar results and spectra.

Given the successful preparation of $[\text{5}^{\text{Cl}}][\text{HNEt}_3]_6$ according to NMR spectroscopy, the synthesis was performed in higher scale in a Schenk tube with proper stirring. 1 eq. of H_6hhtp was deprotonated with 12 eq. of triethylamine in acetonitrile. 24 h after the addition of $2^{\text{Cl}}\cdot(\text{CH}_3\text{CN})_2$ a reaction control was taken, and a conversion could be observed *via* ^1H NMR spectroscopy. Subsequently, the solvent was removed yielding a fine grey powder which was confirmed as $[\text{5}^{\text{Cl}}][\text{HNEt}_3]_6$ by NMR spectroscopy. A clean ^1H NMR spectrum was revealed with two signals in the aromatic region, with an integral ratio of 1:1 (Figure 44). The broader peak at $\delta = 7.58$ ppm can be assigned to the protons of the cations and respectively the other peak at $\delta = 7.47$ ppm, which is interestingly present as doublet, should originate from the *hhtp* core. Also, the peak at around $\delta = 6.5$ ppm, which was obtained in preliminary experiments, was not detected. Thus, it appears that insufficient homogeneous mixing caused by the absence of stirring within a *J Young* NMR tube, for example, may also be a reason for undesired reactivity.

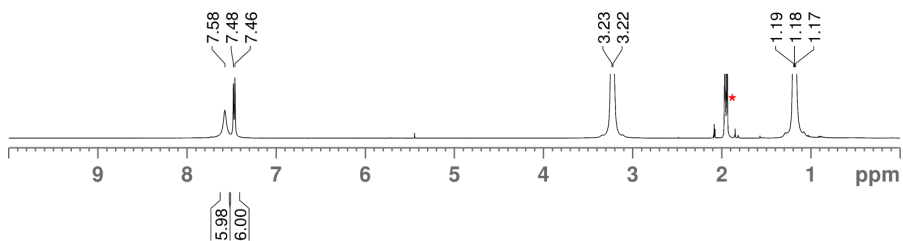


Figure 44: ^1H NMR (600 MHz, CD_3CN^*) spectrum of $[\text{5}^{\text{Cl}}][\text{HNEt}_3]_6$ obtained from preparative scale synthesis.

The origin of the splitting of the signal at $\delta = 7.47$ ppm is satisfactorily explained by the presence of diastereomeric product mixtures. In octahedral complexes, where the

element center is coordinated by three chelating ligands, Δ (delta, Figure 45a) or Λ (lambda) isomers can be existent. Thus, in the trimeric silicon complexes, each of the silicon centers can be present in one of those configurations. Statistically, this can result in 8 combinations, of which four are the mirror images of the other four, meaning they are enantiomeric (see Figure 45b). Of the four remaining combinations, the first one exhibits C_2 symmetry, while the other combinations only show identity as operation element (e). Besides, combinations 2-4 can be transferred into each other by rotation. That means, in total there are two diastereomers present in a ratio of 1:3 (Figure 45b), respectively, which should be distinguishable by NMR spectroscopy. So, this might explain the doublet splitting of the signal in the ^1H NMR spectrum (Figure 44). Yet, discrepancies arise as the integral ratio of the signals at $\delta = 7.48$ and 7.46 ppm (1:1) does not match with the calculated statistical distribution.

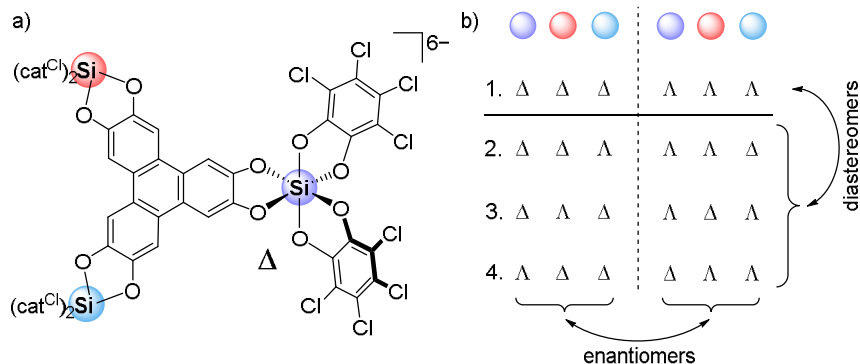


Figure 45: a) Illustration of the Δ configuration for one hexacoordinated silicon center within $[\text{5Cl}]^{6-}$ b) Possible combinations of Δ and Λ for all three silicon centers within $[\text{5Cl}]^{6-}$ summarized in tabular form and the differentiation of enantiomers and diastereomers.

Further, heteronuclear and 2D NMR analyses were conducted. The ^{13}C NMR spectrum showed six signal sets, of which the signal at $\delta = 103.5$ ppm was revealed as CH-type carbon from the *hhtp* core by ^{13}C -DEPT-135 NMR spectroscopy (Figure 46a and b). Here, it can also be observed that multiple signals at similar chemical shifts were obtained, further advocating for the presence of diastereomers. Additionally, the ^1H - ^{13}C -HSQC NMR spectrum showed a cross peak between the protons at $\delta = 7.47$ ppm with the CH-type carbon, both originating from the *hhtp* core. In the ^{29}Si -INVGATE spectrum one single peak at $\delta = -138.6$ ppm was observed

(Figure 46c), indicating chemical equivalent silicon centers within the large bulky trinuclear silicon complexes.

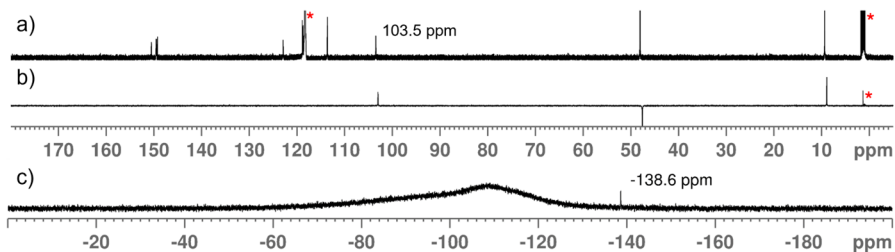


Figure 46: a) ^{13}C , b) ^{13}C -DEPT-135 NMR (151 MHz, CD_3CN^*) and ^{29}Si -INV GATE NMR (119 MHz, CD_3CN) spectra of $[\mathbf{5}^{\text{C1}}][\text{HNEt}_3]_6$ obtained from preparative scale synthesis.

In the IR spectrum, the broad O-H stretching band at $\tilde{\nu} = 3376 \text{ cm}^{-1}$ vanishes after deprotonation and is replaced by the N-H stretching band at $\tilde{\nu} = 3378 \text{ cm}^{-1}$ (Figure 47). After the conversion with the Lewis acid, the C-H stretching bands at $\tilde{\nu} = 2984 \text{ cm}^{-1}$ are more resolved and the N-H ($\tilde{\nu} = 3063 \text{ cm}^{-1}$) stretching vibration bands are shifted to lower wavenumbers.

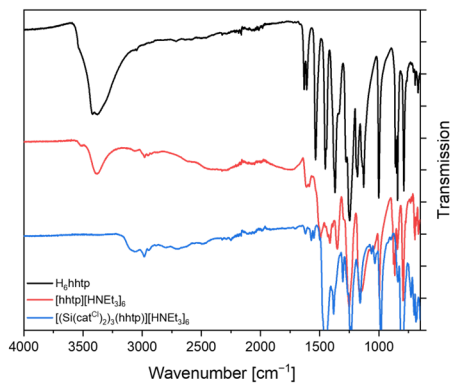


Figure 47: Comparison of the ATR-IR spectra of H_6hhtp (black) with $[\text{hhtp}][\text{HNEt}_3]_6$ (red) and $[\mathbf{5}^{\text{C1}}][\text{HNEt}_3]_6$ (blue).

Regarding the information obtained by NMR and IR spectroscopy, it was concluded that the desired product $[\mathbf{5}^{\text{C1}}][\text{HNEt}_3]_6$ was successfully prepared in yields up to 89 %. Further, salt metathesis with the triethylammonium salt of the chlorinated trimer

was attempted with PPh_4Cl and PNPCl in THF. The solubility of the final products clearly improved, resulting in good solubility even in less polar dichloromethane. Partial crystallization of HNEt_3Cl from the reaction solution was induced when cooled down to $-40\text{ }^\circ\text{C}$. However, the complete isolation of the salt exchange product from HNEt_3Cl seemed to be difficult due to the very similar solubilities. Various crystallization attempts towards $[\mathbf{5}^{\text{Cl}}][\text{HNEt}_3]_6$ were not yet successful either.

3.4.2.2 Method 4: Pyridine

While the approaches described in the preceding method were found crucial for the establishment of a synthetical access towards the aimed systems, the soluble ammonium cations did not yet result in single crystals suitable for scXRD analysis. Therefore, according to the synthesis of the tris(catecholato)silicates (see chapter 3.2.3), the use of pyridine was investigated, since insoluble pyridinium salts also offer the possibility for salt metathesis reactions, in which the side-product pyridinium salts might be separated more easily.

Initial NMR scale experiments showed that the deprotonation of H_6hhtp with the usage of 12 eq. pyridine (used in analogy to triethylamine experiments, see chapter 3.4.2.1) in THF-d_8 led to a clean deprotonation after 1 h shaking. In the ^1H NMR spectrum the signal of the deprotonated *hhtp* core was still observed accompanied by the new signals of the pyridinium cations. Addition of $\mathbf{2}^{\text{Cl}}\cdot(\text{CH}_3\text{CN})_2$ to the purple solution yielded a greenish suspension. The solids were found to be solely soluble in DMSO-d_6 , where the formation of the trinuclear silicon complex was strongly indicated by NMR spectroscopy. For completeness, it shall be mentioned that residues of pyridine originating from the deprotonation were also observed.

The reaction was then conducted in higher scale in Schlenk tubes. After mixing the reagents and adding the Lewis acid, the mixture was stirred for 24 h. A light-yellow precipitate was observed which was collected by filtration. The solids were washed vigorously with pentane and dried *in vacuo*, yielding $[\mathbf{5}^{\text{Cl}}][\text{Hpy}]_6$ as yellow powder in 93 % yields. Thorough examination *via* NMR spectroscopy confirmed a clean conversion. In the ^1H NMR spectrum the signal for the protons at the *hhtp* core was observed as doublet, as in the methods above, but here in an integral ratio of roughly 3:1 (Figure 48), as expected for the diastereomers (see chapter 3.4.2.1).

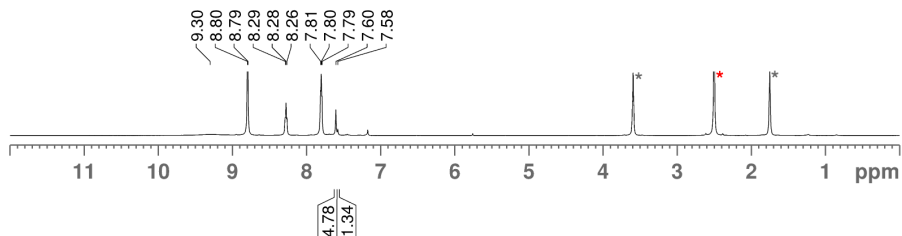


Figure 48: ^1H NMR (600 MHz, DMSO-d_6^*) spectrum of $[\text{5Cl}][\text{Hpy}]_6$ (with residual solvent THF^*) obtained from preparative scale synthesis.

^{13}C NMR measurements revealed nine peaks in the aromatic region, of which, with the help of ^{13}C -DEPT-135 and ^1H - ^{13}C -HSQC NMR spectra, three originate from the pyridinium cations and one from the CH-type carbon from the *hhtp* core (Figure 49a and b). The remaining five signals can be assigned to the quaternary carbon atoms of the *hhtp* core and of the catecholates. Also, a signal at $\delta = -138.1$ ppm was observed in the ^{29}Si -INVGATE NMR spectrum (Figure 49c).

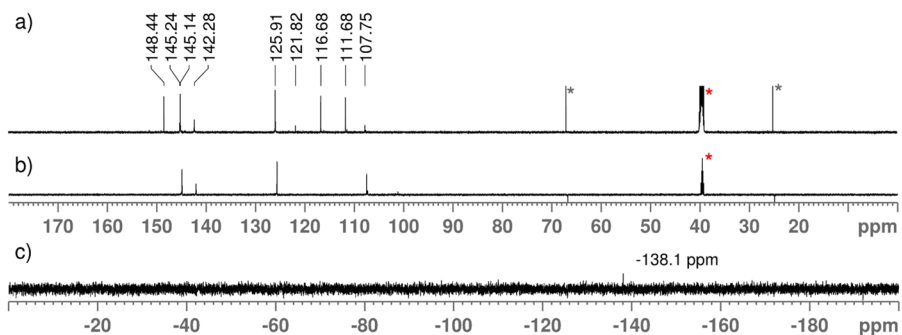


Figure 49: a) ^{13}C and b) ^{13}C -DEPT-135 NMR (151 MHz, DMSO-d_6^*) spectra and c) ^{29}Si -INVGATE NMR (119 MHz, DMSO-d_6) spectrum of $[\text{5Cl}][\text{Hpy}]_6$ (with residual solvent THF^*).

Through IR spectroscopy a successful conversion was also confirmed, whereby for $[\text{5Cl}][\text{Hpy}]_6$ the broad O-H stretching vibration was no longer observed, but broad bands for the C-H and N-H stretching vibrations from $\tilde{\nu} = 3250$ to 2500 cm^{-1} were detected (Figure 50).

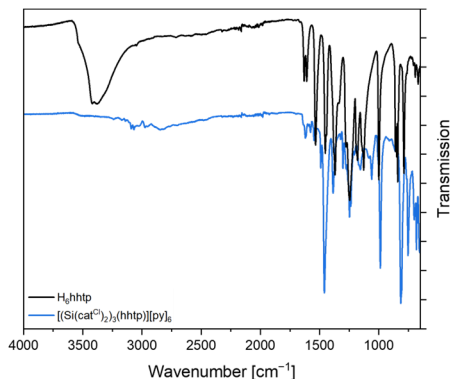


Figure 50: Comparison of the ATR-IR spectra of H₆hhtp (black) with [5^{Ct}][Hpy]₆ (blue).

As proposed, the formed compound was only found to be soluble in DMSO. Thus, salt metathesis reactions of [5^{Ct}][Hpy]₆ was conducted with the following salts: PPh₄Br, PNPCl, NBu₄Br and NEt₄Br. In general, one equivalent of [5^{Ct}][Hpy]₆ was suspended in THF, and 6 eq. of the respective exchange salt were added. After stirring at room temperature for 24 h, the reaction mixtures were examined.

For PPh₄Br no significant change in habitus was observed after the reaction. The solids were still yellow colored and reaction control of the supernatant solution *via* NMR spectroscopy revealed no signal in the ²⁹Si-INVGATE NMR spectrum. After reacting with PNPCl a clear solution with colorless precipitate was obtained. ²⁹Si-INVGATE NMR measurement of the supernatant solution showed a signal at $\delta = -137.7$ ppm, which could be assigned to the desired salt exchange product [5^{Ct}][PNP]₆ (Figure 51a). Conversion with NⁿBu₄Br and NEt₄Br yielded clear solutions with pale-yellow solids. ²⁹Si-INVGATE NMR measurements of the supernatant solutions revealed in both cases signals at $\delta = -139.9$ ppm and $\delta = -140.6$ ppm, respectively (Figure 51b and c). Interestingly, in the ²⁹Si-INVGATE NMR spectra obtained from the salt metathesis reactions above only one singlet peak was observed. Still, crystallization attempts were not successful, yet, and hence further investigations need to be conducted.

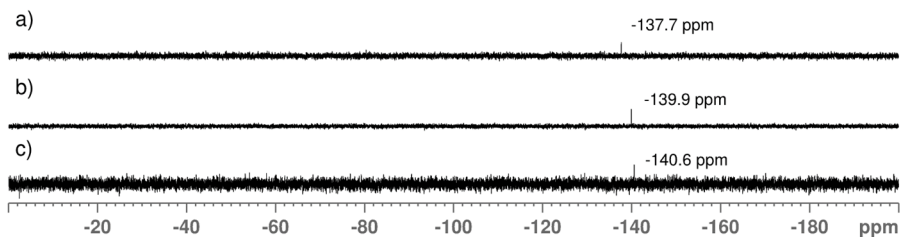


Figure 51: ^{29}Si -INVGATE NMR (119 MHz, THF- d_8) spectra of the supernatant solutions from the salt metathesis reaction between $[\mathbf{5}^{\text{Cl}}][\text{Hpy}]_6$ and a) PNPCL, b) $\text{N}^n\text{Bu}_4\text{Br}$ and c) NEt_4Br .

3.4.2.3 Method 5: Tri-*n*-octylamine

In contrast to the pyridinium salts, a highly soluble representative was expected when using tri-*n*-octylamine as a base and thus tested. Deprotonation of H_6hhtp with tri-*n*-octylamine was at first conducted with 6 eq. in THF- d_8 at 60 °C for 24 h. This led to a blue suspension. ^1H NMR measurements revealed a shifted signal at $\delta = 7.33$ ppm for the *hhtp* core and a new broad peak at $\delta = 8.65$ ppm for the ammonium cations (Figure 52a), according to the integral ratio and ^1H - ^{13}C -HSQC NMR spectrum. Addition of $\mathbf{2}^{\text{Cl}} \cdot (\text{CH}_3\text{CN})_2$ turned the reaction slowly pale brown. A signal at $\delta = 139.1$ ppm arose in the ^{29}Si -INVGATE NMR spectrum (Figure 52b), validating the successful preparation of $[\mathbf{5}^{\text{Cl}}][\text{H}^n\text{NOct}]_6$.

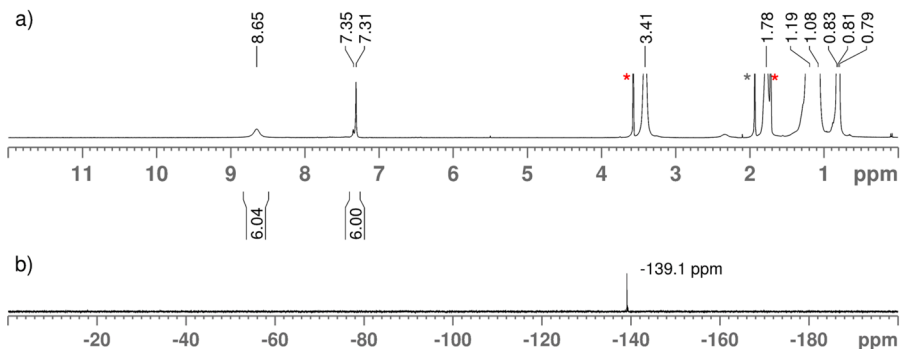


Figure 52: a) ^1H NMR (400 MHz, THF- d_8^*) and ^{29}Si -INVGATE NMR (119 MHz, THF- d_8) spectrum of $[\mathbf{5}^{\text{Cl}}][\text{H}^n\text{NOct}]_6$ (with residual solvent CH_3CN^*) obtained from NMR scale synthesis.

Thus, the reaction was upscaled and conducted in a Schlenk tube. Hereby, the reaction mixture was stirred at 50 °C for 24 h for the first step. Then, the

perchlorinated Lewis acid was added and the mixture was further stirred at 50 °C for 24 h. Strikingly, no precipitate was obtained, meaning with the tri-*n*-octylammonium counteranions the solubility of the hexaanionic complex has tremendously increased. On the contrary, it was not possible at first to precipitate the final product, as it was found to be likewise soluble in very non-polar solvents such as pentane, hexane, and heptane and in highly polar solvents as DMSO, DMF and acetonitrile (albeit only partially). Only in HMDSO the complex salt did not dissolve. Therefore, the product was precipitated and washed with the latter solvent. After isolation, ^1H NMR spectroscopy of the solids showed impurities, as revealed by comparison to the NMR scale experiments. Possible explanation might be given in the application of higher temperatures during the synthesis or the usage of HMDSO for precipitation, possibly leading to decomposition of the trinuclear silicon complex.

Thus, the reaction was repeated at room temperature in THF- d_8 and in the end the solvent was just evaporated. This led to the isolation of analytically pure $[\text{5}^{\text{C}}][\text{H}^n\text{NOct}_3]_6$ as grey and sticky solids in 52 % yields. Accordingly, the ^{13}C NMR spectrum revealed six peaks in the aromatic region, of which the one at $\delta = -108.6$ ppm fits to the tertiary carbon from the hhttp core, validated by ^{13}C -DEPT-135 and ^1H - ^{13}C -HSQC NMR experiments (Figure 53).

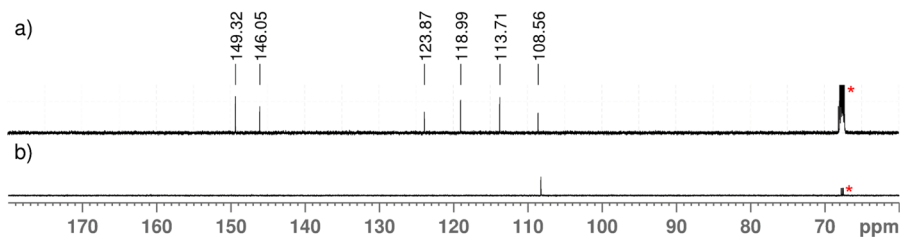


Figure 53: a) ^{13}C and b) ^{13}C -DEPT-135 NMR (151 MHz, THF- d_8 *) spectra of $[\text{5}^{\text{C}}][\text{H}^n\text{NOct}_3]_6$ obtained from preparative scale synthesis.

In the IR spectrum of $[\text{5}^{\text{C}}][\text{H}^n\text{NOct}_3]_6$ (Figure 54), no O-H vibration band was observed anymore, but characteristic bands at $\tilde{\nu} = 3081$ cm^{-1} (br) for N-H stretching vibrations and at $\tilde{\nu} = 2924$ and 2854 cm^{-1} for C-H stretching vibrations.

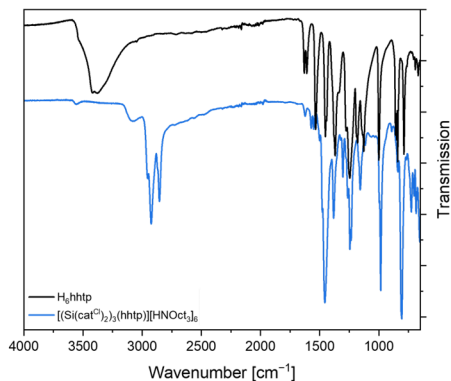


Figure 54: Comparison of the ATR-IR spectra of H_6hhtp (black) with $[5^{C1}][HN^nOct_3]_6$ (blue).

3.4.2.4 Method 6: (*S*)-(-)-1-(2-Naphthyl)ethylamine

Since NMR measurements of the experiments described above have suggested that the obtained products are existent as mixtures of stereoisomers (see chapter 3.4.2.1) and the integral ratios of the signals obtained in the ^{29}Si -INVGATE NMR experiments did not come close to the theoretical one (1:3), it was considered to make use of a chiral base. For this case, (*S*)-(-)-1-(2-naphthyl)ethylamine (NEA) was judged to be suitable for the controlled synthesis of only one preferred stereoisomer.

Deprotonation of H_6hhtp with NEA in THF- d_6 led to pale-green solution after some hours. This was confirmed in the 1H NMR spectrum by the disappearance of the signal for the OH-group and the concurrent appearance of new signals for the protonated bases, especially for the ammonium protons. Then, the Lewis acid $2^{Cl} \cdot (CH_3CN)_2$ was added, and the mixture was stirred at 60 °C until the colorless solids were consumed. Again, a successful conversion was noted *via* NMR spectroscopy. In the 1H NMR spectrum a shift of signals could be observed, as well as in the ^{13}C NMR spectrum. Regarding the ^{29}Si -INVGATE NMR measurements, two silicon peaks at $\delta = -140.9$ ppm were detected (Figure 55), confirming the synthesis of the trimeric silicon complex. Yet, the ratio of the signals was found to be around 1:1, overall, not pledging for a stereospecific synthesis. This led to the conclusion that even though the all- Δ or all- Λ isomer seem preferred, the planned stereospecific control by a proposed preorganized cation is only to a minor extent feasible.

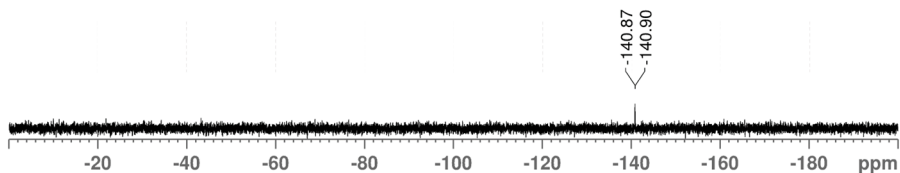
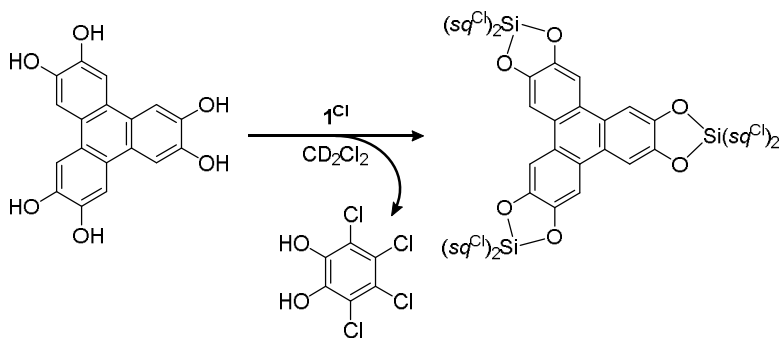


Figure 55: ^{29}Si -INVGATE NMR (119 MHz, THF- d_6) spectrum of NMR scale synthesis of $[\mathbf{5}^{\text{Cl}}][\text{HNEA}]_6$.

3.4.2.5 Base-free Direct Approach Between H_6hhtp and $\mathbf{1}^{\text{Cl}}$

Apart from the reactions between H_6hhtp and $\mathbf{2}^{\text{Cl}}$ under basic conditions, another question arose, namely, whether a direct conversion of H_6hhtp with the neutral silicon diradical $\mathbf{1}^{\text{Cl}}$ was considered, as this would directly lead to the neutral trinuclear silicon semiquinonate complex bridged by the *hhtp* linker (Scheme 25) and therefore would state an attractive alternative.

1 eq. of H_6hhtp was mixed with 3 eq. of $\mathbf{1}^{\text{Cl}}$ in CD_2Cl_2 and the reaction progress was monitored *via* NMR spectroscopy. Immediately after setting up the reaction, signals for the H_6hhtp in the ^1H NMR spectrum were already missing and another broad signal at $\delta = 5.87$ ppm was observed. The ^{13}C NMR spectrum exhibited three new signals in the aromatic region at $\delta = 140.6$, 124.1 and 119.2 ppm. Indeed, these signals altogether agree well with tetrachlorocatechol.³¹ Warming the reaction mixture to 40 °C and stirring for another three days did not lead to any changes in the NMR spectra. It appears that one coordinated *cat*^{Cl} ligand was successfully cleaved from $\mathbf{1}^{\text{Cl}}$ and substituted by the *hhtp* linker as proposed (Scheme 25). Nevertheless, black solid particles were still left in the reaction mixture, leading to the assumption that either $\mathbf{1}^{\text{Cl}}$ was not completely consumed or that reaction products have already precipitated. Moreover, the resulting trinuclear silicon complex is expected to be paramagnetic and therefore NMR spectroscopy cannot provide any further information about the structure. Given these insights, it is still questionable, whether the final product contains three silicon centers bridged by *hhtp* or has only been partially formed or even decomposed.



Scheme 25: Synthetic approach to neutral trimeric silicon complex ($\text{Si}(\text{sq}^{\text{Cl}})_2)_3(\text{hhtp})$ via reaction between H_6hhtp and 1^{Cl} and liberation of $\text{H}_2\text{cat}^{\text{Cl}}$.

Preliminary EPR measurements at room temperature showed a very broad singlet signal that is slightly shifted compared to 1^{Cl} . Additionally the g -value has changed from $g = 2.043$ to $g = 2.003$, indicating that a new compound might have formed, whose unpaired electrons are rather carbon-centered than oxygen-centered.²¹³ From this, it can be postulated that a larger aromatic system for delocalization must be available within the new complex, which would state a first indication for a successful implementation of at least one silicon unit.

Overall, while the preliminary results generally demonstrate the possibility of a direct implementation toward the radical species in base-free environment, the encountered difficulties in this approach yet prevent a full development of an applicable synthetic strategy.

3.4.3 Conclusion

Initial synthetical attempts towards hhtp via oxidation of H_6hhtp were not successful, wherefore the synthesis of the trinuclear silicon polyoxolenes was approached via H_6hhtp . The sixfold deprotonation of tritopic linker was examined with a variety of bases. Preliminary reactions indicated that strong nucleophilic bases, like NaH were found to be unsuitable. Deprotonation with milder amine bases, like triethylamine and pyridine, yielded an equilibrium reaction. Thus, with superstoichiometric amounts of amine base, $[\text{hhtp}]^{6-}$ was finally implemented with $2^{\text{Cl}} \cdot (\text{CH}_3\text{CN})_2$. According to NMR and IR-spectroscopical investigations the trimeric complexes $[\mathbf{5}^{\text{Cl}}][\text{HB}]_6$ ($\text{HB} =$

HEt_3 and *py*) were successfully prepared. Due to the pronounced insolubility of those hexaanionic salts, salt metathesis reactions were approached for $[\mathbf{5}^{\text{Cl}}][\text{Hpy}]_6$ with PNPCL , $\text{N}^n\text{Bu}_4\text{Br}$ and NEt_4Br . Preliminary investigations showed that the exchange salts exhibited increased solubility. Still, attempts to obtain a solid-state molecular structure of $[\mathbf{5}^{\text{Cl}}]^{6-}$ have not been successful yet. With tri-*n*-octylamine, $[\mathbf{5}^{\text{Cl}}][\text{HN}^n\text{Oct}_3]_6$ was synthesized as well and found to be extensively soluble, even in very apolar solvents, such as pentane and heptane.

Furthermore, signal splittings in differing ratios were observed in the ^1H , ^{13}C and ^{29}Si NMR spectra for the hexaanions $[\mathbf{5}^{\text{Cl}}]^{6-}$, rendering the presence of possible diastereomers. Thus, with the chiral base (*S*)-(-)-1-(2-naphthyl)ethylamine (NEA) a controlled synthesis of one preferred stereoisomer was attempted but to no effect.

Preliminary investigations regarding a base-free approach *via* ligand scrambling between H_6hhtp and $\mathbf{1}^{\text{Cl}}$ was also attempted. Thereby, release of $\text{H}_2\text{cat}^{\text{Cl}}$ could be observed by ^{13}C NMR spectroscopy, indicating a successful implementation of at least one silicon unit.

4

SUMMARY

In the context of this work, a series of novel silicon polyoxolenes were prepared and studied regarding their structure, redox and magnetic properties. The mononuclear homoleptic diradical compound $\mathbf{1}^{\text{Cl}}$, whose properties demonstrate a novelty for non-metal compounds, served thereby as inspiration.

The first part of this work dealt with the thorough investigation of the redox properties of $\mathbf{1}^{\text{Cl}}$. Synthesis of the hitherto elusive monoradical anion $[\mathbf{1}^{\text{Cl}}]^{\bullet-}$ finally completed the redox series of $\mathbf{1}^{\text{Cl}}$, and thus of silicon trisdioxolenes in general. The redox potentials were determined as $E_{1/2} = 0.43 \text{ V}$ and 0.88 V (*vs.* Fc/Fc⁺). Guiding redox reactions revealed an even higher redox potential of $E_{1/2} \approx 1.0 \text{ V}$ (*vs.* Fc/Fc⁺), depicting $\mathbf{1}^{\text{Cl}}$ as strong oxidant like $[\text{N}(\text{Ph}-\text{Br}_2)_3]^{\bullet+}$ (*magic blue*) and NO^+ .¹⁶³ However, the latter oxidants suffer limitations due to their charged nature, non-innocence, and effortful synthesis, whereas $\mathbf{1}^{\text{Cl}}$ stands out as neutral oxidant with a straightforward synthesis by only combining two commercially available starting materials. At the same time, upon reduction of $\mathbf{1}^{\text{Cl}}$ an easy-to-handle weakly coordinating anion (*WCA*) is obtained (reminiscent of SbF_5).⁹³ Also, observations of *IVCT* bands in the NIR region for $\mathbf{1}^{\text{Cl}}$ highlighted the suitability of silicon as central atom for the construction of metal-free magnetic materials and electronic devices.¹⁷⁵

Comparing the redox potentials of $\mathbf{1}^{\text{Cl}}$ with *free* q^{Cl} , a massive shift of about 1.2 V became apparent, which outperforms comparable concepts of redox amplification.¹⁵¹⁻¹⁵² Moreover, $\mathbf{1}^{\text{Cl}}$ proved to be an efficient redox catalyst for an oxidative lactonization reaction, for which $\mathbf{1}^{\text{Cl}}$ could be even generated *in situ*. Thus, the new concept of redox amplification through Lewis (super)acid-binding was successfully demonstrated to be a powerful tool for the boost of oxidation potentials.

In the second part of this work, accordingly the homoleptic analogues $\mathbf{1}^{\text{X}}$ ($\text{X} = \text{Br}$, tBu) were prepared. The redox series of $\mathbf{1}^{\text{Br}}$ was completed in analogy to its perchlorinated derivative, exhibiting diradical character and similar structural parameters. Moreover, VT EPR spectroscopy of $\mathbf{1}^{\text{tBu}}$ confirmed a diradical with a triplet ground state. Preliminary CV experiments of $[\mathbf{1}^{\text{X}}][\text{N}^n\text{Bu}_4]_2$ ($\text{X} = \text{F}$, Br , tBu) showed similar oxidation potentials as for $\mathbf{1}^{\text{Cl}}$.

Furthermore, a simple access to the heteroleptic diradicals $\mathbf{1}^{\text{X},\text{Y}}$ ($\text{X} = \text{F}$, Cl , Br , CF_3 and $\text{Y} = \text{tBu}$, iPr) was found by oxidative addition of the quinones q^{Y} to the respective Lewis acids $\mathbf{2}^{\text{X}}$. A pathway utilizing catechol and quinone in a one-pot procedure with HSiCl_3 was also found to be a valuable alternative. Analysis of the heteroleptic representatives $\mathbf{1}^{\text{Cl},\text{tBu}}$ and $\mathbf{1}^{\text{Cl},\text{iPr}}$ *via* VT EPR studies likewise revealed the presence of diradicals with a triplet ground state.

After gaining in-depth insights into the monomeric species, the last two parts of this work investigated the effect of higher nuclearity in extended systems. A straightforward synthesis was established by simply mixing the Lewis acids $\mathbf{2}^{\text{X}}$ ($\text{X} = \text{Cl}$, Br , CF_3 , iPr) with the linker salts $[\text{d}hbq^{\text{Y}}][\text{Na}@15\text{c}5]_2$ ($\text{Y} = \text{Cl}$, Br , Ph , NO_2) yielding a variety of dimeric silicon polyoxolenes $[\mathbf{4}^{\text{X},\text{Y}}][\text{Na}@15\text{c}5]_2$. In contrast to the monomeric forms ($\mathbf{1}^{\text{X}}$ and $\mathbf{1}^{\text{X},\text{Y}}$), the dinuclear complexes $[\mathbf{4}^{\text{X},\text{Y}}]^{2-}$ were found to be stable in coordinating environments, such as acetonitrile and THF. Comparison of the metrical parameters in the complexes with the Lewis formulation $[(\text{cat}^{\text{X}})_2\text{Si}(\text{d}hbq^{\text{Y}})\text{Si}(\text{cat}^{\text{X}})_2]^{2-}$ with the *free* linker salts $[\text{d}hbq^{\text{Y}}]^{2-}$ ($\text{Y} = \text{Cl}$, Ph) revealed a more reduced state of the $\text{d}hbq^{\text{Y}}$ linker. NMR spectroscopy showed sharp signals, however EPR spectroscopy revealed signal patterns for a populated triplet diradical state. Thus, an electron transfer from the external catecholates to the internal $\text{d}hbq$ linker was suspected to be responsible for the EPR activity. By selective combination of more electron-rich bis(catecholato)silanes and electron-poor $\text{d}hbq$ linkers diradicaloid complexes $[\mathbf{4}^{\text{X},\text{Y}}]^{2-}$ ($\text{X} = \text{Cl}$, iPr and $\text{Y} = \text{Cl}$, Br , NO_2) could be finally observed and characterized. The opposite extreme with the smallest diradical character was accomplished by combining electron-poor $\mathbf{2}^{\text{CF}_3}$ and electron-rich $\text{d}hbq^{\text{Ph}}$. Those extremes served as basis for an underlying design principle, which was disclosed by computational analyses. Conclusively, this one-step protocol granted access to diradicaloid dimeric silicon polyoxolenes with adjustable diradical character. Lastly, the trinuclear silicon polyoxolenes $[\mathbf{5}^{\text{Cl}}][\text{HB}]_6$ ($\text{HB} = \text{HNet}_3$, Hpy , HN^nOct_3)

were approached by a sixfold deprotonation of H_6hhtp and subsequent implementation with 2^{Cl} , as indicated by NMR spectroscopy, complicated synthetic approach.

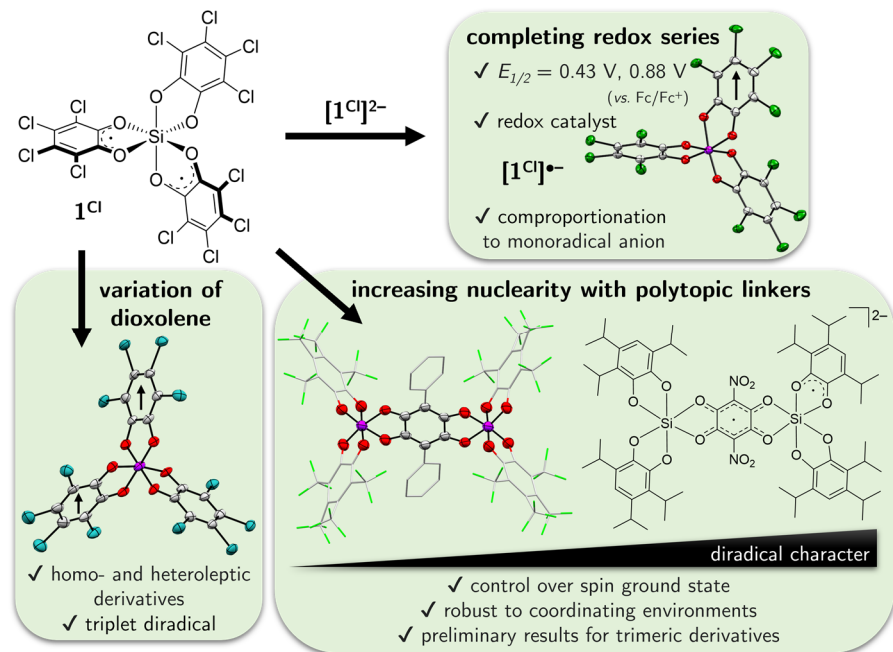


Figure 56: Overview of the results of this work: completion of the redox series and investigation of the redox properties of 1^{Cl} as well as extension towards new silicon polyoxolenes by varying the dioxolene and increasing the nuclearity with polytopic linkers.

Altogether, this work presents a more profound understanding of silicon-bridged redox-active ligands and therefore provides a valuable extension based on a non-metallic main group element to existing works on transition metals.

5

EXPERIMENTAL SECTION

5.1 General Information

5.1.1 Materials and Methods

Unless otherwise stated, all experiments were carried out under inert argon atmosphere using standard Schlenk techniques in flame-dried laboratory glassware or in the gloveboxes *SylaTech* (Y-05-G-7986), *MBraun LABstar* (MB-10-G) and *MBraun LABmaster DP* (MB-20-G) under inert nitrogen atmosphere to prevent oxidation and hydrolysis of air and moisture sensitive compounds. Thereby, the argon used within the Schlenk-line was freed from traces of oxygen with a heated Cu-catalyst²¹⁴ and dried using molecular sieves. All glassware, syringes, needles, and magnetic stirring bars were thoroughly dried. Sensitive compounds were stored in one of the glove boxes under nitrogen atmosphere.

The chemicals and solvents used in this work were obtained from the chemical store of the chemical institutes of Heidelberg University or directly purchased from the respective suppliers: *Sigma Aldrich* (Merck KGaA), *abcr GmbH*, *Alfa Aesar* and *Acros Organics B.V.B.A.* (Thermo Fisher Scientific), *VWR*, *TCI Chemicals*, *Fluorochem*. Prior to use, commercially available solid chemicals were dried under reduced pressure; liquid ones were degassed by saturation with argon and dried by storing over activated molecular sieves (3 or 4 Å) for at least 24 h.

The solvents used were obtained from a solvent purification system (*MB-SPS-800*, *MBraun*). Deuterated solvents were purchased from *Deutero GmbH*, *Eurisotop* or *Sigma Aldrich*. All solvents were degassed with three or four freeze-pump-thaw cycles, and then dried and stored over activated molecular sieves (3 or 4 Å) in *J. Young* or

Normag valve ampoules under dry argon atmosphere for at least 24 h prior to use. In case of acetonitrile and DMSO, the solvents were degassed by saturation with argon.

$\text{H}_2\text{cat}^{\text{Cl}}$,³¹ $2^{\text{X}}\cdot(\text{CH}_3\text{CN})_2$ ($\text{X} = \text{Cl}, \text{Br}$)³¹⁻³² and tris(2,4-dibromophenyl)amine¹⁶⁴ were synthesized according to literature known procedures.

Analytical data of the known compounds were compared to the data of the respective reference and were found to be consistent in all cases. Novel compounds were characterized to the reported structures to the best of our knowledge.

5.1.2 Analytical Methods

Cyclovoltammetry

Electrochemical measurements were performed with a potentiostat (*EmStat3+ Blue, PalmSens Compact Electrochemical Interfaces*) in the *SylaTech* glovebox under nitrogen atmosphere in a glass cell using a three-electrode configuration. A glassy carbon electrode with a working area of 0.07 cm², was used as working electrode, a platinum wire as counter electrode; a silver wire served as quasi reference electrode. The program *PSTrace 5.9* was used to record all measurements. The substances were examined at room temperature with an electrolyte of choice ($[\text{BArF}_{20}][\text{N}^n\text{Bu}_4]$ or $[\text{PF}_6][\text{N}^n\text{Bu}_4]$, $c = 0.1 \text{ M}$, $V = 5 \text{ mL}$) in dichloromethane at a scan rate of 100 mV/s, unless otherwise stated. The solutions were stirred between each measurement and kept under nitrogen atmosphere throughout. As internal standard ferrocene was measured at the very end of each set of measurements.

$[\text{BArF}_{20}][\text{N}^n\text{Bu}_4]$ were prepared according to literature known procedure.²¹⁵⁻²¹⁶ Prior to use, the electrolytes were recrystallized: $[\text{BArF}_{20}][\text{N}^n\text{Bu}_4]$ (dichloromethane/hexane, 4 °C),²¹⁶ $[\text{BArF}_{20}][\text{PF}_6]$ (hot ethanol)²¹⁷, dried *in vacuo* for 24 h and stored in the glovebox.

Electron Paramagnetic Spectroscopy

X-band EPR measurements (9.30-9.55 GHz) at room temperature were conducted on a spectrometer (*MiniScope MS400, magenettech*) with a modulation frequency of 100 kHz. X-band EPR spectra (9.6 MHz) between 4-276 K were obtained with a spectrometer (*Elexsys E500, Bruker*) with a continuous wave dual-mode resonator (*ER 4116DM, Bruker*). The regulation of the temperature for low-temperature

measurements was performed with a *Bruker ER 4112HV-CF42 In-Cavity Cryogen Free VT* system and a temperature controller (*ITC 4, Oxford Instruments*). The low-temperature measurements of solvated samples were directly measured in quartz tubes.

Elemental Analysis

The elemental analyses for the determination of C-, H- and N-content [%] were performed by the staff of the Microanalytical Laboratory of the Institutes of Chemistry at Heidelberg University on an elemental analyzer (*vario EL or vario MICRO cube, Elementar Analysensysteme GmbH*).

GC-MS

All GC-MS measurements were performed on a gas chromatograph (*Agilent Technologies 6890 Series*) with helium as carrier gas, a column (*HP-5MS, 5 % diphenyl polysiloxane and 95 % dimethyl polysiloxane*) and a mass detector (*Agilent 5973 Mass Selective Detector*).

Magnetic Measurements

Magnetic properties were investigated using a SQUID magnetometer (*Quantum Design MPMX-XL 5, 5 T*). Temperature and field dependency of the molar susceptibility (X_m) in a temperature range of 2-300 K and a field range of 0-5 T were measured. To prevent field-induced alignment of the sample during the measurement, the powdered sample was pressed into a polycarbonate capsule and fixed in a plastic straw as a sample holder. The data were adjusted by the diamagnetic contribution of the gelatin capsule, the sample holder, and the sample itself with the help of Pascal constants.

Mass Spectrometry

High resolution mass spectrometry (HR-MS) experiments were performed by the Mass Spectrometry Facility of the Institute of Organic Chemistry of the University of Heidelberg on mass spectrometers (*JEOL AccuTOF GCx* for EI pos., *Bruker ApexQe hybrid 9.4 T FT-ICR* for ESI and MALDI neg. and *Bruker timsTOFfleX* for MALDI neg.).

Nuclear Magnetic Resonance

NMR measurements were carried out by the NMR facilities of the Institute of Inorganic Chemistry of the University of Heidelberg. The spectra were recorded at 298 K with a spectrometer (*DPX 200, Avance II 400 or Avance III 600, Bruker*) and referenced to the respective deuterated solvent in use. ^1H NMR data is reported as follows: chemical shift δ [ppm], multiplicity (s = singlet, br = broad, d = doublet, t = triplet, q = quartet, quin = quintet, sext = sextet, sept = septet, m = multiplet), scalar spin-spin coupling constant ${}^nJ_{AB}$ [Hz], (n = number of chemical bonds between coupled nuclei; A, B = coupled nuclei) integration value. ^{13}C and ^{29}Si INVGATE spectra were recorded ^1H decoupled. Additionally, 2D NMR correlation experiments (^1H - ^{13}C -HSQC) and DEPT-135 NMR spectra were measured for the complete assignment of the signals.

Single Crystal Structure Analysis

Suitable crystals for single-crystal structure determination were taken directly from the mother liquor, submerged in perfluorinated polyether oil, and fixed on a Nylon loop.

For the solid-state molecular structures of chapter 3.1.1, the intensity data were collected at low temperature with a diffractometer (*Enraf-Nonius Kappa CCD, Mo- K_α radiation, sealed X-ray tube, graphite monochromator or Agilent Technologies Supernova-E CCD, Cu- K_α radiation, microfocus X-ray tube, multilayer mirror optics*). Detector frames (w- and j-scans) were integrated by profile fitting.²¹⁸⁻²²⁰ Data were corrected for air and detector absorption, Lorentz and polarization effects²¹⁹⁻²²⁰ and scaled essentially by application of appropriate spherical harmonic functions.^{219, 221-224} Absorption by the crystal was treated with a semiempirical multiscan method (as part of the scaling process), and augmented by a spherical correction,^{219, 221-224} The scXRD measurements were conducted Prof. Dr. H. WADEPOHL and Prof. Dr. L. GREB from the University of Heidelberg. The structures were solved by Prof. Dr. H. WADEPOHL with the charge flip procedure²²⁵⁻²²⁶ and refined by full-matrix least squares methods based on F^2 against all unique reflections.²²⁷⁻²²⁹ All non-hydrogen atoms were given anisotropic displacement parameters. Hydrogen atoms were input at calculated positions and refined with a riding model. The structure of $1^{\text{Cl}}(\text{C}_6\text{H}_6)_4$ was refined as an inversion twin. Combined non-merohedral and inversion twinning was found to be present in the crystals of $1^{\text{Cl}}(\text{C}_6\text{H}_4\text{Cl}_2)_2$. Refinement of one

enantiomorph of this structure was carried out against singles and composites of the first domain. Disordered benzene solvent in the structure of $1^{\text{Cl}}\cdot(\text{CH}_2\text{Cl}_2)_x$ was treated as a rigid planar regular hexagon ($d_{\text{CC}} = 1.390 \text{ \AA}$); rigid body adp restraints were applied.²³⁰ Due to severe disorder, electron density attributed to solvent of crystallization (CH_2Cl_2) was removed from the structures of $1^{\text{Cl}}\cdot(\text{CH}_2\text{Cl}_2)_x$ with the *BYPASS* procedure,²³¹⁻²³² as implemented in *PLATON* (squeeze/hybrid).²³³⁻²³⁴ Partial structure factors from the solvent masks were included in the refinement as separate contributions to F_{calc} .

For the solid-state molecular structures of the remaining chapter, full shells of intensity data were collected at low temperature with a diffractometer (*D8 Venture*, *Bruker*), dual-source (Mo- or Cu- K_α radiation, microfocus X-ray tube, Photon III detector). Data were processed with the standard *Bruker* software package (*SAINTE*, *APEX3* or *APEX4*).²³⁵⁻²³⁶ Multiscan absorption correction was applied using the *SADABS* program.²²¹⁻²²² The scXRD measurements were conducted by the X-ray team of the groups HIMMEL and GREB from the University of Heidelberg. The structures were solved by Prof. Dr. L. GREB, Dr. D. HARTMANN, Dr. M. SCHORPP and D. ROTH by intrinsic phasing^{229,237} and refined using the *SHELXTL* software package (version 2014/6 and 2018/3).^{227-228, 238-239} Graphical handling of the structural data during solution and refinement was performed with *OLEX2*.²⁴⁰ All non-hydrogen atoms were given anisotropic displacement parameters. Hydrogen atoms bound to carbon were input at calculated positions and refined with a riding model.

For data visualization, *Mercury 4.3.1* was used.²⁴¹⁻²⁴³ The thermal displacement ellipsoids are shown at the probability level of 50 %. Already published crystallographic data can be obtained free of charge from the *Cambridge Crystallographic Data Centre* and *FIZ Karlsruhe* joint Access Service via <https://www.ccdc.cam.ac.uk/structures/> under the CCDC numbers given in the respective tables (see Appendix 7.8).

Software

The chemical structures were visualized with *ChemDraw 21.0.0.28* by *PerkinElmer Informatics*. The plot and the evaluation of the spectral data were accomplished using *OriginPro 2021b 9.8.5.212* by *OriginLab Corporation* (IR, UV-vis-NIR, EPR, SQUID), *TopSpin 4.0.6* by *Bruker* (NMR) and *OpenChrom* by *Lablicate* (GC-MS).

UV-vis-NIR Spectroscopy

UV-vis-NIR absorption spectra were recorded at room temperature (298 K) on a spectrophotometer (*Cary 5000, Varian/Agilent*). The substances were measured as dilute solutions in *Normag* quartz glass cuvettes. The solutions were prepared under inert conditions in a glovebox. Before each measurement a background spectrum of the solvent was recorded, and a baseline correction was conducted.

Vibrational Spectroscopy

Infrared (IR) spectra of solids and oils were performed on a FTIR spectrometer (*Cary 630, Agilent*) equipped with a diamond ATR sampling module in the *SylaTech* glovebox under nitrogen atmosphere. Thereby, the samples were directly deposited on the diamond crystal and pressed down with a stamp (in case of solid samples). A baseline correction was conducted. The IR absorption bands are given in wavenumbers $\tilde{\nu}$ [cm^{-1}] and the signal intensities are divided into s = strong, m = medium, w = weak and sh = shoulder, relative to the strongest signal in the respective spectra.

5.1.3 Theoretical Methods

5.1.3.1 Geometry Optimizations, Single Point Energies on Different Spin States of 1^X and Exchange Coupling Constant J (for Chapter 3.1.1)

Geometry optimizations and single point energy calculations have been performed with ORCA 4.0.1²⁴⁴ The RI approximation²⁴⁵ for the Coulomb integrals was used in all cases (RIJCOSX), with application of corresponding auxiliary basis sets.²⁴⁶

The DFT hybrid functional PBE0²⁴⁷ was used in combination with Grimme's semi-empirical dispersion correction,²⁴⁸ Becke-Johnson damping function²⁴⁹⁻²⁵¹ (D3(BJ)) and a def2-TZVPP²⁵²⁻²⁵³ basis set. All calculated geometries have been confirmed as energetic minima on the potential energy surface by analytical calculation of harmonic frequencies, revealing only positive values.

Broken-symmetry Kohn-Sham DFT calculations were used to obtain the magnetic exchange coupling constant J of the two unpaired electrons ($H = -2J^*S_A^*S_B$). Spin-contamination was accounted by means of the Yamaguchi correction scheme ($J =$

$E[\text{HS}] - E[\text{BS}] / (\langle S^2 \rangle_{\text{HS}} - \langle S^2 \rangle_{\text{BS}})$.²⁵⁴⁻²⁵⁷ The use of PBE0 follows a recent advice by Illas and co-workers on the choice of suitable functionals.²⁵⁸

The energies for the open shell triplet, open shell singlet, and closed shell singlet solution for $\mathbf{1}^{\text{Cl}}$ are given in Table 5 (see Appendix). Ferromagnetic exchange coupling constants were obtained for $\mathbf{1}^{\text{X}}$ ($\text{X} = \text{F}, \text{Cl}, \text{Br}, \text{tBu}$; see Appendix, Table 6). Comparison of the computed, characteristic C-O bond lengths of the three different states with the X-ray structure of $\mathbf{1}^{\text{Cl}}$ obtained from CH_2Cl_2 , revealed closest agreement with the triplet state.

5.1.3.2 Transition State for Catecholate Shuffling (for Chapter 3.1.4)

Geometry optimizations and single point energy calculations have been performed with *Orca* 4.2.²⁵⁹ The structures of all involved compounds were optimized with the PBEh-3c/def2-mSVP as implemented in *Orca*, using grid5 settings,²⁶⁰ and confirmed as energetic minima on the potential energy surface by analytical calculation of harmonic frequencies, revealing only positive Hessian eigenvalues, or one negative in case of the transition state. Enthalpies at 298.15 K have been calculated at the same level of theory by using the rigid-rotor harmonic oscillator (RRHO) approximation,²⁶¹ as implemented in *Orca*. The gas phase single point computations were calculated with the hybrid meta exchange-correlation functional PW6B95-D3(BJ),²⁶² in combination with the very large def2-QZVPP basis set.²⁵² SCF settings were tightSCF and integration was performed at a very fine grid7. The RIJCOSX Fock-matrix formation algorithm was used as implemented in *Orca* along with the respective automatically generated auxiliary basis sets (AutoAux)²⁶³. Enthalpies at 298.15 K were calculated with the total thermal and zero-point energy correction from the PBEh-3c calculation combined with the electronic single point energies obtained on the PW6B95-D3(BJ)/def2-QZVPP level of theory.

5.1.3.3 Electron Affinities and Thermodynamic Data (for Chapters 3.1.6, 3.2 and 3.2.5)

Geometry optimizations and single point energy calculations have been performed with *ORCA* 4.0.1.2.^{259,264} The RI approximation²⁴⁵ for the Coulomb integrals was used in all cases (RIJCOSX), with application of corresponding auxiliary basis sets.²⁴⁶ The single point energies were obtained in two steps. First, geometry optimization was performed on BP86.²⁶⁵⁻²⁶⁶ The obtained geometry was taken and further

optimized on PW6B96.²⁶² Both steps included Grimme’s semi-empirical dispersion correction²⁴⁸ with Becke-Johnson damping function²⁴⁹⁻²⁵¹ (D3(BJ) and def2-SVP or def2-TZVPP²⁵²⁻²⁵³ basis set). Solvation correction (CH₂Cl₂) was performed with CPCM in both calculations as implemented in *Orca*.

All calculated geometries have been confirmed as energetic minima on the potential energy surface by analytical calculation of harmonic frequencies at the BP86-D3(BJ)/def2-SVP level, revealing only positive values. Enthalpies at 298 K have been calculated with the same level of theory by using the rigid-rotor harmonic oscillator (RRHO) approximation,²⁶¹ as implemented in *Orca*.

5.1.3.4 Geometry Optimizations, Single Point Energies on Different Spin States and Fractional Occupation Densities (FODs, for Chapter 3.3.4)

All computations were performed with the *Orca 5.0.3* program package.^{244,259} As starting geometries, VSEPR structures preoptimized with UFF were used. Structure optimizations for all compounds were performed with the r2SCAN-3c method (including the def2-mTZVPP basis set, geometrical counter-poise correction scheme (gCP) and the atom-pairwise dispersion correction (D4)),²⁶⁷ as implemented in *Orca*. For the compounds [4^{X,Y}][CH₃CN-Na@15c5]₂ and [d**h**bq^C][Na@15c5]₂, the structures were optimized in the triplet and the singlet manifold. Calculated equilibrium structures were confirmed as energetic minima on the potential energy surface by analytical calculation of harmonic frequencies at the level of optimization, revealing only positive Hessian eigenvalues. Enthalpies at 298.15 K have been calculated by using the rigid-rotor harmonic oscillator (RRHO) approximation,²⁶¹ as implemented in *Orca*.

Single point computations at the singlet- and triplet states were performed at the respective optimized structures of the same spin state. Restricted or unrestricted computations with the PW6B95 functional,²⁶² D4 dispersion correction²⁶⁷ and the def2-QZVPP basis set²⁵² were performed. For the Coulomb Integral, the RI approximation (RIJCOSX) was applied along with the corresponding auxiliary basis sets.²⁴⁶ Broken symmetry solutions were obtained by the implemented feature in *Orca 5.0.3*, on the triplet optimized structures. Coupling constants J are given according to Yamaguchi’s scheme $(-(E[\text{HS}]-E[\text{BS}]) / (\langle \text{S}^{*2} \rangle_{\text{HS}} - \langle \text{S}^{*2} \rangle_{\text{BS}}))$.

Thermochemical corrections to obtain H and G were taken from the structural optimization computations at the r2scan level of theory.

Fractional occupation densities (FODs) were obtained for the respective singlet state structures of $[4^{X,Y}][\text{CH}_3\text{CN-Na@15c5}]_2$ and $[\text{dhhq}^{\text{Cl}}][\text{Na@15c5}]_2$ as implemented in *Orca 5.0.3*, using the originally suggested FT-TPSS/def2-SV(P) ($T_{\text{el}} = 5000$ K) level of theory.^{207,268}

5.1.3.5 Fluoride-Anion-Affinities (FIAs, for Chapter 3.3.5)

For the optimized structures single point energies were calculated with the double-hybrid functional DSD-BLYP,²⁶⁹ the Becke-Johnson damping function (BJ),^{250,270} Grimme's semi-empirical dispersion correction (D3),²⁴⁸⁻²⁴⁹ and the def2-QZVPP basis set.²⁵² For the Coulomb Integral, the RI approximation (RIJCOSX) was applied along with the corresponding auxiliary basis sets.²⁴⁶ This combination is denoted as DSD-BLYP-D3(BJ)/def2-QZVPP.

The FIAs were derived from the thermodynamic data according to a protocol from a comprehensive benchmark study.²⁷¹ Final values were obtained after subtraction of the enthalpy for the isodesmic reaction of the Lewis Acid (LA) with trimethylsilylfluoride ($\text{FSi}(\text{CH}_3)_3$) to the Fluoride adduct of the Lewis acid and the trimethylsilyl cation ($\text{Si}(\text{CH}_3)_3^+$) from the highly accurate CCSD(T)/CBS anchor point for the FIA of the trimethylsilylcation.²⁷¹ The calculated gas phase values are shown in Table 13 (see Appendix).

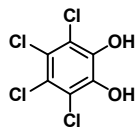
5.2 Syntheses

5.2.1 Precursors	114
5.2.1.1 Tetrachlorocatechol – H_2cat^{Cl}	114
5.2.1.2 3,4,6-Triisopropylcatechol – H_2cat^{iPr}	115
5.2.1.3 Tetrabromo- <i>o</i> -benzoquinone – q^{Br}	116
5.2.1.4 3,4,6-Triisopropyl- <i>o</i> -benzoquinone – q^{iPr}	117
5.2.1.5 Bromanilic acid – H_2dhhbq^{Br}	118
5.2.1.6 3,6-Dibromo-2,5-diphenyl- <i>p</i> -benzoquinone	119
5.2.1.7 Polyporic acid – H_2dhhbq^{Ph}	120
5.2.1.8 $[dhhbq^{NO_2}]Na_2$	121
5.2.1.9 $[dhhbq^H]Na_2$	122
5.2.1.10 2,3,6,7,10,11-Hexamethoxytriphenylene – <i>hmtp</i>	123
5.2.1.11 2,3,6,7,10,11-Hexahydroxytriphenylene – <i>H_6hhtp</i>	124
5.2.2 Silicon Lewis Acids	125
5.2.2.1 $Si(cat^{Cl})_2 \cdot (CH_3CN)_2 - 2^{Cl} \cdot (CH_3CN)_2$	125
5.2.2.2 $Si(cat^{Br})_2 \cdot (CH_3CN)_2 - 2^{Br} \cdot (CH_3CN)_2$	125
5.2.2.3 $Si(cat^{iPr})_2 - 2^{iPr}$	126
5.2.3 Homoleptic Silicon Trisdioxolene Compounds	127
5.2.3.1 $Si(diox^X)_3 - 1^X$ (X = Cl, Br)	127
5.2.3.2 $Si(diox^{tBu})_3 - 1^{tBu}$	128
5.2.3.3 $[Si(cat^X)_3][M]_2 - [1^X][M]_2$ (X = F, Cl, Br, tBu)	129
5.2.3.4 $[Si(diox^X)_3][N^nBu_4] - [1^X][N^nBu_4]$ (X = Cl, Br)	137
5.2.3.5 $[Si(cat^{Cl})_2(cat^{Cl})_2Si(cat^{Cl})_2][H_2N^nPr_2]_2 - [3^{Cl}][H_2N^nPr_2]_2$	139
5.2.4 Heteroleptic Silicon Trisdioxolene Compounds	140
5.2.4.1 $Si(diox^{Cl})_2(diox^{tBu}) - 1^{Cl,tBu}$	140

5.2.4.2	$\text{Si}(\text{diox}^{\text{Cl}})_2(\text{diox}^{\text{iPr}}) - 1^{\text{Cl,iPr}}$	140
5.2.5	Tetraoxolene-bridged Bis(catecholato)silanes	141
5.2.5.1	General Procedure: Preparation of $[\text{dhbq}^{\text{Y}}][\text{Na}@15\text{c}5]_2$	141
5.2.5.2	General Procedure: Preparation of $[(\text{cat}^{\text{X}})_2\text{Si}(\text{dhbq}^{\text{Y}})\text{Si}(\text{cat}^{\text{X}})_2][\text{Na}@15\text{c}5]_2 - [4^{\text{X,Y}}][\text{Na}@15\text{c}5]_2$	143
5.2.6	Hexaoxolene-bridged Bis(catecholato)silanes	147
5.2.6.1	$[\text{hhtp}(\text{Si}(\text{cat}^{\text{Cl}})_2)_3][\text{HB}]_6 - [5^{\text{Cl}}][\text{HB}]_6$	147
5.2.7	Catalysis.....	150
5.2.7.1	Oxidative Lactonization Studies	150
5.2.7.2	Dehydrogenative Coupling of 3,3'',4,4''-Tetramethoxy-o-terphenyl 152	
5.2.7.3	Oxidation of 9,10-Dihydroanthracene.....	152
5.2.8	Miscellaneous.....	153
5.2.8.1	$[2^{\text{Cl}}\text{-N}_3][\text{N}^n\text{Bu}_4]$	153
5.2.8.2	$[2^{\text{Cl}}(\text{N}_3)_2][\text{N}^n\text{Bu}_4]_2$	154

5.2.1 Precursors

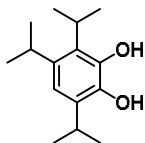
5.2.1.1 Tetrachlorocatechol – $\text{H}_2\text{cat}^{\text{Cl}}$



Freshly sublimated catechol (5.00 g, 45.4 mmol, 1.0 eq.) was dissolved in concentrated acetic acid (50 mL) and concentrated hydrochloric acid (275 mL). The solution was cooled down to 5 °C. Then hydrogen peroxide solution (35%, 15.6 mL, 182 mmol, 4.0 eq.) was added dropwise over a period of 2 h, whereby the color of the reaction changed multiple times. The solution was left to warm up to room temperature slowly leading to precipitation of light brown to orange solids. The precipitate was collected, washed with water, and left to dry in the fume hood for 24 h. The crude product (9.27 g, 37.4 mmol, 82 %) was washed with little amount of cold dichloromethane. It was then recrystallized from hot dichloromethane with the addition of some drops of EtOH. Finally, the crystalline solids were filtrated and dried *in vacuo*, yielding $\text{H}_2\text{cat}^{\text{Cl}}$ (4.26 g, 17.2 mmol, 38 %) as colorless solids. The analytical data was in agreement with the literature data.^{31,272}

$^1\text{H NMR}$ (400 MHz, CD_2Cl_2): $\delta = 5.92$ (s, 2H).

$^{13}\text{C NMR}$ (101 MHz, CD_2Cl_2): $\delta = 140.6$ ($\text{C}_{\text{cat-O}}$), 123.9 ($\text{C}_{\text{cat-Cl}}$), 119.2 ($\text{C}_{\text{cat-Cl}}$).

5.2.1.2 3,4,6-Triisopropylcatechol – $\text{H}_2\text{cat}^{\text{iPr}}$ 

Catechol (2.25 g, 20.4 mmol, 1.0 eq.) was suspended in heptane (6.0 mL) and isopropanol (4.91 g, 6.25 mL, 81.7 mmol, 4.0 eq.) was added. The mixture was heated to reflux. Concentrated sulfuric acid (8.02 g, 4.54 mL, 81.7 mmol, 4.0 eq.) was added over a period of 20 min. The reaction was stirred for further 5 h at around 100 °C. After cooling down, ethyl acetate was added to visibly enhance phase separation. The organic layer was separated and washed twice with diluted aqueous sodium hydroxide solution (0.5 M) and water. The organic phase was dried over Na_2SO_4 . After the solvent was evaporated under reduced pressure a black-brown and viscous residue (3.88 g, 80 %) remained. Purification of the crude material (4.00 g) by silica gel flash column chromatography (petroleum ether: ethyl acetate = 10:1) afforded $\text{H}_2\text{cat}^{\text{iPr}}$ (1.39 g, 5.88 mmol, 35 %) as a brown oil. Single crystals were obtained by solidifying the oil at -40 °C and slowly warming back to room temperature. This led to sublimation yielding in colorless crystals suitable for scXRD analysis. The analytical data was in agreement with the literature data.¹⁸²

^1H NMR (600 MHz, CDCl_3): δ = 6.65 (s, 1H), 5.34 (s, 1H), 4.74 (s, 1H), 3.37 (m, 1H), 3.17 (sept, $^3J_{\text{HH}}$ = 6.7 Hz, 1H), 3.05 (sept, $^3J_{\text{HH}}$ = 6.9 Hz, 1H), 1.40 (d, $^3J_{\text{HH}}$ = 7.2 Hz, 6H), 1.27 (d, $^3J_{\text{HH}}$ = 6.9 Hz, 6H), 1.21 (d, $^3J_{\text{HH}}$ = 6.9 Hz, 6H).

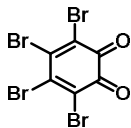
^{13}C NMR (151 MHz, CDCl_3): δ = 143.0 ($\text{C}_{\text{cat-O}}$), 138.8 ($\text{C}_{\text{cat-iPr}}$), 138.6 ($\text{C}_{\text{cat-O}}$), 131.3 ($\text{C}_{\text{cat-iPr}}$), 129.0 ($\text{C}_{\text{cat-iPr}}$), 113.7 ($\text{C}_{\text{cat-H}}$), 29.3 (CH), 27.7 (CH), 26.9 (CH), 24.4 (CH_3), 22.7 (CH_3), 21.2 (CH_3).

Elemental Analysis: calcd. for $\text{C}_{15}\text{H}_{24}\text{O}_2$: C 76.23, H 10.24, found: C 76.22, H 10.42.

GC-MS (EI pos.): m/z 221.2 (30 %) $\text{C}_{14}\text{H}_{21}\text{O}_2^+$ $[\text{M}-\text{CH}_3]^+$, 236.2 (10 %) $\text{C}_{15}\text{H}_{24}\text{O}_2^+$ $[\text{M}]^+$.

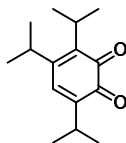
HR-MS (EI pos.): m/z calcd. for $\text{C}_{14}\text{H}_{21}\text{O}_2^+$ $[\text{M}-\text{CH}_3]^+$ 221.1536, found 221.1556; calcd. for $\text{C}_{15}\text{H}_{24}\text{O}_2^+$ $[\text{M}]^+$ 236.1771, found 236.1669.

IR (FT-ATR): $\tilde{\nu}$ = 3359 (br, O-H), 2958 (s, C-H), 2929 (s, C-H), 2869 (s, C-H), 1493 (m), 1440 (s), 1363 (s), 1262 (s), 1187 (s), 1104 (s).

5.2.1.3 Tetrabromo-*o*-benzoquinone – q^{Br} 

A solution of tetrabromocatechol (4.00 g, 9.40 mmol, 1.0 eq.) in warm glacial acetic acid (20 mL) was prepared. Nitric acid (65%, 1.05 mL, 15.0 mmol, 1.6 eq.), diluted with glacial acetic acid (1.5 mL), was added dropwise over 10 min. After the mixture was stirred for 2 h at room temperature, the addition of water (120 mL) precipitated a red solid, which was filtered. The solids were redispersed in dichloromethane and dried over Na_2SO_4 . The solvent was removed under reduced pressure. After drying *in vacuo* for 24 h, q^{Br} (2.24 g, 5.28 mmol, 56 %) was obtained as red crystalline solids. The analytical data was in agreement with the literature data.¹⁷⁶

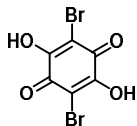
^{13}C NMR (101 MHz, CD_2Cl_2): $\delta = 169.2$ ($\text{C}_{\text{diox-O}}$), 142.7 ($\text{C}_{\text{diox-Br}}$), 128.6 ($\text{C}_{\text{diox-Br}}$).

5.2.1.4 3,4,6-Triisopropyl-*o*-benzoquinone – q^{iPr} 

3,4,6-Triisopropylcatechol (945 mg, 4.00 mmol, 1.0 eq.) was dissolved in diethyl ether (50 mL). A solution of $K_3Fe(CN)_6$ (6.4 g), crushed potassium hydroxide (1.28 g) and Na_2CO_3 (2.2 g) in water (60 mL) was added and the reaction mixture was stirred vigorously at room temperature for 2 h. Then, the phases were separated. The organic phase was washed with water for three times and the aqueous phase was extracted twice with diethyl ether. The combined organic layers were dried over Na_2SO_4 . The solvent was removed under reduced pressure leading to a dark red-brown oil. The oil was dried *in vacuo* for 24 h and afterwards stored at $-40\text{ }^\circ\text{C}$, where the product solidified. Finally, q^{iPr} (790 mg, 3.36 mmol, 84 %) was obtained as sticky dark green solids. The analytical data was in agreement with the literature data.¹⁸²

1H NMR (600 MHz, CD_2Cl_2): δ = 6.74 (d, $^4J_{HH} = 1.0$ Hz, 1H), 3.20 (sept, $^3J_{HH} = 6.9$ Hz, 1H), 3.09 (sept, $^3J_{HH} = 7.1$ Hz, 1H), 2.87 (dsept, $^3J_{HH} = 6.9$ Hz, $^4J_{HH} = 1.0$ Hz, 1H), 1.21 (d, $^3J_{HH} = 7.1$ Hz), 1.14 (d, $^3J_{HH} = 6.9$ Hz), 1.11 (d, $^3J_{HH} = 6.9$ Hz).

^{13}C NMR (101 MHz, CD_2Cl_2): δ = 181.8 ($C_{diox}O$), 181.0 ($C_{diox}O$), 154.0 ($C_{diox}iPr$), 147.1 ($C_{diox}iPr$), 140.5 ($C_{diox}iPr$), 134.1 ($C_{diox}H$), 29.7 (CH), 27.8 (CH), 27.3 (CH), 21.6 (CH_3), 21.2 (CH_3), 20.4 (CH_3).

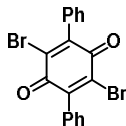
5.2.1.5 Bromanilic acid – $\text{H}_2\text{dhhbq}^{\text{Br}}$ 

2,5-Dihydroxy-*p*-benzoquinone (2.00 g, 14.3 mmol, 1.0 eq.) was suspended in ethanol (25 mL). Bromine (4.56 g, 1.46 mL, 28.6 mmol, 2.0 eq.) was slowly added to the suspension. The reaction mixture was stirred for 20 h at room temperature. Red precipitate was obtained, collected by filtration and washed with pentane and hexane. The crude product was redissolved in hot ethanol, layered with hexane and left to cool down. Red crystalline material formed. After drying *in vacuo* for 24 h, $\text{H}_2\text{dhhbq}^{\text{Br}}$ (1.54 g, 5.17 mmol, 36 %) was obtained as red brown powder. Single crystals were obtained from a saturated solution in hot ethanol layered with hexane. The analytical data was in agreement with the literature data.¹⁹⁰

$^1\text{H NMR}$ (600 MHz, $(\text{CD}_3)_2\text{CO}$): $\delta = 10.95$ (s, br, 2H).

$^{13}\text{C NMR}$ (151 MHz, $(\text{CD}_3)_2\text{CO}$): $\delta = 206.1$ ($\text{C}_q\text{-O}$), 102.1 ($\text{C}_q\text{-Br}$).

Elemental Analysis: calcd. for $\text{C}_6\text{H}_2\text{Br}_2\text{O}_4$: C 24.19, H 0.68, found: C 24.43, H 0.75.

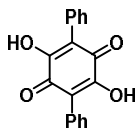
5.2.1.6 3,6-Dibromo-2,5-diphenyl-*p*-benzoquinone

2,5-Diphenyl-*p*-benzoquinone (1.11 g, 4.27 mmol, 1.0 eq.) was dissolved in hot glacial acetic acid (80 mL). Excess of bromine (approx. 5.50 g, 1.76 mL, 34.4 mmol, 8.1 eq.) was dropped to the yellow solution within 20 min. It was stirred at 100 °C for 1 h. After cooling down, water (400 mL) was added to the reaction. An orange suspension was obtained which was again heated to reflux until coagulation of the product was observed. After cooling down to room temperature, the orange solids were collected by filtration and washed with water. The title compound (1.66 g, 3.96 mmol, 93 %) was obtained as orange powder. Single crystals (orange) suitable for scXRD analysis were obtained from a saturated solution in hot *n*-butanol. The analytical data was in agreement with the literature data.¹⁹¹

¹H NMR (600 MHz, CDCl₃): δ = 7.51-7.49 (m, 6H), 7.35-7.33 (m, 4H).

¹³C NMR (151 MHz, CDCl₃): δ = 177.1 (C_q-O), 147.2 (C_q-Br), 136.4 (C_q-Ph), 133.3 (*ipso*-C_{Ph}), 129.9 (C_{Ph}-H), 129.4 (C_{Ph}-H), 128.4 (C_{Ph}-H).

Elemental Analysis: calcd. for C₁₈H₁₀Br₂O₂: C 51.71, H 2.41, found: C 51.98, H 2.54.

5.2.1.7 Polyporic acid – $\text{H}_2\text{dhhbq}^{\text{Ph}}$ 

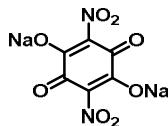
3,6-Dibromo-2,5-diphenyl-*p*-benzoquinone (1.00 g, 2.39 mmol, 1.0 eq.) was suspended in methanol (50 mL). An aqueous solution of sodium hydroxide (10 %, 50 mL) was added, and the reaction immediately turned violet. It was stirred for 2 h at around 50 °C. After cooling down, the mixture was filtrated. The violet solution was acidified with concentrated hydrochloric acid until discoloration and formation of brown precipitate was obtained. Water (50 mL) was added to the suspension. It was heated to reflux until coagulation of the solids was observed. The brown solids were collected by filtration and washed with a vigorous amount of water. After drying *in vacuo* at 50 °C for 2 d, $\text{H}_2\text{dhhbq}^{\text{Ph}}$ (500 mg, 1.71 mmol, 71 %) was obtained as light brown powder. Single crystals (brown) were obtained from a saturated solution in hot toluene. The analytical data was in agreement with the literature data.¹⁹²

$^1\text{H NMR}$ (600 MHz, $(\text{CD}_3)_2\text{SO}$): $\delta = 11.15$ (s, br), 7.43-7.37 (m, 4H), 7.35-7.31 (m, 1H).

$^{13}\text{C NMR}$ (151 MHz, $(\text{CD}_3)_2\text{SO}$): $\delta = 130.8$ (*ipso*- C_{Ph}), 130.5 ($\text{C}_{\text{Ph-H}}$), 127.6 ($\text{C}_{\text{Ph-H}}$), 127.5 ($\text{C}_{\text{Ph-H}}$), 115.6 ($\text{C}_{\text{q-Ph}}$).

Oxygen-bound carbons were not detected.

Elemental Analysis: calcd. for $\text{C}_{18}\text{H}_{12}\text{O}_4$: C 73.97, H 4.14, found: C 72.98, H 4.32.

5.2.1.8 [*dhbq*^{NO₂}]**Na**₂

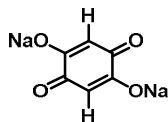
Sodium nitrite (5.00 g, 72.5 mmol, 9.0 eq.) was dissolved in water (200 mL). To the colorless solution tetrachloro-*p*-benzoquinone (2.00 g, 8.13 mmol, 1.0 eq.) was added, resulting in a yellow suspension. The reaction was heated to reflux for 2 h and turned orange. It was filtrated while hot and the solution was left to cool down to room temperature. Orange crystals already formed. The solution was further cooled down to 4 °C for 24 h to increase precipitation. The precipitate was collected by filtration and washed with less amount of water (50 mL). It was left to dry in the fume hood and further dried *in vacuo* for 24 h to yield the product (1.64 g, 5.97 mmol, 73 %) as orange crystalline solids. The analytical data was in agreement with the literature data.¹⁹³

¹H NMR measurements and elemental analysis revealed the presence of 2 eq. of water within 1 eq. of product. Therefore, prior to use, the product was dissolved in dimethyl sulfoxide. The solution was then dried over molecular sieves for 24 h. Then, adding dichloromethane led to precipitation of the product, which was collected by filtration and washed vigorously with dichloromethane and pentane. The solids were dried *in vacuo* for 24 h to yield [*dhbq*^{NO₂}]**Na**₂ as yellow powder in quantitative yields.

¹³C NMR (151 MHz, (CD₃)₂SO): δ = 168.6 (C_q-O), 133.2 (C_q-N).

Elemental Analysis: calcd. for C₆N₂Na₂O₈ x (CH₃)₂SO: C 27.28, H 1.72, N 7.95, found: C 27.58, H 1.99, N 7.66.

IR (FT-ATR): $\tilde{\nu}$ = 1587 (s, N=O, C=O), 1465 (m), 1264 (s), 1032 (s).

5.2.1.9 [*dhbq*^H]**Na**₂

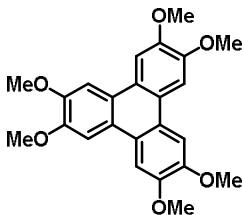
2,5-Dihydroxy-*p*-benzoquinone (500 mg, 3.57 mmol, 1.0 eq.) and NaH (171 mg, 7.14 mmol, 2.0 eq.) were mixed in acetonitrile (11 mL). The reaction mixture turned blood red and was stirred at room temperature until the hydrogen gas development was completed. During the reaction period, the gaseous phase was exchanged frequently. The reaction was further stirred for 18 h at room temperature yielding a brown suspension. The precipitate was collected by filtration and washed once with acetonitrile and several times with dichloromethane. Finally, the brown solids were dried *in vacuo* for 24 h to give [*dhbq*^H]**Na**₂ in quantitative yields.

¹H NMR (200 MHz, D₂O): δ = 5.36 (s, 2H).

¹³C NMR (600 MHz, D₂O): δ = 181.9 (C_q-O), 101.3 (C-H).

Elemental Analysis: calcd. for C₆H₂Na₂O₄: C 39.15, H 1.10, found: C 38.64, H 1.43.

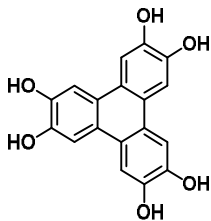
IR (FT-ATR): $\tilde{\nu}$ = 2939 (w, C-H), 1524 (s, C=O), 1400 (s), 1266 (s).

5.2.1.10 2,3,6,7,10,11-Hexamethoxytriphenylene – *hmtp*

Anhydrous iron(III) chloride (12.0 g, 73.9 mmol, 3.4 eq.) was suspended in dichloromethane (65 mL), followed by concentrated sulfuric acid (150 μ L). A solution of 1,2-dimethoxybenzene (3.0 g, 2.77 mL, 21.7 mmol, 1.0 eq.) in dichloromethane (30 mL), was added dropwise over a period of 20 min. The reaction was stirred for 3 h at room temperature. Afterwards it was quenched with methanol (90 mL) leading to a suspension. The precipitate was collected by filtration and washed with methanol (150 mL) and ethanol (100 mL). Drying *in vacuo* for 24 h finally afforded ***hmtp*** (2.58 g, 6.32 mmol, 84 %) as colorless powder. The analytical data was in agreement with the literature data.²⁰⁸

^1H NMR (400 MHz, CD_2Cl_2): $\delta = 7.81$ (s, 6H), 4.08 (s, 18H).

^{13}C NMR (101 MHz, CD_2Cl_2): $\delta = 149.4$ ($\text{C}_{\text{q-O}}$), 123.5 (C_{q}), 104.8 (CH), 56.3 (CH_3).

5.2.1.11 2,3,6,7,10,11-Hexahydroxytriphenylene – **H₆hhtp**

A solution of hexamethoxytriphenylene (500 mg, 1.22 mmol, 1.0 eq.) in dichloromethane (10 mL) was cooled to $-78\text{ }^{\circ}\text{C}$. Boron tribromide (1 M in CH_2Cl_2 , 14.7 mL, 14.7 mmol, 12 eq.) was added dropwise within a period of 20 min. While the reaction was allowed to warm to room temperature, it was further stirred for 16 h. Afterwards the mixture was poured onto ice (50 g) and stirred until the ice was melted. The precipitate was collected by filtration and washed vigorously with water. Drying *in vacuo* for 24 h at $60\text{ }^{\circ}\text{C}$ provided **H₆hhtp** (301 mg, 928 μmol , 76 %) as grey powder. The analytical data was in agreement with the literature data.¹³⁹

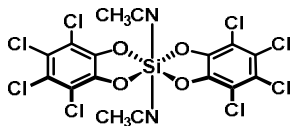
¹H NMR (600 MHz, $(\text{CD}_3)_2\text{SO}$): $\delta = 9.29$ (s, br, 6H), 7.61 (s, 6H).

¹³C NMR (151 MHz, $(\text{CD}_3)_2\text{SO}$): $\delta = 145.2$ ($\text{C}_q\text{-O}$), 121.8 (C_q), 107.8 (CH).

IR (FT-ATR): $\tilde{\nu} = 3418$ (s, br, O-H), 3376 (s, br, O-H), 1631 (m), 1609 (m), 1534 (s), 1452 (s), 1370 (s), 1246 (s), 1180 (s), 1128 (s), 1000 (s).

5.2.2 Silicon Lewis Acids

5.2.2.1 $\text{Si}(\text{cat}^{\text{Cl}})_2(\text{CH}_3\text{CN})_2 - 2\text{Cl}\cdot(\text{CH}_3\text{CN})_2$



$\text{H}_2\text{cat}^{\text{Cl}}$ was recrystallized (see 5.2.1.1), dissolved in acetonitrile and dried over molecular sieves (3 Å) for 24 h prior to use.

HSiCl_3 (296 mg, 221 μL , 2.19 mmol, 1.0 eq.) was slowly dropped to the solution of $\text{H}_2\text{cat}^{\text{Cl}}$ (1.09 g, 4.38 mmol, 2.0 eq.) in acetonitrile (40 mL) while stirring. Evolution of gas bubbles and colorless precipitation could be observed. After the gas development was finished, the solution was warmed up to 40 °C and stirred well for 24 h. The precipitate was collected by filtration, washed with acetonitrile (3 x 10 mL) and dichloromethane (3 x 10 mL). After drying *in vacuo* for 24 h, $2\text{Cl}\cdot(\text{CH}_3\text{CN})_2$ (1.12 g, 1.86 mmol, 85 %) was obtained as colorless solids.

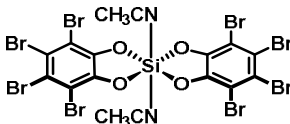
^1H NMR (400 MHz, CD_2Cl_2): $\delta = 2.00$ (s, br, 6H).

^{13}C and ^{29}Si NMR spectra could not be obtained due to limited solubility.

Elemental Analysis: calcd. for $\text{C}_{16}\text{H}_6\text{Cl}_8\text{N}_2\text{O}_4\text{Si}$: C 31.93, H 1.00, N 4.65, found C 31.59, H 1.18, N 4.68.

HR-MS (EI pos.): m/z calcd. for $\text{C}_{12}\text{Cl}_8\text{O}_4\text{Si}^+ [\text{M}-(\text{CH}_3\text{CN})_2]^+$ 519.7010, found: 519.7013.

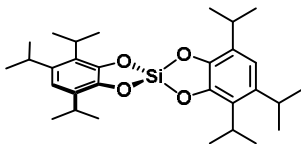
5.2.2.2 $\text{Si}(\text{cat}^{\text{Br}})_2(\text{CH}_3\text{CN})_2 - 2\text{Br}\cdot(\text{CH}_3\text{CN})_2$



$\text{H}_2\text{cat}^{\text{Br}}$ (2.00 g, 4.70 mmol, 2.0 eq.) was suspended in acetonitrile (15 mL). HSiCl_3 (237 μL , 2.35 mmol, 1.0 eq.) was slowly dropped into the solution, whereby evolution of gas bubbles and colorless precipitation could be observed. After the gas development was finished, the solution was warmed up to 40 °C and stirred for 24 h. The precipitate was collected by filtration, washed with acetonitrile and

dichloromethane. After drying *in vacuo* for 24 h, $2^{\text{Br}}\cdot(\text{CH}_3\text{CN})_2$ (2.05 g, 2.14 mmol, 91 %) was obtained as colorless solids. The analytical data was in agreement with the literature data.³²

5.2.2.3 $\text{Si}(\text{cat}^{\text{iPr}})_2 - 2^{\text{iPr}}$



$\text{H}_2\text{cat}^{\text{iPr}}$ (288 mg, 1.22 mmol, 2.0 eq) was dissolved in acetonitrile (5.0 mL) in a broad Schlenk tube resulting in a light brown solution. While stirring HSiCl_3 (78.3 mg, 58.5 μL , 578 μmol , 0.95 eq) was dropped into the solution. The reaction immediately turned greenish black, and development of gas bubbles was observed. It was stirred well for 24 h at room temperature. Over time, it could be observed that the mixture decolorated to light brown and colorless sticky solids formed. The supernatant solution was removed, and the solids were washed with acetonitrile (2 x 5 mL). After drying *in vacuo* 2^{iPr} (183 mg, 368 μmol , 64 %) was obtained as colorless powder.

$^1\text{H NMR}$ (600 MHz, CDCl_3): $\delta = 6.77$ (s, 1H), 3.31 (sept, $^3J_{\text{HH}} = 7.0$ Hz, 1H), 3.21 (sept, $^3J_{\text{HH}} = 6.8$ Hz, 1H), 3.16 (sept, $^3J_{\text{HH}} = 6.9$ Hz, 1H), 1.37 (d, $^3J_{\text{HH}} = 7.0$ Hz, 6H), 1.28 (d, $^3J_{\text{HH}} = 7.0$ Hz, 6H), 1.23 (d, $^3J_{\text{HH}} = 6.8$ Hz, 6H).

$^{13}\text{C NMR}$ (151 MHz, CDCl_3): $\delta = 144.6$ ($\text{C}_{\text{cat}}\text{-O}$), 142.1 ($\text{C}_{\text{cat}}\text{-O}$), 139.9 (C_{cat}), 131.2 (C_{cat}), 129.1 (C_{cat}), 116.1 ($\text{C}_{\text{cat}}\text{-H}$), 29.4 (CH), 28.5 (CH), 27.1 (CH), 24.4 (CH_3), 22.5 (CH_3), 21.2 (CH_3).

$^{29}\text{Si INVGATE NMR}$ (119 MHz, CDCl_3): $\delta = -41.1$.

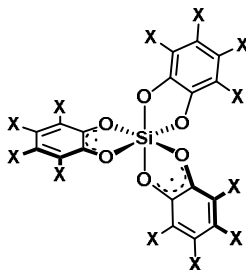
Elemental Analysis: calcd. for $\text{C}_{30}\text{H}_{44}\text{O}_4\text{Si}$: C 72.54, H 8.93, found: C 72.36, H 8.90.

HR-MS (ESI neg.): m/z calcd. for $\text{C}_{30}\text{H}_{45}\text{O}_5\text{Si}^-$ [$\text{M}+\text{OH}$] $^-$ 513.3042, found 513.3045 (100 %).

IR (FT-ATR): $\tilde{\nu} = 2958$ (s, C-H), 2929 (s, C-H), 2870 (s, C-H), 1415 (s), 1309 (s), 1174 (s), 1120 (s), 993 (s).

5.2.3 Homoleptic Silicon Trisdioxolene Compounds

5.2.3.1 $\text{Si}(\text{diox}^{\text{X}})_3 - 1^{\text{X}}$ ($\text{X} = \text{Cl}, \text{Br}$)



SiI_4 and perhalogenated *ortho*-benzoquinone (q^{X}) were dissolved in dichloromethane. The solution was intense red colored in the beginning and was allowed to stand without stirring for several days ($\text{X} = \text{Cl}$) or 24 h ($\text{X} = \text{Br}$). Thereby the mixture darkened to black violet (due to the formed iodine) and big black crystals were observed in the vial. The supernatant solution was removed. The crystalline material was washed several times by suspending in pentane and removing the supernatant until no coloration of the solution was observed anymore. Afterwards the solids were dried *in vacuo* for 24 h to give the products 1^{X} as intense colored powders.

$\text{Si}(\text{diox}^{\text{Cl}})_3 - 1^{\text{Cl}}$: SiI_4 (350 mg, 653 μmol , 1.0 eq.) and q^{Cl} (482 mg, 1.96 mmol, 3.0 eq.) were employed in CH_2Cl_2 (3.0 mL) to give 1^{Cl} (429 mg, 560 μmol , 86 %) as green powder. Single crystals (black) were obtained from a saturated solution in CH_2Cl_2 or by gaseous diffusion of pentane into solutions of CH_2Cl_2 at -40°C or *o*-dcb at room temperature. Crystallization was also possible in TCE by layering with C_6H_6 .

IR (FT-ATR): $\tilde{\nu} = 1502$ (s), 1453 (s), 1387 (sh), 1208 (s), 991 (s).

UV-vis-NIR (CH_2Cl_2 , 5×10^{-4} M): 299, 488, 615, 1025, 1116, 2844.

UV-vis-NIR (*o*-dcb, 5×10^{-4} M): 301, 322, 467, 568, 1130, 2844, 2915.

$\text{Si}(\text{diox}^{\text{Br}})_3 - 1^{\text{Br}}$: SiI_4 (61.9 mg, 116 μmol , 1.0 eq.) and q^{Br} (147 mg, 346 μmol , 3.0 eq.) were employed in CH_2Cl_2 (1.0 mL) to give 1^{Br} (114 mg, 87.8 μmol , 76 %) as purple powder. Single crystals (black violet) suitable for scXRD analysis were obtained from saturated solutions in CH_2Cl_2 or C_6H_6 .

Elemental analysis: calcd. for $C_{18}Br_{12}O_6Si$: C 16.64, found: C 16.90.

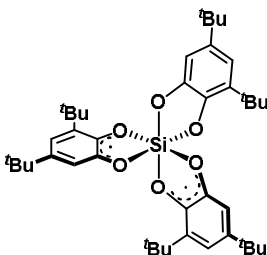
HR-MS (MALDI neg.): m/z calcd. for $C_{18}HBr_{12}O_6Si^- [M+H]^-$ 1299.9626, found 1299.9645 (70 %); calcd. for $C_{12}HBr_8O_5Si^- [Si(cat^{Br})_2+OH]^-$ 892.2983, found 892.2993 (100 %).

IR (FT-ATR): $\tilde{\nu}$ = 1491 (m), 1467 (m), 1416 (s), 1264 (w), 1223 (w), 1359 (m), 1163 (m), 1025 (s).

UV-vis-NIR (CH_2Cl_2 , 10^{-4} M): 277, 468, 575 (sh), 2856.

UV-vis-NIR (*o*-dcb, 10^{-3} M): 491, 1054, 1154, 2852.

5.2.3.2 $Si(diox^{tBu})_3 - 1^{tBu}$

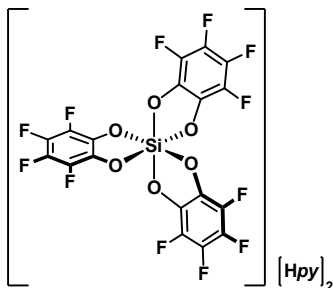


SiI_4 (162 mg, 302 μ mol, 1.0 eq.) and q^{tBu} (200 mg, 908 μ mol, 3.0 eq.) were dissolved in dichloromethane (6.0 mL). The reaction immediately turned dark brown and was stirred at room temperature for 24 h. Afterwards the solvent and iodine (in parts) were removed under reduced pressure. The residual solids were redissolved in dichloromethane and filtered fast over celite and activated charcoal. A black-green solution was obtained. The solvent was removed under reduced pressure. The resulting solids were dried *in vacuo* for 24 h to give 1^{tBu} (107 mg, 155 μ mol, 51 %) as dark green powder.

Elemental Analysis: calcd. for $C_{42}H_{60}O_6Si$: C 73.21, H 8.78, found: C 72.42, H 8.65.

HR-MS (MALDI neg.): m/z calcd. for $C_{42}H_{61}O_6Si^- [M+H]^-$ 689.4243, found 689.4249 (19 %); calcd. for $C_{29}H_{44}O_5Si^- [Si(cat^{tBu})_2+OMe]^-$ 499.2885, found 499.2873.

IR (FT-ATR): $\tilde{\nu}$ = 2954 (s, C-H), 2905 (s, C-H), 2868 (s, C-H); 1574 (w), 1480 (s), 1425 (s), 1362 (m), 1242 (s), 987 (s).

5.2.3.3 $[\text{Si}(\text{cat}^{\text{X}})_3][\text{M}]_2 - [\text{1}^{\text{X}}][\text{M}]_2$ ($\text{X} = \text{F}, \text{Cl}, \text{Br}, \text{tBu}$)

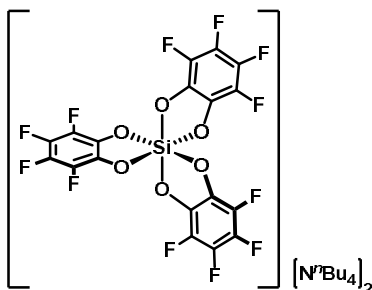
$[\text{Si}(\text{cat}^{\text{F}})_3][\text{Hpy}]_2 - [\text{1}^{\text{F}}][\text{Hpy}]_2$: $\text{H}_2\text{cat}^{\text{F}}$ (100 mg, 549 μmol , 3.0 eq.) was dissolved in acetonitrile (5.0 mL). Then pyridine (28.5 mg, 29.0 μL , 360 μmol , 2.0 eq.) and tetraethyl orthosilicate (37.5 mg, 39.9 μL , 180 μmol , 1.0 eq.) were added and the mixture was stirred for 16 h resulting in an orange solution. The solvent was removed under reduced pressure. The solid was washed with diethyl ether and dried *in vacuo* for 24 h to yield $[\text{1}^{\text{F}}][\text{Hpy}]_2$ (95.0 mg, 130 μmol , 72 %) as brown powder.

^1H NMR (400 MHz, CD_2Cl_2): $\delta = 8.91$ (d, $^3J_{\text{HH}} = 5.2$ Hz, 4H), 8.30 (t, $^3J_{\text{HH}} = 7.8$ Hz, 2H), 7.82 (t, $^3J_{\text{HH}} = 6.8$ Hz, 4H).

^{19}F NMR (376 MHz, CD_2Cl_2): $\delta = -170.7$ (m, 2F), -177.0 (m, 2F).

^{13}C and ^{29}Si NMR spectra could not be obtained due to limited solubility.

HR-MS (ESI neg.): m/z calcd. for $\text{C}_{18}\text{HF}_{12}\text{O}_6\text{Si}^- [\text{Si}(\text{cat}^{\text{F}})_3 + \text{H}]^-$ 568.9356, found 568.9362.



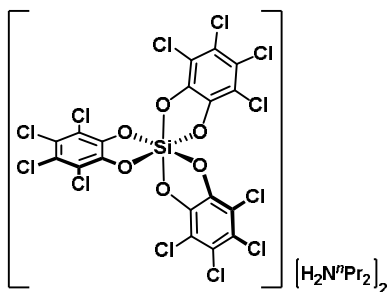
$[\text{Si}(\text{cat}^{\text{F}})_3][\text{N}^t\text{Bu}_4]_2 - [\text{1}^{\text{F}}][\text{N}^t\text{Bu}_4]_2: [\text{1}^{\text{F}}][\text{Hpy}]_2$ (80.0 mg, 110 μmol , 1.0 eq.) was suspended in dichloromethane (20 mL), giving an orange solution. Then $\text{N}^t\text{Bu}_4\text{Br}$ (70.9 mg, 220 μmol , 2.0 eq.) was added and the mixture was stirred for 2 h. Concentrating the solution under reduced pressure and cooling to $-20\text{ }^\circ\text{C}$ resulted in a yellow suspension. The precipitate was removed by filtration and the solution was washed with water (3 x 5 mL). Then the solvent was removed under reduced pressure yielding $[\text{1}^{\text{F}}][\text{N}^t\text{Bu}_4]_2$ (58.0 mg, 55.1 μmol , 50 %) as brown solids which was dried *in vacuo* for 24 h.

$^1\text{H NMR}$ (400 MHz, CD_2Cl_2): $\delta = 3.26$ (m, 16H), 1.66 (m, 16H), 1.31 (m, 16H), 0.90 (t, $^3J_{\text{HH}} = 6.56$ Hz, 24H).

$^{13}\text{C NMR}$ (151 MHz, CD_2Cl_2): $\delta = 59.0$ (N- CH_2), 23.9 (CH_2), 19.7 (CH_2), 13.3 (CH_3). Residual signals were not detected due to intense fluorine content (coupling).

$^{19}\text{F NMR}$ (376 MHz, CD_2Cl_2): $\delta = -172.5$ (m, 2F), -181.0 (m, 2F).

HR-MS (ESI neg.): m/z calcd. for $\text{C}_{18}\text{HF}_{12}\text{O}_6\text{Si}^- [\text{Si}(\text{cat}^{\text{F}})_3 + \text{H}]^-$ 568.9356, found 568.9362; $\text{C}_{34}\text{H}_{36}\text{F}_{12}\text{NO}_6\text{Si}^- [\text{Si}(\text{cat}^{\text{F}})_3 + \text{N}^t\text{Bu}_4 + \text{H}]^-$ calcd. 810.2125, found 810.2130.



[Si(*cat*^{Cl})₃][H₂N^{*n*}Pr₂]₂ – [1^{Cl}][H₂N^{*n*}Pr₂]₂: Di-*n*-propylamine (109 mg, 148 μL, 1.08 μmol, 2.0 eq.) was slowly dropped to a solution of H₂*cat*^{Cl} (402 mg, 1.62 mmol, 3.0 eq.) in acetonitrile (6.0 mL). The reaction mixture turned red brown. Tetraethyl orthosilicate (113 mg, 121 μL, 541 μmol, 1.0 eq.) was slowly added. The reaction was stirred for 1 h at room temperature and heated to reflux for 2 h. After cooling to room temperature, a colorless solid precipitated. Cooling to –20 °C for 1 h promoted further precipitation. The solids were collected by filtration, washed several times with diethyl ether and dried *in vacuo* to give [1^{Cl}][H₂N^{*n*}Pr₂]₂ (268 mg, 276 μmol, 51 %) as colorless crystalline solids. Single crystals (colorless) suitable for scXRD analysis were obtained from a saturated solution in acetonitrile at –20 °C. The analytical data was in agreement with the literature data.⁹²

¹H NMR (600 MHz, CD₂Cl₂): δ = 7.43 (s, 4H), 3.23 (t, ³*J*_{HH} = 7.4 Hz, 8H), 1.71 (sext, ³*J*_{HH} = 7.5 Hz, 4H), 0.96 (t, ³*J*_{HH} = 7.4 Hz, 6H).

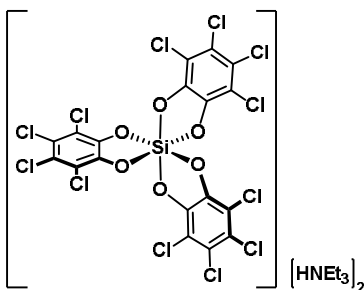
¹³C NMR (151 MHz, CD₂Cl₂): δ = 146.7 (C_{*cat*}-O), 120.3 (C_{*cat*}-Cl), 114.2 (C_{*cat*}-Cl), 49.2 (N-CH₂), 19.7 (CH₂), 10.9 (CH₃).

²⁹Si INVGATE NMR (119 MHz, CD₂Cl₂): δ = –143.7.

Elemental Analysis: calcd. for C₃₀H₃₂Cl₁₂N₂O₆Si: C 37.14, H 3.33, N 2.89, found: C 37.69, H 3.49, N 3.01.

HR-MS (ESI neg.): *m/z* calcd. for C₁₈HCl₁₂O₆Si[–] [Si(*cat*^{Cl})₃+H][–] 766.5721, found: 766.5751.

IR (FT-ATR): $\tilde{\nu}$ = 3230 (m), 2970 (m), 2806 (m), 1568 (m), 1456 (s), 1387 (s), 1305 (w), 1244 (s), 1237 (s), 984 (s).



[Si(*cat*^{Cl})₃][HNEt₃]₂ – [1^{Cl}][HNEt₃]₂: Triethylamine (136 mg, 188 μ L, 1.35 mmol, 2.0 eq.) was slowly dropped to a solution of H₂*cat*^{Cl} (500 mg, 2.02 mmol, 3.0 eq.) in acetonitrile (40 mL). The reaction mixture turned reddish. Then tetraethyl orthosilicate (140 mg, 149 μ L, 672 μ mol, 1.0 eq.) was slowly added. The reaction was stirred for 2 h at room temperature and heated to reflux for 18 h. After cooling to room temperature, colorless solids precipitated. Cooling to -20 °C for 1-2 h promoted further precipitation. The solids were collected by filtration, washed with diethyl ether and pentane, and dried under reduced pressure to give [1^{Cl}][HNEt₃]₂ (400 mg, 412 μ mol, 61 %) as colorless powder.

¹H NMR (200 MHz, CD₂Cl₂): δ = 7.37 (s, 2H), 3.48 (t, ³*J*_{HH} = 5.6 Hz, 12H), 1.26 (t, ³*J*_{HH} = 7.2 Hz, 18H).

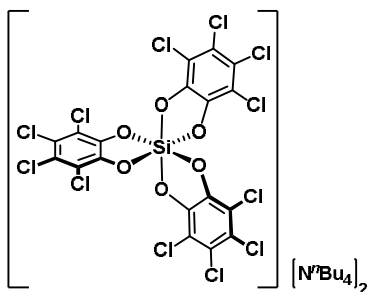
¹³C NMR (151 MHz, CD₂Cl₂): δ = 147.6 (C_{*cat*}-O), 119.9 (C_{*cat*}-Cl), 113.8 (C_{*cat*}-Cl), 48.2 (N-CH₂), 9.0 (N-CH₃).

²⁹Si INVGATE NMR (119 MHz, CD₃CN): δ = -138.3 .

Elemental Analysis: calcd. for C₃₀H₃₂Cl₁₂N₂O₆Si: C 37.14, H 3.33, N 2.89, found: C 37.48, H 3.49, N 3.15.

HR-MS (ESI neg.): *m/z* calcd. for C₁₈HCl₁₂O₆Si⁻ [Si(*cat*^{Cl})₃+H]⁻ 766.5721, found 766.5718.

IR (FT-ATR): $\tilde{\nu}$ = 3118 (m), 2982 (w), 2946 (w), 1571 (w), 1552 (w), 1453 (s), 1396 (sh), 1382 (s), 1304 (m), 1245 (sh), 1231 (m), 983 (s).



[Si(*cat*^{Cl})₃][N^{*t*}Bu₄]₂ – [1^{Cl}][N^{*t*}Bu₄]₂: To a suspension of [1^{Cl}][HNEt₃]₂ (388 mg, 400 μmol, 1.0 eq.) in dichloromethane (50 mL), N^{*t*}Bu₄Cl (222 mg, 800 μmol, 2.0 eq.) was added. The clear and colorless solution was stirred vigorously for 2 h and cooled down to –20 °C overnight to precipitate the side product triethylammonium chloride. Colorless crystals were obtained and removed. The filtrate was washed with water (3 x 50 mL). The organic phase was then dried over anhydrous MgSO₄, and the solvent removed under reduced pressure. The resulting solids were dried *in vacuo* to give [1^{Cl}][N^{*t*}Bu₄]₂ (370 mg, 296 μmol, 74 %) as colorless powder. Single crystals (colorless) were obtained from a saturated solution in dichloromethane at –20 °C.

¹H NMR (600 MHz, CD₂Cl₂): δ = 3.22 (t, ³*J*_{HH} = 8.5 Hz, 16H), 1.69–1.63 (m, 16H), 1.25 (sext, ³*J*_{HH} = 7.4 Hz, 16H), 0.85 (t, ³*J*_{HH} = 7.2 Hz, 24H).

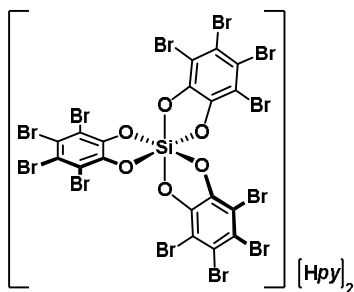
¹³C NMR (151 MHz, CD₂Cl₂): δ = 149.2 (C_{cat}-O), 117.9 (C_{cat}-Cl), 112.6 (C_{cat}-Cl), 59.6 (N-CH₂), 24.4 (CH₂), 20.2 (CH₂), 13.7 (CH₃).

²⁹Si INVGATE NMR (119 MHz, CD₃CN): δ = –138.2.

Elemental Analysis: calcd. for C₅₀H₇₂Cl₁₂N₂O₆Si: C 48.02, H 5.80, N 2.24, found: C 48.24, H 5.91, N 2.18.

HR-MS (ESI neg.): *m/z* calcd. for C₁₈Cl₁₂O₆Si²⁻ [Si(*cat*^{Cl})₃]²⁻ 382.7824, found 382.7813; calcd. for C₁₈HCl₁₂O₆Si⁻ [Si(*cat*^{Cl})₃+H]⁻ 766.5721, found 766.5682; calcd. for C₃₄H₃₆Cl₁₂NO₆Si⁻ [Si(*cat*^{Cl})₃+N^{*t*}Bu₄+H]⁻ 1007.8491, found 1007.8511.

IR (FT-ATR): $\tilde{\nu}$ = 2961 (s), 2932 (sh), 2875 (m), 1568 (w), 1549 (w), 1462 (s), 1379 (s), 1304 (s), 1240 (s), 985 (s).

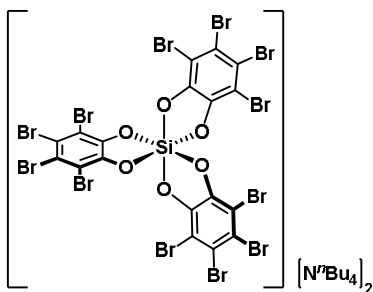


$[\text{Si}(\text{cat}^{\text{Br}})_3][\text{Hpy}]_2 - [1^{\text{Br}}][\text{Hpy}]_2$: $\text{H}_2\text{cat}^{\text{Br}}$ (2.00 g, 4.70 mmol, 3.0 eq.) was suspended in acetonitrile (42 mL). While stirring, first pyridine (248 mg, 252 μL , 3.13 mmol, 3.0 eq.) and then tetraethyl orthosilicate (326 mg, 347 μL , 1.57 mmol, 1.0 eq.) were added. The mixture was stirred for 2 h at room temperature and heated to reflux for further 2 h which led to a yellow precipitation. The solid was collected by filtration and washed with diethyl ether. After drying *in vacuo* at 70 °C for 48 h, $[1^{\text{Br}}][\text{Hpy}]_2$ was obtained as yellow powder (1.55 g, 1.07 mmol, 68 %).

$^1\text{H NMR}$ (600 MHz, CD_2Cl_2): $\delta = 9.20$ (m, 4H), 8.48 (m, 2H), 7.98 (m, 4H).

$^{13}\text{C NMR}$ (151 MHz, CD_2Cl_2): $\delta = 148.7$ ($\text{C}_{\text{cat-O}}$), 146.3 (C_{py}), 142.8 (C_{py}), 127.4 (C_{py}), 114.5 ($\text{C}_{\text{cat-Br}}$), 107.2 ($\text{C}_{\text{cat-Br}}$).

$^{29}\text{Si INVGATE NMR}$ (119 MHz, CD_2Cl_2): $\delta = -142.3$.

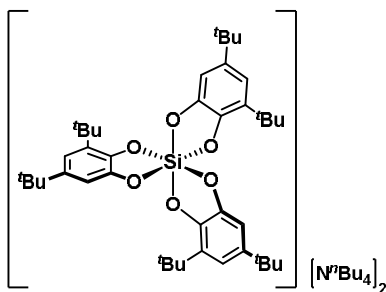


$[\text{Si}(\text{cat}^{\text{Br}})_3][\text{N}^n\text{Bu}_4]_2 - [\text{1}^{\text{Br}}][\text{N}^n\text{Bu}_4]_2: [\text{1}^{\text{Br}}][\text{Hpy}]_2$ (512 mg, 351 mmol, 1.0 eq.) was suspended in dichloromethane (400 mL). Then $\text{N}^n\text{Bu}_4\text{Br}$ (226 mg, 702 mmol, 2.0 eq.) was added and subsequently the mixture was stirred for 2 h at room temperature. The solution was cooled to $-20\text{ }^\circ\text{C}$ and yellow precipitation was observed. The precipitate was removed by filtration. The filtrate was washed with water (3 x 5 mL). The solvent of the organic phase was removed under reduced pressure. The residual was dried *in vacuo* for several days giving $[\text{1}^{\text{Br}}][\text{N}^n\text{Bu}_4]_2$ (332 mg, 186 mmol, 53 %) as light brown powder. Single crystals (colorless) suitable for scXRD analysis were obtained from a saturated solution in dichloromethane at $-40\text{ }^\circ\text{C}$.

$^1\text{H NMR}$ (600 MHz, CD_2Cl_2): $\delta = 3.02$ (m, 16H), 1.53 (m, 16H), 1.29 (sext, $^3J_{\text{HH}} = 7.3$ Hz, 16H), 0.93 (t, $^3J_{\text{HH}} = 7.47$ Hz, 24H).

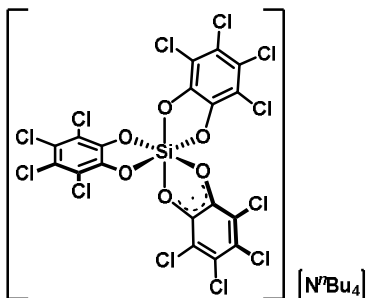
$^{13}\text{C NMR}$ (151 MHz, CD_2Cl_2): $\delta = 151.1$ ($\text{C}_{\text{cat-O}}$), 112.0 ($\text{C}_{\text{cat-Br}}$), 105.6 ($\text{C}_{\text{cat-Br}}$), 59.5 (N- CH_2), 24.3 (CH_2), 20.1 (CH_2), 13.8 (CH_3).

$^{29}\text{Si INVGATE NMR}$ (119 MHz, CD_2Cl_2): $\delta = -141.1$.



$[\text{Si}(\text{cat}^{\text{tBu}})_3][\text{N}^n\text{Bu}_4]_2$ – $[\mathbf{1}^{\text{tBu}}][\text{N}^n\text{Bu}_4]_2$: 3,5-Di-tert-butylcatechol (500 mg, 2.25 mmol, 3.0 eq.) was dissolved in acetonitrile (15 mL). Then pyridine (119 mg, 121 μL , 1.50 mmol, 2.0 eq.) was added over a period of 5 min and tetraethyl orthosilicate (156 mg, 166 μL , 750 μmol , 1.0 eq.) was added within 15 min. The mixture was stirred at room temperature for 30 min and heated to reflux for further 2 h. The solvent was removed under reduced pressure, giving a dark, oily substance. The residue was dissolved in dichloromethane (15.0 mL) and $\text{N}^n\text{Bu}_4\text{Br}$ (484 mg, 1.50 mmol, 2.0 eq) was added. After stirring for 2 h at room temperature the solution was concentrated under reduced pressure to a volume of 5 mL. The solution was washed with water (5 x 5 mL) and the solvent of the organic phase was removed under reduced pressure. Finally, the residue was dried *in vacuo* to give $[\mathbf{1}^{\text{tBu}}][\text{N}^n\text{Bu}_4]_2$ (690 mg, 593 μmol , 79 %) as light brown oil.

^{13}C NMR (101 MHz, CD_2Cl_2): $\delta = 143.5$ ($\text{C}_{\text{cat-O}}$), 142.3 ($\text{C}_{\text{cat-O}}$), 141.4 ($\text{C}_{\text{cat-tBu}}$), 135.8 ($\text{C}_{\text{cat-tBu}}$), 115.7 ($\text{C}_{\text{cat-H}}$), 111.3 ($\text{C}_{\text{cat-H}}$), 59.4 (N- CH_2), 35.1 (C-(CH_3)₃), 34.6 (C-(CH_3)₃), 31.7 (C-(CH_3)₃), 29.8 (C-(CH_3)₃), 24.3 (CH_2), 20.0 (CH_2), 13.8 (CH_3).

5.2.3.4 $[\text{Si}(\text{diox}^{\text{X}})_3][\text{N}^n\text{Bu}_4] - [\text{1}^{\text{X}}][\text{N}^n\text{Bu}_4]$ ($\text{X} = \text{Cl}, \text{Br}$)

$[\text{Si}(\text{diox}^{\text{Cl}})_3][\text{N}^n\text{Bu}_4] - [\text{1}^{\text{Cl}}][\text{N}^n\text{Bu}_4]$: $[\text{1}^{\text{Cl}}][\text{N}^n\text{Bu}_4]_2$ (54.0 mg, 43.2 μmol , 1.0 eq.) was dissolved in dichloromethane (2.0 mL) and cooled down to -40 $^{\circ}\text{C}$. To the colorless solution, $\mathbf{1}^{\text{Cl}}$ (33.1 mg, 43.2 μmol , 1.0 eq.) was added. Immediately, an intense black-green colored reaction mixture was observed. The reaction was maintained at -40 $^{\circ}\text{C}$ without stirring. After 24 h black-green crystals suitable for scXRD analysis were obtained. The supernatant solution was removed. The crystalline solids were dried *in vacuo* to yield the $[\text{1}^{\text{Cl}}][\text{N}^n\text{Bu}_4]$ as intense green powder (55.4 mg, 55.0 μmol , 64 %).

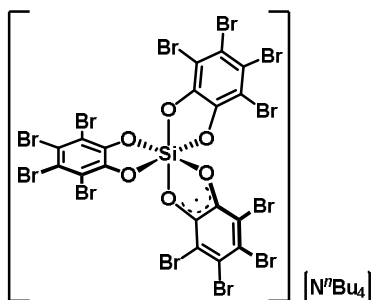
Single crystal structure analysis and elemental analysis revealed one equivalent of dichloromethane per structural unit.

Elemental Analysis: calcd. for $\text{C}_{34}\text{H}_{36}\text{Cl}_{12}\text{NO}_6\text{Si} \times \text{CH}_2\text{Cl}_2$: C 38.46, H 3.50, N 1.28, found: C 38.49, H 3.53, N 1.28.

HR-MS (ESI neg.): m/z calcd. for $\text{C}_{18}\text{HCl}_{12}\text{O}_6\text{Si}^- [\text{1}^{\text{Cl}}+\text{H}]^-$ 766.5721, found 766.5645.

IR (FT-ATR): $\tilde{\nu} = 2874$ (m), 2932 (sh), 2960 (m), 1528 (m), 1448 (s), 1385 (s), 1300 (m), 1287 (m), 1236 (s), 1212 (s), 986 (s).

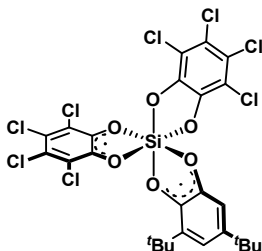
EPR (9.449144 GHz, CH_2Cl_2): $g = 2.0046$.



$[\text{Si}(\text{dioxBr})_3][\text{N}^n\text{Bu}_4] - [\text{1Br}][\text{N}^n\text{Bu}_4]: [\text{1Br}][\text{N}^n\text{Bu}_4]_2$ (30.0 mg, 16.8 μmol , 1.0 eq.) was dissolved in dichloromethane (1.0 mL) and cooled down to -40°C . The colorless solution was dropped to a solution of $\mathbf{1}^{\text{Br}}$ (21.9 mg, 16.8 μmol , 1.0 eq.) in dichloromethane (1.0 mL). Immediately, the reaction mixture turned dark brown. The reaction was maintained at -40°C without stirring. After 24 h the solution was filtrated. Another 24 h at -40°C led to the development of black crystalline solids. The solvent was removed under reduced pressure. The crystalline solids were dried *in vacuo* for 24 h to yield $[\mathbf{1}^{\text{Br}}][\text{N}^n\text{Bu}_4]$ as brown powder in quantitative yields. Single crystals (dark yellow) suitable for scXRD analysis were obtained from a saturated solution in dichloromethane at -40°C .

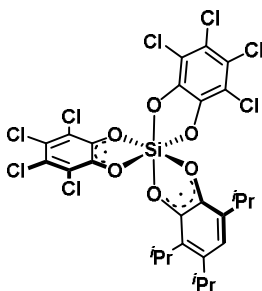
5.2.4 Heteroleptic Silicon Trisdioxolene Compounds

5.2.4.1 $\text{Si}(\text{diox}^{\text{Cl}})_2(\text{diox}^{\text{tBu}}) - 1^{\text{Cl,tBu}}$



$(\mathbf{2}^{\text{Cl}})_n$ (11.0 mg, 21.2 μmol , 1.0 eq.) and q^{tBu} (4.67 mg, 21.2 μmol , 1.0 eq.) were mixed in CD_2Cl_2 (0.5 mL) to give a brown solution. After stirring at room temperature for 48 h a green solution was obtained. The solvent was removed under reduced pressure. The residue was dried *in vacuo* to give $\mathbf{1}^{\text{Cl,tBu}}$ as green solids in quantitative yields.

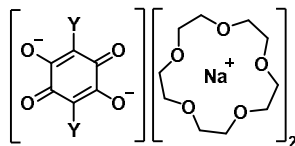
5.2.4.2 $\text{Si}(\text{diox}^{\text{Cl}})_2(\text{diox}^{\text{iPr}}) - 1^{\text{Cl,iPr}}$



$(\mathbf{2}^{\text{Cl}})_n$ (10.2 mg, 19.6 μmol , 1.0 eq.) and q^{iPr} (4.60 mg, 19.6 μmol , 1.0 eq.) were mixed in CD_2Cl_2 (0.5 mL) to give a brown suspension. After stirring at room temperature for 24 h a dark brown-green solution was obtained. The solvent was removed under reduced pressure. The residue was dried *in vacuo* to give $\mathbf{1}^{\text{Cl,iPr}}$ as green solids in quantitative yields.

5.2.5 Tetraoxolene-bridged Bis(catecholato)silanes

5.2.5.1 General Procedure: Preparation of $[d\text{h}bq^Y][\text{Na}@15\text{c}5]_2$



Y = Cl, Br, Ph, NO₂

For Y = Cl, Br and Ph, 1 eq. of substituted dihydroxybenzoquinone (**H₂dhbq^Y**) and 2 eq. of NaH were mixed in acetonitrile. The reaction was stirred at room temperature until the hydrogen gas development was completed. During the reaction period, the gaseous phase was exchanged frequently. The reaction was further stirred for 18 h at room temperature. The precipitate was collected by filtration and washed once with acetonitrile and several times with dichloromethane. After drying *in vacuo* for 24 h, **[dhbq^Y]₂Na₂** (Y = Cl, Br, Ph, NO₂) were suspended in dichloromethane with an excess of 15-crown-5. The mixture was again stirred for 18 h at room temperature to ensure complete complexation. The solids were collected by filtration and washed once with dichloromethane and three times with pentane. The final products **[dhbq^Y][Na@15c5]₂** were dried *in vacuo* for 24 h.

[dhbq^{Cl}][Na@15c5]₂: H₂dhbq^{Cl} (500 mg, 2.39 mmol, 1.0 eq.) and NaH (115 mg, 4.78 mmol, 2.0 eq.) were employed in CH₃CN (5.0 mL) to obtain **[dhbq^{Cl}]₂Na₂** as pink solids in quantitative yields. Complexation of **[dhbq^{Cl}]₂Na₂** (100 mg, 395 μmol, 1.0 eq.) with 15-crown-5 (192 mg, 172 μL, 870 μmol, 2.2 eq.) in CH₂Cl₂ (3.0 mL) yielded the product as magenta-colored solids (210 mg, 303 μmol, 77 %). Single crystals (red) suitable for scXRD analysis were obtained by gaseous diffusion of pentane into solutions of CH₂Cl₂ at -40 °C.

¹H NMR (600 MHz, CD₂Cl₂): δ = 3.72 (s, br, 40H).

¹³C NMR (151 MHz, CD₂Cl₂): δ = 174.1 (C_q-O), 104.8 (C_q-Cl), 69.5 (CH₂).

Elemental Analysis: calcd. for C₂₆H₄₀Cl₂Na₂O₁₄: C 45.03, H 5.81, found: C 44.89, H 5.92.

IR (FT-ATR): $\tilde{\nu}$ = 2905 (s, C-H), 2873 (s, C-H), 1533 (s), 1471 (s), 1353 (m), 1251 (m), 1100 (s).

[*dhbq*^{Br}][Na@15c5]₂: H₂*dhbq*^{Br} (500 mg, 1.68 mmol, 1.0 eq.) and NaH (80.5 mg, 3.36, 2.0 eq.) were employed in CH₃CN (5.0 mL) to obtain [*dhbq*^{Br}]Na₂ as violet solids (482 mg, 1.41 mmol, 84 %). Complexation of [*dhbq*^{Br}]Na₂ (100 mg, 293 μmol, 1.0 eq.) with 15-crown-5 (142 mg, 127 μL, 644 μmol, 2.2 eq.) in CH₂Cl₂ (4.0 mL) yielded the product as pink solids (200 mg, 256 μmol, 87 %).

¹H NMR (600 MHz, (CD₃)₂SO): δ = 3.55 (s, 40H).

¹³C NMR (151 MHz, (CD₃)₂SO): δ = 172.7 (C_q-O), 96.4 (C_q-Br), 69.7 (CH₂).

Elemental Analysis: calcd. for C₂₆H₄₀Br₂Na₂O₁₄: C 39.91, H 5.15, found: C 39.62, H 5.07.

IR (FT-ATR): $\tilde{\nu}$ = 2905 (s, C-H), 2870 (s, C-H), 1631 (w, C=O), 1538 (s), 1473 (s), 1352 (m), 1251 (m), 1100 (s).

[*dhbq*^{Ph}][Na@15c5]₂: H₂*dhbq*^{Ph} (200 mg, 684 μmol, 1.0 eq.) and NaH (32.8 mg, 1.37 mmol, 2.0 eq.) were employed in CH₃CN (8.0 mL) to obtain [*dhbq*^{Ph}]Na₂ as lilac solids (219 mg, 650 μmol, 95 %). Complexation of [*dhbq*^{Ph}]Na₂ (192 mg, 571 μmol, 1.0 eq.) with 15-crown-5 (440 mg, 400 μL, 1.82 mmol, 3.2 eq.) in CH₂Cl₂ (4.0 mL) yielded the product as pink solids (400 mg, 515 μmol, 90 %). Single crystals (red) suitable for scXRD analysis were obtained by gaseous diffusion of pentane into a solution of dimethyl sulfoxide or from a saturated solution in dichloromethane at room temperature.

¹H NMR (600 MHz, (CD₃)₂SO): δ = 7.63 (d, ³*J*_{HH} = 7.0 Hz, 4H), 7.13 (t, ³*J*_{HH} = 7.7 Hz, 4H), 6.92 (t, ³*J*_{HH} = 7.3 Hz, 2H), 3.56 (s, br, 40H).

¹³C NMR (151 MHz, (CD₃)₂SO): δ = 177.7 (C_q-O), 139.1 (*ipso*-C_{Ph}), 130.8 (C_{Ph}-H), 125.9 (C_{Ph}-H), 122.6 (C_{Ph}-H), 111.0 (C_q-Ph), 69.7 (CH₂).

Elemental Analysis: calcd. for C₃₈H₅₀Na₂O₁₄: C 58.76, H 6.49, found: C 58.15, H 6.21.

IR (FT-ATR): $\tilde{\nu}$ = 2908 (s, C-H), 2873 (s, C-H), 1585 (w), 1522 (sh), 1508 (s), 1436 (m), 1351 (m), 1278 (m), 1251 (m), 1103 (s).

[*dhbq*^{NO₂}][Na@15c5]₂: Complexation of [*dhbq*^{NO₂}]Na₂ (200 mg, 730 μmol, 1.0 eq) with 15-crown-5 (334 mg, 300 μL, 1.46 mmol, 2.1 eq) in CH₂Cl₂ (5.0 mL) yielded the product as yellow solids (368 mg, 515 μmol, 71 %). Single crystals (yellow) suitable for scXRD analysis were obtained from concentrated solutions in dimethyl sulfoxide at room temperature.

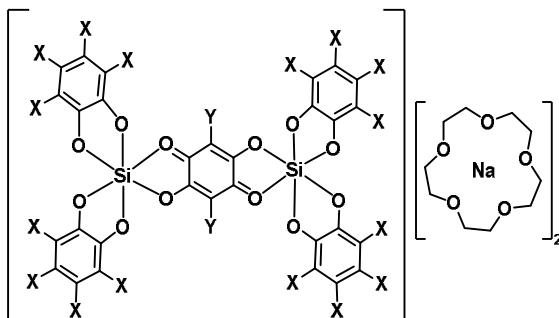
¹H NMR (600 MHz, (CD₃)₂SO): δ = 3.55 (s, br, 40H).

^{13}C NMR (151 MHz, $(\text{CD}_3)_2\text{SO}$): $\delta = 168.5$ ($\text{C}_q\text{-O}$), 133.3 ($\text{C}_q\text{-N}$), 69.5 (CH_2).

IR (FT-ATR): $\tilde{\nu} = 2916$ (s, C-H), 2880 (s, C-H), 1578 (s, N=O, C=O), 1493 (s), 1464 (s), 1353 (s), 1296 (s), 1251 (s), 1097 (s).

Elemental Analysis: calcd. for $\text{C}_{26}\text{H}_{40}\text{N}_2\text{Na}_2\text{O}_{18} \times \text{CH}_2\text{Cl}_2$: C 40.56, H 5.29, N 3.50, found: C 40.28, H 4.95, N 3.76.

5.2.5.2 General Procedure: Preparation of
 $[(\text{cat}^{\text{X}})_2\text{Si}(\text{d}hbq^{\text{Y}})\text{Si}(\text{cat}^{\text{X}})][\text{Na}@15\text{c}5]_2 - [4^{\text{X,Y}}][\text{Na}@15\text{c}5]_2$



X = Cl, Br, CF_3 , iPr
Y = Cl, Br, Ph, NO_2

To a suspension of 2 eq. of $2^{\text{X}}\cdot(\text{CH}_3\text{CN})_2$ ($\text{X} = \text{Cl}, \text{Br}$) or $2^{\text{CF}_3}\cdot(\text{sulfolane})_2$, or to a solution of 2^{iPr} in dichloromethane, 1 eq. of $[\text{d}hbq^{\text{Y}}][\text{Na}@15\text{c}5]_2$ ($\text{Y} = \text{Cl}, \text{Br}, \text{Ph}, \text{NO}_2$) was added. The reaction was stirred for 18 h at room temperature. For $\text{X}, \text{Y} = \text{Cl}, \text{Br}$ grey solids were collected by filtration and washed once with dichloromethane and three times with pentane. For $\text{X} = \text{Cl}$ or CF_3 and $\text{Y} = \text{Ph}$ a dark colored solution was obtained. Addition of pentane led to precipitation of colored solids, which were collected by filtration and washed with pentane. For $\text{X} = \text{iPr}$ and $\text{Y} = \text{Cl}, \text{Br}$ or NO_2 red-brown reaction solutions were obtained. They were filtrated and the solvent was removed under reduced pressure yielding in colored residual solids. The final products $[4^{\text{X,Y}}][\text{Na}@15\text{c}5]_2$ were dried *in vacuo* for 24 h.

$[4^{\text{Cl,Cl}}][\text{Na}@15\text{c}5]_2$: $[\text{d}hbq^{\text{Cl}}][\text{Na}@15\text{c}5]_2$ (75.0 mg, 108 μmol , 1.0 eq.) and $2^{\text{Cl}}\cdot(\text{CH}_3\text{CN})_2$ (130 mg, 216 μmol , 2.0 eq.) were employed in CH_2Cl_2 (4.0 mL) to obtain the product as grey solids (167 mg, 96.3 μmol , 89 %). Single crystals (red) suitable for scXRD analysis were obtained by gaseous diffusion of CH_2Cl_2 into solutions of CH_3CN at -40°C .

^1H NMR (600 MHz, CD_2Cl_2): $\delta = 3.62$ (s, 40H).

^{13}C NMR (151 MHz, CD_2Cl_2): $\delta = 170.6$ (C_{dhbq}O), 146.8 (C_{cat}O), 120.6 (C_{cat}Cl), 114.6 (C_{cat}Cl), 102.3 (C_{dhbq}Cl), 69.1 (CH_2).

^{29}Si INVGATE NMR (119 MHz, CD_2Cl_2): $\delta = -130.1$.

Elemental Analysis: calcd. for $\text{C}_{50}\text{H}_{40}\text{Cl}_{18}\text{Na}_2\text{O}_{22}\text{Si}_2$: C 34.65, H 2.33, found: C 34.57, H 2.47.

IR (FT-ATR): $\tilde{\nu} = 2922$ (m, C-H), 2879 (m, C-H), 1552 (s), 1450 (s), 1384 (s), 1247 (s), 1235 (s), 1093 (s).

HR-MS (ESI neg.): m/z calcd. for $\text{C}_{12}\text{HCl}_8\text{O}_5\text{Si}^- [\mathbf{2}^{\text{Cl}}+\text{OH}]^-$ 536.7047, found: 536.7049; calcd. for $\text{C}_{13}\text{H}_3\text{Cl}_8\text{O}_5\text{Si}^- [\mathbf{2}^{\text{Cl}}+\text{OMe}]^-$ 550.7204, found: 550.7203; calcd. for $\text{C}_{18}\text{Cl}_{10}\text{O}_8\text{Si}^- [(\text{dhbq}^{\text{Cl}})\text{Si}(\text{cat}^{\text{Cl}})_2]^-$ 748.6272, found: 748.6288; calcd. for $\text{C}_{18}\text{Cl}_{10}\text{NaO}_8\text{Si}^- [(\text{dhbq}^{\text{Cl}})\text{Si}(\text{cat}^{\text{Cl}})_2+\text{Na}]^-$ 726.6091, found: 726.6096.

$[\mathbf{4}^{\text{Br,Br}}][\text{Na}@15\text{c}5]_2$: $[\text{dhbq}^{\text{Br}}][\text{Na}@15\text{c}5]_2$ (75.0 mg, 95.9 μmol , 1.0 eq.) and $\mathbf{2}^{\text{Br}}\cdot(\text{CH}_3\text{CN})_2$ (184 mg, 192 μmol , 2.0 eq.) were employed in CH_2Cl_2 (4.0 mL) to obtain the product as grey solids (227 mg, 89.7 μmol , 94 %). Single crystals (dark red) suitable for scXRD analysis were obtained by gaseous diffusion of CH_2Cl_2 into solutions of CH_3CN at -40°C .

^1H NMR (600 MHz, CD_3CN): $\delta = 3.61$ (s, 40H).

^{13}C NMR (151 MHz, CD_3CN): $\delta = 172.6$ (C_{dhbq}O), 149.0 (C_{cat}O), 115.7 (C_{cat}Br), 107.7 (C_{cat}Br), 90.3 (C_{dhbq}Br), 69.4 (CH_2).

^{29}Si INVGATE NMR (119 MHz, CD_3CN): $\delta = -133.1$.

Elemental Analysis: calcd. for $\text{C}_{50}\text{H}_{40}\text{Br}_{18}\text{Na}_2\text{O}_{22}\text{Si}_2$: C 23.71, H 1.59, found: C 23.45, H 1.84.

IR (FT-ATR): $\tilde{\nu} = 2921$ (m, C-H), 2874 (m, C-H), 1599 (sh), 1551 (s), 1442 (s), 1383 (s), 1351 (s), 1273 (m), 1222 (s), 1085 (s).

$[\mathbf{4}^{\text{Cl,Br}}][\text{Na}@15\text{c}5]_2$: $[\text{dhbq}^{\text{Br}}][\text{Na}@15\text{c}5]_2$ (75.0 mg, 95.9 μmol , 1.0 eq.) and $\mathbf{2}^{\text{Cl}}\cdot(\text{CH}_3\text{CN})_2$ (115 mg, 192 μmol , 2.0 eq.) were employed in CH_2Cl_2 (4.0 mL) to obtain the product as grey solids (145 mg, 79.6 μmol , 83 %). Single crystals (violet) suitable for scXRD analysis were obtained by gaseous diffusion of CH_2Cl_2 into solutions of CH_3CN at -40°C .

^1H NMR (600 MHz, CD_3CN): $\delta = 3.62$ (s, 40H).

^{13}C NMR (151 MHz, CD_3CN): $\delta = 172.7$ (C_{dhbq}O), 147.0 (C_{cat}O), 121.3 (C_{cat}Cl), 115.1 (C_{cat}Cl), 90.4 (C_{dhbq}Br), 69.4 (CH_2).

^{29}Si INVGATE NMR (119 MHz, CD_3CN): $\delta = -131.1$.

IR (FT-ATR): $\tilde{\nu}$ = 2920 (m, C-H), 2878 (m, C-H), 1557 (s), 1450 (s), 1378 (s), 1235 (s), 1109 (s, sh), 1093 (s).

Elemental Analysis: calcd. for $C_{50}H_{40}Cl_{16}Br_2Na_2O_{22}Si_2$: C 32.96, H 2.21, found: C 33.15, H 2.37.

[4^{Br,Cl}][Na@15c5]₂: [*dhbq*^{Cl}][Na@15c5]₂ (75.0 mg, 108 μ mol, 1.0 eq.) and **2^{Br}**·(CH₃CN)₂ (207 mg, 216 μ mol, 2.0 eq.) were employed in CH₂Cl₂ (4.0 mL) to obtain the product as grey solids (216 mg, 88.4 μ mol, 82 %). Single crystals (red) were obtained by gaseous diffusion of CH₂Cl₂ into solutions of CH₃CN at -40 °C.

¹H NMR (600 MHz, CD₃CN): δ = 3.62 (s, 40H).

¹³C NMR (151 MHz, CD₃CN): δ = 171.5 (C_{*dhbq*O}), 148.9 (C_{*cat*O}), 115.7 (C_{*cat*Br}), 107.7 (C_{*cat*Br}), 102.9 (C_{*dhbq*Cl}), 69.4 (CH₂).

²⁹Si INVGATE NMR (119 MHz, CD₃CN): δ = -132.2 .

Elemental Analysis: calcd. for $C_{50}H_{40}Cl_2Br_{16}Na_2O_{22}Si_2$: C 24.57, H 1.65, found: C 24.93, H 1.95.

IR (FT-ATR): $\tilde{\nu}$ = 2919 (m, C-H), 2878 (m, C-H), 1550 (s), 1442 (s), 1383 (m), 1352 (m), 1273 (m), 1222 (m), 1106 (s, sh), 1092 (s).

[4^{Cl,Ph}][Na@15c5]₂: [*dhbq*^{Ph}][Na@15c5]₂ (42.9 mg, 55.2 μ mol, 1.0 eq.) and **2^{Cl}**·(CH₃CN)₂ (66.4 mg, 110 μ mol, 2.0 eq.) were employed in CH₂Cl₂ (1.5 mL) to obtain the product as green solids (78 mg, 42.9 μ mol, 78 %). Single crystals (dark green) suitable for scXRD analysis were obtained from a saturated solution in CH₂Cl₂ at room temperature.

¹H NMR (600 MHz, CD₂Cl₂) δ = 7.44 (d, ³*J*_{HH} = 7.5 Hz, 4H), 7.31 (t, ³*J*_{HH} = 7.5 Hz, 4H), 7.26 (t, ³*J*_{HH} = 7.4 Hz, 2H), 3.59 (s, 40H).

¹³C NMR (151 MHz, CD₂Cl₂) δ = 173.1 (C_{*dhbq*O}), 147.3 (C_{*cat*O}), 130.1 (C_{Ph-H}), 128.8 (*ipso*-C_{Ph}), 128.5 (C_{Ph-H}), 128.4 (C_{Ph-H}), 120.2 (C_{*cat*Cl}), 114.4 (C_{*cat*Cl}), 110.5 (C_{*dhbq*Ph}), 69.2 (CH₂).

²⁹Si INVGATE NMR (119 MHz, CD₂Cl₂) δ = -132.7 .

Elemental Analysis: calcd. for $C_{62}H_{50}Cl_{16}Na_2O_{22}Si_2$: C 41.00, H 2.77, found: C 41.01, H 2.93.

IR (FT-ATR): $\tilde{\nu}$ = 2917 (m, C-H), 2874 (m, C-H), 1540 (s), 1452 (s), 1368 (s), 1234 (s), 1087 (s).

[4^{CF₃,Ph}][Na@15c5]₂: [*dhbq*^{Ph}][Na@15c5]₂ (9.7 mg, 12.5 μ mol, 1.0 eq.) and **2^{CF₃}**·(sulfolane)₂ (25.7 mg, 25.0 μ mol, 2.0 eq.) were employed in CH₂Cl₂ (2.0 mL) to obtain the product as light brown solids (27.3 mg, 11.6 μ mol, 93 %). Single crystals

(brown) suitable for scXRD analysis were obtained by gaseous diffusion of CH₂Cl₂ into solutions of CH₃CN at room temperature.

¹H NMR (600 MHz, CD₂Cl₂): δ = 7.23 (m, 10H), 3.62 (s, 40H).

¹³C NMR (151 MHz, CD₂Cl₂): δ = 173.5 (C_{dhbq}-O), 154.3 (C_{cat}-O), 129.8 (C_{Ph}-H), 128.9 (C_{Ph}-H), 128.4 (C_{Ph}-H), 127.9 (*ipso*-C_{Ph}), 111.0 (C_{dhbq}-Ph), 69.2 (CH₂).

Residual signals were not detected due to limited concentration and intense fluorine content (coupling).

¹⁹F NMR (376 MHz, CD₂Cl₂): δ = -50.8 - -51.3 (m, 24F), -56.4 - -57.1 (m, 24F).

²⁹Si INVGATE NMR (119 MHz, CD₂Cl₂): δ = -132.8.

Elemental Analysis: calcd. for C₇₈H₅₀F₄₈Na₂O₂₂Si₂: C 39.81, H 2.14, found: C 40.13, H 2.92.

IR (FT-ATR): $\tilde{\nu}$ = 2923 (m, C-H), 2878 (m, C-H), 1551 (m), 1482 (s), 1351 (m), 1269 (sh), 1251 (sh), 1219 (s), 1152 (sh), 1137 (sh), 1109 (s), 1095 (s).

[⁴iPr,^{Cl}][Na@15c5]₂: [dhbq^{Cl}][Na@15c5]₂ (34.9 mg, 50.3 μmol, 1.0 eq.) and **2^{iPr}** (50.0 mg, 101 μmol, 2.0 eq.) were employed in CH₂Cl₂ (2.5 mL) to obtain the product as red solids in quantitative yields.

Elemental Analysis: calcd. for C₈₆H₁₂₈Cl₂Na₂O₂₂Si₂ x 0.5 CH₂Cl₂: C 60.07, H 7.52, found: 60.10, 7.24.

IR (FT-ATR): $\tilde{\nu}$ = 2955 (s, C-H), 2919 (s, C-H), 2868 (s, C-H), 1563 (s), 1456 (sh), 1430 (s), 1352 (s), 1331 (sh), 1303 (sh), 1250 (m), 1114 (s), 1091 (s), 1001 (s).

HR-MS (ESI neg.): *m/z* calcd. for C₂₁H₂₃Cl₂O₇Si⁻ [(dhbq^{Cl})Si(cat^{iPr})+OH]⁻ 485.0595, found 485.0599; calcd. for C₂₂H₂₅Cl₂O₇Si⁻ [(dhbq^{Cl})Si(cat^{iPr})+OMe]⁻ 499.0752, found: 499.0756; calcd. for C₃₀H₄₅O₅Si⁻ [2^{iPr}+OH]⁻ 513.3041, found: 513.3040; calcd. for C₃₁H₄₇O₅Si⁻ [2^{iPr}+OMe]⁻ 527.3198, found: 527.3198; calcd. for C₄₅Cl₆₇O₆Si⁻ [Si(cat^{iPr})₃+H]⁻ 731.4712, found: 731.4717.

[⁴iPr,^{Br}][Na@15c5]₂: [dhbq^{Br}][Na@15c5]₂ (39.4 mg, 50.3 μmol, 1.0 eq.) and **2^{iPr}** (50.0 mg, 101 μmol, 2.0 eq.) were employed in CH₂Cl₂ (2.0 mL) to obtain the product as red solids in quantitative yields.

Elemental Analysis: calcd. for C₈₆H₁₂₈Br₂Na₂O₂₂Si₂ x CH₂Cl₂: C 56.16, H 7.04, found: 56.36, 6.70.

IR (FT-ATR): $\tilde{\nu}$ = 2955 (s, C-H), 2919 (s, C-H), 2868 (s, C-H), 1563 (s), 1456 (sh), 1430 (s), 1352 (s), 1331 (sh), 1303 (sh), 1250 (m), 1114 (s), 1091 (s), 1001 (s).

HR-MS (ESI neg.): *m/z* calcd. for C₃₀H₄₅O₅Si⁻ [2^{iPr}+OH]⁻ 513.3041, found: 513.3040; calcd. for C₃₁H₄₇O₅Si⁻ [2^{iPr}+OMe]⁻ 527.3198, found: 527.3199; calcd. for C₂₁H₂₃Br₂O₇Si⁻ [dhbq^{Br}Si(cat^{iPr})+OH]⁻ 574.9564, found: 574.9569; calcd. for

$C_{22}H_{25}Br_2O_7Si^- [dhbq^{Br}Si(cat^{iPr})+OMe]^-$ 588.9721, found: 588.9724; calcd. for $C_{45}Cl_6O_6Si^- [Si(cat^{iPr})_3+H]^-$ 731.4712, found: 731.4718.

$[4^{iPr,NO_2}][Na@15c5]_2$: $[dhbq^{NO_2}][Na@15c5]_2$ (36.0 mg, 50.3 μ mol, 1.0 eq.) and $Si(cat^{iPr})_2$ (50.0 mg, 101 μ mol, 2.0 eq.) were employed in CH_2Cl_2 (2.5 mL) to obtain the product as green solids in quantitative yields.

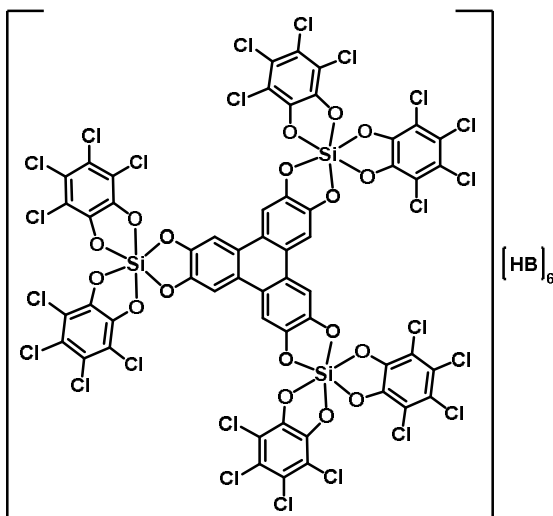
Elemental Analysis: calcd. for $C_{86}H_{128}N_2Na_2O_{26}Si_2 \times 0.5 CH_2Cl_2$: C 59.35, H 7.43, N 1.60, found: 58.82, 7.38, 1.83.

IR (FT-ATR): $\tilde{\nu} = 2957$ (s, C-H), 2926 (s, C-H), 2870 (s, C-H), 1596 (s, N=O), 1525 (m), 1458 (sh), 1430 (s), 1353 (s), 1327 (s), 1250 (m), 1114 (s), 1092 (s), 1001 (s).

HR-MS (ESI neg.): m/z calcd. for $C_{30}H_{45}O_5Si^- [2^{iPr}+OH]^-$ 513.3041, found: 513.3039; calcd. for $C_{31}H_{47}O_5Si^- [2^{iPr}+OMe]^-$ 527.3198, found: 527.3201.

5.2.6 Hexaaxolene-bridged Bis(catecholato)silanes

5.2.6.1 $[hhtp(Si(cat^{Cl})_2)_3][HB]_6 - [5^{Cl}][HB]_6$



$[5^{Cl}][HNET_3]_6$: To a suspension of H_6hhtp (50.0 mg, 154 μ mol, 1.0 eq.) in acetonitrile (10 mL) triethylamine (187 mg, 256 μ L, 1.88 mmol, 12 eq.) was added and stirred for 30 min. Then, $2^{Cl} \cdot (CH_3CN)_2$ (278 mg, 462 μ mol, 3.0 eq.) was added to the solution and stirred for further 24 h at room temperature. Afterwards the solvent was removed

under reduced pressure yielding the product (342 mg, 137 μmol , 89 %) as grey crystalline solids.

^1H NMR (400 MHz, CD_3CN): $\delta = 7.57$ (s, 6H), 7.47 (d, 6H), 3.22 (q, $^3J_{\text{HH}} = 7.1$ Hz), 1.18 (t, $^3J_{\text{HH}} = 6.1$ Hz).

^{13}C NMR (101 MHz, CD_3CN) $\delta = 150.5$ (C-O), 149.4 (C-O), 122.9 (C_q), 118.9 (C_q), 113.6 (C_q), 103.5 (C_{hhtp}-H), 48.1 (N-CH₂), 9.4 (CH₃).

^{29}Si NMR (80 MHz, CD_3CN): $\delta = -138.6$.

IR (FT-ATR): $\tilde{\nu} = 3063$ (m, C-H, N-H), 2984 (m, C-H, N-H), 2947 (m, C-H, N-H), 2704 (m, br, C-H, N-H), 1450 (s), 1382 (m), 1245 (s), 1234 (s), 1158 (m), 984 (s).

[hhtp(Si(cat^{Cl})₂)₃][Hpy]₆: To a solution of H₆hhtp (20.0 mg, 61.7 μmol , 1.0 eq.) in THF (5.0 ml), pyridine (59.6 μL , 740 μmol , 12.0 eq.) was added, resulting in a dark brown, suspension. The mixture was stirred for 24 h at room temperature. Then, **2^{Cl}**·(CH₃CN)₂ (111 mg, 185 μmol , 3.0 eq.) was added and subsequently yellow precipitation was observed. The reaction was stirred for further 4 d at room temperature. The solids were collected by filtration and washed with pentane. After drying *in vacuo*, the product (140 mg, 59.4 μmol , 96 %) was obtained as yellow solids.

^1H NMR (600 MHz, (CD₃)₂SO): $\delta = 9.3$ (br s), 8.79 (d, 12H), 8.28 (t, $^3J_{\text{HH}} = 7.2$ Hz, 6H), 7.80 (t, $^3J_{\text{HH}} = 6.0$ Hz, 12H), 7.59 (m, 6H).

^{13}C NMR (151 MHz, (CD₃)₂SO): $\delta = 148.4$ (C-O), 145.2 (C-O), 145.1 (C_{py}), 142.3 (C_{py}), 125.9 (C_{py}), 121.8 (C_q), 116.7 (C_q), 111.7 (C_q), 107.7 (C_{hhtp}-H).

^{29}Si INVGATE NMR (119 MHz, (CD₃)₂SO): $\delta = -138.1$.

IR (FT-ATR): $\tilde{\nu} = 3091$ (w, C-H, N-H), 3069 (w, C-H, N-H), 2973 (w, C-H, N-H), 2845 (w, C-H, N-H), 1459 (s), 1386 (m), 1248 (m), 1237 (m), 987 (s).

[5^{Cl}][HNⁿOct]₃: To a solution of H₆hhtp (20.0 mg, 61.7 μmol , 1.0 eq.) in THF (5.0 mL), tri-*n*-octylamine (162 μL , 370 μmol , 6.0 eq.) was added. The mixture turned dark blue and was stirred for 24 h at room temperature. Then, **2^{Cl}**·(CH₃CN)₂ (111 mg, 185 μmol , 3.0 eq.) was added and the reaction was stirred for further 4 d at room temperature forming a green solution. The solvent under was removed under reduced pressure. After drying *in vacuo*, the product (128 mg, 32.0 μmol , 52 %) was obtained as light green solids.

^1H NMR (600 MHz, THF-d₈): $\delta = 8.65$ (br s, 6H), 7.33 (m, 6H), 3.41 (s, 36H), 1.78 (s, 36H) 1.37-1.01 (m, 180H), 0.81 (t, $^3J_{\text{HH}} = 7.0$ Hz, 54H).

^{13}C NMR (151 MHz, THF- d_8): $\delta = 149.3$ (C-O), 146.1 (C-O), 123.9 (C_q), 119.0 (C_q), 113.7 (C_q), 108.6 (C_{hhtr}-H), 54.6 (N-CH₂), 32.8 (CH₂), 30.2 (CH₂), 30.1 (CH₂), 27.8 (CH₂), 23.5 (2CH₂), 14.6 (CH₃).

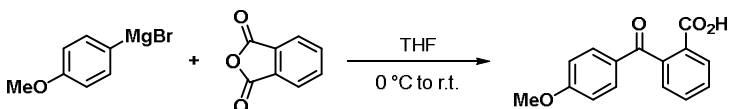
^{29}Si INVGATE NMR (119 MHz, THF- d_8): $\delta = -139.1$.

IR (FT-ATR): $\tilde{\nu} = 3081$ (w, br, N-H), 2954 (s, sh, C-H), 2924 (s, C-H), 2854 (s, C-H), 1571 (w), 1549 (w), 1456 (s), 1383 (s), 1304 (m), 1263 (m, sh), 1245 (s), 1235 (s), 1157 (m), 984 (s).

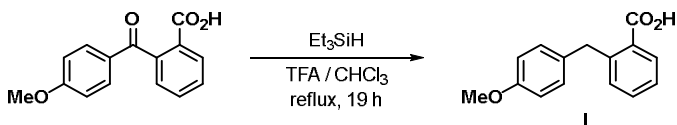
5.2.7 Catalysis

5.2.7.1 Oxidative Lactonization Studies

Substrate Synthesis



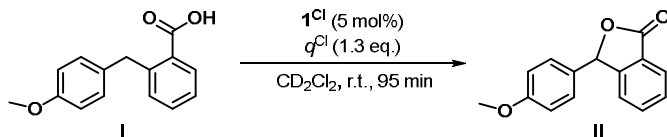
2-(4-Methoxybenzoyl)benzoic acid: 4-Methoxyphenylmagnesium bromide (9.46 mL, 0.50 M in THF, 4.73 mmol, 1.0 eq.) was added dropwise to a solution of phthalic anhydride (701 mg, 4.73 mmol, 1.0 eq.) in THF (10 mL) at 0 °C. The light-yellow reaction was warmed to room temperature after 1 h and stirred for 24 h. The blurry and colorless reaction mixture was quenched with aqueous HCl solution (1 M) and extracted with diethyl ether. The combined organic phases were extracted twice with aqueous NaOH solution (1 M), and the resulting aqueous phases were acidified with concentrated HCl solution. The mixture was then extracted with diethyl ether, washed with brine solution, and dried over MgSO₄. The solvent was removed under reduced pressure to obtain the crude product (857 mg, 3.34 mmol, 71 %). Recrystallisation in diethyl ether yielded the product as colorless crystals (464 mg, 1.81 mmol, 38 % yield). The spectral data matched with previously reported ones.¹⁷¹⁻¹⁷²



2-(4-Methoxybenzyl)benzoic acid: Trifluoroacetic acid (3.0 mL) was added dropwise to a solution of 2-(4-methoxybenzoyl)benzoic acid (460 mg, 1.80 mmol, 1.0 eq.) and triethylsilane (860 μL, 5.39 mmol, 3.0 eq.) in chloroform (3.0 mL) at 0 °C. Then the solution was warmed up to room temperature and heated at reflux for 19 h. After the reaction was cooled down to room temperature, it was diluted with diethyl ether and washed twice with aqueous HCl solution (1 M). The combined organic phases were extracted twice with aqueous NaOH solution (1 M), and the resulting aqueous phases were acidified with concentrated HCl solution. The mixture

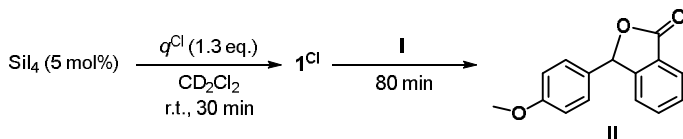
was then extracted with diethyl ether, washed with brine solution, and dried over MgSO_4 . The solvent was removed under reduced pressure to yield the product **I** as colorless solids (380 mg, 1.57 mmol, 87% yield). The spectral data of **I** matched with previously reported ones.¹⁷¹

Catalysis



1Cl (2.50 mg, 3.27 μmol , 5 mol%), $q\text{Cl}$ (20.9 mg, 84.9 μmol , 1.3 eq.) and **I** (15.8 mg, 65.3 μmol , 1.0 eq.) were mixed and cooled down to -40°C . Cold CD_2Cl_2 (0.5 mL) was slowly added. The reaction mixture was maintained for 5 min at 4°C and then stirred at room temperature. Over time the reaction turned from intense dark red to yellow. Within less than 95 min the reaction was completed. Product conversions were determined by ^1H NMR analysis of the crude reaction. **II** is a known compound and the spectral data matched with previously reported ones.²⁷³

in situ Catalysis



SiI_4 (1.70 mg, 3.10 μmol , 5 mol%) and $q\text{Cl}$ (19.8 mg, 80.5 μmol , 1.3 eq.) were mixed and CD_2Cl_2 (0.25 mL) was added. A bright red solution was obtained. After 30 min, a solution of **I** (15.0 mg, 61.9 μmol , 1.0 eq) in CD_2Cl_2 (0.25 mL) was added to the reaction. Within less than 80 min the reaction was completed. Product conversions were determined by ^1H NMR analysis of the crude reaction. **II** is a known compound and the spectral data matched with previously reported ones.²⁷³

5.2.7.2 Dehydrogenative Coupling of 3,3'',4,4''-Tetramethoxy-*o*-terphenyl

1^{Cl} (2.00 mg, 2.61 μmol , 10 mol%), q^{Cl} (8.35 mg, 34.0 μmol , 1.3 eq.) and 3,3'',4,4''-tetramethoxy-*o*-terphenyl **III** (9.15 mg, 26.1 μmol , 1.0 eq.) were mixed and cooled down to -40 °C. Cold CD_2Cl_2 (0.5 mL) was added and a dark green solution was obtained. It was maintained for 5 min at -40 °C, then it was slowly warmed up to room temperature. The reaction was stirred for 24 h, then colorless crystals precipitated. The supernatant solution was removed. The crystals were dried under reduced pressure to give the product 1,2,11,12-tetramethoxytriphenylene **IV** cocrystallized with $\text{H}_2\text{cat}^{\text{Cl}}$ as light brown powder in quantitative yields. **IV** is a known compound and the spectral data matched with previously reported ones.¹⁷⁴ Product identity was also confirmed by scXRD analysis (Figure 57).

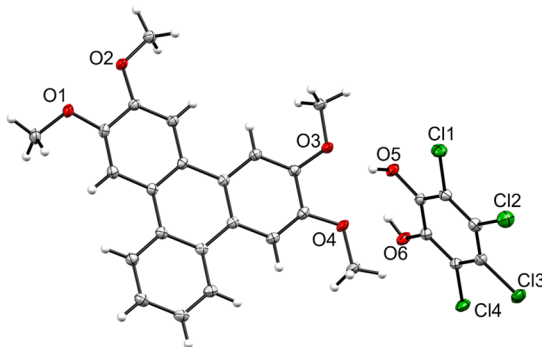
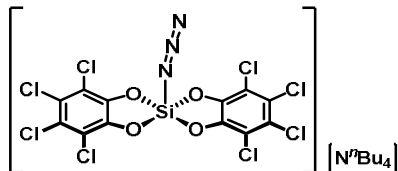


Figure 57: Solid-state molecular structure of **IV** cocrystallized with $\text{H}_2\text{cat}^{\text{Cl}}$. The thermal displacement ellipsoids are shown at the probability level of 50 %.

5.2.7.3 Oxidation of 9,10-Dihydroanthracene

1^{Cl} (2.00 mg, 2.61 μmol , 5 mol%), q^{Cl} (16.1 mg, 65.3 μmol , 2.5 eq.) and 9,10-dihydroanthracene (4.70 mg, 26.1 μmol , 1.0 eq.) were mixed and CD_2Cl_2 (0.5 mL) was added. A dark red solution was obtained, which decolorized within few minutes to a colorless to light yellow suspension. It was stirred at room temperature. After 65 h the reaction was completed. Product conversions were determined by ^1H NMR analysis of the crude reaction. Anthracene is a known compound and the spectral data matched with previously reported ones.²⁷⁴

5.2.8 Miscellaneous

5.2.8.1 $[2^{\text{Cl}}\text{-N}_3][\text{N}^n\text{Bu}_4]$ 

A suspension of $2^{\text{Cl}}\cdot(\text{CH}_3\text{CN})_2$ (100 mg, 166 μmol , 1.0 eq.) and $\text{N}^n\text{Bu}_4\text{N}_3$ (47.3 mg, 166 μmol , 1.0 eq.) in *o*-dcb (1.5 mL) was stirred at room temperature for 18 h. A clear colorless solution was obtained. The solution was filtered through a syringe filter to remove any fine insoluble solids (starting materials). The solvent was removed *in vacuo* and $[2^{\text{Cl}}\text{-N}_3][\text{N}^n\text{Bu}_4]$ was obtained in quantitative yields as colorless solids. Single crystals (colorless) suitable for scXRD analysis were obtained by gaseous diffusion of pentane into solutions of *o*-dcb at room temperature.

$^1\text{H NMR}$ (600 MHz, *o*- $\text{C}_6\text{H}_4\text{Cl}_2\text{:C}_6\text{D}_6$ (50:1)): δ = 2.71 (m, 8H), 1.30-1.24 (m, 8H), 1.11 (sext, $^3J_{\text{HH}} = 7.42$ Hz, 8H), 0.75 (t, $^3J_{\text{HH}} = 7.30$ Hz, 12H).

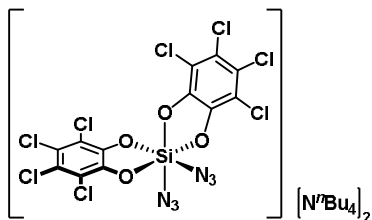
$^{13}\text{C NMR}$ (151 MHz, *o*- $\text{C}_6\text{H}_4\text{Cl}_2\text{:C}_6\text{D}_6$ (50:1)): δ = 146.3 ($\text{C}_{\text{cat-O}}$), 122.1 ($\text{C}_{\text{cat-Cl}}$), 115.1 ($\text{C}_{\text{cat-Cl}}$), 59.0 (N- CH_2), 23.9 (CH_2), 19.9 (CH_2), 13.7 (CH_3).

$^{29}\text{Si NMR}$ (119 MHz, *o*- $\text{C}_6\text{H}_4\text{Cl}_2\text{:C}_6\text{D}_6$ (50:1)): δ = -99.9.

$^{15}\text{N NMR}$ (61 MHz, *o*- $\text{C}_6\text{H}_4\text{Cl}_2\text{:C}_6\text{D}_6$ (50:1)): δ = 249.2 (Si-N=N=N $^-$), 236.0 (Si-N=N=N $^-$), 175.4 (Si-N=N=N $^-$).

Elemental Analysis: calcd. for $\text{C}_{28}\text{H}_{36}\text{Cl}_8\text{N}_4\text{O}_4\text{Si}$: C 41.81, H 4.51, N 6.97, found: C 42.05, H 4.35, N 7.02.

IR (FT-ATR): $\tilde{\nu}$ = 2963 (m), 2934 (m), 2876 (m), 2137 (s), 1454 (s), 1387 (s), 1315 (m), 1302 (m), 1249 (m), 1234 (m), 988 (s).

5.2.8.2 $[2^{\text{Cl}}\text{-(N}_3)_2][\text{N}^n\text{Bu}_4]_2$ 

A solution of $\text{N}^n\text{Bu}_4\text{N}_3$ (7.10 mg, 24.9 μmol , 1.0 eq.) and $[2^{\text{Cl}}\text{-N}_3][\text{N}^n\text{Bu}_4]$ (20.0 mg, 24.9 μmol , 1.0 eq.) in *o*-dcb (0.5 mL) was stirred at room temperature for 18 h. A clear colorless solution was obtained. The solvent was removed *in vacuo* and $[2^{\text{Cl}}\text{-(N}_3)_2][\text{N}^n\text{Bu}_4]_2$ was obtained in quantitative yields as colorless solids. Single crystals (colorless) suitable for scXRD analysis were obtained by gaseous diffusion of pentane into solutions of *o*-dcb at room temperature.

^1H NMR (600 MHz, *o*- $\text{C}_6\text{H}_4\text{Cl}_2$: C_6D_6 (50:1)): δ = 3.03 (m, 16H), 1.51-1.45 (m, 16H), 1.22 (sext, $^3J_{\text{HH}} = 7.5$ Hz, 16H), 0.80 (t, $^3J_{\text{HH}} = 7.4$ Hz, 24H).

^{13}C NMR (151 MHz, *o*- $\text{C}_6\text{H}_4\text{Cl}_2$: C_6D_6 (50:1)): δ = 149.5 ($\text{C}_{\text{cat-O}}$), 118.2 ($\text{C}_{\text{cat-Cl}}$), 112.9 ($\text{C}_{\text{cat-Cl}}$), 59.0 (N- CH_2), 24.1 (CH_2), 20.1 (CH_2), 13.8 (CH_3).

^{29}Si NMR (119 MHz, *o*- $\text{C}_6\text{H}_4\text{Cl}_2$: C_6D_6 (50:1)): δ = -155.1.

Elemental Analysis: calcd. for $\text{C}_{44}\text{H}_{72}\text{Cl}_8\text{N}_8\text{O}_4\text{Si}$: C 48.54, H 6.67, N 10.29 found: C 48.24, H 6.46, N 10.60.

IR (ATR): $\tilde{\nu}$ 2961 (m), 2933 (w), 2875 (w), 2120 (s), 2086 (s), 1461 (s), 1379 (m), 1303 (m), 1243 (m), 988 (s).

6

REFERENCES

1. V. Lyaskovskyy, B. de Bruin, *ACS Catal.* **2012**, *2*, 270.
2. D. L. J. Broere, R. Plessius, J. I. van der Vlugt, *Chem. Soc. Rev.* **2015**, *44*, 6886.
3. N. P. van Leest, F. J. de Zwart, M. Zhou, B. de Bruin, *JACS Au* **2021**, *1*, 1101.
4. P. W. Van Leeuwen, *Homogeneous Catalysis: Understanding the Art*, Springer Science & Business Media, 2006.
5. S. Blanchard, E. Derat, M. Desage - El Murr, L. Fensterbank, M. Malacria, V. Mouriès - Mansuy, *Eur. J. Inorg. Chem.* **2012**, *2012*, 376.
6. F. Press, R. Siever, J. P. Grotzinger, *Allgemeine Geologie*, Spektrum, Akad. Verlag, 2008.
7. H. Grützmacher, *Angew. Chem. Int. Ed.* **2008**, *47*, 1814.
8. J. I. van der Vlugt, J. N. Reek, *Angew. Chem. Int. Ed.* **2009**, *48*, 8832.
9. J. I. van der Vlugt, *Chemistry* **2019**, *25*, 2651.
10. W. Kaim, B. Schwederski, *Coord. Chem. Rev.* **2010**, *254*, 1580.
11. P. J. Chirik, K. Wieghardt, *Science* **2010**, *327*, 794.
12. O. R. Luca, R. H. Crabtree, *Chem. Soc. Rev.* **2013**, *42*, 1440.
13. C. K. Jørgensen, *Coord. Chem. Rev.* **1966**, *1*, 164.
14. D. Schröder, S. Shaik, H. Schwarz, *Acc. Chem. Res.* **2000**, *33*, 139.
15. W. Griffith, *Transition Met. Chem.* **1993**, *18*, 250.
16. H. Reinsch, in 'Repertorium für die Pharmacie', Johann Leonhard Schrag, Nürnberg, **1839**, 49.
17. C. G. Pierpont, R. M. Buchanan, *Coord. Chem. Rev.* **1981**, *38*, 45.
18. A. L. Balch, *J. Am. Chem. Soc.* **1973**, *95*, 2723.
19. J. A. Ladd, M. M. Olmstead, A. L. Balch, *Inorg. Chem.* **1984**, *23*, 2318.
20. C. G. Pierpont, *Coord. Chem. Rev.* **2001**, *219–221*, 415.
21. P. Zanello, M. Corsini, *Coord. Chem. Rev.* **2006**, *250*, 2000.
22. K. Martyanov, V. Kuropatov, *Inorganics* **2018**, *6*, 48.
23. W. I. Dzik, J. I. van der Vlugt, J. N. H. Reek, B. de Bruin, *Angew. Chem. Int. Ed.* **2011**, *50*, 3356.
24. F. F. Khan, A. D. Chowdhury, G. K. Lahiri, *Eur. J. Inorg. Chem.* **2020**, *2020*, 1138.

25. A. E. Thorarinsdottir, T. D. Harris, *Chem. Rev.* **2020**, *120*, 8716.
26. L. S. Xie, G. Skorupskii, M. Dinca, *Chem. Rev.* **2020**, *120*, 8536.
27. F. H. Osman, F. A. El-Samahy, *Chem. Rev.* **2002**, *102*, 629.
28. C. A. Ramsden, in 'Adv. Heterocycl. Chem.' (Ed.: A. R. Katritzky), Academic Press, **2010**, 1.
29. M. G. Chegrev, A. V. Piskunov, *Russ. J. Coord. Chem.* **2018**, *44*, 258.
30. I. V. Ershova, A. V. Piskunov, *Russ. J. Coord. Chem.* **2020**, *46*, 154.
31. R. Maskey, M. Schädler, C. Legler, L. Greb, *Angew. Chem. Int. Ed.* **2018**, *57*, 1717.
32. D. Hartmann, M. Schädler, L. Greb, *Chem. Sci.* **2019**, *10*, 7379.
33. T. Thorwart, D. Roth, L. Greb, *Chem. Eur. J.* **2021**, *27*, 10422.
34. D. Roth, H. Wadepohl, L. Greb, *Angew. Chem. Int. Ed.* **2020**, *59*, 20930
35. R. Maskey, L. Greb, in 'Encyclopedia of Inorganic and Bioinorganic Chemistry' (Ed.: R. A. Scott), **2022**.
36. L. Greb, *Eur. J. Inorg. Chem.* **2021**, e202100871.
37. E. Evangelio, D. Ruiz-Molina, *Eur. J. Inorg. Chem.* **2005**, *2005*, 2957.
38. D. R. Eaton, *Inorg. Chem.* **1964**, *3*, 1268.
39. G. A. Abakumov, E. S. Klimov, V. V. Ershov, I. S. Belostotskaya, *Bull. Acad. Sci. USSR, Div. Chem. Sci.* **1975**, *24*, 841.
40. D. M. Adams, A. Dei, A. L. Rheingold, D. N. Hendrickson, *Angew. Chem. Int. Ed.* **1993**, *32*, 391.
41. A. Ozarowski, B. R. McGarvey, A. El-Hadad, Z. Tian, D. G. Tuck, D. J. Krovich, G. C. DeFotis, *Inorg. Chem.* **1993**, *32*, 841.
42. S. R. Sofen, D. C. Ware, S. R. Cooper, K. N. Raymond, *Inorg. Chem.* **1979**, *18*, 234.
43. S. D. Chemerisov, G. D. Perekhodtsev, D. S. Tipikin, Y. S. Lebedev, A. I. Prokof'ev, A. I. Aleksandrov, A. A. Dubinskii, K. Möbius, O. G. Poluektov, J. Schmidt, *J. Chem. Soc., Faraday Trans.* **1996**, *92*, 1959.
44. G. D. Perekhodtsev, Y. S. Lebedev, *J. Struct. Chem.* **1997**, *38*, 884.
45. A. V. Piskunov, I. N. Meshcheryakova, A. V. Maleeva, A. S. Bogomyakov, G. K. Fukin, V. K. Cherkasov, G. A. Abakumov, *Eur. J. Inorg. Chem.* **2014**, *2014*, 3252.
46. A. V. Piskunov, A. V. Maleeva, G. K. Fukin, E. V. Baranov, A. S. Bogomyakov, V. K. Cherkasov, G. A. Abakumov, *Dalton Trans.* **2011**, *40*, 718.
47. H. B. Stegmann, K. B. Ulmschneider, K. Scheffler, U. Bösenberg, *J. Organomet. Chem.* **1975**, *101*, 145.
48. P. Rivière, A. Castel, J. Satgé, D. Guyot, *J. Org. Chem.* **1986**, *315*, 157.
49. A. V. Lado, A. V. Piskunov, I. V. Zhdanovich, G. K. Fukin, E. V. Baranov, *Russ. J. Coord. Chem.* **2008**, *34*, 251.
50. A. A. El-Hadad, B. R. McGarvey, B. Merzougui, R. G. W. Sung, A. K. Trikha, D. G. Tuck, *J. Chem. Soc., Dalton Trans.* **2001**, 1046.

51. M. Glavinovic, M. Krause, L. Yang, J. A. McLeod, L. Liu, K. M. Baines, T. Friscic, J. P. Lumb, *Sci. Adv.* **2017**, *3*, 1.
52. E. N. Nikolaevskaya, E. A. Saverina, A. A. Starikova, A. Farhati, M. A. Kiskin, M. A. Syroeshkin, M. P. Egorov, V. V. Jouikov, *Dalton Trans.* **2018**, *47*, 17127.
53. L. B. Vaganova, A. V. Maleeva, A. V. Piskunov, D. F. Grishin, *Russ. Chem. Bull.* **2011**, *60*, 1620.
54. T. A. Annan, D. G. Tuck, *Can. J. Chem.* **1989**, *67*, 1807.
55. R. R. Rakhimov, P. M. Solozhenkin, V. S. Pupkov, A. I. Prokof'ev, *Bull. Acad. Sci. USSR, Div. Chem. Sci.* **1990**, *39*, 1385.
56. H. B. Stegmann, R. Schrade, H. Saur, P. Schuler, K. Scheffler, *J. Org. Chem.* **1981**, *214*, 197.
57. T. A. Annan, R. K. Chadha, D. G. Tuck, K. D. Watson, *Can. J. Chem.* **1987**, *65*, 2670.
58. T. A. Annan, B. R. McGarvey, A. Ozarowski, D. G. Tuck, R. K. Chadha, *J. Chem. Soc., Dalton Trans.* **1989**, 439.
59. A. G. Davies, J. A. A. Hawari, *J. Org. Chem.* **1983**, *251*, 53.
60. H. E. Mabrouk, D. G. Tuck, *J. Chem. Soc., Dalton Trans.* **1988**, 2539.
61. A. V. Lado, A. I. Poddel'sky, A. V. Piskunov, G. K. Fukin, E. V. Baranov, V. N. Ikorskii, V. K. Cherkasov, G. A. Abakumov, *Inorg. Chim. Acta* **2005**, *358*, 4443.
62. A. V. Lado, A. V. Piskunov, V. K. Cherkasov, G. K. Fukin, G. A. Abakumov, *Russ. J. Coord. Chem.* **2006**, *32*, 173.
63. E. V. Ilyakina, A. I. Poddel'sky, G. K. Fukin, A. S. Bogomyakov, V. K. Cherkasov, G. A. Abakumov, *Inorg. Chem.* **2013**, *52*, 5284.
64. E. V. Ilyakina, A. I. Poddel'sky, A. V. Piskunov, N. V. Somov, G. A. Abakumov, V. K. Cherkasov, *Inorg. Chim. Acta* **2013**, *394*, 282.
65. M. G. Chegerev, A. V. Piskunov, A. V. Maleeva, G. K. Fukin, G. A. Abakumov, *Eur. J. Inorg. Chem.* **2016**, *2016*, 3813.
66. A. V. Piskunov, A. V. Lado, G. K. Fukin, E. V. Baranov, L. G. Abakumova, V. K. Cherkasov, G. A. Abakumov, *Heteroat. Chem.* **2006**, *17*, 481.
67. G. M. Barnard, M. A. Brown, H. E. Mabrouk, B. R. McGarvey, D. G. Tuck, *Inorg. Chim. Acta* **2003**, *349*, 142.
68. E. V. Ilyakina, A. I. Poddel'sky, V. K. Cherkasov, G. A. Abakumov, *Mendelev Commun.* **2012**, *22*, 208.
69. F. Ramirez, S. Dershowitz, *J. Org. Chem.* **1957**, *22*, 856.
70. F. Ramirez, S. B. Bhatia, A. V. Patwardhan, E. H. Chen, C. P. Smith, *J. Org. Chem.* **1968**, *33*, 20.
71. F. Ramirez, A. Patwardhan, H. Kugler, C. Smith, *Tetrahedron* **1968**, *24*, 2275.
72. J. Gloede, H. Gross, *J. prakt. Chem.* **1970**, *312*, 326.
73. A. Waked, S. Chitnis, D. W. Stephan, *Chem. Commun.* **2019**, *55*, 8971.
74. T. A. Annan, Z. Tian, D. G. Tuck, *J. Chem. Soc., Dalton Trans.* **1991**, 19.

75. F. Ramirez, A. J. Bigler, C. P. Smith, *Tetrahedron* **1968**, *24*, 5041.
76. M. Wieber, B. Eichhorn, J. Götz, *Chem. Ber.* **1973**, *106*, 2738.
77. V. K. Cherkasov, G. A. Abakumov, E. V. Grunova, A. I. Poddel'skiy, G. K. Fukin, E. V. Baranov, Y. V. Kurskii, L. G. Abakumova, *Chem. Eur. J.* **2006**, *12*, 3916.
78. I. V. Smolyaninov, A. I. Poddel'skiy, N. T. Berberova, V. K. Cherkasov, G. A. Abakumov, *Russ. J. Coord. Chem.* **2010**, *36*, 644.
79. I. V. Smol'yaninov, A. I. Poddel'skii, S. A. Smol'yaninova, N. O. Movchan, *Russ. J. Gen. Chem.* **2014**, *84*, 1761.
80. P. Antikainen, P. Mälkönen, *Z. anorg. allg. Chem.* **1959**, *299*, 292.
81. O. Lindqvist, *Acta Chem. Scand.* **1967**, *21*, 1473.
82. T. A. Annan, A. Ozarowski, Z. Tian, D. G. Tuck, *J. Chem. Soc., Dalton Trans.* **1992**, 2931.
83. J. M. Kieser, L. O. Jones, N. J. Lin, M. Zeller, G. C. Schatz, S. C. Bart, *Inorg. Chem.* **2021**, *60*, 3460.
84. A. Rosenheim, O. Sorge, *Ber. Dtsch. Chem. Ges.* **1920**, *53*, 932.
85. A. Rosenheim, B. Raibmann, G. Schendel, *Z. Anorg. Allg. Chem.* **1931**, *196*, 160.
86. A. Weiss, G. Reiff, A. Weiss, *Z. Anorg. Allg. Chem.* **1961**, *311*, 151.
87. J. J. Flynn, F. P. Boer, *J. Am. Chem. Soc.* **1969**, *91*, 5756.
88. A. I. Prokof'ev, T. I. Prokof'e'va, N. N. Bubnov, S. P. Solodovnikov, I. S. Belostotskaya, V. V. Ershov, M. I. Kabachnik, *Bull. Acad. Sci. USSR, Div. Chem. Sci.* **1978**, *27*, 1726.
89. A. K. Chekalov, A. I. Prokof'ev, N. N. Bubnov, S. P. Solodovnikov, A. A. Zhdanov, M. I. Kabachnik, *Bull. Acad. Sci. USSR, Div. Chem. Sci.* **1981**, *30*, 2064.
90. A. I. Prokof'ev, T. I. Prokof'e'va, N. N. Bubnov, S. P. Solodovnikov, I. S. Belostotskaya, V. V. Ershov, M. I. Kabachnik, *Dokl. Akad. Nauk SSSR* **1977**, *234*, 603.
91. A. I. Prokof'ev, T. I. Prokof'e'va, N. N. Bubnov, S. P. Solodovnikov, I. S. Belostotskaya, V. V. Ershov, M. I. Kabachnik, *Dokl. Akad. Nauk SSSR* **1977**, *236*, 897.
92. A. Doddi, J. V. Kingston, v. Ramkumar, M. Suzuki, M. Hojo, M. N. S. Rao, *Phosphorus, Sulfur, and Silicon and the Related Elements* **2011**, *187*, 343.
93. R. Maskey, Master thesis, **2018**.
94. A. L. Liberman-Martin, R. G. Bergman, T. D. Tilley, *J. Am. Chem. Soc.* **2015**, *137*, 5328.
95. L. O. Müller, D. Himmel, J. Stauffer, G. Steinfeld, J. Slattey, G. Santiso - Quiñones, V. Brecht, I. Krossing, *Angew. Chem. Int. Ed.* **2008**, *47*, 7659.
96. L. Greb, *Chem. Eur. J.* **2018**, *24*, 17881.
97. T. Thorwart, L. Greb, in 'Encyclopedia of Inorganic and Bioinorganic Chemistry' (Ed.: R. A. Scott), **2021**.
98. D. H. McDaniel, H. C. Brown, *J. Org. Chem.* **1958**, *23*, 420.

-
99. A. Cronstedt, *Svenska Vetenskaps Akademiens Handlingar Stockholm* **1756**, 17, 120.
 100. L. E. Smart, E. A. Moore, *Solid State Chemistry: an Introduction*, CRC press, 2012.
 101. F. S. Xiao, X. Meng, *Hierarchically Structured Porous Materials: From Nanoscience to Catalysis, Separation, Optics, Energy, and Life Science* **2011**, 435.
 102. J. D. Sherman, *Proc. Natl. Acad. Sci. U.S.A.* **1999**, 96, 3471.
 103. G. Boyd, A. W. Adamson, L. Myers Jr, *J. Am. Chem. Soc.* **1947**, 69, 2836.
 104. D. Breck, J. Smith, *Sci. Am.* **1959**, 200, 85.
 105. D. M. Rasmus, C. K. Hall, *AlChE J.* **1991**, 37, 769.
 106. A. G. Slater, A. I. Cooper, *Science* **2015**, 348, aaa8075.
 107. A. F. Masters, T. Maschmeyer, *Microporous Mesoporous Mater.* **2011**, 142, 423.
 108. J. García-Martínez, K. Li, G. Krishnaiah, *Chem. Commun.* **2012**, 48, 11841.
 109. J. Martens, P. Jacobs, J. Weitkamp, *Appl. Catal.* **1986**, 20, 239.
 110. O. Yaghi, H. Li, *J. Am. Chem. Soc.* **1995**, 117, 10401.
 111. H. Li, M. Eddaoudi, T. L. Groy, O. Yaghi, *J. Am. Chem. Soc.* **1998**, 120, 8571.
 112. H.-C. Zhou, J. R. Long, O. M. Yaghi, *Chem. Rev.* **2012**, 112, 673.
 113. S. Yuan, L. Feng, K. Wang, J. Pang, M. Bosch, C. Lollar, Y. Sun, J. Qin, X. Yang, P. Zhang, Q. Wang, L. Zou, Y. Zhang, L. Zhang, Y. Fang, J. Li, H.-C. Zhou, *Adv. Mater.* **2018**, 30, 1704303.
 114. O. M. Yaghi, M. O'Keeffe, N. W. Ockwig, H. K. Chae, M. Eddaoudi, J. Kim, *Nature* **2003**, 423, 705.
 115. M. O'Keeffe, M. A. Peskov, S. J. Ramsden, O. M. Yaghi, *Acc. Chem. Res.* **2008**, 41, 1782.
 116. G. M. Espallargas, E. Coronado, *Chem. Soc. Rev.* **2018**, 47, 533.
 117. M. Ko, L. Mendecki, K. A. Mirica, *Chem. Commun.* **2018**, 54, 7873.
 118. L. Sun, M. G. Campbell, M. Dincă, *Angew. Chem. Int. Ed.* **2016**, 55, 3566.
 119. A. Morozan, F. Jaouen, *Energy Environ. Sci.* **2012**, 5, 9269.
 120. I. Stassen, N. Burtch, A. Talin, P. Falcaro, M. Allendorf, R. Ameloot, *Chem. Soc. Rev.* **2017**, 46, 3185.
 121. L. E. Darago, M. L. Aubrey, C. J. Yu, M. I. Gonzalez, J. R. Long, *J. Am. Chem. Soc.* **2015**, 137, 15703.
 122. I.-R. Jeon, B. Negru, R. P. Van Duyne, T. D. Harris, *J. Am. Chem. Soc.* **2015**, 137, 15699.
 123. M. Hmadeh, Z. Lu, Z. Liu, F. Gándara, H. Furukawa, S. Wan, V. Augustyn, R. Chang, L. Liao, F. Zhou, E. Perre, V. Ozolins, K. Suenaga, X. Duan, B. Dunn, Y. Yamamoto, O. Terasaki, O. M. Yaghi, *Chem. Mater.* **2012**, 24, 3511.
 124. N. T. Nguyen, H. Furukawa, F. Gándara, C. A. Trickett, H. M. Jeong, K. E. Cordova, O. M. Yaghi, *J. Am. Chem. Soc.* **2015**, 137, 15394.

125. D. Sheberla, J. C. Bachman, J. S. Elias, C.-J. Sun, Y. Shao-Horn, M. Dincă, *Nat. Mater.* **2017**, *16*, 220.
126. A. Mähringer, A. C. Jakowetz, J. M. Rotter, B. J. Bohn, J. K. Stolarczyk, J. Feldmann, T. Bein, D. D. Medina, *ACS Nano* **2019**, *13*, 6711.
127. S.-Y. Ding, W. Wang, *Chem. Soc. Rev.* **2013**, *42*, 548.
128. C. S. Diercks, O. M. Yaghi, *Science* **2017**, *355*, eaal1585.
129. M. S. Lohse, T. Bein, *Adv. Funct. Mater.* **2018**, *28*, 1705553.
130. A. P. Cote, A. I. Benin, N. W. Ockwig, M. O'Keeffe, A. J. Matzger, O. M. Yaghi, *Science* **2005**, *310*, 1166.
131. X. Feng, X. Ding, D. Jiang, *Chem. Soc. Rev.* **2012**, *41*, 6010.
132. J. H. Small, D. J. McCord, J. Greaves, K. Shea, *J. Am. Chem. Soc.* **1995**, *117*, 11588.
133. J. B. Lambert, S. R. Singer, *J. Organomet. Chem.* **2004**, *689*, 2293.
134. J. L. Holmes, B. F. Abrahams, A. Ahveninen, B. A. Boughton, T. A. Hudson, R. Robson, D. Thinagaran, *Chem. Commun.* **2018**, *54*, 11877.
135. C. M. Hong, M. Morimoto, E. A. Kapustin, N. Alzakhem, R. G. Bergman, K. N. Raymond, F. D. Toste, *J. Am. Chem. Soc.* **2018**, *140*, 6591.
136. Y. Kawakami, T. Ogishima, T. Kawara, S. Yamauchi, K. Okamoto, S. Nikaido, D. Souma, R. H. Jin, Y. Kabe, *Chem. Commun.* **2019**, *55*, 6066.
137. K. Shea, D. Loy, J. Small, *Chem. Mater.* **1992**, *4*, 255.
138. J. Roeser, D. Prill, M. J. Bojdys, P. Fayon, A. Trewin, A. N. Fitch, M. U. Schmidt, A. Thomas, *Nat. Chem.* **2017**, *9*, 977.
139. O. Yahiaoui, A. N. Fitch, F. Hoffmann, M. Fröba, A. Thomas, J. r. m. Roeser, *J. Am. Chem. Soc.* **2018**, *140*, 5330.
140. J. Guo, Y. Xu, S. Jin, L. Chen, T. Kaji, Y. Honsho, M. A. Addicoat, J. Kim, A. Saeki, H. Ihee, *Nat. Commun.* **2013**, *4*, 1.
141. Y. Zhang, S. N. Riduan, J. Wang, *Chem. Eur. J.* **2017**, *23*, 16419.
142. Z. Meng, R. M. Stolz, K. A. Mirica, *J. Am. Chem. Soc.* **2019**, *141*, 11929.
143. Y. Tsuji, R. Hoffmann, M. Strange, G. C. Solomon, *Proc. Natl. Acad. Sci. U.S.A.* **2016**, *113*, E413.
144. Y. Morita, S. Nishida, T. Murata, M. Moriguchi, A. Ueda, M. Satoh, K. Arifuku, K. Sato, T. Takui, *Nat. Mater.* **2011**, *10*, 947.
145. M. B. Smith, J. Michl, *Chem. Rev.* **2010**, *110*, 6891.
146. V. A. Dediu, L. E. Hueso, I. Bergenti, C. Taliani, *Nat. Mater.* **2009**, *8*, 707.
147. S. Kitagawa, S. Kawata, *Coord. Chem. Rev.* **2002**, *224*, 11.
148. K. S. Min, A. G. DiPasquale, J. A. Golen, A. L. Rheingold, J. S. Miller, *J. Am. Chem. Soc.* **2007**, *129*, 2360.
149. A. Barthram, R. Cleary, M. Ward, *Chem. Commun.* **1998**, 2695.
150. Y. Suenaga, H. Inada, M. Inomata, R. Yamaguchi, T. Okubo, M. Maekawa, T. Kuroda-Sowa, *Chem. Lett.* **2014**, *43*, 562.
151. R. L. Spicer, A. D. Stergiou, T. A. Young, F. Duarte, M. D. Symes, P. J. Lusby, *J. Am. Chem. Soc.* **2020**, *142*, 2134.

-
152. A. K. Turek, D. J. Hardee, A. M. Ullman, D. G. Nocera, E. N. Jacobsen, *Angew. Chem. Int. Ed.* **2016**, *55*, 539.
 153. A. Vlček, *Comments Inorg. Chem.* **1994**, *16*, 207.
 154. C. G. Pierpont, C. W. Lange, in 'Prog. Inorg. Chem.', John Wiley & Sons, Inc., **2007**, 331.
 155. H.-C. Chang, T. Ishii, M. Kondo, S. Kitagawa, *J. Chem. Soc., Dalton Trans.* **1999**, 2467.
 156. H.-C. Chang, H. Miyasaka, S. Kitagawa, *Inorg. Chem.* **2001**, *40*, 146.
 157. S. Stoll, A. Schweiger, *J. Magn. Reson.* **2006**, *178*, 42.
 158. S. N. Brown, *Inorg. Chem.* **2012**, *51*, 1251.
 159. R. Foster, M. I. Foreman, in 'The Chemistry of Quinonoid Compounds' (Ed.: S. Patai), John Wiley & Sons Ltd., Chichester, **1974**.
 160. T. J. Kistenmacher, T. E. Phillips, D. O. Cowan, *Acta Crystallogr. B Struct. Sci.* **1974**, *30*, 763.
 161. R. M. Buchanan, H. H. Downs, W. B. Shorthill, C. G. Pierpont, S. L. Kessel, D. N. Hendrickson, *J. Am. Chem. Soc.* **1978**, *100*, 4318.
 162. R. Gupta, M. Lechner, Chemical shifts and coupling constants for Silicon-29, Springer, 2008.
 163. N. G. Connelly, W. E. Geiger, *Chem. Rev.* **1996**, *96*, 877.
 164. S. L. Matthews, D. M. Heinekey, *Inorg. Chem.* **2011**, *50*, 7925.
 165. M. Schorpp, S. Rein, S. Weber, H. Scherer, I. Krossing, *Chem. Commun.* **2018**, *54*, 10036.
 166. D. M. D'Alessandro, F. R. Keene, *Dalton Trans.* **2004**, 3950.
 167. R. J. Crutchley, in 'Adv. Inorg. Chem.' (Ed.: A. G. Sykes), Academic Press, **1994**, 273.
 168. M. B. Robin, P. Day, in 'Advances in inorganic chemistry and radiochemistry', Elsevier, **1968**, 247.
 169. D. J. McCord, J. H. Small, J. Greaves, Q. N. Van, A. J. Shaka, E. B. Fleischer, K. J. Shea, *J. Am. Chem. Soc.* **1998**, *120*, 9763.
 170. D. Hartmann, L. Greb, *Angew. Chem. Int. Ed.* **2020**, *59*, 22510.
 171. W. v. E. Doering, T. Kitagawa, *J. Am. Chem. Soc.* **1991**, *113*, 4288.
 172. J. Miao, H. Ge, *Org. Lett.* **2013**, *15*, 2930.
 173. L. Zhai, R. Shukla, S. H. Wadumethrige, R. Rathore, *J. Org. Chem.* **2010**, *75*, 4748.
 174. U. Wild, O. Hübner, H.-J. Himmel, *Chem. Eur. J.* **2019**.
 175. A. Heckmann, C. Lambert, *Angew. Chem. Int. Ed.* **2012**, *51*, 326.
 176. T. Zincke, *Chem. Ber.* **1887**, *20*, 1776.
 177. S. Ramanathan, D. Sang, V. Kumar, D. M. Lemal, Wiley Online Library, **2012**.
 178. V. Kumar, S. Ramanathan, D. Sang, X. Chen, D. M. Lemal, *J. Org. Chem.* **2012**, *77*, 966.
 179. D. M. Lemal, S. Ramanathan, J. Shellito, *J. Org. Chem.* **2008**, *73*, 3392.
 180. P. Sah, S. Peoples, *Arzneimittel-Forschung* **1961**, *11*, 27.

181. G. Furin, G. Grebenschikova, A. Y. Lvova, V. Vlasov, G. Yakobson, in 'Syntheses of Fluoroorganic Compounds', Springer, **1985**, 109.
182. G. A. Abakumov, N. N. Vavilina, Y. A. Kurskii, V. I. Nevodchikov, V. K. Cherkasov, A. S. Shavyr, *Russ. Chem. Bull.* **2003**, *52*, 1847.
183. D. Hartmann, T. Thorwart, R. Müller, J. Thusek, J. Schwabedissen, A. Mix, J.-H. Lamm, B. Neumann, N. W. Mitzel, L. Greb, *J. Am. Chem. Soc.* **2021**, *143*, 18784.
184. A. Mianowski, M. Owczarek, A. Marecka, *Energy Sources A: Recovery Util. Environ. Eff.* **2007**, *29*, 839.
185. T. Thorwart, ongoing PhD thesis, **2023**.
186. J. M. Zachara, C. C. Ainsworth, C. E. Cowan, B. L. Thomas, *Environmental science & technology* **1987**, *21*, 397.
187. D. Ripin, D. Evans, *Chem* **2006**, **2005**.
188. N. Ansmann, D. Hartmann, S. Sailer, P. Erdmann, R. Maskey, M. Schorpp, L. Greb, *Angew. Chem. Int. Ed.* **2022**, *61*, e202203947.
189. M. Abe, *Chem. Rev.* **2013**, *113*, 7011.
190. Y. Tsuji, Y. Morisaki, Y. Chujo, *Polym. Chem.* **2013**, *4*, 5361.
191. R. L. Frank, G. R. Clark, J. N. Coker, *J. Am. Chem. Soc.* **1950**, *72*, 1824.
192. P. Shildneck, R. Adams, *J. Am. Chem. Soc.* **1931**, *53*, 2373.
193. A. E. Thorarinsdottir, R. Bjornsson, T. D. Harris, *Inorg. Chem.* **2020**, *59*, 4634.
194. H. N. Zhang, Y. Lu, W. X. Gao, Y. J. Lin, G. X. Jin, *Chem. Eur. J.* **2018**, *24*, 18913.
195. R. Murase, B. F. Abrahams, D. M. D'Alessandro, C. G. Davies, T. A. Hudson, G. N. Jameson, B. Moubaraki, K. S. Murray, R. Robson, A. L. Sutton, *Inorg. Chem.* **2017**, *56*, 9025.
196. M. Essers, G. Haufe, *J. Chem. Soc., Perkin Trans. 1* **2002**, 2719.
197. Z. Zhu, H. Li, J. Liang, Z. Tao, J. Chen, *Chem. Commun.* **2015**, *51*, 1446.
198. H. N. Colli, V. Gold, J. E. Pearson, *J. Chem. Soc., Chem. Commun.* **1973**, 408.
199. H. Jia, A. P. Häring, F. Berger, L. Zhang, T. Ritter, *J. Am. Chem. Soc.* **2021**.
200. F. Uhlig, H. C. Marsmann, *Gelest Catalog* **2008**, 208.
201. K. Heinze, G. Huttner, L. Zsolnai, A. Jacobi, P. Schober, *Chem. Eur. J.* **1997**, *3*, 732.
202. A. I. Krylov, in 'Rev. Comput. Chem.', **2017**, 151.
203. S. Dong, T. Y. Gopalakrishna, Y. Han, H. Phan, T. Tao, Y. Ni, G. Liu, C. Chi, *J. Am. Chem. Soc.* **2019**, *141*, 62.
204. C. Chen, H. Ruan, Z. Feng, Y. Fang, S. Tang, Y. Zhao, G. Tan, Y. Su, X. Wang, *Angew. Chem. Int. Ed.* **2020**, *59*, 11794.
205. A. Maiti, F. Zhang, I. Krummenacher, M. Bhattacharyya, S. Mehta, M. Moos, C. Lambert, B. Engels, A. Mondal, H. Braunschweig, P. Ravat, A. Jana, *J. Am. Chem. Soc.* **2021**.

-
206. S. Grimme, A. Hansen, *Angew. Chem. Int. Ed.* **2015**, *54*, 12308.
 207. C. A. Bauer, A. Hansen, S. Grimme, *Chem. Eur. J.* **2017**, *23*, 6150.
 208. M. Morshedi, A. C. Willis, N. G. White, *CrystEngComm* **2016**, *18*, 4281.
 209. S. N. Talapaneni, J. Kim, S. H. Je, O. Buyukcakir, J. Oh, A. Coskun, *Journal of Materials Chemistry A* **2017**, *5*, 12080.
 210. S. N. Talapaneni, J. Kim, S. H. Je, O. Buyukcakir, J. Oh, A. Coskun, *Journal of Materials Chemistry A* **2019**, *7*, 18159.
 211. H. Zheng, K. Li, G. D. Cody, C. A. Tulk, X. Dong, G. Gao, J. J. Molaison, Z. Liu, M. Feygenson, W. Yang, *Angew. Chem. Int. Ed.* **2016**, *55*, 12040.
 212. E. Oikawa, K. Mori, G. Saito, *Bull. Chem. Soc. Jpn.* **1966**, *39*, 1182.
 213. B. Dellinger, S. Lomnicki, L. Khachatryan, Z. Maskos, R. W. Hall, J. Adoukpe, C. McFerrin, H. Truong, *Proc. Combust. Inst.* **2007**, *31*, 521.
 214. M. Schütze, *Angew. Chem.* **1958**, *70*, 697.
 215. L. Omann, M. Oestreich, *Organometallics* **2017**, *36*, 767.
 216. R. J. LeSuer, C. Buttolph, W. E. Geiger, *Anal. Chem.* **2004**, *76*, 6395.
 217. M. Vaidyanathan, R. Balamurugan, U. Sivagnanam, M. Palaniandavar, *J. Chem. Soc., Dalton Trans.* **2001**, 3498.
 218. W. Kabsch, in 'International Tables for Crystallography, Volume F, Chapter 11.3: Integration, scaling, space-group assignment and post refinement', Kluwer, **2001**, 218.
 219. Z. Otwinowski, W. Minor, D. Borek, M. Cymborowski, **2012**.
 220. *CrysAlisPro*, Agilent Technologies UK Ltd., Oxford, UK 2011-2014 and *Rigaku Oxford Diffraction*, Rigaku Polska Sp.z o.o., Wrocław, Poland 2015-2018.
 221. G. M. Sheldrick, SADABS, Bruker AXS GmbH, Karlsruhe, Germany, **2004-2014**.
 222. L. Krause, R. Herbst-Irmer, G. M. Sheldrick, D. Stalke, *J. Appl. Crystallogr.* **2015**, *48*, 3.
 223. R. H. Blessing, *Acta Crystallogr. Sect. A: Found. Crystallogr.* **1995**, *51*, 33.
 224. *SCALE3 ABSPACK CrysAlisPro*, Agilent Technologies UK Ltd., Oxford, UK, 2011-2014, and *Rigaku Oxford Diffraction*, Rigaku Polska Sp.z o.o., Wrocław, Poland, 2015-2018.
 225. L. Palatinus, *SUPERFLIP*, EFP Lausanne, Switzerland and Fyzikální ústav AV ČR, v. v. i., Prague, Czech Republic, **2007-2014**.
 226. L. Palatinus, G. Chapuis, *J. Appl. Crystallogr.* **2007**, *40*, 786.
 227. G. M. Sheldrick, SHELXL-20xx, University of Göttingen and Bruker AXS GmbH, Karlsruhe, Germany, **2012-2018**.
 228. G. M. Sheldrick, *Acta Cryst.* **2008**, *A64*, 112.
 229. G. M. Sheldrick, *Acta Cryst.* **2015**, *A71*, 3.
 230. P. Müller, R. Herbst-Irmer, A. Spek, T. Schneider, M. Sawaya, *Crystal Structure Refinement: A Crystallographer's Guide to SHELXL*, Vol. 8, OUP Oxford, 2006.

231. P. Van der Sluis, A. Spek, *Acta Crystallogr. Sect. A: Found. Crystallogr.* **1990**, *46*, 194.
232. A. L. Spek, *Acta Crystallographica Section C: Structural Chemistry* **2015**, *71*, 9.
233. A. Spek, *J. Appl. Crystallogr.* **2003**, *36*, 7.
234. A. L. Spek, PLATON, Utrecht University, The Netherlands, <http://www.platonsoft.nl>.
235. Z. Otwinowski, W. Minor, *Methods Enzymol.* **1997**, *276*, 307.
236. SAINT, Bruker AXS GmbH, Karlsruhe, Germany, **2016**.
237. G. M. Sheldrick, SHELXT, Program for Crystal Structure Solution, University of Göttingen, Germany, **2014-2018**.
238. W. Robinson, G. M. Sheldrick, (Eds.: N. W. Isaaks, M. R. Taylor), Ch. 22, IUCr and Oxford University Press, Oxford, UK, **1988**.
239. G. M. Sheldrick, *Acta Cryst.* **2015**, *C71*, 3.
240. O. V. Dolomanov, L. J. Bourhis, R. J. Gildea, J. A. K. Howard, H. Puschmann, *J. Appl. Crystallogr.* **2009**, *42*, 339.
241. I. J. Bruno, J. C. Cole, P. R. Edgington, M. Kessler, C. F. Macrae, P. McCabe, J. Pearson, R. Taylor, *Acta Crystallogr. B Struct. Sci.* **2002**, *58*, 389.
242. C. F. Macrae, P. R. Edgington, P. McCabe, E. Pidcock, G. P. Shields, R. Taylor, M. Towler, J. Streek, *J. Appl. Crystallogr.* **2006**, *39*, 453.
243. C. F. Macrae, I. Sovago, S. J. Cottrell, P. T. Galek, P. McCabe, E. Pidcock, M. Platings, G. P. Shields, J. S. Stevens, M. Towler, *J. Appl. Crystallogr.* **2020**, *53*, 226.
244. F. Neese, **2018**.
245. K. Eichkorn, O. Treutler, H. Öhm, M. Häser, R. Ahlrichs, *Chem. Phys. Lett.* **1995**, *240*, 283.
246. K. Eichkorn, F. Weigend, O. Treutler, R. Ahlrichs, *Theor. Chem. Acc.* **1997**, *97*, 119.
247. C. Adamo, V. Barone, *J. Chem. Phys.* **1999**, *110*, 6158.
248. S. Grimme, J. Antony, S. Ehrlich, H. Krieg, *J. Chem. Phys.* **2010**, *132*, 154104.
249. S. Grimme, S. Ehrlich, L. Goerigk, *J. Comput. Chem.* **2011**, *32*, 1456.
250. A. D. Becke, E. R. Johnson, *J. Chem. Phys.* **2005**, *122*, 154104.
251. E. R. Johnson, A. D. Becke, *J. Chem. Phys.* **2005**, *123*, 024101.
252. F. Weigend, R. Ahlrichs, *Phys. Chem. Chem. Phys.* **2005**, *7*, 3297.
253. A. Schäfer, C. Huber, R. Ahlrichs, *J. Chem. Phys.* **1994**, *100*, 5829.
254. L. Noodleman, *J. Chem. Phys.* **1981**, *74*, 5737.
255. K. Yamaguchi, F. Jensen, A. Dorigo, K. Houk, *Chem. Phys. Lett.* **1988**, *149*, 537.
256. R. Caballol, O. Castell, F. Illas, I. de PR Moreira, J. Malrieu, *J. Phys. Chem. A* **1997**, *101*, 7860.

-
257. T. Soda, Y. Kitagawa, T. Onishi, Y. Takano, Y. Shigeta, H. Nagao, Y. Yoshioka, K. Yamaguchi, *Chem. Phys. Lett.* **2000**, *319*, 223.
258. R. Costa, D. Reta, I. d. P. Moreira, F. Illas, *J. Phys. Chem. A* **2018**, *122*, 3423.
259. F. Neese, *Wiley Interdiscip. Rev.-Comput. Mol. Sci.* **2012**, *2*, 73.
260. S. Grimme, J. G. Brandenburg, C. Bannwarth, A. Hansen, *J. Chem. Phys.* **2015**, *143*, 054107.
261. S. Grimme, *Chem. Eur. J.* **2012**, *18*, 9955.
262. Y. Zhao, D. G. Truhlar, *J. Phys. Chem. A* **2005**, *109*, 5656.
263. G. L. Stoychev, A. A. Auer, F. Neese, *J. Chem. Theory Comput.* **2017**, *13*, 554.
264. F. Neese, *Wiley Interdiscip. Rev.-Comput. Mol. Sci.* **2017**, *8*, 73.
265. J. P. Perdew, *Phys. Rev. B* **1986**, *33*, 8822.
266. A. D. Becke, *Phys. Rev. A* **1988**, *38*, 3098.
267. S. Grimme, A. Hansen, S. Ehlert, J.-M. Mewes, *J. Chem. Phys.* **2021**, *154*, 064103.
268. S. Grimme, A. Hansen, *Angew. Chem. Int. Ed.* **2015**, *54*, 12308.
269. S. Kozuch, D. Gruzman, J. M. Martin, *J. Phys. Chem. C* **2010**, *114*, 20801.
270. A. D. Becke, E. R. Johnson, *J. Chem. Phys.* **2005**, *123*, 154101.
271. P. Erdmann, J. Leitner, J. Schwarz, L. Greb, *ChemPhysChem* **2020**, *21*, 987.
272. H. Lübbecke, P. Boldt, *Tetrahedron* **1978**, *34*, 1577.
273. D. C. Gerbino, D. Augner, N. Slavov, H.-G. Schmalz, *Org. Lett.* **2012**, *14*, 2338.
274. AIST, *Integrated Spectral Database System of Organic Compounds (Data were obtained from the National Institute of Advanced Industrial Science and Technology, Japan)*.
275. E. A. C. Lucken, *J. Chem. Soc.* **1962**, 4963.
276. J. O. Howell, J. M. Goncalves, C. Amatore, L. Klasinc, R. M. Wightman, J. Kochi, *J. Am. Chem. Soc.* **1984**, *106*, 3968.
277. L. Ebersson, O. Persson, F. Radner, M. P. Hartshorn, *Res. Chem. Intermed.* **1996**, *22*, 799.

7

APPENDIX

7.1 List of Abbreviations

15c5	15-crown-5	Cp	cyclopentadiene
2D	two-dimensional	CS	closed shell
a.u.	atomic unit	CV	cyclic voltammetry
anhyd.	anhydrous	<i>cw</i>	continuous wave
ATR	attenuated total reflection	d/D	doublet/donor
<i>av</i>	average	DBU	diazabicycloundecene
B	base	DDQ	2,3-dichloro-5,6-dicyano-1,4-benzoquinone
BArF ₂₀	tetrakis(pentafluorophenyl)borate	DEPT	distortionless enhancement by polarization transfer
BArF ₂₄	tetrakis(3,5-bis(trifluoromethyl)phenyl)borate	DFT	density functional theory
bipy	2,2'-bipyridine	<i>dhbq</i>	2,5-dihydroxy-1,4-benzoquinone
br	broad	<i>diox</i>	dioxolene
<i>BS</i>	broken symmetry	DIPEA	diisopropylethylamine
BTPP	(tbutylimino)tris-(pyrrolidino)phosphorane	DMF	dimethylformamide
calc.	calculated	DMSO	dimethyl sulfoxide
<i>cat</i>	catechol	dtb	di- <i>tert</i> -butyl
COF	covalent organic framework	<i>dtbpy</i>	2,6-di- <i>t</i> -butylpyridine
conc.	concentrated		

<i>e.g.</i>	for example	iPr	<i>iso</i> -propyl
<i>EA</i>	electron affinity	IR	infrared
EI	electron ionization	<i>IVCT</i>	intervalence charge transfer
EPR	electron paramagnetic resonance	L	ligand
eq.	equivalent	<i>LAG</i>	liquid-assisted grinding
ESI	electrospray ionization		lithium
Et	ethyl	LiHMDS	bis(trimethylsilyl)-amide
<i>et al.</i>	and others	LLCT	ligand-ligand charge transfer
exp.	experimental	LUMO	lowest unoccupied molecular orbital
Fc	ferrocene	m/M	multiplet or medium /metal
FCC	fluid catalytic cracking	MALDI	matrix assisted laser desorption/ionization
FIA	fluoride ion affinity	MAS	magic-angle spinning
FOD	fractional occupation density	MOF	metal organic framework
GC	gas chromatography	MOS	metrical oxidation state
hhtp	2,3,6,7,10,11-hexahydroxytriphenylene	MS	mass spectrometry
hktp	2,3,6,7,10,11-hexaketotriphenylene	<i>n</i>	normal
HMB	hexamethylbenzene	<i>n</i> Bu	<i>n</i> -butyl
HMDSO	hexamethyl-disiloxane	NEA	(<i>S</i>)-(-)-1-(2-naphthyl)ethylamine
hmtp	2,3,6,7,10,11-hexamethoxytriphenylene	neg.	negative
HOAc	acetic acid	NIR	near-IR
HOMO	highest occupied molecular orbital	NMO	N-methylmorpholine-N-oxide
HR	high resolution	NMR	Nuclear magnetic resonance
HSQC	heteronuclear single quantum coherence	<i>n</i> Pr	<i>n</i> -propyl
INVGATE	inverse-gated	<i>o</i> -	<i>ortho</i> -
i	<i>iso</i>		

Oct	octyl	t/T	<i>tert</i> or triplet/triplet
<i>o</i> -dfb	<i>o</i> -difluorobenzene	tBu	<i>tert</i> -butyl
ORTEP	Oak Ridge thermal ellipsoid plot	TCE	1,1,2,2-tetrachloroethane
OTf	trifluoromethanesulfonate	TCNQ	Tetracyanoquinodimethane
ox	oxidation	TEOS	tetraethyl orthosilicate
<i>p</i> -	<i>para</i> -	<i>terpy</i>	terpyridine
Ph	phenyl	THF	tetrahydrofuran
phen	1,10-phenantroline	tip	tri- <i>iso</i> -propyl
q	quaternary	TMB	1,2,3,4-tetramethylbenzene
red	reduction	TMEDA	Tetramethylethylenediamine
s	strong or singlet	triphos	1,1,1-tris(diphenylphosphinomethyl)ethane
scXRD	single crystal X-ray diffraction	TS	transition state
SET	single electron transfer	TT	thianthrene
sext	sextet	TTF	tetrathiafulvalene
sept	septet	UV	ultraviolet
sh	shoulder	vis	visual
sim	simulated	<i>vs.</i>	<i>versus</i>
<i>solv</i>	solvated	VT	variable temperature
<i>sq</i>	semiquinone	w	weak
SQUID	superconducting quantum interference device	<i>WCA</i>	weakly coordinating anion
sub	substrate		

7.2 List of Symbols

\angle	angle between two planes [°]
\ddagger	activation-
B	magnetic field [mT] or [G]
D / E	zero-field splitting parameters [G]
E	energy [Hartree] or [kJ·mol ⁻¹]
$E / E_{ox} / E_{1/2}$	potential / oxidation potential / half-wave potential [V]
F	Faraday constant
g	proportionality factor
G	Gibbs free energy [kJ·mol ⁻¹]
H	enthalpy [kJ·mol ⁻¹]
I	nuclear spin or intensity
J	exchange coupling constant [Hz]
K_c	comproportionation constant
\ln	logarithmus naturalis
m/z	mass-to-charge ratio
${}^nJ_{AB}$	NMR coupling constant [Hz]
pK_a	negative common logarithm of the acid dissociation constant
ppm	parts per million
r	distance [Å]
R	universal gas constant
S	electron spin
T	temperature [°C] or [K]
$\tilde{\nu}$	wavenumber [cm ⁻¹]
δ	chemical shift [ppm]
Δ	difference
m_s	spin quantum number
ϵ	extinction coefficient
λ	wavelength [nm]
μ_B	Bohr magneton
σ_m	(meta) Hammett parameter

7.3 Computational Data Tables

7.3.1 Data Tables for Chapters 3.1 and 3.2

Table 5: Computed energies for the singlet, triplet, and broken-symmetry state of 1^{Cl} .

	Exp.	<i>T</i>	<i>BS</i>	<i>CS</i> singlet
Energy [Hartree] and [kJ·mol ⁻¹]	--	-6946.799556	-6946.799553	-6946.775549
		-18252715.833	-18252715.826	-18252652.8
C-O bond lengths ^[a] [Å]	1.350 / 1.290 / 1.282	1.337 / 1.276 / 1.276	1.317 / 1.311 / 1.311	1.302 / 1.292 / 1.291

^[a] average of two bonds in one ring

Table 6: Computed exchange coupling constants *J* for 1^{X} .

Compound	<i>J</i> [cm ⁻¹]
1^{Br}	4.57
1^{Cl}	1.83
1^{F}	6.58
1^{tBu}	13.52

Table 7: Computed energies of $[3^{\text{Cl}}]^{2-}$ and the transition state (TS, Figure 58) for the catecholate shuffling.

	Thermal + ZPE correction from PBEh- 3c [kJ·mol ⁻¹]	Entropy*29 8K from PBEh-3c [kJ·mol ⁻¹]	E [Hartree] PW6B95- D3(BJ)/def 2-QZVPP	E [kJ·mol ⁻¹]	H [kJ·mol ⁻¹]	G [kJ·mol ⁻¹]
$[3^{\text{Cl}}]^{2-}$	848.8	379.9	-11690.5	-30693465.2	-30692616.4	-30692996.2
TS	845.6	369.4	-11690.5	-30693423.0	-30692577.4	-30692946.7
				ΔE	ΔH	ΔG
			Exchange	42.3	39.1	49.5

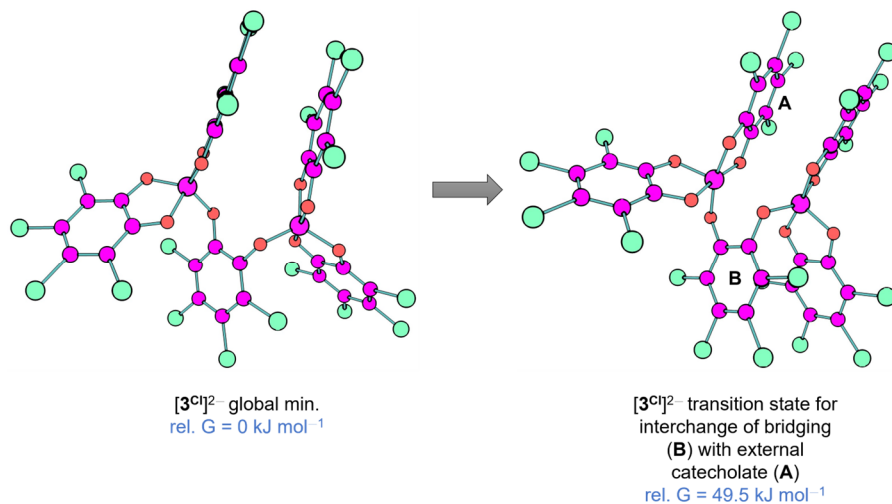


Figure 58: Calculated structures of the global minimum and the transition state for catecholate shuffling of [3Cl]²⁻.

Table 8: Computed energies of the compounds for the calculation of solvent corrected (CH₂Cl₂, CPCM) electron affinities (EA_{solv}).

Compound	E [Hartree] PW6B95/ TZVPP D3	Compound	E [Hartree] PW6B95/ TZVPP D3	ΔE [Hartree]	EA_{solv} [eV]
q^{Cl}	-2221.9411	sq^{Cl}	-2222.1073	0.166279	4.52
q^{Br}	-10680.8075	sq^{Br}	-10680.9749	0.167487	4.56
q^F	-779.5900	sq^F	-779.7540	0.163935	4.46
q^{tBu}	-697.1296	sq^{tBu}	-697.2677	0.138110	3.76
$[q^{Cl}SiI_3]^+$	-3405.3447	$q^{Cl}SiI_3$	-3405.5874	0.242728	6.61
$[q^{Br}SiI_3]^+$	-11864.2130	$q^{Br}SiI_3$	-11864.4551	0.242146	6.59
$[q^FSiI_3]^+$	-1962.9870	q^FSiI_3	-1963.2326	0.245632	6.68
$[q^{tBu}SiI_3]^+$	-1880.5467	$q^{tBu}SiI_3$	-1880.7823	0.235668	6.41
1^{Cl}	-6955.914073	[1^{Cl}]^{•-}	-6956.113474	0.199401	5.43
1^{Br}	-32332.517281	[1^{Br}]^{•-}	-32332.717732	0.200451	5.45
1^F	-2628.849286	[1^F]^{•-}	-2629.048230	0.198944	5.41
1^{tBu}	-2381.470549	[1^{tBu}]^{•-}	-2381.633851	0.163302	4.44

Table 9: Computed energies for the compounds for the calculation of thermodynamic data.

Compound	E [Hartree]			E [Hartree]		
	PW6B95/ TZVPP D3	E [kJ·mol ⁻¹]	H [kJ·mol ⁻¹]	PW6B95/ TZVPP D3	E [kJ·mol ⁻¹]	H [kJ·mol ⁻¹]
q^{Bu}	-695.5112956	-1826064.9	-1825228.6	-697.1161162	-1830278.4	-1829442.0
q^{Br}	-10675.28404	-28027958.3	-28027810.9	-10680.79641	-28042431.0	-28042283.6
q^{Cl}	-2219.2036	-5826519.1	-5826368.1	-2221.930492	-5833678.5	-5833527.6
q^{F}	-777.8217274	-2042170.9	-2042011.0	-779.5784565	-2046783.2	-2046623.3
SiI_4	-1480.982507	-3888319.6	-3888285.0	-1481.513765	-3889714.4	-3889679.8
I_2	-595.7008273	-1564012.5	-1564001.2	-595.8041515	-1564283.8	-1564272.5
$\mathbf{1}^{\text{Br}}$	-32315.6174	-84844653.5	-84844186.3	-32332.49937	-84888977.1	-84888509.9
$\mathbf{1}^{\text{Cl}}$	-6947.37272	-18240327.1	-18239851.3	-6955.897599	-18262709.1	-18262233.3
$\mathbf{1}^{\text{F}}$	-2623.218566	-6887260.3	-6886750.8	-2628.830886	-6901995.5	-6901485.9
$\mathbf{1}^{\text{tBu}}$	-2376.304897	-6238988.5	-6236456.0	-2381.450649	-6252498.7	-6249966.2

Table 10: Calculation of thermodynamic data for the synthesis of the diradicals $\mathbf{1}^{\text{X}}$.

	$\Delta H_{\text{R}} = \text{H}(\text{Products}) - \text{H}(\text{Educts})$ [kJ·mol ⁻¹]
$\text{SiI}_4 + 3 q^{\text{Cl}} = \mathbf{1}^{\text{Cl}} + 2 \text{I}_2$	-515.7571849
$\text{SiI}_4 + 3 q^{\text{Br}} = \mathbf{1}^{\text{Br}} + 2 \text{I}_2$	-524.1063048
$\text{SiI}_4 + 3 q^{\text{F}} = \mathbf{1}^{\text{F}} + 2 \text{I}_2$	-481.1388778
$\text{SiI}_4 + 3 q^{\text{tBu}} = \mathbf{1}^{\text{tBu}} + 2 \text{I}_2$	-505.2201607

7.3.2 Data Tables for Chapter 3.3

Table 11: Computed energies for the singlet, triplet, and broken-symmetry states and for the energies of the highest occupied molecular orbital (HOMO) and the lowest unoccupied molecular orbital (LUMO).

Compound ^[a]	State ^[b]	E ^{SP}	E ^{SP}	H ^{SP}	G ^{SP}	HOMO	LUMO	Gap
		[Hartree]	[kJ·mol ⁻¹]	[kJ·mol ⁻¹]	[kJ·mol ⁻¹]	[eV]	[eV]	[eV]
[d _h bq ^{Cl}]	<i>CS</i>	-3317.6824	-8710575.1	-8708695.8	-8709017.6	-4.698	-1.027	-3.7
	<i>T</i>	-3317.6279	-8710432.1	-8708560.3	-8708880.0			
	<i>BS</i>	-- ^[c]	-- ^[c]					
[4 ^{Cl,Cl}]	<i>CS</i>	-13052.0031	-34268034.2	-34265217.6	-34265842.1	-5.202	-4.111	-1.1
	<i>T</i>	-13051.9913	-34268003.2	-34265189.6	-34265816.8			
	<i>BS</i>	-13051.9917	-34268004.3					
[4 ^{iPr,Cl}]	<i>CS</i>	-7110.0808	-18667517.2	-18661571.4	-18662334.9	-4.220	-3.322	-0.9
	<i>T</i>	-7110.0826	-18667521.9	-18661578.2	-18662343.8			
	<i>BS</i>	-7110.0826	-18667521.8					
[4 ^{Cl,Ph}]	<i>CS</i>	-12595.0061	-33068188.4	-33064882.3	-33065532.8	-5.235	-3.907	-1.3
	<i>T</i>	-12594.9900	-33068146.3	-33064844.9	-33065501.6			
	<i>BS</i>	-12594.9911	-33068149.2					
[4 ^{Cl,NO₂}]	<i>CS</i>	-12541.6785	-32928176.9	-32925292.9	-32925932.3	-5.318	-4.510	-0.8
	<i>T</i>	-12541.6752	-32928168.1	-32925286.9	-32925928.8			
	<i>BS</i>	-12541.6752	-32928168.3					
[4 ^{CF₃,Ph}]	<i>CS</i>	-10636.4231	-27925928.9	-27921940.3	-27922767.0	-6.349	-4.128	-2.2
	<i>T</i>	-10636.3898	-27925841.3	-27921860.9	-27922681.5			
	<i>BS</i>	-- ^[c]	-- ^[c]					
[4 ^{iPr,NO₂}]	<i>CS</i>	-6599.7606	-17327671.4	-17321658.1	-17322436.3	-4.533	-3.691	-0.8
	<i>T</i>	-6599.7762	-17327712.3	-17321699.8	-17322478.5			
	<i>BS</i>	-6599.7761	-17327712.1					

^[a] all compounds computed as salts with two [CH₃CN-Na@15c5]⁺, ^[b] *CS* = closed shell, *T* = triplet open shell, *BS* = broken symmetry open shell singlet, ^[c] no stable broken symmetry solution obtained.

Table 12: Computed energies for the calculation of fractional occupation densities (FODs) and exchange coupling constant *J*.

Compound ^[a]	State ^[b]	ΔE ^{SP}	ΔH ^{SP}	ΔG ^{SP}	FOD	<i>J</i> [cm ⁻¹]
		[kJ·mol ⁻¹]	[kJ·mol ⁻¹]	[kJ·mol ⁻¹]		
[d _h bq ^{Cl}]	<i>CS</i>	0.0	0.0	0.0	0.4966	
	<i>T</i>	143.0	135.5	137.6		
[4 ^{Cl,Cl}]	<i>CS</i>	0.0	0.0	0.0	1.6785	
	<i>T</i>	30.9	28.1	25.3		
	<i>BS</i>	29.9				-79.0
[4 ^{iPr,Cl}]	<i>CS</i>	0.0	0.0	0.0	1.9018	

	<i>T</i>	-4.7	-6.9	-8.9		
	<i>BS</i>	-4.6				+4.1
	<i>CS</i>	0.0	0.0	0.0	1.6329	
[4 ^{Cl,Ph}]	<i>T</i>	42.1	37.5	31.2		
	<i>BS</i>	39.2				-207.0
	<i>CS</i>	0.0	0.0	0.0	1.8689	
[4 ^{Cl,NO₂}]	<i>T</i>	8.8	5.9	3.5		
	<i>BS</i>	8.6				-15.7
	<i>CS</i>	0.0	0.0	0.0	1.3967	
[4 ^{CF₃,Ph}]	<i>T</i>	87.6	79.4	85.4		
	<i>BS</i>					
	<i>CS</i>	0.0	0.0	0.0	2.3026	
[4 ^{iPr,NO₂}]	<i>T</i>	-40.8	-41.7	-42.2		
	<i>BS</i>	-40.6				+18.8

^[a] all compounds computed as salts with two [MeCN-Na@15c5]⁺, ^[b] *CS* = closed shell, *T* = triplet open shell, *BS* = broken symmetry open shell singlet.

Table 13: Computed energies for the calculation of *vacuum* FIAs.

Compound	Level of Optimization (r2scan)			Single-Point (SP) Level (DSD-BLYP-D3(BJ)/def2-QZVPP)			FIA [kJ·mol ⁻¹] (SP Level)
	E _{el} ^{Opt} [Hartree]	H ^{Opt} [Hartree]	H ^{Opt} [kJ·mol ⁻¹]	E _{el} ^{SP} [H]	E _{el} ^{SP} [kJ·mol ⁻¹]	H _{el} ^{SP} [kJ·mol ⁻¹]	
Si(CH ₃) ₃ ⁺	-408.9138	-408.7967	-1073295.8	-408.6882	-1073011.0	-1072703.5	
FSi(CH ₃) ₃	-509.1207	-508.9986	-1336375.9	-508.8755	-1336052.6	-1335732.0	
2 ^{iPr}	-1759.9347	-1759.2130	-4618814.2	-1759.0601	-4618412.7	-4616518.0	386
[F-2 ^{iPr}] ⁻	-1859.9291	-1859.2054	-4881344.0	-1859.0288	-4880880.6	-4878980.3	
2 ^{Cl}	-4729.1168	-4728.9923	-12415970.3	-4727.2579	-12411416.5	-12411089.7	488
[F-2 ^{Cl}] ⁻	-4829.1533	-4829.0254	-12678607.1	-4827.2665	-12673989.2	-12673653.5	
2 ^{CF₃}	-3748.8453	-3748.5907	-9841925.7	-3747.5521	-9839198.8	-9838530.4	566
[F-2 ^{CF₃}] ⁻	-3848.9092	-3848.6526	-10104638.2	-3847.5890	-10101845.8	-10101172.1	

FIA = $-\Delta H(\text{LA} + \text{F}^- \rightarrow \text{LA}\cdot\text{F}^-)$, LA = Lewis Acid,

Anchor Point (AP) = $-\Delta H(\text{Si}(\text{CH}_3)_3^+ + \text{F}^- \rightarrow \text{Si}(\text{CH}_3)_3)$,

AP^{CCSD(T)/CBS} = 952.5 kJ·mol⁻¹,

FIA^{LA} = AP^{CCSD(T)/CBS} - [$\Delta H(\text{LA} + \text{FSi}(\text{CH}_3)_3 \rightarrow \text{LA}\cdot\text{F}^- + \text{Si}(\text{CH}_3)_3^+)$]

= AP^{CCSD(T)/CBS} - [$\text{H}(\text{LA}\cdot\text{F}^-) + \text{H}(\text{Si}(\text{CH}_3)_3^+) - \text{H}(\text{LA}) - \text{H}(\text{FSi}(\text{CH}_3)_3)$].

7 Appendix

Table 14: Computed energies for the energies of the highest occupied molecular orbital (HOMO) of the respective Lewis acid (vacuum, DSD-BLYP-D3(BJ)/def2-QZVPP//r2SCAN-3c level of theory).

Compound	Energy of the highest occupied molecular orbital (HOMO) at the Single-Point Calculation Level [eV]
2^{Pr}	-7.5354
2^{Cl}	-8.7651
2^{CF₃}	-10.1264

7.4 Computation of Metrical Oxidation State

The metrical oxidation state (MOS) was calculated with the Excel sheet provided in the supporting information of: S. N. BROWN, *Inorg. Chem.* **2012**, *51*, 1251-1260.¹⁵⁸

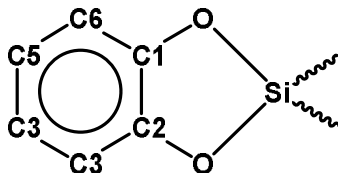


Table 15: Calculated MOS for the following silicon polyoxolene compounds.

Compound	<i>diox</i> ^X	C-O _{av}	C1-C2	C2-C3 _{av}	C3-C4 _{av}	C4-C5	Calc. MOS
1^{Cl}	Ring 1	1.2900	1.4430	1.4035	1.3740	1.4340	-1.15
	Ring 2	1.2905	1.4480	1.4045	1.3770	1.4360	-1.13
	Ring 3	1.3520	1.4100	1.3780	1.3985	1.3940	-1.97
	sum						-4.25
1^{Cl}(C₆H₆)₄	Ring 1	1.3015	1.4220	1.4140	1.3765	1.4250	-1.32
	Ring 2						-1.32
	Ring 3	1.3580	1.3860	1.3820	1.3990	1.3900	-2.10
	sum						-4.75
1^{Cl}(<i>o</i>-dcb)	Ring 1	1.3180	1.4270	1.3880	1.3850	1.4170	-1.52
	Ring 2						-1.52
	Ring 3	1.2840	1.4400	1.4090	1.3800	1.4430	-1.10
	sum						-4.14
1^{Br}	Ring 1	1.2785	1.4680	1.3900	1.3770	1.4790	-0.85
	Ring 2	1.2850	1.4380	1.4035	1.3810	1.4200	-1.21
	Ring 3	1.3480	1.4080	1.3785	1.3895	1.3760	-2.01
	sum						-4.08
[1^{Cl}][NBu₄]	Ring 1	1.2805	1.4470	1.4135	1.3760	1.4370	-1.05
	Ring 2	1.3435	1.4090	1.3765	1.4030	1.3860	-1.97
	Ring 3	1.3460	1.3970	1.3810	1.4025	1.3910	-1.99

7 Appendix

						sum	−5.01
$[1\text{Br}][\text{NBu}_4]$	Ring 1	1.285	1.453	1.4075	1.3725	1.447	−1.02
	Ring 2	1.3425	1.409	1.3835	1.402	1.388	−1.93
	Ring 3	1.343	1.419	1.376	1.401	1.397	−1.87
						sum	−4.82
$[1\text{Cl}][\text{H}_2\text{N}(\text{}^n\text{Pr})_2]_2$	Ring 1	1.3430	1.4090	1.3775	1.4025	1.3890	−1.95
	Ring 2	1.3400	1.3990	1.3910	1.4030	1.3880	−1.93
	Ring 3	1.3430	1.4090	1.3775	1.4025	1.3890	−1.95
						sum	−5.82
$[3\text{Cl}][\text{H}_2\text{N}(\text{}^n\text{Pr})_2]_2$	Ring 1	1.3620	1.3820	1.3790	1.3965	1.3970	−2.11
	Ring 2	1.3565	1.3870	1.3780	1.3930	1.3970	−2.06
	Ring 3 (linker)	1.3685	1.3940	1.3880	1.3835	1.3860	−2.11
	Ring 4	1.3630	1.3910	1.3785	1.3950	1.3900	−2.12
	Ring 5	1.3575	1.3950	1.3685	1.3985	1.4000	−2.07
						sum	−10.48
$[4\text{Cl,Cl}][\text{Na}@15\text{c}5]_2$	Ring 1	1.3520	1.3960	1.3845	1.4015	1.3950	−2.00
	Ring 2	1.3440	1.4140	1.3750	1.4080	1.3980	−1.92
	Ring 3	1.3440	1.4140	1.3750	1.4080	1.3980	−1.92
	Ring 4	1.3520	1.3960	1.3845	1.4015	1.3950	−2.00
						sum	−7.84
$[4\text{Br,Br}][\text{Na}@15\text{c}5]_2$	Ring 1	1.3430	1.4070	1.3795	1.4015	1.3890	−1.95
	Ring 2	1.3385	1.4040	1.3785	1.4050	1.3840	−1.96
	Ring 3	1.3385	1.4040	1.3785	1.4050	1.3840	−1.96
	Ring 4	1.3430	1.4070	1.3795	1.4015	1.3890	−1.95
						sum	−7.82
$[4\text{Cl,Br}][\text{Na}@15\text{c}5]_2$	Ring 1	1.3410	1.4050	1.3810	1.4030	1.3910	−1.93
	Ring 2	1.3445	1.3990	1.3820	1.4035	1.3930	−1.96
	Ring 3	1.3445	1.3990	1.3820	1.4035	1.3930	−1.96
	Ring 4	1.3410	1.4050	1.3810	1.4030	1.3910	−1.93
						sum	−7.79
$[4\text{Cl,Ph}][\text{Na}@15\text{c}5]_2$	Ring 1	1.3470	1.4110	1.3855	1.4105	1.3930	−1.94
	Ring 2	1.3475	1.4090	1.3890	1.4105	1.3880	−1.96
	Ring 3	1.3475	1.4090	1.3890	1.4105	1.3880	−1.96
	Ring 4	1.3470	1.4110	1.3855	1.4105	1.3930	−1.94
						sum	−7.80

7.5 EPR Spectroscopy

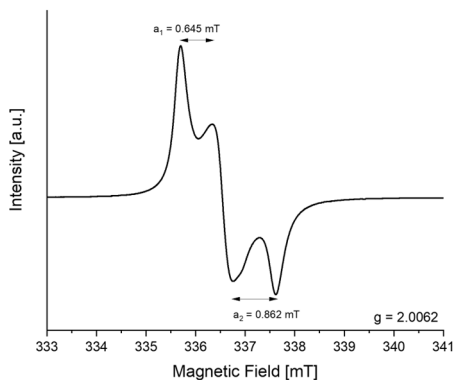


Figure 59: EPR spectrum of the reaction between 1Cl and thianthrene at room temperature in dichloromethane. The observed signals are in agreement with previous studies of the thianthrene radical cation.²⁷⁵ Parameters: $B_0 = 3364$ G, sweep = 100 G, sweep time = 20 s, modulation = 2000 mG, microwave power = 10 mW, gain = 7.

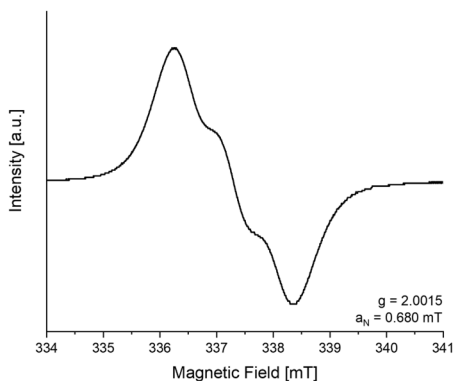


Figure 60: EPR spectrum of the reaction between 1Cl and tris(4-bromophenyl)amine at room temperature in dichloromethane. The broad signal with hyperfine splitting indicates a radical localized at the nitrogen. EPR parameters: $B_0 = 3370$ G, sweep = 200 G, sweep time = 20 s, modulation = 2000 mG, microwave power = 10 mW, gain = 9.

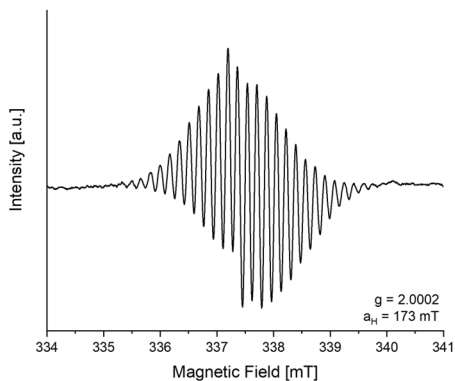


Figure 61: EPR spectrum of the reaction between 1Cl and PMB at room temperature in dichloromethane. The observed hyperfine coupling validates the successful oxidation reaction of PMB. The asymmetry in the signal can be explained by the presence of the underlying radical anion of 1Cl . Due to the short-lived nature and light-sensitivity of the primary oxidation products, no further isolation or characterization was attempted.²⁷⁶⁻²⁷⁷ Parameters: $B_0 = 3370 \text{ G}$, sweep = 100 G, sweep time = 20 s, modulation = 2000 mG, microwave power = 10 mW, gain = $4 \cdot 10^2$.

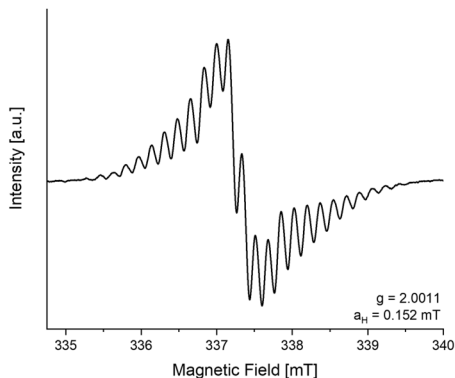


Figure 62: EPR spectra of the reaction between 1Cl and TMB at room temperature in dichloromethane. The observed hyperfine coupling validates the successful oxidation reaction of TMB. The asymmetry in the signal can be explained by the presence of the underlying radical anion of 1Cl . Due to the short-lived nature and light-sensitivity of the primary oxidation products, no further isolation or characterization was attempted.²⁷⁶⁻²⁷⁷ Parameters: $B_0 = 3370 \text{ G}$, sweep = 100 G, sweep time = 30 s, modulation = 2000 mG, microwave power = 10 mW, gain = $2 \cdot 10^2$.

7.6 NMR Spectroscopy

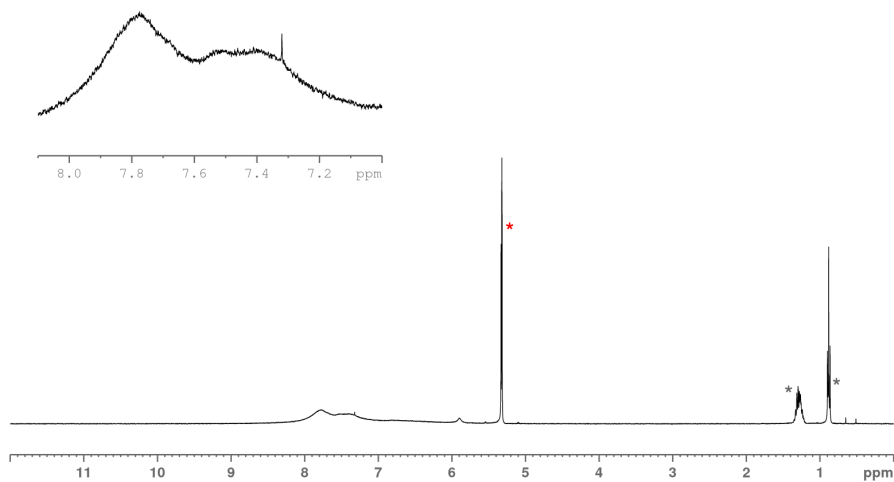


Figure 63: ^1H NMR ($^*\text{CD}_2\text{Cl}_2$) of a reaction mixture of 1^{Cl} and tris(2,4-dibromophenyl)amine. Contains residual * pentane.

7.7 Cyclic Voltammetry Experiments

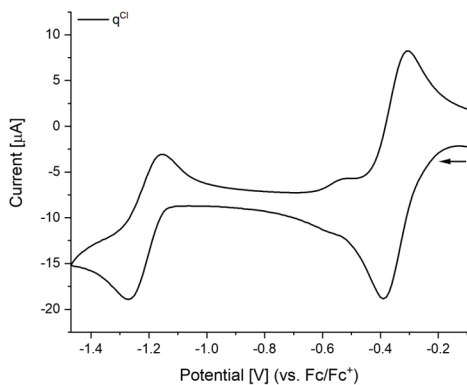


Figure 64: CV measurement of q^{Cl} in dichloromethane with [BArF₂₀][NⁿBu₄] at 100 mV/s.

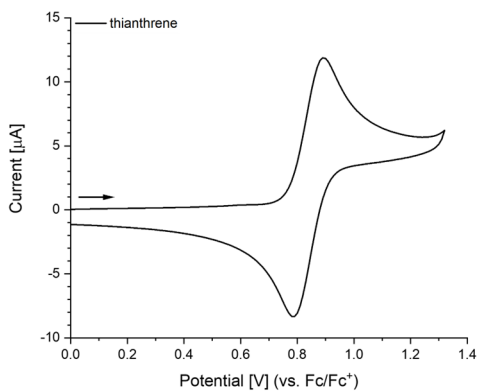


Figure 65: CV measurement of thianthrene in dichloromethane with [PF₆][NⁿBu₄] at 100 mV/s.

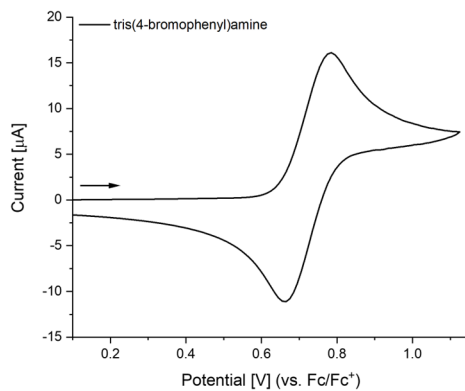


Figure 66: CV measurement of tris(4-bromophenyl)amine in dichloromethane with $[\text{PF}_6][\text{N}^n\text{Bu}_4]$ at 100 mV/s

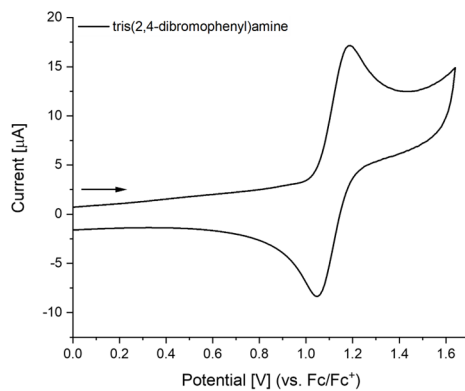


Figure 67: CV measurement of tris(2,4-bromophenyl)amine in dichloromethane with $[\text{PF}_6][\text{N}^n\text{Bu}_4]$ at 100 mV/s.

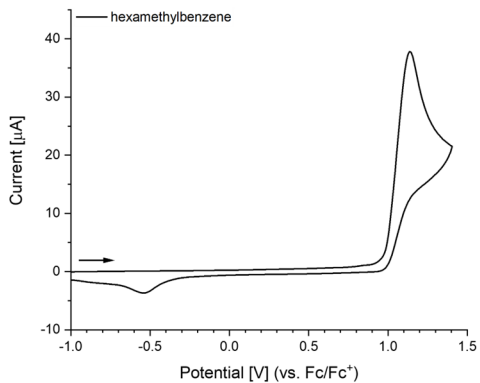


Figure 68: CV measurement of HMB in dichloromethane with $[\text{PF}_6][\text{N}^+\text{Bu}_4]$ at 100 mV/s.

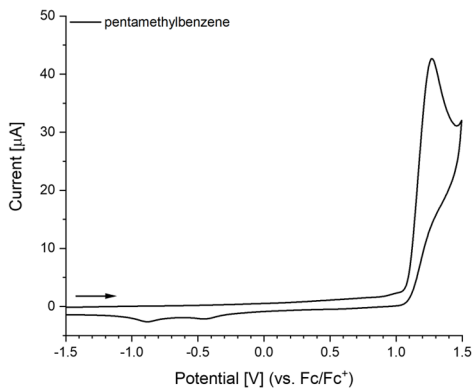


Figure 69: CV measurement of PMB in dichloromethane with $[\text{PF}_6][\text{N}^+\text{Bu}_4]$ at 100 mV/s.

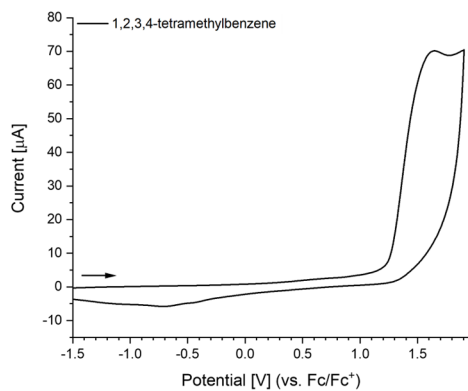


Figure 70: CV measurement of TMB in dichloromethane with $[\text{PF}_6][\text{N}^t\text{Bu}_4]$ at 100 mV/s.

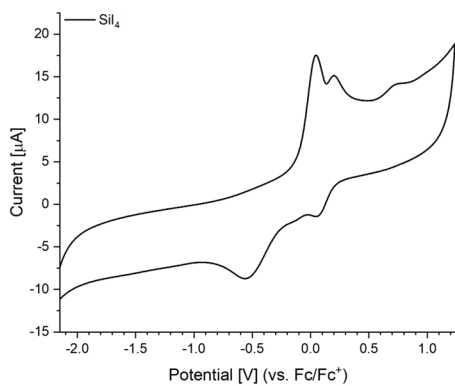


Figure 71: CV measurement of SiI_4 in dichloromethane with $[\text{PF}_6][\text{N}^t\text{Bu}_4]$ at 100 mV/s.

7.8 Crystallographic Data

Compound	H ₂ cat ^{Pr}	3,6-Br-2,5-Ph- <i>p</i> -benzoquinone
Identification code	mo_rm701c_0m_a	mo_RM617_0m_a
CCDC number	2182203	2182196
Empirical formula	C ₁₅ H ₂₄ O ₂	C ₁₈ H ₁₀ Br ₂ O ₂
Formula weight	236.37	418.08
Temperature [K]	100.00	100.0
Crystal system	monoclinic	monoclinic
Space group	<i>C</i> 2/ <i>c</i>	<i>P</i> 2 ₁ / <i>n</i>
<i>a</i> [Å]	19.6049(12)	6.1461(4)
<i>b</i> [Å]	21.0294(12)	7.2515(4)
<i>c</i> [Å]	21.3612(14)	17.5582(11)
α [°]	90	90
β [°]	91.195(3)	99.493(2)
γ [°]	90	90
Volume [Å ³]	8804.9(9)	771.83(8)
<i>Z</i>	24	2
<i>ρ</i> _{calc} [g·cm ³]	1.070	1.799
μ [mm ⁻¹]	0.069	5.255
<i>F</i> (000)	3121.0	408.0
Crystal size [mm ³]	0.394 × 0.364 × 0.238	0.44 × 0.339 × 0.124
Radiation	Mo- <i>K</i> _α (λ = 0.71073 Å)	Mo- <i>K</i> _α (λ = 0.71073 Å)
2Θ range [°]	3.814 to 54.51	4.704 to 59.208
Index ranges	-25 ≤ <i>h</i> ≤ 25, -26 ≤ <i>k</i> ≤ 27, -27 ≤ <i>l</i> ≤ 27	-8 ≤ <i>h</i> ≤ 8, -10 ≤ <i>k</i> ≤ 10, -24 ≤ <i>l</i> ≤ 24
Reflections collected	169045	31132
Independent reflections	9821 [<i>R</i> _{int} = 0.0778, <i>R</i> _{sigma} = 0.0358]	2173 [<i>R</i> _{int} = 0.0626, <i>R</i> _{sigma} = 0.0258]
Data/Restraints/Parameters	9821/913/805	2173/0/100
Goodness-of-fit on <i>F</i> ²	1.050	1.061
Final <i>R</i> indexes [<i>I</i> ≥ 2σ(<i>I</i>)]	<i>R</i> ₁ = 0.0792, <i>wR</i> ₂ = 0.2332	<i>R</i> ₁ = 0.0225, <i>wR</i> ₂ = 0.0588
Final <i>R</i> indexes [all data]	<i>R</i> ₁ = 0.0891, <i>wR</i> ₂ = 0.2425	<i>R</i> ₁ = 0.0245, <i>wR</i> ₂ = 0.0597
Largest peak/hole [e·Å ⁻³]	0.40/-0.28	0.59/-0.78

Compound	$1^{\text{Cl}}(\text{CH}_2\text{Cl}_2)_x$	$1^{\text{Cl}}(\text{C}_6\text{H}_6)_4$
Identification code	rm270_sq_file002	rm277_file003
CCDC number	1877563	1877564
Empirical formula	$\text{C}_{18}\text{Cl}_{12}\text{O}_6\text{Si} (\text{CH}_2\text{Cl}_2)_x$	$\text{C}_{42}\text{H}_{24}\text{Cl}_{12}\text{O}_6\text{Si}$
Formula weight	765.67	1078.10
Temperature [K]	100	100
Crystal system	monoclinic	tetragonal
Space group	$P 2_1/n$	$P 4_12_12$
a [Å]	13.760(3)	13.3140(19)
b [Å]	31.108(6)	90
c [Å]	14.872(3)	24.662(5)
α [°]	90	90
β [°]	95.44(3)	90
γ [°]	90	90
Volume [Å ³]	6337(2)	4371.7(15)
Z	8	4
ρ_{calc} [g·cm ³]	1.605	1.638
μ [mm ⁻¹]	1.117	0.836
$F(000)$	2992	2168
Crystal size [mm ³]	$0.65 \times 0.30 \times 0.30$	$0.60 \times 0.50 \times 0.35$
Radiation	Mo- $K\alpha$ ($\lambda = 0.71073$ Å)	Mo- $K\alpha$ ($\lambda = 0.71073$ Å)
2Θ range [°]	1.5 to 25.1	2.2 to 26.4
Index ranges	$-16 \leq h \leq 16, -37 \leq k \leq 37, -17 \leq l \leq 17$	$-16 \leq h \leq 16, -11 \leq k \leq 11, -30 \leq l \leq 30$
Reflections collected	89964	12734
Independent reflections	11315 [$R_{\text{int}} = 0.0872, R_{\text{sigma}} = 0.0571$]	4474 [$R_{\text{int}} = 0.0340, R_{\text{sigma}} = 0.0473$]
Data/Restraints/Parameters	11315/0/667	4474/72/253
Goodness-of-fit on F^2	1.025	1.034
Final R indexes [$I \geq 2\sigma(I)$]	$R_1 = 0.0484, wR_2 = 0.1008$	$R_1 = 0.0468, wR_2 = 0.1118$
Final R indexes [all data]	$R_1 = 0.0759, wR_2 = 0.1099$	$R_1 = 0.0796, wR_2 = 0.1263$
Largest peak/hole [e·Å ⁻³]	0.845, -0.553	0.698, -0.298
Flack parameter	n/a	0.37(14)*

* inversion twin

7 Appendix

Compound	1^{Cl}(<i>o</i>-dcb)₄	1^{Br}
Identification code	gr_rm1_4_file004	mo_RM422_0m_a
CCDC number	1877565	n/a
Empirical formula	C ₄₂ H ₁₆ Cl ₂₀ O ₆ Si	Br ₁₂ C ₁₉ Cl ₂ O ₆ SiH _{0.12}
Formula weight	1353.64	1382.23
Temperature [K]	120	100.00
Crystal system	orthorhombic	monoclinic
Space group	<i>F d d 2</i>	<i>C 2/c</i>
<i>a</i> [Å]	24.6052(3)	21.6357(10)
<i>b</i> [Å]	24.2681(4)	20.2942(8)
<i>c</i> [Å]	16.5848(2)	16.3581(7)
α [°]	90	90
β [°]	90	119.468(2)
γ [°]	90	90
Volume [Å ³]	9903.1(2)	6253.3(5)
<i>Z</i>	8	8
ρ_{calc} [g·cm ³]	1.816	2.936
μ [mm ⁻¹]	10.775	15.618
<i>F</i> (000)	5360	5041.0
Crystal size [mm ³]	0.104 × 0.080 × 0.065	0.092 × 0.133 × 0.088
Radiation	Cu- <i>K</i> α ($\lambda = 1.54184$ Å)	Mo- <i>K</i> α ($\lambda = 0.71073$ Å)
2 Θ range [°]	3.7 to 71.0	4.014 to 50.048
Index ranges	-30 ≤ <i>h</i> ≤ 30, -29 ≤ <i>k</i> ≤ 29, -20 ≤ <i>l</i> ≤ 20	-25 ≤ <i>h</i> ≤ 25, -24 ≤ <i>k</i> ≤ 24, -19 ≤ <i>l</i> ≤ 19
Reflections collected	75635	118156
Independent reflections	4621 [<i>R</i> _{int} = 0.0684, <i>R</i> _{sigma} = 0.0283]	5523 [<i>R</i> _{int} = 0.1141, <i>R</i> _{sigma} = 0.0445]
Data/Restraints/Parameters	4621/1/313	5523/0/361
Goodness-of-fit on <i>F</i> ²	1.027	1.061
Final <i>R</i> indexes [<i>I</i> ≥ 2 σ (<i>I</i>)]	<i>R</i> ₁ = 0.0314, <i>wR</i> ₂ = 0.0723	<i>R</i> ₁ = 0.0627, <i>wR</i> ₂ = 0.1620
Final <i>R</i> indexes [all data]	<i>R</i> ₁ = 0.0348, <i>wR</i> ₂ = 0.0733	<i>R</i> ₁ = 0.0789, <i>wR</i> ₂ = 0.1744
Largest peak/hole [e·Å ⁻³]	0.397, -0.250	3.02/-1.25
Flack parameter	0.054(18)	n/a

Compound	[1 ^{Cl}][H ₂ N ₂] ₂	[1 ^{Cl}][NBu ₄]
Identification code	rm264_2_c2	mo_rm498_0m
CCDC number	2035360	2035362
Empirical formula	C ₃₀ H ₃₂ Cl ₁₂ N ₂ O ₆ Si	C ₃₅ H ₃₈ Cl ₁₄ NO ₆ Si
Formula weight	970.06	1093.05
Temperature [K]	120	101.0
Crystal system	monoclinic	triclinic
Space group	<i>C</i> 2/ <i>c</i> (15)	<i>P</i> $\bar{1}$ (2)
<i>a</i> [Å]	20.646(4)	10.9650(8)
<i>b</i> [Å]	12.467(3)	12.4668(9)
<i>c</i> [Å]	16.175(3)	17.8053(13)
α [°]	90	101.534(3)
β [°]	108.56(3)	100.805(3)
γ [°]	90	102.979(3)
Volume [Å ³]	3946.8(15)	2254.0(3)
<i>Z</i>	4	2
ρ_{calc} [g·cm ³]	1.633	1.611
μ [mm ⁻¹]	0.917	0.927
<i>F</i> (000)	1968.0	1110.0
Crystal size [mm ³]	0.13 × 0.12 × 0.11	0.181 × 0.089 × 0.062
Radiation	Mo- <i>K</i> _α ($\lambda = 0.71073$ Å)	Mo- <i>K</i> _α ($\lambda = 0.71073$ Å)
2 Θ range [°]	3.874 to 60.09	3.686 to 54.326
Index ranges	-29 ≤ <i>h</i> ≤ 29, -17 ≤ <i>k</i> ≤ 17, -22 ≤ <i>l</i> ≤ 22	-14 ≤ <i>h</i> ≤ 14, -15 ≤ <i>k</i> ≤ 15, -22 ≤ <i>l</i> ≤ 22
Reflections collected	10939	71748
Independent reflections	5772 [<i>R</i> _{int} = 0.0376, <i>R</i> _{sigma} = 0.0528]	9956 [<i>R</i> _{int} = 0.0599, <i>R</i> _{sigma} = 0.0332]
Data/Restraints/Parameters	5772/0/244	9956/0/518
Goodness-of-fit on <i>F</i> ²	1.034	1.049
Final <i>R</i> indexes [<i>I</i> ≥ 2σ(<i>I</i>)]	<i>R</i> ₁ = 0.0415, <i>wR</i> ₂ = 0.0920	<i>R</i> ₁ = 0.0398, <i>wR</i> ₂ = 0.0910
Final <i>R</i> indexes [all data]	<i>R</i> ₁ = 0.0699, <i>wR</i> ₂ = 0.1021	<i>R</i> ₁ = 0.0513, <i>wR</i> ₂ = 0.0979
Largest peak/hole [e·Å ⁻³]	0.69/-0.59	0.69/-0.61

7 Appendix

Compound	[1 ^{Br}][N ⁿ Bu ₄] ₂	[1 ^{Br}][NBu ₄]
Identification code	mo_rm574_2_0ma	mo_x_rm573_0m_a
CCDC number	n/a	n/a
Empirical formula	C ₅₀ H ₇₂ Br ₁₂ N ₂ O ₆ Si	C _{17.50} H ₁₉ Br ₆ ClN _{0.50} O ₃ Si _{0.50}
Formula weight	1784.10	813.29
Temperature [K]	100.0	100(2)
Crystal system	orthorhombic	triclinic
Space group	<i>P</i> 2 ₁ 2 ₁ 2 (18)	<i>P</i> $\bar{1}$ (2)
<i>a</i> [Å]	20.4286(10)	11.2987(7)
<i>b</i> [Å]	27.8404(12)	12.7356(8)
<i>c</i> [Å]	13.9042(6)	17.8079(13)
α [°]	90	100.533(3)
β [°]	90	99.093(3)
γ [°]	90	105.045(3)
Volume [Å ³]	7907.9(6)	2375.3(3)
<i>Z</i>	4	4
ρ_{calc} [g·cm ³]	1.499	2.274
μ [mm ⁻¹]	6.129	10.298
<i>F</i> (000)	3472	1542
Crystal size [mm ³]	n/a	0.069 × 0.053 × 0.046
Radiation	Mo- <i>K</i> α ($\lambda = 0.71073$ Å)	Mo- <i>K</i> α ($\lambda = 0.71073$ Å)
2 Θ range [°]	4.14 to 55.05 (0.77 Å)	3.82 to 62.08 (0.69 Å)
Index ranges	-26 ≤ <i>h</i> ≤ 26, -35 ≤ <i>k</i> ≤ 36, -16 ≤ <i>l</i> ≤ 18	-16 ≤ <i>h</i> ≤ 16, -18 ≤ <i>k</i> ≤ 18, -25 ≤ <i>l</i> ≤ 25
Reflections collected	72409	143094
Independent reflections	18184 [<i>R</i> _{int} = 0.0664, <i>R</i> _{sigma} = 0.0706]	15192 [<i>R</i> _{int} = 0.0814, <i>R</i> _{sigma} = 0.0427]
Data/Restraints/Parameters	18184/602/612	15192/0/518
Goodness-of-fit on <i>F</i> ²	1.304	1.029
Final <i>R</i> indexes [<i>I</i> ≥ 2σ(<i>I</i>)]	<i>R</i> ₁ = 0.1104, <i>wR</i> ₂ = 0.3114	<i>R</i> ₁ = 0.0323, <i>wR</i> ₂ = 0.0610
Final <i>R</i> indexes [all data]	<i>R</i> ₁ = 0.1358, <i>wR</i> ₂ = 0.3343	<i>R</i> ₁ = 0.0557, <i>wR</i> ₂ = 0.0676
Largest peak/hole [e·Å ⁻³]	5.93/-2.60	1.24/-0.95
Flack parameter	0.043(8)	n/a

Compound	[3 ^{C1}][H ₂ N ⁿ Pr ₂] ₂	[<i>dhbq</i> ^{C1}][Na@15c5] ₂
Identification code	rm317_p1	mo_rmaj119_0m
CCDC number	2035361	2182195
Empirical formula	C ₄₂ H ₃₂ N ₂ O ₁₀ Si ₂ Cl ₂₀	C ₂₆ H ₄₀ Cl ₂ Na ₂ O ₁₄
Formula weight	1489.87	693.46
Temperature [K]	293(2)	100.0
Crystal system	triclinic	triclinic
Space group	<i>P</i> $\bar{1}$ (2)	<i>P</i> $\bar{1}$
<i>a</i> [Å]	11.029(2)	8.704(4)
<i>b</i> [Å]	15.799(3)	9.531(4)
<i>c</i> [Å]	17.369(4)	20.274(6)
α [°]	87.78(3)	83.028(10)
β [°]	74.42(3)	78.044(11)
γ [°]	85.75(3)	74.702(12)
Volume [Å ³]	2906.8(11)	1583.2(11)
<i>Z</i>	2	2
ρ_{calc} [g·cm ³]	1.702	1.455
μ [mm ⁻¹]	1.035	0.299
<i>F</i> (000)	1492.0	728.0
Crystal size [mm ³]	0.105 × 0.09 × 0.085	0.188 × 0.111 × 0.098
Radiation	Mo- <i>K</i> α ($\lambda = 0.71073$ Å)	Mo- <i>K</i> α ($\lambda = 0.71073$ Å)
2 Θ range [°]	2.586 to 55	4.118 to 61.176
Index ranges	-14 ≤ <i>h</i> ≤ 14, -20 ≤ <i>k</i> ≤ 20, -22 ≤ <i>l</i> ≤ 22	-12 ≤ <i>h</i> ≤ 12, -13 ≤ <i>k</i> ≤ 13, -28 ≤ <i>l</i> ≤ 28
Reflections collected	24720	98060
Independent reflections	13332 [<i>R</i> _{int} = 0.0797, <i>R</i> _{sigma} = 0.1439]	9716 [<i>R</i> _{int} = 0.0487, <i>R</i> _{sigma} = 0.0235]
Data/Restraints/Parameters	13332/0/689	9716/0/397
Goodness-of-fit on <i>F</i> ²	0.923	1.055
Final <i>R</i> indexes [<i>I</i> ≥ 2 σ (<i>I</i>)]	<i>R</i> ₁ = 0.0523, <i>wR</i> ₂ = 0.0913	<i>R</i> ₁ = 0.0304, <i>wR</i> ₂ = 0.0690
Final <i>R</i> indexes [all data]	<i>R</i> ₁ = 0.1631, <i>wR</i> ₂ = 0.1195	<i>R</i> ₁ = 0.0392, <i>wR</i> ₂ = 0.0744
Largest peak/hole [e·Å ⁻³]	0.44/-0.34	0.41/-0.22

7 Appendix

Compound	[<i>dhbq</i> ^{Pb}][Na@15c5] ₂	[<i>dhbq</i> ^{NO₂}][Na@15c5] ₂
Identification code	mo_RM631_0m	mo_rm692_0m_4_a
CCDC number	2182197	2182198
Empirical formula	C ₄₀ H ₅₄ Cl ₄ Na ₂ O ₁₄	C ₂₈ H ₄₆ N ₂ Na ₂ O ₁₉ Si ₂
Formula weight	473.30	792.71
Temperature [K]	293.15	100.00
Crystal system	triclinic	triclinic
Space group	<i>P</i> $\bar{1}$	<i>P</i> $\bar{1}$
<i>a</i> [Å]	9.153(4)	8.3219(7)
<i>b</i> [Å]	10.574(6)	11.2322(9)
<i>c</i> [Å]	12.640(8)	11.4895(10)
α [°]	79.04(3)	63.487(3)
β [°]	72.713(17)	80.017(4)
γ [°]	82.615(15)	79.825(4)
Volume [Å ³]	1143.5(10)	940.44(14)
<i>Z</i>	1	1
ρ_{calc} [g·cm ³]	1.375	1.400
μ [mm ⁻¹]	0.340	0.188
<i>F</i> (000)	496.0	418.0
Crystal size [mm ³]	0.125 × 0.1 × 0.088	0.202 × 0.177 × 0.145
Radiation	Mo- <i>K</i> _α ($\lambda = 0.71073$ Å)	Mo- <i>K</i> _α ($\lambda = 0.71073$ Å)
2 Θ range [°]	3.934 to 61.944	6.818 to 54.334
Index ranges	-13 ≤ <i>h</i> ≤ 13, -15 ≤ <i>k</i> ≤ 15, -18 ≤ <i>l</i> ≤ 18	-10 ≤ <i>h</i> ≤ 10, -12 ≤ <i>k</i> ≤ 14, 0 ≤ <i>l</i> ≤ 14
Reflections collected	57063	4108
Independent reflections	7182 [<i>R</i> _{int} = 0.0455, <i>R</i> _{sigma} = 0.0277]	4108 [<i>R</i> _{int} = 0.0822, <i>R</i> _{sigma} = 0.0556]
Data/Restraints/Parameters	7182/0/271	4108/40/255
Goodness-of-fit on <i>F</i> ²	1.063	1.129
Final <i>R</i> indexes [<i>I</i> ≥ 2σ(<i>I</i>)]	<i>R</i> ₁ = 0.0446, <i>wR</i> ₂ = 0.1085	<i>R</i> ₁ = 0.1305, <i>wR</i> ₂ = 0.3413
Final <i>R</i> indexes [all data]	<i>R</i> ₁ = 0.0577, <i>wR</i> ₂ = 0.1150	<i>R</i> ₁ = 0.1492, <i>wR</i> ₂ = 0.3519
Largest peak/hole [e·Å ⁻³]	0.59/-0.67	1.79/-1.16

Compound	[4 ^{Cl,Cl}][Na@15c5] ₂	[4 ^{Br,Br}][Na@15c5] ₂
Identification code	mo_rm579_1_0m	mo_rmse77_pentan_0m
CCDC number	2182199	2182200
Empirical formula	C ₅₄ H ₄₆ Cl ₁₈ N ₂ Na ₂ O ₂₂ Si ₂	C ₅₄ H ₄₆ Br ₁₈ N ₂ Na ₂ O ₂₂ Si ₂
Formula weight	1815.19	2615.47
Temperature [K]	100.00	100.00
Crystal system	triclinic	triclinic
Space group	$P\bar{1}$	$P\bar{1}$
<i>a</i> [Å]	10.7482(13)	10.9161(4)
<i>b</i> [Å]	13.2987(16)	13.6199(4)
<i>c</i> [Å]	14.0893(18)	14.3745(5)
α [°]	115.674(5)	114.9450(10)
β [°]	95.090(5)	95.9130(10)
γ [°]	100.826(5)	100.8530(10)
Volume [Å ³]	1749.5(4)	1862.75(11)
<i>Z</i>	1	1
ρ_{calc} [g·cm ³]	1.723	2.332
μ [mm ⁻¹]	0.827	9.784
<i>F</i> (000)	916.0	1240.0
Crystal size [mm ³]	0.177 × 0.145 × 0.102	0.145 × 0.131 × 0.095
Radiation	Mo- <i>K</i> _α ($\lambda = 0.71073$ Å)	Mo- <i>K</i> _α ($\lambda = 0.71073$ Å)
2 Θ range [°]	4.564 to 50	3.882 to 57.462
Index ranges	-12 ≤ <i>h</i> ≤ 12, -15 ≤ <i>k</i> ≤ 15, -16 ≤ <i>l</i> ≤ 16	-14 ≤ <i>h</i> ≤ 14, -18 ≤ <i>k</i> ≤ 18, -19 ≤ <i>l</i> ≤ 19
Reflections collected	45958	52652
Independent reflections	6141 [<i>R</i> _{int} = 0.1252, <i>R</i> _{sigma} = 0.0711]	9655 [<i>R</i> _{int} = 0.0710, <i>R</i> _{sigma} = 0.0488]
Data/Restraints/Parameters	6141/9/453	9655/0/452
Goodness-of-fit on <i>F</i> ²	1.030	1.016
Final <i>R</i> indexes [<i>I</i> ≥ 2σ(<i>I</i>)]	<i>R</i> ₁ = 0.0570, <i>wR</i> ₂ = 0.1398	<i>R</i> ₁ = 0.0320, <i>wR</i> ₂ = 0.0585
Final <i>R</i> indexes [all data]	<i>R</i> ₁ = 0.0778, <i>wR</i> ₂ = 0.1614	<i>R</i> ₁ = 0.0524, <i>wR</i> ₂ = 0.0657
Largest peak/hole [e·Å ⁻³]	0.55/-0.52	0.90/-0.79

7 Appendix

Compound	[4 ^{Cl,Br}][Na@15c5] ₂	[4 ^{Cl,Pb}][Na@15c5] ₂
Identification code	mo_rm599_1_0m_a	mo_rm626_0m_a
CCDC number	2182201	2182202
Empirical formula	C ₅₄ H ₄₆ Br ₂ Cl ₁₆ N ₂ Na ₂ O ₂₂ Si ₂	C ₆₈ H ₆₀ Cl ₂₀ N ₂ Na ₂ O ₂₂ Si ₂
Formula weight	1904.11	2068.34
Temperature [K]	100.00	100.00
Crystal system	triclinic	monoclinic
Space group	$P\bar{1}$	$P2_1/n$
<i>a</i> [Å]	10.7198(6)	19.818(11)
<i>b</i> [Å]	13.3617(7)	11.020(4)
<i>c</i> [Å]	14.1849(7)	20.503(8)
α [°]	116.011(2)	90
β [°]	94.312(2)	104.773(17)
γ [°]	101.051(2)	90
Volume [Å ³]	1762.66(16)	4330(3)
<i>Z</i>	1	2
ρ_{calc} [g·cm ³]	1.794	1.586
μ [mm ⁻¹]	1.878	0.738
<i>F</i> (000)	952.0	2096.0
Crystal size [mm ³]	0.117 × 0.105 × 0.09	0.14 × 0.12 × 0.08
Radiation	Mo- <i>K</i> _α ($\lambda = 0.71073$ Å)	Mo- <i>K</i> _α ($\lambda = 0.71073$ Å)
2 Θ range [°]	3.506 to 56.64	4.11 to 54.11
Index ranges	$-14 \leq h \leq 14$, $-17 \leq k \leq 17$, $-18 \leq l \leq 18$	$-25 \leq h \leq 25$, $-14 \leq k \leq 14$, $-26 \leq l \leq 25$
Reflections collected	64482	106568
Independent reflections	8772 [$R_{int} = 0.0420$, $R_{\sigma} = 0.0227$]	9453 [$R_{int} = 0.0656$, $R_{\sigma} = 0.0273$]
Data/Restraints/Parameters	8772/0/452	9453/0/524
Goodness-of-fit on F^2	1.058	1.069
Final <i>R</i> indexes [$I \geq 2\sigma(I)$]	$R_1 = 0.0315$, $wR_2 = 0.0873$	$R_1 = 0.0347$, $wR_2 = 0.0809$
Final <i>R</i> indexes [all data]	$R_1 = 0.0371$, $wR_2 = 0.0907$	$R_1 = 0.0458$, $wR_2 = 0.0872$
Largest peak/hole [e·Å ⁻³]	0.61/−1.29	0.62/−0.70

Compound	[2 ^{Cl} -N ₃][N ⁿ Bu ₄]	[2 ^{Cl} -(N ₃) ₂][N ⁿ Bu ₄] ₂
Identification code	mo_rm590_0m	rm615_P21c_a
CCDC number	2130731	2132184
Empirical formula	C ₂₈ H ₃₆ Cl ₈ N ₄ O ₄ Si	C ₄₄ H ₇₂ Cl ₈ N ₈ O ₄ Si
Formula weight	804.30	1088.78
Temperature [K]	100.0	100(2)
Crystal system	triclinic	monoclinic
Space group	$P\bar{1}$ (2)	$P2_1/c$ (14)
<i>a</i> [Å]	10.1621(4)	9.8208(12)
<i>b</i> [Å]	11.4174(5)	14.8040(15)
<i>c</i> [Å]	16.5904(7)	36.978(5)
α [°]	93.958(2)	90
β [°]	98.166(2)	94.199(4)
γ [°]	111.533(2)	90
Volume [Å ³]	1756.98(13)	5361.7(11)
<i>Z</i>	2	4
ρ_{calc} [g·cm ³]	1.520	1.349
μ [mm ⁻¹]	0.716	0.490
<i>F</i> (000)	828	2296
Crystal size [mm ³]	0.301 × 0.161 × 0.098	0.300 × 0.150 × 0.080
Radiation	Mo- <i>K</i> _α ($\lambda = 0.71073$ Å)	Mo- <i>K</i> _α ($\lambda = 0.71073$ Å)
2 Θ range [°]	3.87 to 57.45 (0.74 Å)	4.16 to 54.62 (0.77 Å)
Index ranges	-13 ≤ <i>h</i> ≤ 13, -15 ≤ <i>k</i> ≤ -22 ≤ <i>l</i> ≤ 22	-12 ≤ <i>h</i> ≤ 12, -19 ≤ <i>k</i> ≤ -47 ≤ <i>l</i> ≤ 47
Reflections collected	37613	211540
Independent reflections	8973 [$R_{int} = 0.0487$, $R_{sigma} = 0.0360$]	11960 [$R_{int} = 0.0667$, $R_{sigma} = 0.0272$]
Data/Restraints/Parameters	8973/0/410	11960/387/671
Goodness-of-fit on F^2	1.060	1.056
Final <i>R</i> indexes [$I \geq 2\sigma(I)$]	$R_1 = 0.0301$, $wR_2 = 0.0765$	$R_1 = 0.0463$, $wR_2 = 0.1043$
Final <i>R</i> indexes [all data]	$R_1 = 0.0370$, $wR_2 = 0.0793$	$R_1 = 0.0584$, $wR_2 = 0.1123$
Largest peak/hole [e·Å ⁻³]	0.45/-0.28	0.92/-0.70

DANKSAGUNG

An dieser Stelle möchte ich mich bei all jenen Menschen bedanken, die mich während meiner Promotion begleitet und mich auf unterschiedlichste Art und Weise unterstützt haben! Ohne euch wäre die Fertigstellung dieser Arbeit so nicht möglich gewesen.

Ein besonderer Dank geht zuallererst an meinen Doktorvater Prof. Dr. *Lutz Greb*. Ich bin sehr froh darüber, dass ich damals als Master Studentin zu deinem (Drei-Menschen-)Arbeitskreis gefunden habe. Schon seit dem Forschungspraktikum über die Master-Arbeit bis hin zur Promotion hast du mir stets interessante und herausfordernde Themen anvertraut. Danke für dieses Vertrauen in mich und für den immerwährenden Glauben an mich, meine Projekte und natürlich an die Radikale! Durch dich habe ich meine Begeisterung für die Anorganische-Chemie entdeckt. Es war schön bei deinem Werdegang von Habilitand-Lutz zu Prof. Lutz dabei zu sein. Danke auch für die hervorragende Betreuung, die, obwohl wir immer größer wurden, nie nachgelassen hat. 😊

Für die Übernahme des Zweitgutachtens danke ich herzlich Prof. Dr. Dr. *Hans-Jörg Himmel*. Danke für die Eingliederung des AK Grebs in deinen Arbeitskreis und für die vollumfängliche Unterstützung in den letzten Jahren, mit deiner fachlichen Expertise bei den Seminarvorträgen und für die Bereitstellung der nötigen Infrastruktur.

Ein weiterer Dank gilt allen Mitarbeitern der analytischen Einrichtungen des gesamten Chemischen Instituts sowie den Reinigungskräften, Feinmechanikern, Schlossern, Elektrikern und Glasbläsern. Insbesondere danke ich *Marion Kerscher* für die Einführung am *großen* EPR-Spektrometer und auch *Sebastian Haaf*, dafür, dass ihr mir mit Rat und Tat zur Seite standet, wenn das Gerät wieder Probleme bereitete.. meist jedes Mal. 😊

Ein sehr großer Dank geht ebenfalls an das X-Ray-Team mit aktuellen und ehemaligen Mitgliedern des AK Greb und AK Himmel für die Zeit, die ihr geopfert habt beim Kristalle suchen aus meinen Proben, die nicht farblos waren, für das Messen und das anschließende Lösen der Strukturen.

Vielen Dank auch an meine fleißigen Praktikant:innen *Christoph, Simone, Angi, Jonas, Coco* und *Annabelle* für eure engagierte Mitarbeit bei den jeweiligen Forschungsthemen und dementsprechend für eure Beiträge zu dieser Arbeit.

Ganz herzlichen Dank auch an meine sorgfältigen Korrekturleser *Thaddäus Thorwart, Nils Ansmann, Daniel Roth, Heiko Ruppert, Ravi Yadav* und *Christoph Bendel*. Die Arbeit wurde damit signifikant besser, ich schwöre!

Ein großes Dankeschön geht auch an alle aktuellen und ehemaligen Mitglieder des *AK Himmel* für die herzliche Aufnahme in den Arbeitskreis. Danke für die zahlreichen FABs, die familiäre Atmosphäre, Hilfsbereitschaft bei jeglichen Problemen und für die gemeinsamen Social Events, wie Skiseminare, Grillabende, Motto-Tage und andere coole außeruniversitären Ausflüge.

Auch danke ich meinem geliebten Freundeskreis. *Sophia Fehrenbach*, *Mathias Scherpe*, ihr seid die besten Freunde, die man sich wünschen kann. Ohne euch, wäre ich wohl zu einer sozial-inkompetenten Zombie-Chemikerin geworden, die sich in Arbeit vergräbt und Instant-Nudeln isst (nichts gegen Instant Nudeln 🍝). Zum Glück habt ihr dafür gesorgt, dass ich regelmäßig aus dem Labor-Alltag komme, was anderes esse und vor allem auch andere Leute sehe. Danke auch für den tollen *co-working space* bei euch! Da machte Home-Office gleich dreimal so viel Spaß; mit Karli sogar noch viel mehr 😊 (wäre da nicht dieser Berg..). *Franziska Hess*, *Jana Trabold*, *Natascha Böttinger* und *Lukas Arnecke*, danke, dass ihr immer ein offenes Ohr für mich habt und für mich da seid, egal welches Wehwechen ich habe. Danke für all' die schönen gemeinsamen (Sonntag-)Abende, Unternehmungen (außer das Wandern 😊) und einfach dafür, dass ich bei euch genauso sein kann, wie ich bin.

Lieber *Thaddäus*, ich weiß gar nicht wie ich dir danken soll. Ich bin einfach so froh dich zu haben. Du hast mir immer vor Augen gehalten, was ich alles geschafft habe, worauf ich stolz sein kann und dass ich für mich einstehen kann, genauso, wie ich bin. Danke, für jegliche (Kaffee-)Pause, für die vielen Unternehmungen außerhalb des Instituts, für das Gutzureden, Mut machen, Aufheitern und überhaupt einfach fürs Dasein und Halten gegen Ende der Promotion, als ich das Gefühl hatte innerlich zu zerbrechen. ❤️ Du hast mir oft guten Input gegeben, wenn ich an meiner Chemie verzweifelt bin. Daher habe ich immer großen Wert auf den Austausch mit dir gelegt. Danke, dass du dich in den letzten Monaten um mich gekümmert und so viele Teile dieser Arbeit korrekturgelesen hast. Ohne dich hätte ich das mental nicht überstanden. Du bist ein wunderbarer Mensch. Und falls du jemals Zweifel an dir haben solltest, egal in welcher Situation, ich versichere dir, Du schaffst das!

Danke auch an die Greb-Alumnis *Nina Kramer*, *Deborah Hartmann*, *Fabian Ebner* und *Yael Ginzburg* für die damals liebevolle Aufnahme in den Arbeitskreis. Liebe *Nina*, leider gab es keine Réunion in Berlin und auch wenn wir nun physisch nicht sehr nah waren, hast du immer geschaut, dass wir den Kontakt halten, und warst aus der Ferne immer für mich da. Danke dafür, dass du mich aufgebaut hast und mir immer versichert hast, dass ich das alles schaffe und bald das Leben rosiger aussehen wird. Ich verstehe nun sehr gut, wie es dir damals ging. #wirkömmendasjetzt ❤️ Liebe *Debbie*, du bist ein herzensguter Mensch. Danke, dass du mir immer zur Seite standest und gegen Ende der Promotion sehr unter die Arme gegriffen und geschaut hast, dass dieses elendige Paper vorankommt. Es ist schön, dass wir #grebgurls unseren monatlichen Skype/Heiconf/Zoom-Call haben und uns auf dem Laufenden halten. Ich freue mich schon auf das nächste Mal, aber gerne auch *in natura*. Lieber *Fabi*, ich war gern dein Laborbuddy, leider hat Lutz uns getrennt. 😊 Danke für dein offenes Ohr und dafür, dass du immer gemerkt hast, wenn es mir nicht gut ging. Du hast mir gezeigt, wie man sich durchsetzt. Durch dich habe ich viel Selbstbewusstsein und Ehrgeiz gewonnen. Dear *Yael*, you always knew how to cheer me up. Thank you for your loving nature and for always telling me that I am an awesome person. That has strengthened my being and gave me courage. It was good to know that you cared about me. I can't wait to finally visit you in Groningen! Ich danke euch von Herzen, für die schöne Zeit mit unvergesslichen Unternehmungen und außerchemischen Gesprächen. #akfallobst 🍷

Qingqing Luo a.k.a *Coco*, ich weiß du wolltest eigentlich nach Schweden, aber ich habe mich sehr gefreut, dass du zur Promotion hier im Arbeitskreis geblieben bist. Ich hoffe ich war dir eine gute Betreuerin! Danke, dass du immer nach mir schaust, mir Snacks zum Probieren mitbringst und neue Restaurants oder Spiele zeigst. Wir teilen die Liebe zum Essen, das gefällt mir. Ich freue mich auch auf weitere Switch Abende. 😊

Lieber *Nils*, es freut mich sehr, dass du in unseren AK gefunden hast. Somit habe ich nicht nur einen neuen Laborkollegen, sondern auch noch einen neuen Mitbewohner bekommen! Danke, dass du da warst als ich meinen *ground zero* erreicht hatte. Du hast mir immer gut zugeredet und mir andere Sichtweisen aufgezeigt. Das letzte Jahr war für uns beide sehr holprig, aber dadurch, dass ich dich als Freund dazu gewonnen habe, wurde es für mich auf jeden Fall erträglicher. Ich hoffe ich konnte dir zeigen, dass auch platonische Freundschaften zwischen Männer und Frauen funktionieren 😊
#brotherfromanothermother..and father, obviously.

Lieber *Heiko*, danke für deine herzliche Art und für deinen fantastischen Humor. Deine *Dad-Jokes* haben mich fast (immer) zum Schmunzeln gebracht. Es war auch schön zu wissen, dass man die Wochenenden oder die Tage zwischen den Jahren nicht allein an der Uni verbringen musste. Danke, dass du uns bei diversen Ausflügen immer mit dem richtigen Getränk versorgst. 😊

Lieber *Daniel*, lieber *Lukas Sigmund*, Labor -1.06 4Life würde ich sagen. Mit euch habe ich meine Promotion gestartet und ohne euch beenden müssen. 😊 Ihr habt mir in den letzten Monaten gefehlt, aber ich hoffe ihr habt/hattet eine gute Zeit in Murrrrrica. Danke für eure Hilfsbereitschaft und Ratschläge jeglicher Art.

Philipp Erdmann, danke für das Organisieren der Hütte für das AK-Wochenende. Es war eine optimale Ortschaft, um aus dem Uni-Stress rauszukommen!

Lucas Kistner, danke dass du mir gezeigt hast, wie man richtig Badminton spielt und für die vielen wilden Karaoke und Wii Party Abende.

Marco Werr, *Jean Thusek* und *Lukas Lohmeyer*, meine Leidensgenossen, danke für eure aufbauenden Worte, Rückhalt in der stressigen Phase und die vielen hilfreichen Ratschläge. Ich freue mich wieder auf eine gediegene Runde Spike-Ball im Sommer.

Lena Steuer, tausend Dank an dich für deine mentale Unterstützung und dass du immer verfügbar warst, wenn ich jemanden zum Reden brauchte, um meinen Ballast loszuwerden. Du hast mir gezeigt, dass ich mir sehr viel mehr wert sein kann und mich aufgebaut, als ich am Tiefpunkt war. Danke für deine ehrliche und besonders herzliche Art.

Großen Dank geht auch an alle Jungdoktoranden und Masteranden. Danke *Paulchen*, für deine außergewöhnliche Einstellung zum Leben. 😊 Immer auf Krawall gebürstet, oder bin ich das. 😊 Außerdem hast du mich überzeugt mich beim Venice anzumelden, was ein sehr willkommenes Ventil in der stressigen Zeit war. *Christoph* a.k.a. *Crispy Bacon*, schön, dass du es auch zu uns geschafft hast. Aber nach der gelungen Bachelor-Arbeit in der wirklich wahren GREB-Chemie, hatte ich nichts anderes erwartet. *Valentin*, mein Schreibkumpel, es war schön, wenigstens eine gewisse Zeit lang nicht ganz allein im Computerzimmer vor dieser Arbeit zu hocken. *Senta*, danke für deine offene Art und dass du dich nicht scheust Fragen zu stellen! #frauenpower 😊 *Lennart*, danke für deine herzliche Art und optimistische Einstellung. Ich hoffe es gibt bald wieder eine Kneipentour mit dir! *Lijun*, nice that you joined our group, you're fun at parties!

Simon Barth, ich danke dir, dass du für mich da warst in den Anfängen meiner Promotion. Bei dir bin ich immer gut aus dem *Chemiversum* gekommen, auch wenn ich vor Erschöpfung dann meist einfach irgendwo eingeschlafen bin (sorry). Ich habe mich immer sehr wohl gefühlt bei dir und deiner

Familie. Danke, dass ihr immer an mich geglaubt und bis zum Schluss mitgefiebert habt. Endlich geschafft!

Für die Hilfe bei bürokratischen und labor-alltäglichen Problemen danke ich herzlich *Karin Gissmann*, *Silke Dussel*, *Ute Eisendick* und *Maik Jakob*. Danke, dass ihr immer wieder nach mir schaut und ein offenes Ohr für mich habt.

Marcel Schorpp, du warst wirklich eine Bereicherung für unseren AK. Vor allem warst du einer der ersten (neben Lutz), die meine Chemie und die Farben meiner Substanzen gefeiert hat. Dear *Ravi*, dear *Avijit*, I am very pleased that you joined our group. *Ravi*, thank you for your good advices and *Avijit*, it's great that somebody else is so enthusiastic about the radical stuff! Also, drinking events are much more fun with you both. 😊

Zu guter Letzt, obwohl das der wichtigste Part ist, danke ich meinen Eltern und meinem Bruder *Sohir*. Danke *Mama* und *Papa* für eure unendliche Unterstützung in allen Bereichen, überhaupt für das Ermöglichen meines Studiums und die Hilfe, wenn es auch mal um was Fachliches ging. In gewisser Weise habe ich mir das mit der Chemie ja bei euch abgeschaut. 😊 Danke fürs Kochen und Kümmern, wenn ich mal krank oder einfach KO war. Ihr habt meine wechselnden Launen ertragen müssen, aber euch nie darüber beschwert. Danke *Babu*, dass du immer für mich da bist trotz der Entfernung. Auf euch ist immer Verlass. ❤️

EIDESSTATTLICHE VERSICHERUNG

GESAMTFAKULTÄT FÜR MATHEMATIK, INGENIEUR-
UND NATURWISSENSCHAFTEN
COMBINED FACULTY OF MATHEMATICS, ENGINEERING
AND NATURAL SCIENCES

RUPRECHT-KARLS-
UNIVERSITÄT
HEIDELBERG



Eidesstattliche Versicherung gemäß § 8 der Promotionsordnung für die Gesamtfakultät für Mathematik, Ingenieur- und Naturwissenschaften der Universität Heidelberg / Sworn Affidavit according to § 8 of the doctoral degree regulations of the Combined Faculty of Mathematics, Engineering and Natural Sciences at Heidelberg University

1. Bei der eingereichten Dissertation zu dem Thema / **The thesis I have submitted entitled**

Synthesis and Characterization of Silicon Polyoxolenes

handelt es sich um meine eigenständig erbrachte Leistung / **is my own work.**

2. Ich habe nur die angegebenen Quellen und Hilfsmittel benutzt und mich keiner unzulässigen Hilfe Dritter bedient. Insbesondere habe ich wörtlich oder sinngemäß aus anderen Werken übernommene Inhalte als solche kenntlich gemacht. / **I have only used the sources indicated and have not made unauthorised use of services of a third party. Where the work of others has been quoted or reproduced, the source is always given.**

3. Die Arbeit oder Teile davon habe ich wie folgt/bislang nicht¹⁾ an einer Hochschule des In- oder Auslands als Bestandteil einer Prüfungs- oder Qualifikationsleistung vorgelegt. / **I have not yet/have already¹⁾ presented this thesis or parts thereof to a university as part of an examination or degree.**

Titel der Arbeit / **Title of the thesis:**

Hochschule und Jahr / **University and year:**

Art der Prüfungs- oder Qualifikationsleistung / **Type of examination or degree:**

4. Die Richtigkeit der vorstehenden Erklärungen bestätige ich. / **I confirm that the declarations made above are correct.**

5. Die Bedeutung der eidesstattlichen Versicherung und die strafrechtlichen Folgen einer unrichtigen oder unvollständigen eidesstattlichen Versicherung sind mir bekannt. / **I am aware of the importance of a sworn affidavit and the criminal prosecution in case of a false or incomplete affidavit.**

Ich versichere an Eides statt, dass ich nach bestem Wissen die reine Wahrheit erklärt und nichts verschwiegen habe. / **I affirm that the above is the absolute truth to the best of my knowledge and that I have not concealed anything.**

Ort und Datum / **Place and date**

Unterschrift / **Signature**

¹⁾ Nicht Zutreffendes streichen. Bei Bejahung sind anzugeben: der Titel der andernorts vorgelegten Arbeit, die Hochschule, das Jahr der Vorlage und die Art der Prüfungs- oder Qualifikationsleistung. / **Please cross out what is not applicable. If applicable, please provide: the title of the thesis that was presented elsewhere, the name of the university, the year of presentation and the type of examination or degree.**

The German text is legally binding.